Magma fragmentation and tephra dispersal in explosive eruptions

The 1991 and 1845 Hekla eruptions

Jónas Guðnason

Faculty of Earth Sciences
University of Iceland
2017

Magma fragmentation and tephra dispersal in explosive eruptions: The 1991 and 1845 Hekla eruptions

Jónas Guðnason

Dissertation submitted in partial fulfilment of a
Philosophiae Doctor degree in 2017

Advisors and PhD Committee
Professor Þorvaldur Þórðarson, University of Iceland
Professor Bruce Houghton, University of Hawai'i at Mānoa
Emeritus Research Professor Guðrún Larsen, University of Iceland

Opponents
Dr. Eliza Calder
Senior Lecturer in Volcanology, University of Edinburgh, United Kingdom
Dr. Dave McGarvie
Senior Lecturer, The Open University, United Kingdom

Faculty of Earth Sciences
School of Engineering and Natural Sciences
University of Iceland
Reykjavik, July 2017

Magma fragmentation and tephra dispersal in explosive eruptions: The 1991 and 1845 Hekla eruptions
Magma fragmentation and tephra dispersal in explosive volcanic eruptions
Dissertation submitted in partial fulfilment of a *Philosophiae Doctor* degree in Geology

Faculty of Earth Sciences
School of Engineering and Natural Sciences
University of Iceland
Sturlugata 7
101, Reykjavik
Iceland

Telephone: 525 4000

Bibliographic information:
Jónas Guðnason, 2017, *Magma fragmentation and tephra dispersal in explosive volcanic eruptions: The 1991 and 1845 Hekla eruptions*, PhD dissertation, Faculty of Earth Sciences, University of Iceland, 135 pp.

ISBN 978-9935-9306-5-1

Printing: Háskólaprent
Reykjavik, Iceland, July 2017

Abstract

Iceland is one of the most volcanically active terrestrial regions on Earth. Hazards posed from volcanic eruptions to local population and life stock is well known in Iceland and the wider effects from volcanic activity have been elevated in recent years with increasing globalization, tourism and air traffic. Even small to medium size explosive eruptions can influence areas beyond their immediate surroundings. The high eruptive frequency, in combination with short warning times and dispersion of air borne pyroclasts, make Hekla an important volcano to study and monitor. The aim of this thesis is to add on to the growing collection of studies that focus on explosive volcanism in Iceland, by studying the opening phase of the 1991 and 1845 Hekla eruptions.

Paper 1 focuses on the 1991 eruption. Temporal variation in plume activity during the 50-minute-long opening phase was revealed by mapping out the proximal tephra fall. The 1991 eruption produced an eruption plume that rose to 11.5 km (a.s.l.) in 10 minutes. The mass eruption rate for the opening phase was 2.6×10^6 kg s^{-1}, and total mass of tephra 8.6×10^9 kg. The principal axis of tephra sedimentation was to the NNE of Hekla, with systematic grain-size fractionation during the first 65 km of transport. Beyond 65 km from the source, the tephra layer has a consistent grain-size distribution but decreasing mass, indicating sedimentation from a laminar regime in the volcanic plume. The opening phase of the 1991 eruption was pulsating, as revealed from changes in grain-size and vesicle number density with time. The vesicle number density indicates that peak intensity was reached towards the end of the opening phase before transitioning into effusive activity (paper 3).

In paper 2, the 1845 tephra fall is mapped and the one-hour-long opening phase constrained. The average plume height during the 1845 eruption was 19 km (a.s.l.), with a mass eruption rate of 2.1×10^7 kg s^{-1} and total tephra volume of 0.13 km^3 (0.03 km^3 dense rock equivalent) and total mass of 7.5×10^{10} kg. The plume was dispersed to the ESE of Hekla at speeds of 16–19 m s^{-1} and the tephra fall reached ships and islands as far away as 700–1100 km from Hekla. Over the course of the opening phase, a gradual decrease in intensity was inferred both from normal grading of the tephra deposit at proximal locations and from decreasing vesicle number densities (paper 3). Sedimentation of tephra from the 1845 opening phase produced bimodal grain-size distributions, primarily due to enhanced deposition of ash-sized particles by aggregation.

Paper 3 quantifies the vesiculation processes of the 1991 and 1845 opening phases. Decreasing vesicle number densities with time (1991 and 1845) and across conduit (1845) show that effective separation of the gas phase increases with decreasing ascent rate. This process finally leads to the transition from explosive to effusive activity in the 1991 and 1845 eruptions.

The results presented in this thesis contribute to enhanced understanding of vesiculation and fragmentation mechanisms during eruptions of Hekla. The patterns of sedimentation will aid in hazard mitigation and provide a basis for hazard modelling through both new and revised eruption source parameters, such as plume height, eruptive volume, mass eruption rate and total grain-size distribution.

Útdráttur

Vá vegna eldgosa er vel þekkt á Íslandi. Gosvá vegna Heklu er einna best þekkt, þar sem ræktarlönd, úthagar og vatnsból geta spillst vegna gjóskufalls. Með aukinni flugumferð á N-Atlantshafssvæðinu og í Evrópu geta jafnvel lítil til miðlungs stór eldgos valdið alvarlegum truflunum utan landsteinanna. Há gostíðni í Heklu, stuttur viðvörunartími og sprengivirkni veldur því að Hekla er eitt þeirra íslensku eldfjalla sem hvað best er fylgst með. Markmið þessarar ritgerðar er að bæta við ört vaxandi þekkingu á íslenskum þeytigosum, með rannsókn á opnunarfasa Heklugosanna árin 1991 og 1845 og skilgreiningu á kennistærðum þeirra (þ.e. eruption source parameters). Þeim eru gerð skil í þrem greinum.

Grein 1 fjallar um 50 mínútna langan opnunarfasa í Heklugosinu árið 1991. Gosmökkurinn reis á 10 mínútum upp í um 11.5 km hæð (yfir sjó), heildarrúmmál gjóskunnar var 0.017 km^3 (0.003 km^3 þétt berg), framleiðnin var að meðaltali 2.6 x 10^6 kg s^{-1} og heildarmassi gjóskunnar 8.6 x 10^9 kg. Heildarkornastærð gjóskunnar er tvítoppa en fínefni er lítið. Gjóskufall var til NNA og breyting í kornastærðardreifingu gjóskunnar er hvað mest fyrstu 65 km þar sem stærstu gjósku kornin féllu hratt úr gosmekkinum. Lengra frá Heklu varð kornastærð gjóskunnar stöðug, aðeins varð breyting á massa af gjósku sem féll á flatareiningu. Breytingar í kornastærð með tíma (grein 1) og blöðruinnihald gjóskunnar (grein 3) benda til þess að opnunarfasi Heklugossins 1991 hafi verið óstöðugur og komið í tveim hrinum, sú síðari var kraftmesti þáttur gossins í Heklu árið 1991.

Grein 2 fjallar um opnunarfasa gossins árið 1845. Hann var um 1 klukkustundar langur og ákvarðaður með samtímalýsingum á gosinu. Heildar rúmmál gjóskunnar var 0.13 km^3 (0.03 km^3 þétt berg), framleiðnin var 2.1 x 10^7 kg s^{-1}, heildarmassinn 7.5 x 10^{10} kg og hæð gosmakkarins um 19 km (yfir sjó). Gjóskufall var til ASA. Þess varð vart á skipum og eyjum 700–1100 km frá Heklu og barst það þangað með hraðanum 16–19 m s^{-1}. Opnunarfasinn árið 1845 náði hámarki í framleiðni skömmu eftir upphaf gossins, ákvarðað út frá lóðgreiningu gjósku í nágrenni Heklu og breytingu í blöðruinnihaldi gjóskunnar með tíma (grein 3). Heildarkornastærðin er tvítoppa. Kornastærðargreiningar sýna að tveir ferlar voru ráðandi þegar gjóska féll úr mekkinum. Grófara gjósku-fylkið sýnir að stærstu korn falla hratt úr gosmekkinum með flutningi. Fínna gjósku-fylkið sýnir mjög stöðuga stærðardreifingu óháð fjarlægð frá upptökum og er best skýrt með samloðun fínna öskukorna. Slíkt samsafn agna fellur fyrr og jafnar til jarðar en ella.

Í Grein 3 er blöðrumyndun í kvikunni í opnunarfasa gosanna 1991 og 1845 magngreind. Í opnunarfasa beggja gosanna fækkar blöðrum og þær stækka með tíma. Í gosinu 1845 fækkar blöðrum og þær stækka til jaðranna í gosrásinni. Þetta sýnir að gasið skilur sig hraðar frá kvikunni þegar uppstreymishraðinn minnkar og verður til þess að gas fer að rísa upp í gegnum kvikuna, sem að lokum leiðir til tveggja fasa flæðis og breytingar frá þeytigosi yfir í flæðigos.

Niðurstöður rannsóknanna bæta við þá þekkingu sem nú er til staðar um blöðrumyndun og sundrun kviku í þeytigosum í Heklu og skilgreint magnbundið lykil kennistærðir þessara gosa. Breytingar í kornastærð með flutningi frá eldfjallinu og greining á heildarkornastærðardreifingu gjóskunnar munu nýtast við gerð líkana á gjóskudreifingu og bæta mat á vá frá þeytigosum.

This work is dedicated to the memory of

my father

Guðni Tómasson (1953–2016)

and my father-in-law

Ólafur Emilsson (1948–2013)

Preface

The work towards this PhD thesis was carried out at the Institute of Earth Sciences at the University of Iceland, accompanied with a visit to the University of Hawai'i at Mānoa. The aim of the project was to examine and quantify eruption source parameters in small to medium sized magmatic explosive eruptions, including: duration of the explosive phase, plume height, volume and mass of the deposit, mass eruption rate and the degree of magma fragmentation by reconstructing the total grain-size distribution. The chosen volcano for this purpose is Hekla, as it is the most frequently erupting volcano in Iceland that has no ice cover over vent area. The chosen eruptions were the 1991 and 1845 events.

The primary motivation for undertaking this work was the wish to know more about volcanism, to get the opportunity to do fieldwork, to collect, process, and analyse samples, and to finally deliver a product that adds on to our knowledge about physical processes of explosive eruptions and the eruptive history of Hekla. A volcano that has impacted the Icelandic nation for centuries.

Vættaslagur

Illvættir:

Snæfells-ás,
Stormi blás!
Eyfjalla ár,
Ógnir og fár!
Heklu-glóð!
Hamra-þjóð!
Dvergar, dökkálfar,
Dólgar, hraunbjálfar:

Æsið, hræsið,
emjið, lemjið,
bölvið, mölvið,
blótið, skjótið,
hrækið, skrækið,
hendið, sendið
út yfir sjóinn eldinn og grjótið!

Höf. Matthías Jochumsson

Table of Contents

List of Original Papers

Paper 1 Gudnason, J., Thordarson, T., Houghton, B.F., Larsen, G., 2017. The opening subplinian phase of the Hekla 1991 eruption: properties of the tephra fall deposit. Bulletin of Volcanology. 79.

Paper 2 Gudnason, J., Thordarson, T., Houghton, B.F., Larsen., G., 2017. The 1845 Hekla eruption: grain-size characteristics of a tephra layer. Submitted to Journal of Volcanology and Geothermal Research

Paper 3 Gudnason, J., Houghton, B.F., Thordarson, T., 2017. The 1991 and 1845 eruptions at Hekla: Nature of the explosive opening phases inferred from vesicle volume distributions. In preparation for Bulletin of Volcanology.

List of Figures

Acknowledgements

This project has been helped in many ways, I firstly want to thank my supervisors: Þorvaldur Þórðarson for introducing me to physical volcanology, for his insight into the eruptive history of Iceland and Hekla, and paving the path for me in so many ways. Bruce Houghton for teaching me to understand fall deposits and fragmentation mechanisms, for fantastic time at the University of Hawaii, for coming to Iceland to help me and always being ready to assist me. Guðrún Larsen I want to thank for teaching me the value of careful sampling, the importance of good datasets, insight into the volcanic history of Iceland and the Hekla 1991 activity and her willingness to help me. Fellow students have also been valuable and shared the pain, especially William Moreland who helped in many ways, fieldwork, laboratory work and deciphering data, this task would not have been the same without him. I was very lucky to be able to stay and work at the University of Hawaii early on in my Ph.D, this was made possible by Bruce Houghton and Alison Houghton who also made our time there fantastic.

Help during fieldwork was valuable and came from multiple directions, Chris Lofthouse, William Moreland, Sigurður Gústafsson, Simon Norman Lauritsen, Lee Masson, Delphine Klaessens, Bergrún Arna Óladóttir, Sigurjón Valgeir Hafsteinsson, Maria Janebo, John Stevenson and even my wife Elísa Ólafsdóttir and our older son Emil Óli Jónasson came to search for tephra during vacations. My father, my mother and Ragnar gave their vehicles up for use (or abuse) during fieldwork along with tents and camping gear. I got also fantastic help during laboratory work, Carolyn Parcheta, Maria Janebo and Kristine helped with bubble work in Hawaii and made our time there even better. Maria Janebo, Inga Berg and Hannah Reynolds proofread the thesis and manuscripts, and deserve special thanks for that effort. Good company of fellow students/co-workers at the University of Iceland aided with discussions and helped lubricating life with good company, coffee and beer: Ásgeir, Sigurjón, Snorri, Birgir, Rob, Esther, Bergrún, Sófus, Olga, Sigrún, Hreggviður, Ívar, Johanne, Gro, Steini, Sveinbjörn, Þorsteinn, Svandís, Níels, Hannah, Catherine, Ágúst, Becca, Deirdre, Sandra, Ármann, Olgeir, Magnús, Dísa and Þórhallur.

Lastly I want to thank my family, my boys Emil Óli and Viggó Guðni for all the sleepless nights. My wife Elísa Ólafsdóttir deserves special thanks for putting up with my nonsense, crazy ideas and sharing her life with me.

The project was funded by Rannís, the Icelandic Centre for Research, grant 110077-0061, Orkurannsóknarsjóður Landsvirkjunar or the National Energy Research Fund, grant 02-2012 and Vísinda og Rannsóknasjóður Suðurlands the South Iceland Research fund, grant year 2014.

1 Introduction

Explosive volcanism is the most powerful and destructive type of volcanic activity, and one of the most instantaneous and far reaching natural hazards on Earth. Injections of large volumes of tephra (ash) into the atmosphere during explosive volcanic activity have immediate (and long term) effects on the local environment, infrastructure, and the local population (e.g. Carey and Sparks, 1986; Gudmundsson et al., 2012; Horwell and Baxter, 2006; Houghton et al., 2004; Thordarson and Self, 2003). Far reaching effects of volcanism have increased in recent years, due to globalisation and increased transport of people and goods around the world. This was exemplified by the 2010 Eyjafjallajökull eruption, when ash rich plumes caused widespread disruption to air traffic across Europe (Gudmundsson et al., 2012).

The 2010 event highlighted the need for better characterization of explosive volcanism in Iceland, in particular small to medium sized explosive volcanic eruptions which are the most frequent (e.g. Thordarson and Larsen, 2007). The fundamental process behind explosive volcanism is the formation of pyroclasts when a contiguous volume of magma is broken into pieces, either by magmatic fragmentation or by water-magma interaction (e.g. Gonnermann, 2015). Tephrochronology has been used for many years to study explosive volcanism in Iceland, and has provided valuable insight into eruptive history of individual volcanic systems (Gudmundsdottir et al., 2016; Larsen, 2010; Larsen et al., 1999, 1979; Gudrún Larsen et al., 2013; Óladóttir et al., 2011, 2008, 2007, Thorarinsson, 1968, 1967a). Quantification of eruption source parameters (i.e. plume height, mass eruption rate, mass, and volume) has typically been associated with ongoing or recent events (e.g. Grönvold et al., 1983; Gudmundsson et al., 1992, 2012, 1997; Hreinsdóttir et al., 2014; Larsen et al., 1979; Oddsson et al., 2012; Thorarinsson and Sigvaldason, 1972a, 1962). Additional parameters, aimed at understanding eruption dynamics and tephra dispersal in Icelandic eruptions, have received increased attention in recent years (Carey et al., 2009a, 2009b, 2008, Janebo et al., 2016a, 2016b; Jude-Eton et al., 2012; Sharma et al., 2008; Sparks et al., 1981), in particular quantification of fragmentation processes through reconstructed total grain-size distributions (TGSD), thereby rendering it possible to asses injection of fine particles into the atmosphere in given volcanic events (Janebo, 2016; Stevenson et al., 2015). This study is aimed at filling the gap in the already growing collection of thoroughly studied Icelandic explosive events, by the addition of eruption source parameters, TGSD, and vesicle size analysis of two small to medium sized explosive events: the 1991 and 1845 Hekla eruptions.

1.1 Explosive volcanism

In explosive eruptions, pyroclastic material (tephra) is cascaded high up into the atmosphere by thrust and thermal expansion, and transported through the atmosphere. The tephra is later deposited by gravitational separation of clasts, leaving a time marker (a tephra layer) in soils, marine, and lacustrine environments. Physical characteristics and chemistry of the pyroclastic fall deposit provide the information necessary to interpret, classify, and understand ascent dynamics, explosive activity, and the chemical processes that generated

the erupted pyroclasts (Bursik et al., 1992; Dingwell, 1996; Houghton and Wilson, 1989; Kaminski and Jaupart, 1998; Klug and Cashman, 1996, 1994; McBirney and Murase, 1970; Pyle, 1989; Sparks, 1978; Verhoogen, 1951; Walker, 1973).

The schematic diagram of an erupting volcano in Figure 1 can be divided into four parts, each of which exhibit different processes: 1) deep magma source, where magma is generated and released to the volcano; 2) magma chamber at some depth in the crust, where the melt collects; 3) the conduit to the surface, a connection of comparatively small dimensions; 4) the atmosphere, where lavas are emplaced or volcanic plumes are formed. For this study parts 3–4 are of most importance.

1.1.1 Magma storage

It is in the magma storage region (i.e. magma chamber) where overpressure is attained to drive volcanic eruptions (Figure 1). Exhumed magma chambers on the Earth´s surface vary greatly in structure, in both volume and shape (e.g. Marsh, 2015). Crustal magma chambers are established where the rise of buoyant magma is inhibited by colder, lower density, increasingly brittle upper crustal rocks (Gudmundsson, 2012). It is here that the chemical composition of the erupting magma is dictated, i.e. either mafic, intermediate or felsic (or a mixture thereof). The chemical composition of the erupting magma is an important parameter, as volatiles (primarily H_2O and CO_2) are enriched in felsic magmas compared to mafic (e.g. Baker and Alletti, 2012; Métrich and Wallace, 2008; Wallace et al., 2015), and the viscosity of felsic magma is high compared to mafic (Dingwell, 1996; Eichelberger, 1995; Gonnermann, 2015; Houghton and Gonnermann, 2008). Thus, it is in the magma storage region where the pre-conditions for the style of volcanic activity and size of the volcanic eruption are set (Carey and Sigurdsson, 1989; Eichelberger, 1995). For a volcanic eruption to occur, a roof failure of the magma chamber is needed, followed by a fluid driven rupture (dike) through the overlying crust. If the dike reaches the surface, a pathway (conduit) is established (Carey and Sigurdsson, 1989; Gudmundsson, 2012). Initiation of the roof failure can be caused by various sources: e.g. excess pressure from the magma chamber (Carey and Sigurdsson, 1989; Gudmundsson, 2012); pressure built up as a result of crystallization of anhydrous phase (e.g. Cashman, 2004); increased pressure gradient from the magma chamber by mass removal, like the slope failure in the 1980 Mt. St. Helens eruption (Criswell, 1987) and water drainage from lake Grímsvötn in Iceland, like the 2004 and 1934 eruptions (Thorarinsson, 1953; Vogfjörð et al., 2005); the intrusion of mafic magma into more evolved magma bodies like in the Eyjafjallajökull 2010 (Sigmundsson et al., 2010) a combination of rifting and intrusion like the 1477 Veiðivötn eruption (Blake, 1984; Larsen, 1984); or a rifting event like the 2014–2015 Holuhraun eruption (Gudmundsson et al., 2016; Sigmundsson et al., 2015). Once the conduit is established, the excess pressure between the magma chamber and the surface drives the magma ascent, and theoretically the eruption ceases when the overpressure drops below a critical threshold (Gudmundsson, 2012).

1.1.2 Bubble nucleation

The concentration of dissolved volatiles is strongly pressure dependant; solubility of volatiles in the magma decreases with decreasing pressure as the magma ascends towards the surface. The volatiles exsolve (degas) and nucleate to produce bubbles, forming a gas phase primarily composed of H_2O, CO_2 and SO_2 (Baker et al., 2012; Behrens and Gaillard, 2007). Nucleation of bubbles will only start after a certain degree of supersaturation of volatiles is obtained (Mourtada-Bonnefoi and Laporte, 2004, 2002; Sparks, 1978), and is either heterogeneous (on existing crystal phases) or homogeneous (within the melt) (Cashman, 2004). After nucleation

of bubbles, degassing will either continue through diffusion of volatile species into bubbles (Proussevitch and Sahagian, 1996; Sparks, 1978; Toramaru, 1989), or continue to nucleate new bubbles (Cashman, 2004). At very high rates of decompression, bubble nucleation becomes continuous and homogeneous (Mangan et al., 2004; Mourtada-Bonnefoi and Laporte, 2002). During ascent and degassing, magma rheology changes by: 1) increasing viscosity as a consequence of H_2O loss, 2) increased viscosity due to degassing induced crystallisation, and 3) addition of bubbles to the melt, inducing shear-thinning rheology (Cashman, 2004, 1992). The viscosity of the magma will also influence the rate of degassing and the ability of bubbles to migrate through the melt (Gonnermann and Manga, 2007). After a bubble nucleates, it will grow through diffusion, decompression driven expansion and/or coalescence (Sparks, 1978; Toramaru, 1989). Diffusion is affected by density, viscosity, solubility, surface tension, and the diffusion coefficient of the magma (Sparks, 1978). Growth induced by decompression dominates for large bubbles and at low pressures (Sparks, 1978). Coalescence of bubbles is more common in lower viscosity magmas, where bubbles can move independently of the surrounding magma (e.g. Houghton and Gonnermann, 2008; Parfitt, 2004), or in slowly advancing high viscosity magmas (Klug and Cashman, 1996). A high degree of coalescence will result in high permeability, creating an interconnected network of bubbles which facilitates outgassing and dissipates overpressure, i.e. open system degassing (Gonnermann, 2015; Rust and Cashman, 2004). In a closed system, the rate of bubble nucleation and expansion must exceed coalescence and outgassing to facilitate explosive fragmentation. In highly explosive eruptions (Plinian), high eruption rates are attributed to high initial volatile content of the magma (Melnik, 2000) or late onset of vesiculation (Mourtada-Bonnefoi and Laporte, 2004, 1999). Decoupled degassing can occur in mafic or low viscosity magmas, resulting in open system gas loss and lower explosivity (Melnik et al., 2005; Polacci et al., 2008), while coupled degassing more commonly occurs in more viscous melts (e.g. Papale et al., 1998). However, lower viscosity magmas may erupt explosively, possibly by rheological stiffening of the magma by microlites, resulting in brittle fragmentation (Houghton and Gonnermann, 2008; Sable et al., 2006; Taddeucci et al., 2004). In highly explosive eruptions, regardless of magma composition, vesiculation starts after supersaturation of the volatile species is obtained. This results in rapid nucleation and high vesicle number densities (Mourtada-Bonnefoi and Laporte, 2002, 1999).

1.1.3 Magma fragmentation

If magma ascends fast enough to inhibit outgassing, the feedback in the conduit from growing and nucleating bubbles is acceleration of the mixture up towards the surface. This in turn decreases pressure and triggers more degassing, and the ultimate result of this process is magmatic fragmentation. Magmatic fragmentation occurs when bubble overpressure surpasses the tensile strength of the surrounding melt (McBirney and Murase, 1970) or when the strain rate is higher than what viscous liquid can compensate for by elastic deformation (Dingwell, 1996; Papale, 1999), resulting in conversion of melt (+/- crystals) with dispersed bubbles of gas into a gas phase with dispersed pyroclasts. In magmatic fragmentation, experiments have shown that regardless of composition the fragmentation threshold depends dominantly on porosity, and that during high decompression rates, brittle deformation dominates over ductile (Spieler et al., 2004). Another process which triggers fragmentation is the interaction with external water (i.e. phreatomagmatic fragmentation). In phreatomagmatic eruptions, it is the expansion of the external water heated up by the erupting magma that fragments the magma (Wohletz, 1986; Zimanowski et al., 2015).

1.1.4 Volcanic plumes

After fragmentation of the magma, the two phases (gas and pyroclasts) accelerate by gas thrust to sonic velocities up through the conduit (Papale et al., 1998). When exiting the conduit/vent, the gas and particle mixture is denser then the surrounding atmosphere. The lowest part of the volcanic plume, the jet (Figure 1), continues to be momentum driven and there the mixture is carried upwards (Carey and Sparks, 1986). In the jet, larger clasts can be ejected from the plume following a ballistic trajectory (Figure 1). Originally accelerated by the gas thrust (Carey and Sparks, 1986), these clasts give no information about plume dynamics as their distribution reflects the initial velocity, although some acceleration in the jet may occur (Wilson, 1972). The jet can be several kilometres high, and is highly turbulent (Sparks et al., 1997). The jet progressively slows down due to atmospheric drag and decreasing gas thrust. Above the jet, in the convective phase, relatively cold air is entrained in turbulent eddies on the margins of the plume, and expands as it heats up. This results in decreasing plume density, increasing buoyancy, and increased width of the volcanic plume with height (e.g. Figure 1; Sparks et al., 1997). The convective phase of the volcanic plume strongly depends on atmospheric conditions and can be sub-vertical or bent-over (Bonadonna and Phillips, 2003). Strong plumes have higher vertical velocities than the atmospheric wind velocity (sub-vertical), while weak plumes have lower vertical velocities than the wind velocities (bent-over) (Bonadonna et al., 2005; Bonadonna and Phillips, 2003; Carey and Sparks, 1986). Figure 1 is a schematic illustration of a strong plume. As a strong plume reaches the level of neutral buoyancy (H_u), it will rise further (H_t) due to momentum and feed the lateral spread which is governed by the surrounding wind field (Carey and Sparks, 1986). The height of a volcanic plume can be inferred by an empirical relationship with the erupted mass and the mass eruption rate (Mastin et al., 2009; Sparks et al., 1997).

1.1.5 Sedimentation

Sedimentation of pyroclasts (tephra) is governed by their shape, size, and density. The majority of tephra fall comes from the laterally spreading current, as deposition from the plume margins is normally only within 1–15 km from the vent, although this is dependent on plume height (Bonadonna et al., 1998; Bonadonna and Phillips, 2003; Sparks et al., 1992). According to Bursik et al. (1992), there are four classes of pyroclasts deposited from a volcanic plume, based on their dispersal behaviour: 1) Coarse fragments which are ejected from the crater and follow ballistic trajectories; 2) pyroclasts that sediment from the margins of the convective phase of the plume; 3) pyroclasts that fallout from the laterally spreading plume; and 4) fine particles which are transported in the spreading current and often dispersed far away from source. Decreasing turbulence during the lateral spreading of a volcanic plume causes individual particles (class 3 and 4) to settle in accordance with their terminal fall velocity. Thus, particles will sediment when the settling velocity overcomes the turbulent diffusion within the plume (Bonadonna and Phillips, 2003; Carey and Sparks, 1986). Very fine particles (<0.03 mm diameter; class 4) have low settling velocities and can remain in suspension for days or weeks (Rose and Durant, 2011). Class 4 particles can also sediment prematurely by aggregation or due to gravitational instabilities, and will thus sediment with class 3 particles (Bonadonna and Phillips, 2003; Brown et al., 2012; Manzella et al., 2015). Early sedimentation of fine particles is an important process to recognize for the assessment of hazards to local populations and/or the effectiveness of models of particle distribution from volcanic eruptions.

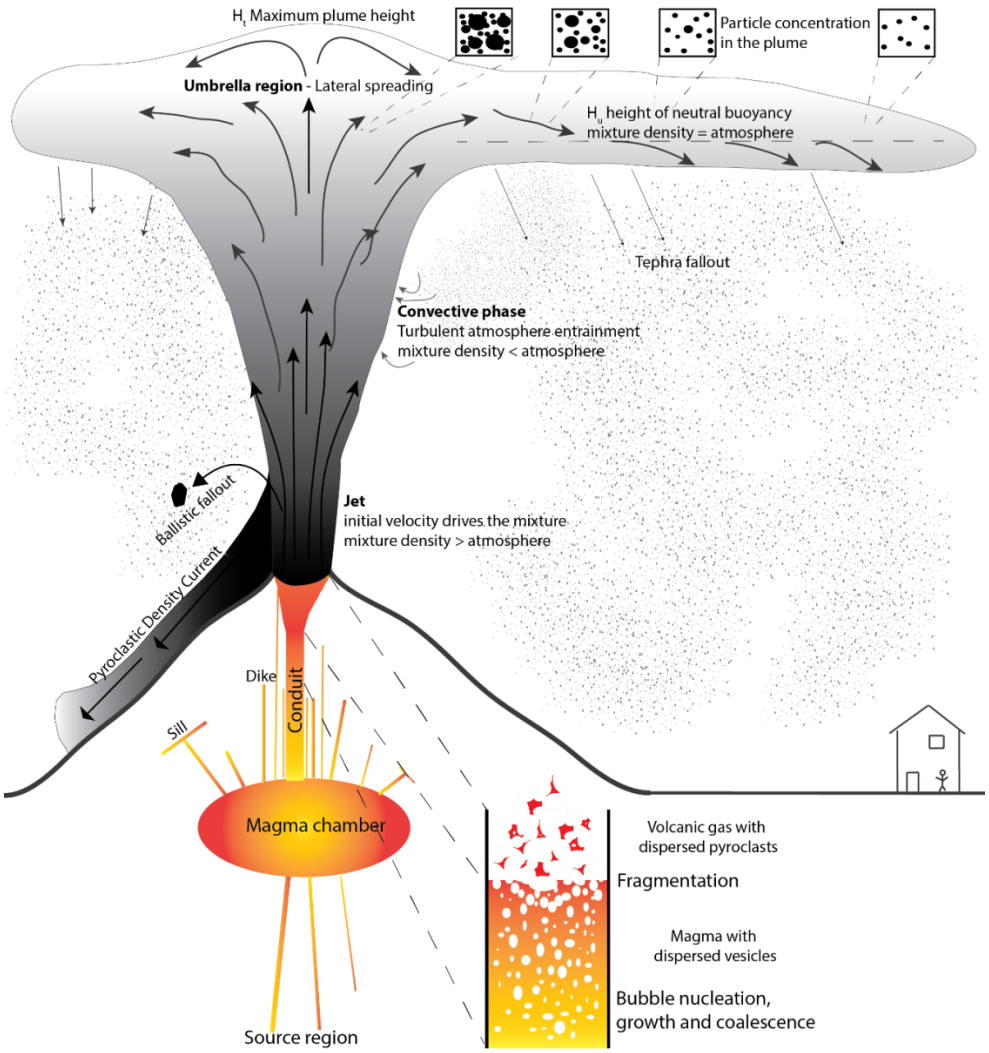

Figure 1: Schematic illustration of an erupting volcano and formation of pyroclasts in the conduit. The pyroclasts are lifted in the eruptive plume and deposited away from the volcano.

Tephra deposition from volcanic plumes generally shows elongation in the direction of the prevailing wind field, as represented by their isopach or isomass maps (e.g. Carey et al., 2009a; Carey and Sigurdsson, 1982; Janebo et al., 2016b). Presentation of isopach data can minimize distortion by this downwind elongation and facilitate comparison between eruptions, if presented on semilog plots of thickness versus the square root of isopach area (Pyle, 1989).

From the semilog plot, information regarding tephra sedimentation, the volume of the deposits, and quality of the sample cover can be inferred. Sedimentation regimes can be inferred by fitting line segments to the data set (Bonadonna and Phillips, 2003; Bursik et al., 1992) and quality of the sample cover inferred from the number of line segments (Bonadonna and Phillips, 2003). The volume of the tephra fall deposits is calculated by integration on the semilog plot after fitting exponential, power law, or Weibull curves to the

data (Bonadonna and Costa, 2012; Bonadonna and Houghton, 2005; Fierstein and Nathenson, 1992; Pyle, 1989). Further information regarding sedimentation of tephra can be obtained from individual grain-size samples across the tephra fall deposits, including clast size fractionation during transport and premature sedimentation of fine particles (e.g. Bonadonna et al., 2015; Eychenne and Pennec, 2012). However, the grain-size distribution of tephra fall deposits may be modified by e.g. the formation of pyroclastic density currents (PDC) and sedimentation from the co-PDC cloud (Eychenne et al., 2015). The grain-size distribution of tephra fall deposits can also give insight into the fragmentation process through a reconstructed TGSD. The TGSD can give quantitative information of the size distribution of pyroclasts created by the fragmentation processes. By that the TGSD is a crucial parameter for tephra dispersal modelling and for hazard assessment from volcanic eruptions (Bonadonna and Houghton, 2005).

1.1.6 Eruption source parameters

Eruption source parameters are set of physical parameters used to characterize eruptions and as input into modelling of volcanic hazards. These parameters are; eruption duration, erupted mass or volume, plume height, mass eruption rate (MER) and the TGSD.

Eruption duration is not directly obtainable from tephra fall deposits. However, it is a parameter often obtainable from contemporary descriptions. In the case of the Hekla eruptions studied here, the duration was obtained from contemporary descriptions for the 1845 opening phase.

MER is most commonly inferred from the eruption duration and the mass of the deposit. This results in time averaged MER. If the duration is not known, the MER can be inferred from the plume height using an empirical relationship based on buoyant plume theory (Mastin et al., 2009; Sparks et al., 1997). The relationship is approximately to the fourth power, resulting in large uncertainty on the MER estimates if the plume height is badly constrained.

Volume or mass of the erupted material is obtained from the field mapping. The associated uncertainties are poor exposure of the deposit and/or poor coverage (Bonadonna and Houghton, 2005; Pyle, 1989). The most common technique for estimating volume and mass of tephra fall deposit is from the deposit isopach map as described in section 1.1.5.

Plume height is in current eruptions estimated with remote sensing, this will give values for the H_t. However, plume height estimates from the tephra fall deposit will give estimates of the H_u (Figure 1). Although the plume height is readily available for current eruptions through remote sensing the uncertainty can be of 10–40 %, e.g. in the 2004 Grímsvötn eruption (Oddsson et al., 2012). Plume height from past eruptions can be inferred by empirical models using volume of the tephra fall deposit (Mastin et al., 2009), or isopleth maps (Carey and Sparks, 1986), and the MER (Mastin et al., 2009; Sparks et al., 1997).

TGSD is calculated from the sampled tephra fall deposit. he largest uncertainty to TGSD calculation is bad exposure and poor sample coverage (Bonadonna et al., 2015b). Many techniques have been used to estimate TGSD. Here the Voronoi Tesselation is used (Bonadonna and Houghton, 2005), see section 4.6 for details and comparison.

Thus, the necessary information to infer all the processes described above can be drawn from the deposited tephra by performing the following: detailed field sampling and mapping of the tephra fall deposit; grain-size analyses; vesicle-size analyses; measurements of chemical composition; volume estimations of the tephra deposit and reconstructing the TGSD.

2 Iceland

2.1 Geological setting

Iceland is a volcanic island in the North Atlantic, sitting astride the mid-Atlantic ridge. The active spreading of the Eurasian and North American plate, coupled with higher magma productivity from the Icelandic mantle plume, results in one of the world's most active terrestrial volcanic regions (Bjarnason, 2008; Einarsson, 2008, 1991; Thordarson and Höskuldsson, 2008). Volcanism in Iceland is confined to volcanically active regions, or volcanic zones, most importantly the West (WVZ), East (EVZ), and North (NVZ) volcanic zones (Figure 2). Most of the active spreading in Iceland occurs along the axial rift that is defined by these volcanic zones. The average spreading rate is 19–20 mm per year (Geirsson et al., 2006; Sella et al., 2002). The mid-Atlantic plate boundary comes ashore and connects to the WVZ in the SW of Iceland, and the active plate spreading connects to the EVZ across the south Iceland seismic zone (SISZ), to continue north through the country along the NVZ (Geirsson et al., 2006). Volcanism also takes place in zones outside of the axial rift, in the Öræfajökull (ÖVZ), the Snæfellsnes (SVZ) flank zones, and at the southern, propagating, tip of the EVZ.

2.2 Volcanic systems

The volcanic zones are subdivided into volcanic systems (Figure 2). The volcanic systems can be viewed as the principal volcanic structures in Iceland, and each volcanic system is composed of a central volcano and/or a fissure (dike) swarm (Sæmundsson, 1979).

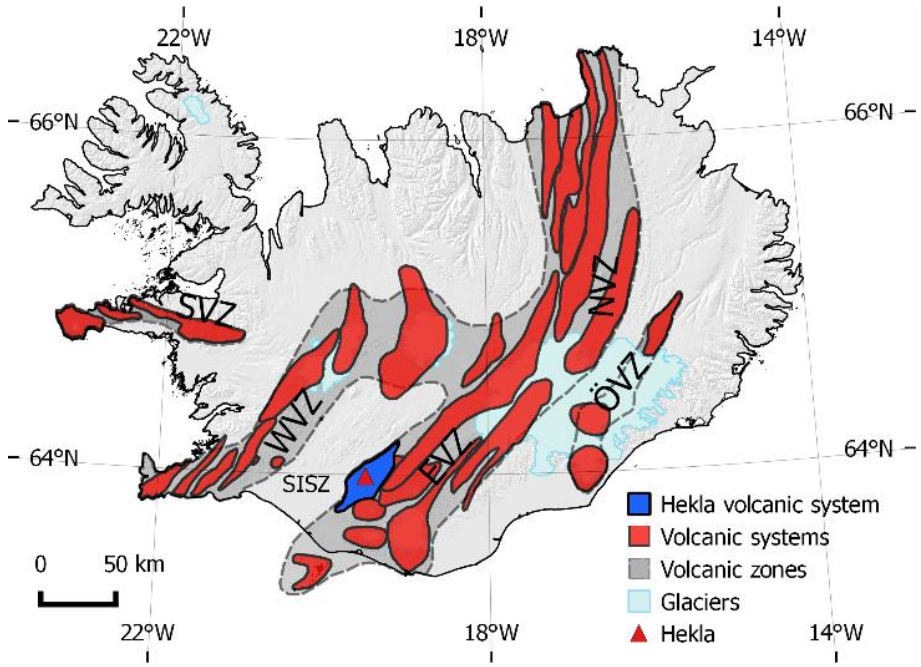

Figure 2: Iceland and the neovolcanic zones: the western volcanic zone (WVZ), northern volcanic zone (NVZ); and eastern volcanic zone (EVZ). The flank zones, Snæfellsnes volcanic zone (SVZ), Öræfajökull volcanic zone (ÖVZ), and the south Iceland seismic zone (SISZ) are also indicated. Hekla volcano is indicated with red triangle and the Hekla volcanic system is in blue. Boundaries of all terrestrial volcanic systems in Iceland are indicated. Based on Jóhannesson and Sæmundsson (1998).

These systems are defined by identifying the spatial distribution of tectonic fissures and eruptive vents, and based on the chemical composition of eruptive products (Gudmundsson and Högnadóttir, 2007; Jakobsson, 1979; Jakobsson et al., 2008; Jóhannesson and Sæmundsson, 1998; Sæmundsson, 1979). The fissure swarms are 7–200 km long and 7–38 km wide features, subparallel to the plate boundary (Figure 2). Of the 30 terrestrial volcanic systems in Iceland, 19 have a central volcano (some have two), where there is locus of volcanic activity and magma production, and 26 have produced eruptions during the Holocene (Thordarson and Höskuldsson, 2008; Thordarson and Larsen, 2007). Iceland is one of the most productive terrestrial volcanic environments on Earth, with an estimated 566 km^3 (recalculated as dense rock; DRE) of material erupted in 2434 events. Thereof the EVZ has been the most active part of the neovolcanic zones with an estimated 2023 events, where 163 are effusive events (Figure 3) and 1860 are explosive (estimated). The volume of material produced during the Holocene in the EVZ is 174 km^3 of lava and 163 km^3 of tephra. That is 44% of the lava volume erupted in Iceland and 94% of the tephra (Thordarson and Höskuldsson, 2008). Thus, the volcanic systems of the EVZ, which includes the Hekla volcanic system, are the most productive in Iceland (Figure 2).

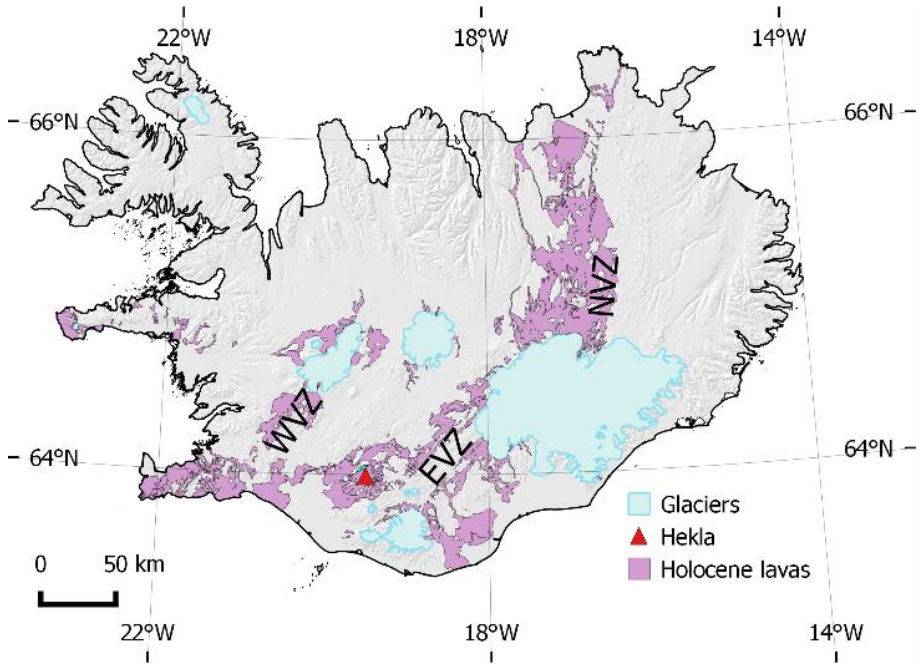

Figure 3: Distribution and cover of Holocene lavas in Iceland. Based on Jóhannesson and Sæmundsson (1998).

2.3 Explosive volcanism in Iceland

Explosive volcanism in Iceland spans the range from mafic to felsic magma compositions and in terms of style of activity from "wet" eruptions (i.e. Surtseyan to phreatoplinian) to "dry" eruptions (Strombolian to Plinian) (Carey et al., 2009a, 2009b, 2008, Gudmundsson et al., 1992, 2012; Janebo et al., 2016b; Jude-Eton et al., 2012; Larsen et al., 1999; Larsen, 2000, 1984; Larsen and Eiríksson, 2008; Moore, 1985; Pedersen et al., 2017; Sæmundsson, 1991; Sparks et al., 1981; Thorarinsson, 1968, 1967b, 1958; Thorarinsson and Sigvaldason, 1972b; Thordarson and Larsen, 2007; Thordarson and Self, 2003, 1993). The vast majority of eruptions in Iceland occur at central volcanos, ~70% of which are small basaltic eruptions, and the remaining events are confined to fissure swarms (Thordarson and Larsen, 2007). During the Holocene, most of the active central volcanos were ice capped, and thus phreatomagmatic activity is common (Figure 4). Magma that otherwise might erupt effusively was hence erupted explosively. Explosive volcanism accounts for ~80% of the predicted volcanic events and of those 83% of the events occurred in the EVZ (Thordarson and Höskuldsson, 2008). Similarly, the EVZ has produced about 80% of verified events during historical times (i.e. since 874 CE).

The volume of tephra (DRE) erupted explosively in Iceland during historical times is 19 km^3 of basaltic tephra, whereas the volume of intermediate tephra is 2 km^3 and silicic 3.5 km^3, and Hekla is the major contributor of intermediate tephra. The four most productive volcanic systems in terms of tephra volume (DRE) are Katla with 6–7 km^3, Grímsvötn with 6 km^3, Bárðarbunga/Veiðivötn with 5 km^3 and Hekla with 2 km^3 (Figure 4) (Thordarson and Larsen, 2007).

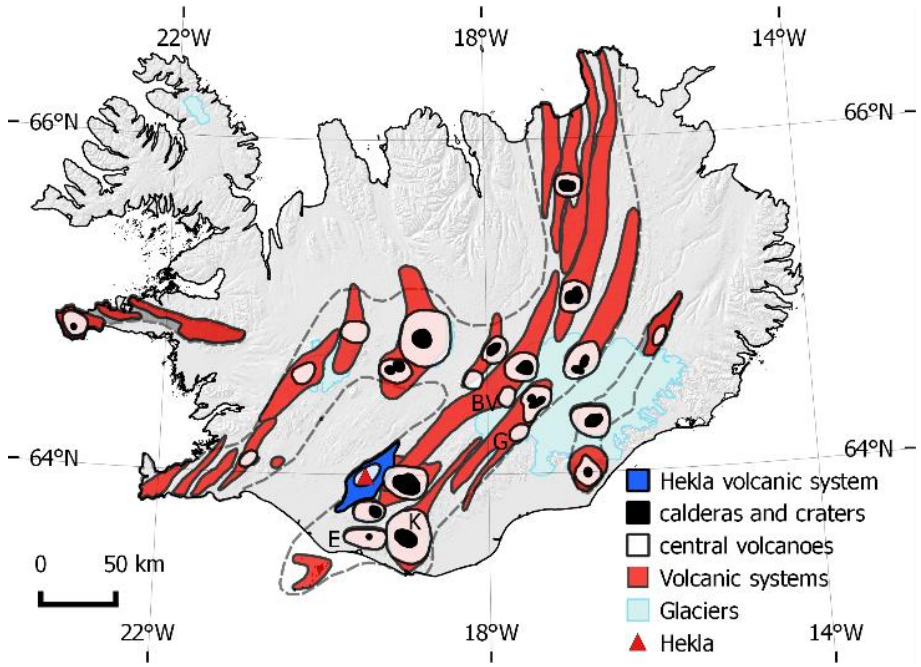

Figure 4: Distribution of central volcanoes and surrounding volcanic systems in the volcanic zones. The labelled central volcanoes of the EVZ are BV – Bárðarbunga/Veiðivötn, E – Eyjafjallajökull, K – Katla, and G – Grímsvötn.

The smallest explosive event recorded occurred during the Krafla fires, when about 1 m^3 of tephra (DRE) was produced through a borehole (Larsen et al., 1979). Apart from this event are the smallest explosive events normally phreatomagmatic and of basaltic composition, on the order of ~0.01–0.5 km^3 (DRE) as typified by the 2004 Grímsvötn eruption which is one of the 70 historical events of the Grímsvötn volcanic system (Gudmundsson et al., 2004; Jude-Eton et al., 2012; Oddsson et al., 2012; Thordarson and Larsen, 2007). However, the largest explosive events of basaltic composition in Iceland normally occur on the fissure swarms of the volcanic systems. In ~870 and 1477 CE, fissure eruptions on the Bárðarbunga/Veiðivötn fissure swarm surfaced in areas with a high ground water table. Explosive activity dominated the wet areas and 5–10 km^3 of tephra were produced (Larsen, 1984), which makes them some of the largest tephra layers deposited in historical times (Thordarson and Larsen, 2007). The largest (Plinian and phreatoplinian) explosive silicic (dacite and rhyolite) events are mostly confined to 7 central volcanoes and about 60 eruptions (Hekla, Torfajökull, Öræfajökull, Askja, Snæfellsjökull, Eyjafjallajökull and Katla) during the Holocene, (Larsen, 2002, 2000; Larsen and Eiríksson, 2008). Of these, three are historical Plinian eruptions: Hekla 1104, Öræfajökull 1362, and Askja 1875 (Carey et al., 2009a; Janebo et al., 2016b; Sparks et al., 1981; Thorarinsson, 1958).

Hybrid eruptions are defined as featuring both explosive activity and effusive activity, and are most often produced by volcanism of intermediate magma (Thordarson and Larsen, 2007). During historical times, the eruption of Heimaey 1974 is the only event other than eruptions from Hekla to display hybrid activity (see section 3.1 for details). Only 3 volcanic systems have erupted intermediate magma and produced tephra during the Holocene (Grímsvötn, Hekla, Öræfajökull), and the number of events is >40, dominated by the intermediate tephras from Hekla which amount to at least 35 during the Holocene (Larsen and Eiríksson, 2008).

3 Hekla volcanic system

Hekla volcanic system is situated in southern Iceland, along the western margin of the EVZ (Figure 2). To the west of Hekla is the South Iceland Seismic Zone (SISZ; Figure 2), with a series of en-echelon surface fractures with an orientation of N°60 (Einarsson and Eiríksson, 1982). Hekla central volcano (63.98°N, 19.70°W) rises 1490 m above sea level and sits within a SW–NE trending fissure swarm which is ~40km long and ~7 km wide (Figure 2) and includes Vatnafjöll, although Vatnafjöll has sometimes been considered a separate system (Jakobsson, 1979). In this overview, the Vatnafjöll region is included with the Hekla system in concordance to Jakobsson et al. (2008), Jóhannesson and Einarsson (1990) and Larsen et al. (2013).

Hekla´s northwest to southeast profile has the conical form that typifies stratovolcanoes, while its southwest to northwest profile is more elongated (Figure 5). The elongation reflects a ~5 km-long linear vent system that becomes partly or fully active during most eruptions (Grönvold et al., 1983; Gudmundsson et al., 1992; Gudnason et al., 2017; Höskuldsson et al., 2007; Larsen et al., 1992; Thorarinsson, 1968; Thorarinsson and Sigvaldason, 1972a). The Hekla system has produced a wide range of magma compositions, from mafic to silicic, where the mafic (< 51 wt% SiO_2) magmas are mildly alkali in character but the intermediate to silicic (51–62 wt% SiO_2) magmas are tholeiitic (i.e. sub-calcic). The production of basaltic magmas (< 51 wt% SiO_2) is confined to the fissure swarm, while eruption of basaltic icelandite and more evolved magmas is confined to the central volcano (Jakobsson, 1979; Sigmarsson et al., 1992).

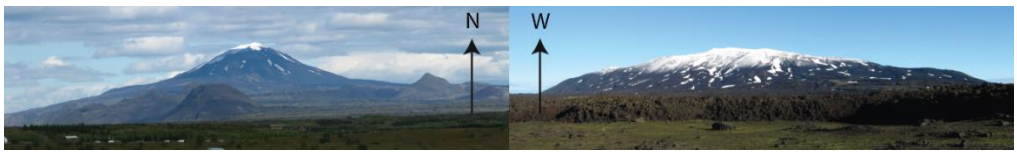

Figure 5: Hekla seen from the south and the east, illustrating the conical shape along the Hekla fissure and perpendicular to the fissure Hekla is like an inverted boat.

Hekla volcano might be a young structure, and Hekla's current form may have grown from a caldera to an edifice in approximately 4500 years (Jóhannesson and Einarsson, 1990). In the period 4500 and 1400 years ago no basaltic lavas erupted within the central volcano although explosive activity emitting silicic tephra continued. Hyaloclastites are also absent from the edifice while in other Icelandic central volcanoes they are common (Jóhannesson and Einarsson, 1990). The absence of hyaloclastites is attributed to post glaciation build up of the edifice, and the absence of basaltic lavas is thought to indicate a period of caldera infill by the lavas (Jóhannesson and Einarsson, 1990).

As mentioned above, Hekla lies within the EVZ, which has been the most productive volcanic zone in Iceland during historical times (i.e. since 874 C.E.) and has produced 82% of the erupted magma volume (DRE). The Hekla volcanic system has accounted for 19% of the erupted volume (DRE) during this time (Thordarson and Larsen, 2007). The eruptive products of Hekla during historical times are 13 km^3, split into 11 km^3 of lava and 2 km^3

(DRE) of tephra (Thordarson and Larsen, 2007). These products were produced in 23 eruptions, 18 events on the central volcano and 5 on the fissure swarm.

The presence of and the depth to an inferred Hekla magma chamber is still debated. A depth of 5–11 km has been proposed in a series of geodetic studies (Kjartansson and Grönvold, 1983; Sigmundsson et al., 1992; Sturkell et al., 2005), and depth of 5–6 km centred 4–6 km northwest of Hekla from optical levelling tilt measurements (Tryggvason, 1994). Nonetheless, following the 2000 eruption Soosalu and Einarsson (2004) concluded that a considerable magma volume cannot be present in the 4–14 km depth range beneath Hekla due to the lack of any S-wave attenuation. Ofeigsson et al. (2011) observed a broad inflation signal from 1993–1999 and from 2003–2008 using InSAR, and inferred that it was generated at a depth of 14–20 km, and furthermore reported superimposed deflation following the 2000 eruption at depth of 14–18 km. Similarly, was the pre-eruptive depth of crystal/melt equilibrium at 14 km for the 2000 eruption (Höskuldsson et al., 2007), and this depth is also the maximum depth earthquakes were recorded in the 2000 eruption and thought to give an estimate on minimum depth of the Hekla magma chamber (Soosalu et al., 2005).

3.1 Hekla volcanism

The postglacial eruptive history of Hekla is of three types, based on composition of eruptive products and type of activity (Larsen and Thorarinsson, 1977).

The three types are: (I) Effusive fissure eruptions, primarily basaltic; (II) Plinian eruptions often with starting composition of ~70% SiO_2; and (III) hybrid events primarily of intermediate composition.

Type I events take place on the Hekla fissure swarm, and there have been periods of high basaltic productivity during the Holocene (Jakobsson, 1979), firstly from 9000 to 5000 B.P. to the south of Hekla, followed by activity to the north of Hekla, while activity in Vatnafjöll (south east of Hekla) was more continuous from 7000 to 1000 B.P. Type I effusive events during historical times are: the 1913 Lambafitjahraun, 1913 Mundafell, 1878 Nýjahraun, 1725 Trippafjallahraun, 1554 Pálsteinshraun, and an unnamed lava from 1440 (Jakobsson, 1979; Thordarson and Larsen, 2007)

Type II events take place at the central volcano, producing tephra deposit of silicic composition. In the period from 7050 to 3000 yr. B.P. (calibrated ^{14}C ages) Hekla erupted up to eight times, with long repose periods and type II eruptions dominating the explosive activity. During this time three of the largest tephra layers from Hekla were deposited; the H5, H4, and H3 layers. The H5 tephra layer is the oldest tephra layer (7050 B.P.) to be traced back to Hekla and is classified as a VEI 5 event. The H5 tephra layer covers about 60% of Iceland (Larsen and Thorarinsson, 1977). Five smaller tephra layers with less area coverage were formed in between the larger eruptions, including the Hekla Ö (6100 B.P.) and Hekla DH (6600 B.P.) (Gudmundsdóttir et al., 2011). Following those the H4 (4200 B.P.), HS (3800 B.P.), and H3 (3000 B.P.) tephra layers were formed (Dugmore et al., 1995; Larsen and Thorarinsson, 1977). The H4 and H3 (about 2 km^3 DRE each) are two of the largest tephra layers found in Iceland, and are estimated to cover more than 80% of Iceland (Larsen and Thorarinsson, 1977; Stevenson et al., 2015). Hekla activity changed character after the formation of H3, when seven bicoloured tephra layers were produced from 2900 to 2500 B.P, all of which have a lighter base and darker top (Larsen and Eiríksson, 2008; Larsen and Vilmundardóttir, 1992; Róbertsdóttir, 1992). Furthermore, the H3 was a potential caldera forming event (Jóhannesson and Einarsson, 1990). The last type II eruption at Hekla was the 1104 eruption, often referred to as H1 (Janebo et al., 2016b; Larsen and Thorarinsson, 1977).

The 1104 was the first historical eruption at Hekla. It was a VEI 4 to 5 event and produced some 1 km^3 of tephra (Janebo et al., 2016b).

The type III are hybrid events. They are found in the stratigraphy predating H3 but are best represented in the stratigraphy from Hekla after 2500 yr. B.P, when dark coloured tephra layers dominate the tephra sequence into the historical part of the volcanic activity in Hekla. This eruption type is typical for the historical Hekla activity. Many of the best documented historical events indicate powerful but short (minutes–hours) tephra-producing opening phases, which transition into effusive activity and lava production (weeks–months). Events of confirmed hybrid character are for example the 1693, 1766, 1845, 1947, 1970, 1991, 1980, and 2000 eruptions (Grönvold et al., 1983; Gudmundsson et al., 1992; Gudnason et al., 2017; Höskuldsson et al., 2007; Janebo et al., 2016b; Larsen et al., 1992; Thorarinsson, 1968; Thorarinsson and Sigvaldason, 1972a). The typical proceedings of type III eruption is: an explosive tephra producing opening phase, and in recent eruptions the maximum plume height (>10 km a.s.l.) is attained in minutes. The opening phase is short, e.g. in the 1991 and 1845 eruptions is lasted about 1 hour. The opening phase is followed by a sharp decrease in magma discharge and a transition into dominantly effusive activity producing icelandite to basaltic icelandite lavas. The switch to a linear vent system occurs during the transitional phase, when intense fountaining activity starts along the crest of Hekla, producing relatively fast moving fountain-fed lava flows. After the transitional phase, activity becomes localized to single lower lying vents with Strombolian activity with relatively low discharge rates (<20 $m^3\ s^{-1}$).

The repose time of all types of Hekla eruptions during historical times is 41 ± 19 years with a maximum repose time of 78 years before the 1845 Hekla eruption and a minimum of 9 years before the 2000 eruption. For eruptions from Hekla proper (excluding type I eruptions), the repose time is 53 ± 33 years in historical times, with a maximum time of 120 years before the eruption in 1510 and minimum of 9 years before the eruption in 2000. The repose time of Hekla eruptions during historical times is calculated here after the eruption compilation of Thordarson and Larsen (2007). In the tephra deposits from the historical eruptions, Sigurður Þórarinsson (Thorarinsson, 1968, 1967a) noticed a correlation with SiO_2, volume, intensity, and the preceding repose time. His findings indicated that longer repose time results in a more evolved magma erupted. For example, the latest four eruptions in 1970, 1980, 1991, and 2000 have been typified by short repose times and low SiO_2 (Figure 6A). Despite the low volumes of recent eruptions, the high frequency of Hekla eruptions seems to keep up with the magma production rates of early historical times as the cumulative output of erupted material is nearly constant (Figure 6B).

Another feature of Hekla eruptions is the temporal variation of chemical composition within a single eruption. This is observed in both tephra fall deposits and lavas of type II eruptions during historical times and in the type II and III eruptions of pre-historic times (Sverrisdottir, 2007; Thorarinsson, 1968, 1967a). The SiO_2 content of the large explosive eruptions (type II) generally exceeds 70 wt%, with minor proportions of the magma containing as little as 56 wt% (Sverrisdottir, 2007), in the medium sized type III eruptions, however the SiO_2 content ranges from 54 wt% to 63 wt%. In the smallest studied Hekla eruptions (i.e. 20^{th} century events) the SiO_2 content does not show variation with time and is ~54 wt% SiO_2 (Grönvold et al., 1983; Gudmundsson et al., 1992; Gudnason et al., 2017; Höskuldsson et al., 2007; Thorarinsson and Sigvaldason, 1972a). In the chemically zoned deposits the magma containing higher SiO_2 erupts first, thus the tephra fall deposits are inverted with respect to silica content. The largest observed variance of this sort is in the H3 and H4 fall deposits, the SiO_2 ranges from 72% to 56% with a spectrum from rhyolite to dacite to basaltic icelandite (Sverrisdottir, 2007). Sigmarsson et al. (1992) illustrated that the basaltic icelandites erupted at Hekla are formed by crystal fractionation from basaltic magma, and the more evolved silicic compositions erupted at Hekla are derived from partial melting of metabasalts in the

crust. The fact that less evolved magmas are commonly erupted around Hekla (type I eruptions) and more evolved magmas at Hekla proper (type II and III eruptions) has implications for subsurface structures and magma formations under Hekla. Sigmarsson et al. (1992) inferred an elongated magma chamber that has a cyclic behaviour i.e. during long repose periods SiO_2 content increases possibly resulting in type II eruption, during a short repose periods there is less time to form evolved magmas. The shape, size and nature of Hekla magma chamber is not up for discussion here. These observations are, however, extremely important as they indicate that, with increased repose the possibility of larger more intense events increases. Nonetheless, as illustrated by the 1991 and 1845 eruption the relatively small Hekla events are a potential source for disruption of various kinds to modern society and will have health related hazards associated with them and therefore are of no less importance than large explosive events at Hekla.

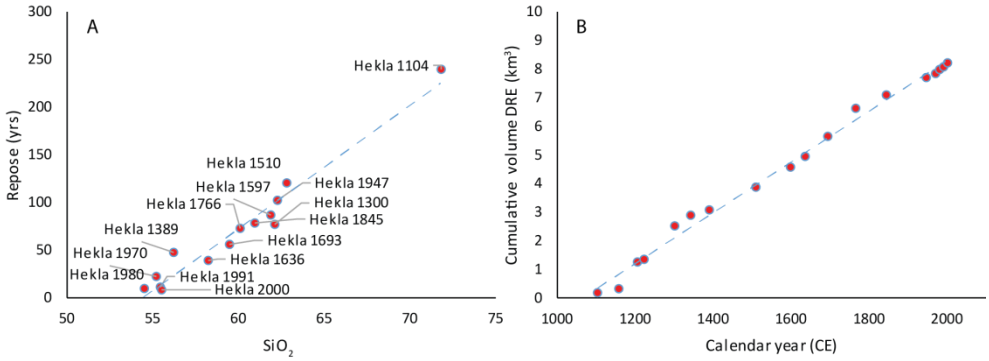

Figure 6: Historical eruptions in Hekla. A) length of repose and SiO_2 content of the erupting magma. B) cumulative DRE volume of historical eruptions in Hekla, indicating steady output of magma over the last 1000 yrs (Grönvold et al., 1983; Gudmundsson et al., 1992; Gudnason et al., 2017; Höskuldsson et al., 2007; Janebo et al., 2016b; Thorarinsson, 1967a; Thorarinsson and Sigvaldason, 1972a; Thordarson and Larsen, 2007).

3.2 The 1991 Hekla eruption

The 17th historical eruption of Hekla started at 17:01 on 17th January 1991 (Soosalu et al., 2003). The eruption lasted for 53 days and exhibited the typical hybrid (type III) course of events. The opening phase started abruptly with little precursors. Volcanic tremor started at 17:01 (Iceland standard time), elevated seismicity started only some 30 minutes earlier (Soosalu et al., 2003). First sightings indicated gas rich jets from the top craters of Hekla that were followed by a dark tephra laden eruption cloud (Þráinsson, 1991). The eruption plume reached 11.5 km a.s.l. height in only 10 minutes (Gudmundsson et al., 1992; Gudmundsson and Sæmundsson, 1992; Larsen et al., 1992). The opening phase of the 1991 eruption was 50 minutes long. A sharp earthquake at 17:52 marked the start of the transitional phase and the transition into effusive dominated eruption. The eruption attained peak discharge of 2.9 x 10^6 kg s^{-1} during the opening phase (Gudnason et al., 2017; paper 3), the discharge dropped quickly to 2–5 x 10^4 kg s^{-1} and during the transitional and effusive phase was on a steady decline until 31st of January (Gudmundsson et al., 1992). On 1st February temporary minimum in discharge was measured at 2.6 x 10^3 kg s^{-1} for two weeks or until on 13th February when the discharge picked up again and was around 3 x 10^4 kg s^{-1} and lava was flowing from five separate vents. On 23rd February the discharge had decreased again to 5 x

10^3 kg s^{-1} and on 6th March was down to about 2.6 x 10^3 kg s^{-1} until on the evening of 10th March volcanic tremor declined rapidly and dropped below detection on 11th March 1991 (Gudmundsson et al., 1992). The total volume of erupted material is dominated by lava over tephra. The lava field covers some 23 km^2 and the estimated volume is 0.15 km^3 (Gudmundsson et al., 1992), and the volume of tephra is 0.003 km^3 DRE (Gudnason et al., 2017). Only minimal amounts of tephra were produced in the transitional and effusive phases of the eruption. On the third day of the eruption, activity was typified by fountaining on a short fissure segment, supporting only a weak convective plume. This fissure segment became known as the East cone. The activity at the East cone was typified by a gas rich fountain, carrying sporadic bombs to height of few hundred meters. At the same time, lava was discharged from vents at the base of the East cone.

The 1991 Hekla eruption was the first eruption in Iceland where the volcanic plume was monitored remotely in time and space. Daylight and weather conditions on 17th January 1991 were poor, so the newly installed weather radar at the Keflavík airport (operated by the Icelandic Meterological office) gave valuable insight into the plume dynamics (Larsen et al., 1992). The focus of paper 1 and 3 is the opening phase of the 1991 eruption, however detailed observations during the eruption of the effusive phase are important in terms of the ascend dynamics and give insight into effective separation of gas and magma in the Hekla conduit system.

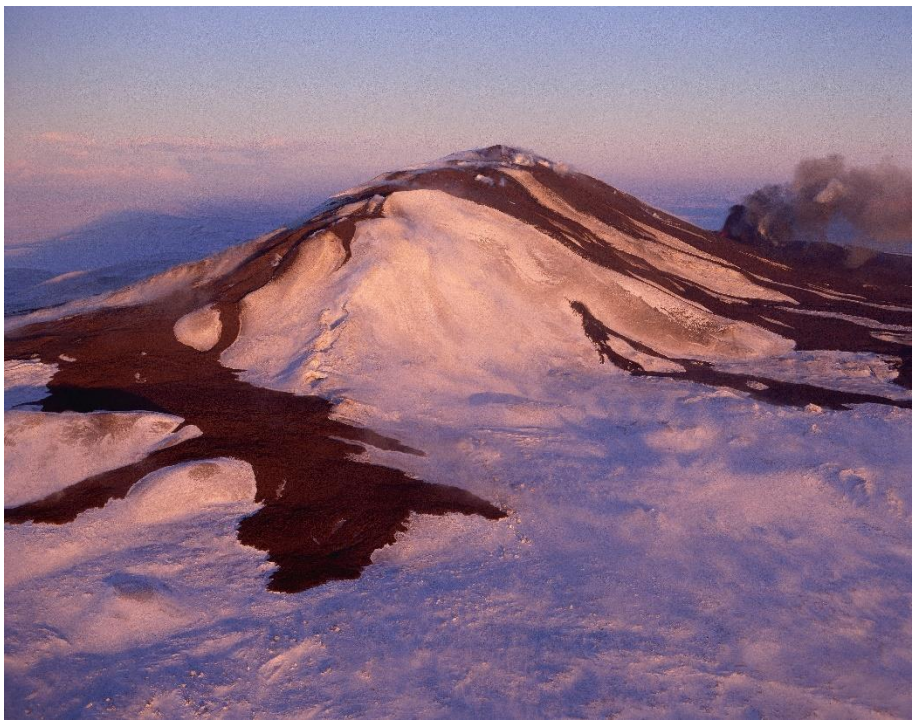

Figure 7: Hekla seen from the south during latter phases of the 1991 eruption. Opening phase vents are on the crest of the volcano. Location of activity during phase 3 in the east cone is seen here by dark grey cloud of tephra. Photo taken by Mats Wibe Lund.

3.3 The 1845 Hekla eruption

The 13th historical Hekla eruption started on 2nd September1845 after repose of 77 years, and ended on 5th to 10thApril 1846. The 1845 Hekla eruption is the best documented event of Hekla apart from the 20th century eruptions (Thorarinsson 1968). Contemporary descriptions are available from nearby farms, in particular a journal written by the farmer Oddur Erlendsson from Þúfa some 30 km west of Hekla. He documents all events from the onset of the eruption until activity in craters and lava flow ceased on 5th to 10th April 1846. He also noticed some possible renewed activity in August 1846 (Erlendsson, 1847). Observations made by Páll Melsteð at the farm Hjálmholt in Flói 50 km west of Hekla (Melsted, 1846), Jóhann Björnsson at the farm Kirkjubær á Rangárvöllum 35 km south west of Hekla (Björnsson, 1846) are also important sources for the onset of the eruption and proceedings of it. The summer after the eruption, scientists visited Iceland to study the eruptive products, amongst those were Robert Bunsen, W. Sartorius von Walterhausen, A. des Cloizeaux, H. Mathiesen and J.C. Schythe (Thorarinsson, 1968). Schythe published a book on his findings: Hekla og dens sidste udbrud. In his book he compiled accounts of the length, onset and nature of the tephra fall (Schythe, 1847). The detailed observations made by Erlendsson (1847), and the compilation of observations, timing and description of the tephra fall made by Schythe (1847) are valuable contributions and provide insight in to the 1845 activity at Hekla. Furthermore, the eruption was studied by the late Sigurður Thorarinsson and was amongst other eruptions in his contribution on historical activity in Hekla (Thorarinsson, 1968, 1967a).

The phenomena associated with the onset of the eruption and sequence of events is best described by Oddur Erlendsson (1847), and is quoted below as translated by Sigurður Thorarinsson (1967a) with his omissions.

> Tuesday, 2 September, 1845. —The weather was quiet, the sky cloudy so the sun was not visible, a gentle breeze from the west now lifted, now dropped, and gave every prospect of a lovely day… All of sudden towards 9 a.m. rumbles and violent murmurings became audible in the east with such sub-terranean din that the ground shook under foot; this roaring noise was most like what one would hear in the most terrifying river chasms or the noise of the fiercest breakers. People who were indoors felt moderate earth tremors, three of four of them those who were nearest the mountains but only one those who were farther off, and people working outside did not notice them at all. Then the sky in the ENE was covered by a huge blue-black cloud which suddenly spread over the whole northern sky to the WNW and right up to the zenith, so that out into the middle of the farmlands here it was almost as if half-dusk were the shadow of it struck the ground, and people who were under that shadow said that it was only just light enough to work as long as that darkness lasted. And this darkness was as ominous as the worst thunderclouds, yet not like them in appearance for this was most like sheer obscurity and not like clouds save where small ash-grey mist-clouds were visible scattered here and there. It covered all the mountains that lay beneath it with its pitch-blackness and it was as if dark night brooded over them. — I know of nothing if it was not this that could give witnesses of it a better idea of Egypt´s ancient darkness and how that must have appeared to the children of Israel dwelling in Goshen … Many were terrified at what they saw or heard; some thought it was thunder, but closer attention soon showed it was not; others thought it heralded a terrible wind from the east, which often begins here with great murmuring in

the eastern mountains, and indeed from the eastern sky this looked not unlikely, but such a murmur hat never been heard before as this frightening murmur now; there were also some who thought the end of the world was at hand. But majority, however knew by sight and sound that this was the work of Hekla, the volcano which so often in the past had terrorised the country with destruction and death……

The darkness soon began to clear away, but the sky was very terrifying to see in the breaks, for here and there in the north sky, when it began to be visible through the obscurity, there were what looked like ash-grey-yellow wind rifts; and gradually it dissipated in this way and moved to the mountains; and then the great darkness fled away. Now great crashes and reports came every now and then from the direction of the mountain, but it could not be seen from here because of the mist cloud that hid the mountains. At once there came so great a flood in Rangá ytri — which has its source WNW of the mountain and runs alongside it to the sea, west of Næfurholtsfjöll — that it rose over its banks and nearly boiled; that brought with it a great glacial mud so that the river was light blue in colour — at other times it is clear spring water — and it was impossible to cross in any way; all the trout were killed in it, and many of them were washed up; about 200 were found on a few farmlands in the middle part along the river, and the smallest of these trout was rotted through from the heat that had come into the river; it went down nevertheless in the evening and was fordable. People also heard that a flood had come in Markarfljót which divides Landmannaafréttur and Rangvellingaafréttur ENE of Hekla and which runs into Þverá; that brought the flood into this river along with a deposit of pumice; these floods arose because the ice-cap on the mountain, which had become large after so many years, melted and rushed down the mountain in two directions. People saw that the flood which entered Rangá came plunging down from the NW of the mountain, then flowed north of Sauðafell, which is the same direction, and into an old snow-thaw channel to the north of it and then fell into the march which is the eastern source of Rangá, which lies west of the mountain; it dug itself down deep as a river-bed into the boulder-strewn and stony ground in the channel, although signs were seen that it had also flooded west over the sand plain, as far west as western Rangárbotnar which lie NW from there. All the ash cloud now moved ESE over Rangvellingaafréttur, east to Skaftártunga, Síða and the whole of Meðalland — There after 9 a.m. an ash fall was felt which gradually increased so that it got dark and it was necessary to light lamps in the houses. People hardly saw their own hand lifted in front of them when they were outside, and that lasted full three hours; much ash and small pumice fell there. As the day passed on, constant rumbles began to come from the direction of the mountain and terribly great booms and sudden crashes, so that it was just as if the earth shook under one´s feet. Yet none were as awful as two crashes about midway which were so sharp and piercing that animals were frightened by them; but one which came about sunset was the biggest of all; it happened that I was out by myself in the meadows turning hay for drying, since the sky cleared in the evening and it seemed likely that the weather would turn dry, and a dog was with me that had never parted from me wherever I had been, — he lay down there by me and I went to work, and when I had been at it for a little while, there was this appalling crash and a shiver ran through me … it was as a shock, and the dog jumped up howling and ran back to the farm, he was so frightened.

> Now the sky was so clear that the mountain was visible and the fire that was spewed up out of the western part of it — it was towards the top of the cleft in the western part of the mountain; the fire surged high into the air, and when it began to get dark the fire-flood could be seen coursing down along the cleft just mentioned and into a hollow below the mountain; And the lava flow had halted there and filled up the hollow and a great blaze shut up there as it stopped, and beyond the top there were fires burning no smaller than this one and the ash cloud came from there; people saw clearly how showers of glowing rocks, which in their un-melted state must have been great crags, were flung up into the air and in various directions from the blaze. Various opinions were held about the nature of the darkness which was seen in the morning, because it could not be an ash cloud for the wind was in the wrong direction and even though it might be that the tremendous strength of Hekla could have driven the cloud against the wind there was no sign that this was so, for then after all some ash fall must have occurred where the darkness passed over, but since this was not observed, people had to imagine other causes. — One of the likeliest explanations seems to be that the ash cloud was at the outset so terribly intense and thick and reached so enormously high because of the tremendous force of the eruption that it eclipsed the sun in the districts where the darkness fell, and the darkness was thus no more than the shadow of the ash cloud; I consider this probable from the way in which the darkness gradually cleared and could be seen through here and there, so that the sky was visible through it, both close to the mountain and far from it; and that was when the main force which burst the mountain open – and which may be reasonably assumed to have been greatest at the outset – began to abate, and the ash spout gradually got lower and thinner, so that the sun began to shoot its rays through the thinnest parts of it; that great quantity of steam which arose from the glacial flood as it melted could also have helped a lot to increase the size and shadow of the cloud; people saw some traces of this steam rise up from the upper part of Rangá, after the flood came into it, - it was a great smoky vapour like out of a charcoal pit, and yet it was probably but little compared to what arose from the melting ice flood itself before it fell into the river; but that the obscurity was the vapour itself is still less likely than what has been put forward above, although people´s opinions are their own.
>
> It was especially remarked how strongly Hekla was heard in remote parts of the country, in Langanes in the east, in Ísafjarðarsýsla in the west and in Grindavík in Gullbringusýsla in the south, so much so that in this last place horses were frightened by it; and I have seen from a letter from Eyjafjarðarsýsla that people have prided themselves on how bad is was there (Thorarinsson, 1967a, p.127-130).

This clearly indicates that the opening phase of the 1845 eruption was, similarly to 20th century eruptions, explosive and produced a high eruption column in a matter of minutes. As Oddur describes, tephra fall occurred mainly during the opening phase towards the ESE, and his conclusions on why there was dusk upwind of the volcano and no tephra fall in his district exhibits an understanding of natural phenomena. The dusk in the Land district was due to the shadow cast by the rising eruption column and the position of the morning sun position to the east of the volcano.

On 3rd September Oddur Erlendsson (1847) wrote, as translated by author:

> Wind is slow from WSW. Forcing the eruption plume to the E onto the highlands; the plume height is as at minimum three times the height of Hekla not seeing clearly the top of it due to its direction. Rumbles and violent murmurs could be heard with constant subterranean din, the fires could be seen morning and evening with similar size and the lava constantly growing with smoke and haze; glares and cascading glowing rocks are seen around the fissure…. Two farmers herding sheep in the highlands on the first days reported, the river Tungnaá to the north of Hekla was filled with pumice to such a degree that clear drinking water could not be collected (Erlendsson, 1847 p. 12).

Here Oddur states that it is difficult to assess the plume height because he cannot see the top of the plume due to its direction, which indicates that the plume is bent over. He also describes what could be fire fountaining activity, on the second day of the eruption, similar to Hekla 1991 and other 20th century eruptions which transitioned to fire fountaining activity soon following a short opening phase. In the Hekla eruption of 1947 the transition from a tephra producing opening phase to fire fountaining activity and outpouring of lava was rather early, with the first lava observed just 30 minutes after the onset of the eruption and the lava production increased as tephra production diminished (Thorarinsson, 1968, 1967a). All of this indicates the same activity sequence as in other historical Hekla eruptions (e.g. Grönvold et al 1983, Gudmunsson et al 1992, Höskuldsson et al 2007, Larsen et al 1992, Thorarinsson and Sigvaldason 1972, Thorarinsson 1949, Thorarinsson 1968).

Sigurður Þórarinsson studied the Hekla 1845 eruption and published his findings in his monographs (Thorarinsson, 1968, 1967a). He located the active vents on Hekla, the top vent and another along the Hekla fissure to the SW. The tephra fallout was mapped to the ESE of Hekla (Figure 8). According to Thorarinsson (1968. 1967a) the volume of the tephra from the opening phase is 23 km^3 as freshly fallen. However, as pointed out in paper 3 this value is a mistake, because when the volume of the tephra deposit is calculated using the thickness and area values listed in his monographs (Thorarinsson 1968, 1967a), the volume amounts to 0.09 km^3, which is equal to 0.14 km^3 of freshly fallen tephra using his conversion factor of 1.6 (Thorarinsson, 1958, 1968). It is noteworthy that the 0.23 km^3 of freshly fallen tephra is a factor of 1.6 larger than the value of 0.14 km^3 obtained in the recalculation (Thorarinsson, 1968, 1967a). Effusive activity started on the first day of the eruption and Thorarinsson (1968) mapped the total area of the lava to be 25 km^2 and estimated the average thickness to be 25 m, resulting in lava volume estimate of 0.63 km^3. The total amount of tephra produced was roughly estimated 0.07 km^3 DRE. Thus, total output from the 1845 eruption was 0.7 km^3 of DRE. Tephra fallout from the effusive phase was minimal, but over time formed semi-circular isopach around Hekla (Figure 8). The fallout from the effusive phase brought large problems for the local population as continuous deposition of tephra brought Fluorine and resulted in fluorosis in sheep and cattle in southern Iceland (Thorarinsson, 1968).

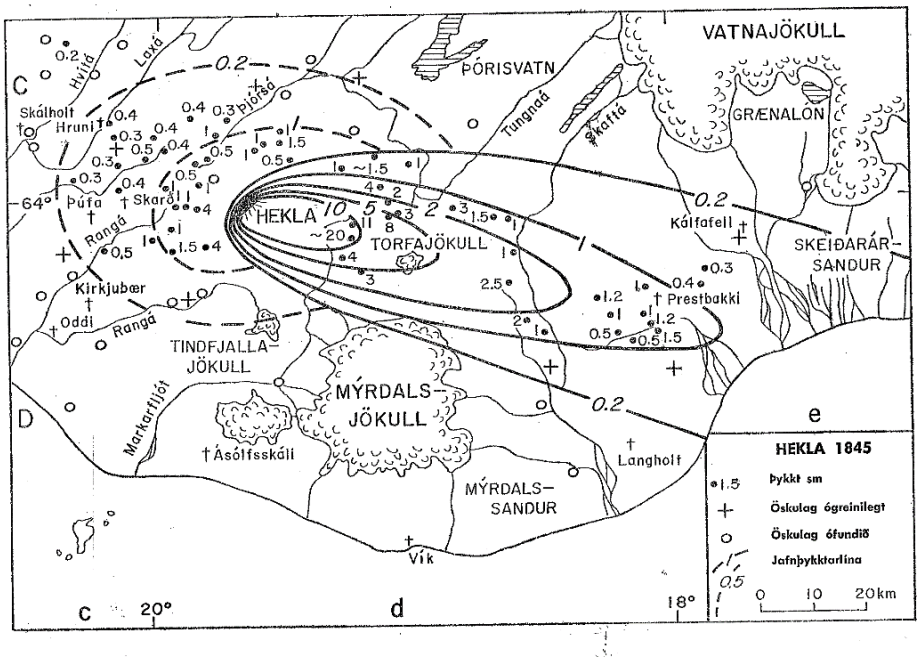

Figure 8: The isopach map of the 1845 deposit by Sigurður Þórarinsson as published in Thorarinsson (1968).

In addition to what Sigurður Þórarinsson contributed to our knowledge of the 1845 Hekla eruption (Thorarinsson, 1968, 1967a), and the abundant contemporary observation by Björnsson (1846), Erlendsson (1847) and Melsted (1846), some additions have been made. See paper 2 for further details.

4 Methods

4.1 Grain-size analysis

For analysis of grain-sizes of pyroclastic material that spans several orders of magnitude (i.e. from 20 cm to 10 μm) the Φ scale is used; D is particle diameter in mm.

$$\Phi = -log_2 D$$

Samples were sieved down to 63 μm (4Φ) on half Φ intervals. The samples were shaken by hand to minimize breakage of fragile surface features of the clasts. The sample portion smaller than 63 μm was analysed on two machines; majority of samples (all from 1845 and half of 1991) were analysed at the University of Iceland, where a SediGraph 5120 X-ray particle analyser was used to analyse particles from 3Φ (125 μm) down to 10Φ (1 μm). At the University of Edinburgh, a Beckmann Coulter Counter was used for part of the samples from the 1991 eruption of Hekla. The coulter counter analyzes grain-sizes < 1 mm (0Φ).

The SediGraph uses X-rays to measure particle concentration in the liquid. The Beer-Lambert law describes how photons (X-rays) are attenuated when passing through matter. The intensity of the incident beam I_i is reduced exponentially to I_f as a function of the absorptivity ε, of the system. Concentration of the absorber (c) and the path length (d) through the absorber.

$$\frac{I_f}{I_i} = exp(-\varepsilon cd) = T$$

which defines transmittance (T). T can have a range of values from 0 to 1, where 0 signifies total absorbance of X-rays by the matter and 1 signifies no absorbance. Before each round of analysis, a baseline measurement is done. This is to establish the background absorbance of the liquid and cell windows before the sample is introduced.

The machine measures the absorbance of the sample while in suspension (sample mass fraction 100%), and after the sample is allowed to settle out any signal level between the two extremes is due to the absorbance of X-rays by some mass fraction between 0 and 100%. At any time, t, the mass fraction in the measurement zone of the instrument (M_t) can be calculated from the X-ray transmission, T_t, at that time using:

$$M_t = \frac{ln\ T_t}{lnT_i}$$

The SediGraph 5120 thus measures absorbance of matter at any given time in the sample cell. To measure grain-size of the particles the SediGraph then uses the settling velocity of the particles in the liquid medium. Particles settling in a liquid will achieve terminal velocity (V_t) when the gravitational forces balance the particle buoyancy and drag forces. This is dependent on the particle density and the viscosity of the liquid. For the analysis with the SediGraph all variables are known, and the resulting settling velocity of particles is

proportional to the particle size. The SediGraph thus utilizes Stoke´s law to calculate particle size as the density of the particles and viscosity of the liquid are known.

$$D = V_t^{1/2}[(18\eta)/(\rho - \rho_0)g]^{1/2}$$

For the particle, D is diameter of a spherical particle, V_t its equilibrium sedimentation velocity, and ρ its density. The fluid is characterized by viscosity η and density ρ_0, and the gravitational force is g. The largest particles settle out at the highest velocity, so after a certain time all particles larger than certain size will have settled below the measurement zone of the instrument.

Stoke´s law assumes laminar flow, and that particles are spherical with smooth surfaces and that material is homogeneous. When analysing volcanic material, the spherical shape, smooth surface of particles and the homogeneity cannot be controlled. The laminar flow can be controlled by increasing viscosity of the liquid if dealing with larger particles. At the University of Iceland (UI) the dispersing liquid is a glycerol-H_2O mixture, proportions selected ensure high enough viscosity so laminar flow can be assumed.

The Beckmann Coulter Counter LS230 applies laser diffraction to analyse grain-size distribution of the samples. The grain-size information is obtained through measurements of scattering intensity as a function of the scattering angle, the wavelength and polarization of light based on applicable scattering models. The instrument produces a light source that generates a monochromatic beam. This beam is then collimated which illuminates the particles in the scattering volume. The particles scatter light, generating unique angular scattering patterns. These patterns (I(Q)) are then Fourier transformed into a spatial intensity pattern (I(r)). The intensity pattern is then detected by a multi element array of photodetectors. The current is digitized and a flux pattern created (f(Q)). Computer software utilizing appropriate scattering theory converts the flux of values into particle-size distribution (q(d)). The method assumes spheres and can thus measure one parameter which is the particle diameter. This diameter is obtained through the Mie theory of scattering pattern from a spherical particle, illuminated by vertically and horizontally polarized incident light.

In both methods, the analysed particles are assumed to be spherical. This is an approximation, resulting in analysed size differing from the actual dimensions.

Similarly, for the sieving, the diameter obtained represents the minimum diameter of a particle as it passes through the mesh of each sieve. Particle shapes that are elongated will be underestimated in terms of volume, while near spherical particles will be affected to a much lesser extent. Elongation of the 1845 and 1991 tephra as a result of tubular vesicles was not a problem in this study.

4.2 Deconvolution

Grain-size analysis of pyroclastic fall deposits give information into the fragmentation mechanisms, changes with time and/or insight into transportation of the pyroclastic mixture. Traditionally grain-size distributions are plotted using the phi scale and in wt%, and theoretically they should be unimodal. If multiple populations are present in the deposits, they will show as polymodal distributions. Reasons for polymodal distributions in pyroclastic deposits can by contamination (i.e. aeolian), secondary granulation in the conduit or plume (e.g. Rose and Durant, 2009), sedimentation from a co-pyroclastic cloud (e.g. Engwell et al., 2014; Eychenne et al., 2015), and premature fallout of small particles by

aggregation and/or gravitational instabilities (e.g. Bonadonna et al., 2011; Brown et al., 2012; Manzella et al., 2015). Statistical information (i.e. median grain-size and sorting) of the grain-size distribution will give poor results if two or more populations are present. Deconvolution is therefore used in this study on the 1845 tephra fall deposit, to separate the grain-size populations present in the deposits. The program Decolog (www.decolog.org) was used for this purpose. The program has previously been used for tephra fall deposits, e.g. from the 1980 Mt. St. Helens eruption (Eychenne et al., 2015), and to separate between the B and C fall units of Askja 1875 (Janebo, 2016). The decolog program fits Weibull or Power law functions to the mixture and separates them without any selective process of the operator. The program can identify up to three separate populations, solve for either log-normal or Weibull distributions, and allow distributions with right tailed (positive skewness) and/or both positive and negative skewness (left tailed). Raw output from Decolog theoretically equals 1, and the individual populations are fractions of 1. The program thus delivers the fraction of each subpopulation as a percentage of the total distribution, and also statistical information (Folk and Ward, 1957). For this study the median diameter ($Md_\varphi = {}_\varphi 50$) and sorting ($\sigma_\varphi$) are used:

$$\sigma_\varphi = \frac{\varphi 84 - {}_\varphi 16}{4} + \frac{\varphi 95 - {}_\varphi 5}{6.6}$$

The sorting and median diameter were used to infer particle fractionation during transport for each subpopulation in paper 2 (Figure 9). An example of how the deconvolution can be used to separate two populations within a grain-size distribution is shown in Figure 10.

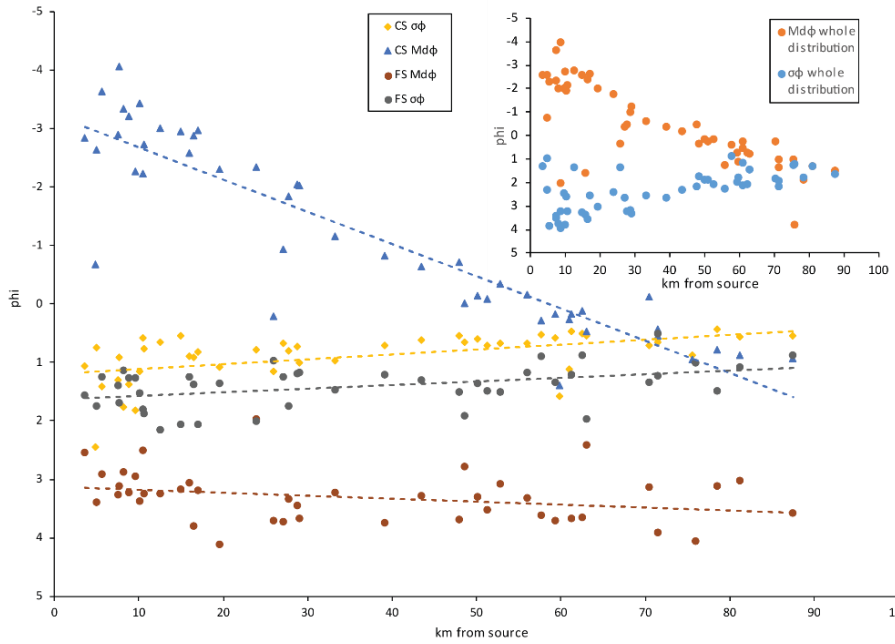

Figure 9: Example from paper 2 of how the deconvolution facilitated understanding of sedimentation mechanisms of two subpopulations of the Hekla 1845 deposit. The small inset illustrates the whole distribution. The large plot illustrates the rapid fractionation of the coarse subpopulation (CS) compared to relatively stable fractionation of the fine subpopulation (FS). See paper 2 for full details.

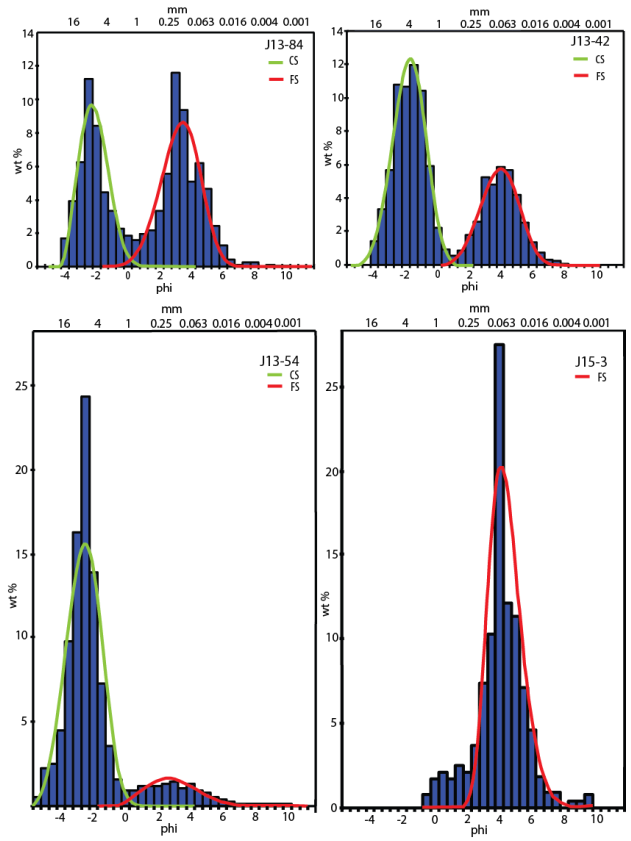

Figure 10: Examples of deconvolved grain-size distributions from the 1845 Hekla tephra fall deposit. The green curve represents the coarse subpopulation (CS) and the red represents the fine subpopulation (FS). The blue bars are original wt% values obtained with sieving. See paper 2 for full details.

4.3 Chemical analyses

In this study, glass chemistry of the 1991 and 1845 tephra was analysed on two sets of materials, firstly shards from the 125 µm sieve fraction were mounted in epoxy and analysed on a WDS Cameca SX100 electron microprobe at the Laboratoire Magmas et Volcans, Clermont –Ferrand (LMV), and secondly thin sections of individual lapilli sized pyroclasts initally prepared for image analysis (see section 1.6.5) on a Jeol jxa-8230 superprobe at the Institute of Earth Sciences, University of Iceland (UI). At LMV the analytical conditions used were a voltage of 15 kV, a current of 4 nA, and a 10 µm beam diameter. At UI a voltage of 15 kV voltage, a current of 10 nA and a 5 µm beam diameter was used. The standard used at both laboratories was natural glass from Kilauea (A99). The counting time was 10 s for Na, Ca, Ti, P and Si; 20 s for Mg and Al; 30 s for Mn and finally 40 s for Fe and K. Before the session, 10 point analyses were done on the standard. When compared to other reported results they are indistinguishable apart from systematically higher titanium at LMV (Jarosewich et al., 1980; Óladóttir et al., 2011; Thornber et al., 2002). The results from the chemical analyses are published as supplementary material in all papers.

4.4 Vesicularity analysis

Samples for density/vesicularity analysis were collected from vertically narrow stratigraphic intervals at the type localities selected for the 1991 and 1845 eruptions (see papers 1 and 3). Each sample contained a minimum of 100 clasts. The clast size sampled was 8–32 mm, because clasts > 32 mm can show secondary, post-fragmentation expansion whereas smaller pyroclasts normally do not. The lower cut-off is because smaller pyroclasts lack the largest primary vesicles (Houghton and Wilson, 1989). The samples collected were analysed after Houghton and Wilson (1989). Preparation for measurements involves making each pyroclast water tight, with either a thin layer of wax film or with water proofing spray. The general vesicle size of the sample set determines which approach is better. Coarser vesicles (e.g. scoria) need wrapping, while fine vesiculated clasts (e.g. pumice) can be sprayed. For this study, all samples were wrapped. The measurement involves weighing each pyroclast dry, and then submerged in water (weighed down if needed), and the specific gravity for each pyroclast is calculated using:

$$S.G. = \frac{(W_c)air}{(W_c)air + (W_s)water - (W_{c+s})}$$

Subscript s refers to wax film and c refers to clast. According to Houghton and Wilson (1989), the wrapping of clasts with wax film consistently gives values of ≤1% lower than the spray technique, which is less than the reproducibility of measurements for most samples.

To calculate the vesicularity of the pyroclast from the specific gravity, melt density needs to be known. To measure the melt density of the 1991 and 1845 tephra, the <63µm fraction was measured using a water pycnometer. The resulting melt density for Hekla 1845 is 2470 kg m^{-3} and Hekla 1991 is 2620 kg m^{-3}.

$$vesicularity\ V(\%) = \frac{100(DRE\ density - clast\ density)}{DRE\ density}$$

Vesicularity analysis were done on the 1991 and 1845 tephra and the results presented in paper 1 and paper 3.

4.5 Vesicle size analysis

From the vesicularity samples described in section 4.4, subsets of clasts were selected from each eruption for image analysis. Sample selection and vesicle analysis was based on Shea et al. (2010), see paper 3 for details and justification.

To quantify vesicles in volcanic pyroclasts, which commonly contain vesicles with diameters spanning 4–5 orders of magnitude (e.g. Klug et al., 2002), images are collected at several magnifications, using a flatbed scanner to image the whole clasts, and a scanning electron microscope (SEM) using backscatter electron detectors to image smaller areas in more detail (Shea et al., 2010). Images at four magnifications were used in nested trees following Shea et al. (2010). The scanned images were obtained with transmitted light at 1200 to 3200 dpi (47.2 to 126.0 dpmm). For the higher magnifications, two SEMs were used between 25x to 250x magnification, at the University of Hawaii (UH) and the University of Iceland (UI). From Hekla 1991, clasts were imaged at UH on a JEOL-5900lv operating with a 15kV acceleration voltage and at UI with a TM3000 Hitachi table top microscope, with a 15 kV acceleration voltage. The lowest possible magnification for the TM3000 instrument is 50x opposed to 25x on the JEOL. To minimize the magnification jump from scan to SEM, and to

be comparable to other studies (e.g. Carey et al., 2009b; Gurioli et al., 2008; Houghton et al., 2010; Janebo et al., 2016a; Parcheta et al., 2013), a set of 5 images at 50x magnification was collected with overlap of at least 30% on the TM3000 instrument, and combined into one image (Figure 11). In other magnifications, no adjustments are needed.

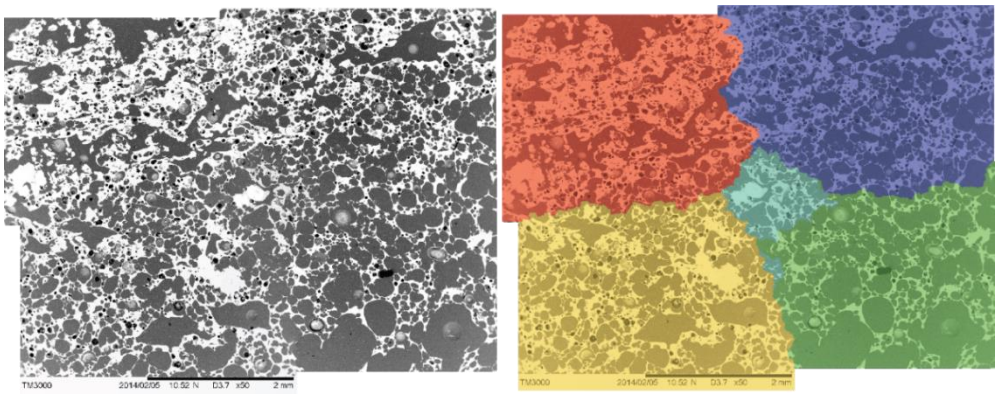

Figure 11: Example of combined images from the TM3000 scanning electron microscope, using 50x magnification. The 5 images stitched together in Photoshop. The colors on the right indicate individual images after stitching. The black bar on the bottom is 2 mm.

The images were merged using the photomerge command in Photoshop, choosing the reposition layout so that the images were not distorted. As a result, the 50x image covers the same or a larger area compared to the 25x magnification images used in other studies (Gurioli et al., 2008; Janebo et al., 2016a), and is thus large enough to record the largest bubbles that would be recorded in a 25x image (Figure 11). The images were processed in Photoshop and made binary; melt (and microlites) is white and vesicles are black (Figure 11). The open source software ImageJ was then used to measure the area of each vesicle in 2D and to count the number density per unit area relative to glass content (N_a) (Schneider et al., 2012). Conversion to 3D was made using the stereological conversion (Sahagian and Proussevitch, 1998) and vesicles per unit volume of melt (N_v), vesicle volume distributions (VVD) and vesicle size distributions (VSD) were calculated. The stereological conversion technique takes into account that small vesicles are less likely than large vesicles to be intersected and the probability of not cutting a vesicle at the largest diameter (Sahagian and Proussevitch, 1998). The drawback is that the method assumes spherical vesicle shapes. In the case of the Hekla pyroclasts studied here, spherical shapes are more common amongst the smaller vesicles (Figure 11). No alternative method is available for converting irregular shaped bubbles. Correction for the vesicle volume (N_{Vm}) was also applied to avoid underestimating number densities, which can be an issue in highly vesicular samples (Klug et al., 2002). Because of acquiring images on two SEMs with different resolutions the lower limit of measured vesicles was set at 22 pixels on images from the Jeol and 15 pixels on images from the TM3000, at 250x magnification this results in a minimum size equivalent diameter of 9 µm. This relatively large cut-off minimizes the error from misinterpreted pixels (Shea et al., 2010). Despite the high cut off limits, there is not an issue with under-representation of small vesicles. That is illustrated on Figure 12 for the 1845 sample set, indicating that lowering the cut off to 10 or 5 pixels does not increase the number of vesicles counted per volume of melt.

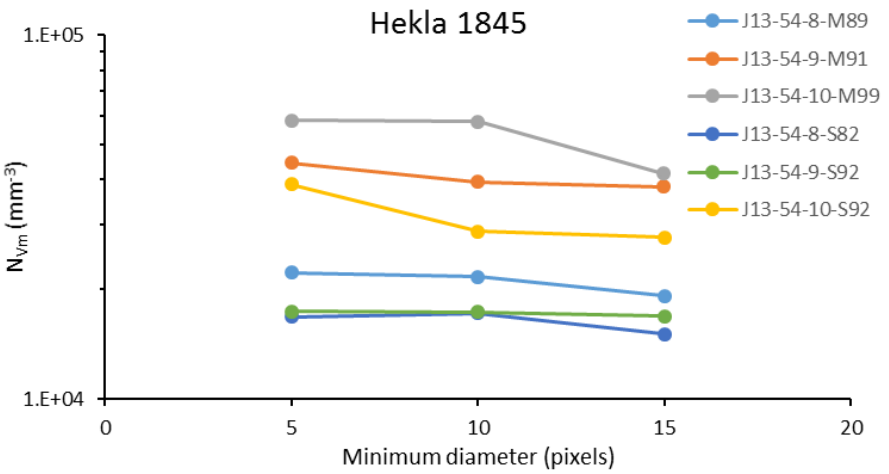

Figure 12: The 1845 sample set, y-axis illustrates the volume corrected number densities of vesicles for three different lower cut offs, i.e. 15 pixels 10 pixels and 5 pixels as represented by the x-axis. There is not a significant addition of vesicles by lowering the cut off.

Furthermore on Figure 13 it is shown that if the lower cut of is set at 5 pixels rather than 15 the trend becomes saw-toothed and irregular, indicating that the size threshold has been reached and measurements become unreliable (Shea et al., 2010).

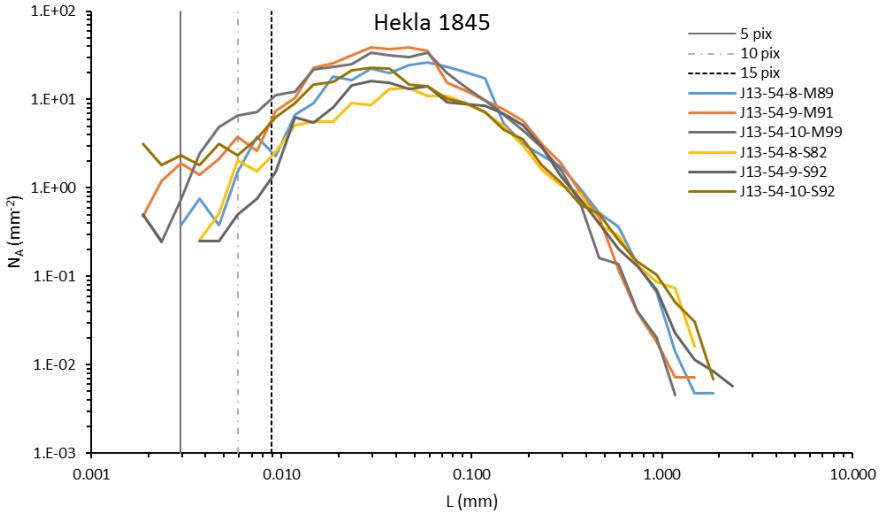

Figure 13: Diagram illustrating the different lower pixel cut-offs for each sample of the 1845 sample set. X-axis is the equivalent diameter and y-axis is the number of vesicles per area.

4.6 Total Grain-Size Distribution

Samples are collected to best represent the tephra fall deposit. The TGSD combines multiple grain-size analyses into one integrated distribution and does not reflect transportation, but rather the fragmentation and eruption style, and as such it can become an important parameter for classification of fall deposits (Houghton and Carey, 2015).

Methods that have been used to calculate TGSD are: unweighted averaging of all available grain-size analyses (Walker, 1981); average grain-size distribution of isopachs weighted with corresponding isopach volume percentage (Murrow et al., 1980); for the Askja 1875 deposit weighted grain-size data was integrated with the segmented isopach map of the deposit (Sparks et al., 1981); the tephra fall from the Mt. St. Helens eruption in 1980 was divided into 13 polygons and the total mass within each calculated and grain-size within each averaged (Carey and Sigurdsson, 1982). A more recent method, which has been used in this study, is the Voronoi Tesselation method (Bonadonna and Houghton, 2005). This method has been the most widely used in recent years (Andronico et al., 2014; Bonadonna et al., 2015a; Gjerløw et al., 2015), but the other techniques have not been totally abandoned, e.g. the approach of Murrow et al. (1980) was used to calculate the TGSD for the eruption in El Chichón in 1982 (Rose and Durant, 2009a), and the approach of Carey and Sigurdsson (1982) was used on the eruption of Mt. Spurr in 1992 (Durant and Rose, 2009). The Voronoi Tesselation method is a statistical method for spatial analysis. It partitions the plane so that each data point contains all locations closer to that point than to any other (e.g. Bonadonna and Houghton, 2005). Data needed for each point is grain-size distribution of the tephra and known mass per unit area. The TGSD is obtained as the area-weighted average of all Voronoi cells over the whole deposit. The advantage of the Voronoi Tesselation method over the others are e.g. no arbitrary selection of sectors of the analysed deposit. When data sets are non-uniform, it is statistically better than weighted averages of grain-size distributions (Bonadonna and Houghton, 2005), and it provides an automated platform to calculate TGSD (Biass and Bonadonna, 2014) which allows for comparison between different eruptions.

5 Present study

The present study adds on the available data sets on Icelandic explosive eruptions through: investigation of eruptive behaviour and transport of tephra from the 1991 Hekla eruption (paper 1); detailed study on eruptive processes of the 1845 Hekla eruption along with the characteristics, dimensions, and sedimentation patterns of the tephra fall deposit (paper 2); and a combined study of shallow conduit process of small to medium sized explosive events at Hekla (1991 and 1845 eruptions; paper 3).

The main objectives of the project are the following:

1. Investigate eruption mechanisms of small to medium size explosive eruptions at Hekla, Iceland by quantifying the processes that drive magma degassing and fragmentation.
2. Describe processes of tephra sedimentation and investigate mass contribution and distribution of fine particles in the tephra fall deposits.
3. Describe proceedings of explosive activity at Hekla to underpin understanding of these highly explosive and hazardous events.

5.1 Paper 1: The opening subplinian phase of the Hekla 1991 eruption: properties of the tephra fall deposit

5.1.1 Summary

The explosive nature of the opening phase of Hekla eruptions is of great importance, due to its immediate effect on the local environment and infrastructure. Hazards associated with Hekla eruptions are primarily sourced from the opening phase and a result of the ejected pyroclasts and subsequent tephra fall. Since the Hekla eruptive frequency increased after the 1970 eruption, the primary focus of studies on Hekla volcanism have been on course of events and eruption source parameters, such as mass eruption rate, volume, plume height (Grönvold et al., 1983; Gudmundsson et al., 1992; Höskuldsson et al., 2007; Thorarinsson and Sigvaldason, 1972a). The focus of the paper was therefore to add quantitative information on the nature of the 1991 tephra fall deposit, add details in terms of grain-size variations with transport and to produce a TGSD.

5.1.2 Main results

The opening phase of the 1991 Hekla eruption was a 50-minute-long explosive phase of subplinian intensity. Volume produced and deposited to the NNE of Hekla was 8.6×10^9 kg and 0.017 km^3 (0.003 km^3 DRE) of basaltic icelandite tephra with mean vesicularity of 77–79%. Grain-size analysis of the tephra fall deposit indicate early sedimentation of fine particles over the first 25 km. The general trend over the first 65 km of transport furthermore illustrate the gradual decrease in the plume capacity to carry pyroclasts, with effective size

fractionation up until 65 km from Hekla. From 65 km and onwards particle sedimentation transitioned from a turbulent to laminar regime, the deposited mass gradually decreases while sorting (σ_φ) and median diameter (Md_φ) are almost constant (Figure 14). The total grain-size distribution of the deposit calculated with 29 samples is bimodal. There is a primary coarse peak at -3.5 to -2.5 φ and a fine peak at 2.5 to 3.5 φ. The bimodality of the deposit is not attributed to secondary fragmentation in the conduit and/or eruption cloud. The bimodality is on the contrary attributed to the primary fragmentation of the magma in the shallow conduit.

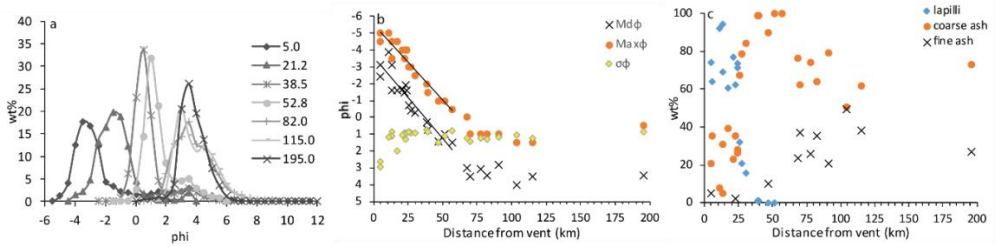

Figure 14: Grain-size variation with distance from vent in the 1991 tephra fall deposit. a) illustrates the changes in grain-size along the dispersal axis, b) illustrates the variation in maximum grain-size, median grain size and the sorting of the sample set versus distance from vent, and c) illustrates the different size components of the tephra fall deposit. Original figure is presented in paper 1.

5.2 Paper 2: The 1845 Hekla eruption: grain-size characteristics of a tephra layer

5.2.1 Summary

The opening phase from the 1845 Hekla eruption was the focus of paper 2. The 1845 eruption typifies the 1500–1970 activity at Hekla. The tephra fall deposits from this period have previously been mapped and the chronology of events compiled (Thorarinsson, 1968). Since the original mapping of the 1845 deposit, progress has been made on methods to calculate tephra volume (Bonadonna and Costa, 2012; Bonadonna and Houghton, 2005; Pyle, 1989) and estimate plume height (Mastin et al., 2009; Sparks et al., 1997). Recent work on historical Hekla eruptions has shown that a second look at the deposit results in comparable or larger volume estimates (Janebo et al., 2016b). Therefore the 1845 tephra fall deposit was remapped, volume and plume height estimated and total grain-size distribution calculated. This resulted in new estimates of the volume of the tephra fall deposit, provided basis for a second look at the duration of the opening phase and provided better estimates of the MER during the 1845 opening phase.

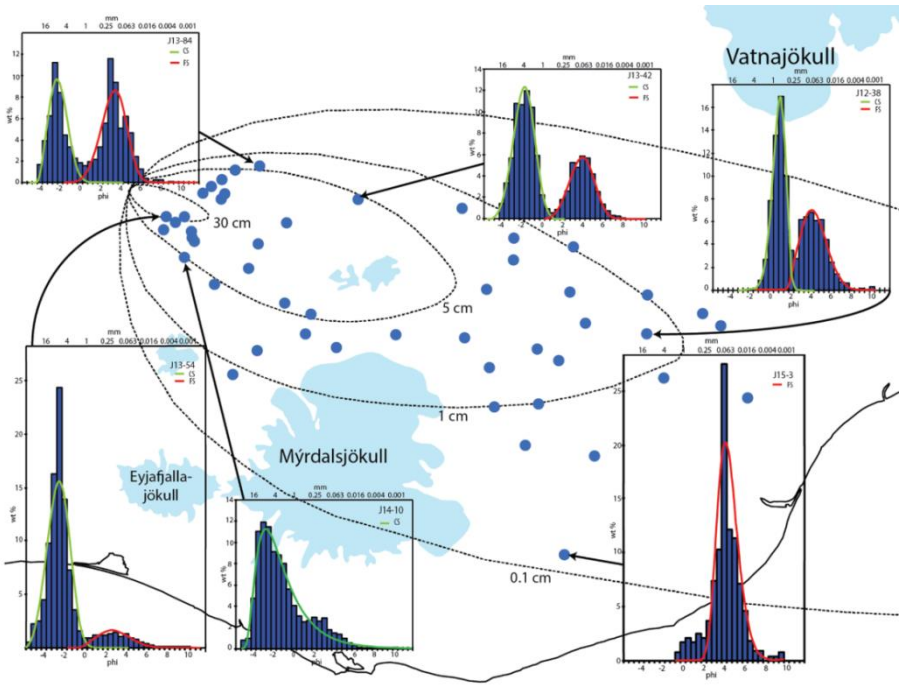

Figure 15: Examples of grain-size subpopulations in the 1845 tephra fall deposit. Samples are randomly selected for illustration. The two subpopulations were revealed through grain-size analysis. Original figure is presented in paper 2.

5.2.2 Main results

The 1845 opening phase started abruptly and peaked in intensity soon after onset. Tephra fall was to the ESE of Hekla over the highlands and towards the coastal regions. The volume of the 1845 tephra fall is estimated to be 0.13 km^3 (0.03 km^3 DRE) and 7.5 x 10^{10} kg. The duration of the opening phase was one hour long, and the time averaged plume height estimated 19 km a.s.l. The tephra was transported to locations in Iceland and to ships around the Faroe and Shetland islands, some 700 to 1100 km away with speed of 16–19 m s^{-1}. The tephra deposit is composed of two grain-size populations (coarse and fine subpopulations) that after deconvolution reveal systematic differences in sedimentation patterns (Figure 15). The coarse subpopulation depositional trends reveal gradual fining of the grain-size population as the carrying capacity of the volcanic plume decreases with distance from source (Figure 9). The fine subpopulation however, is not fractionated as strongly and reflects deposition by aggregation. The total grain-size distribution is bimodal with a dominating coarse mode at -2.5 φ and a subordinate fine mode at 3 to 4.5 φ.

5.3 Paper 3: The 1991 and 1845 eruptions at Hekla: Nature of the explosive opening phases inferred from vesicle volume distributions

5.3.1 Summary

The focus of the third paper was to quantify the processes in the shallow conduit, from vesiculation to fragmentation of the magma, during the 1991 and 1845 opening phases by applying microtextural analysis on the tephra and measure the vesicle population preserved in the erupted pumices. Two type locations were selected from the mapping of the tephra fall deposits presented in paper 1 and paper 2. Analytical methods and sample selection followed Shea et al. (2010). Systematic quantification of the vesiculation process has only been done on one Hekla eruption, the 1158 eruption (Janebo et al., 2016a). Paper 3 will therefore add valuable insight into the vesiculation and fragmentation process of small to medium sized explosive events at Hekla.

5.3.2 Main results

There is a temporal variation observed for the opening phase of both the 1991 and 1845 eruptions. However, there is a difference in the progression.

The 1991 opening phase is typified by two depositional units that range in vesicle number densities (VND) from the base to the top, illustrating the decreasing rate of each ascending magma batch with time. This is seen in the lower fall unit where VND changes with time from 2.3 to 1.5 x 10^4 mm^{-3}, similarly in the upper fall unit, the VND changes with time from 4.7 to 2.4 x 10^4 mm^{-3}. This is interpreted as: The lower fall unit represents the magma responsible for opening the conduit, during the ascent vesicles grew by coalescence and the magma vas affected by outgassing. The upper fall unit represents higher ascent rates and the most intense part of the 1991 opening phase.

The 1845 opening phase peaked in intensity soon after onset of the eruption, the intensity progressively decreased until the tephra production stopped. This is seen in drop in VND values from 4.15 to 1.92 x 10^4 mm^{-3} for the microvesicular (M) componentry group and from 2.77 to 1.51 x 10^4 mm^{-3} for the scoriaceous (S) componentry group. As the opening phase progressed and ascent rate decreased, increased velocity variance was observed across the conduit. The S group is interpreted as representing slower ascending magma along the conduit walls, and represents magma type that increased in proportions with time (Figure 16). The M group represents faster ascending magma in the centre of the conduit, that with decreasing intensity, decreases in proportion with time. Finally, is the high intensity of the 1991 and 1845 opening phases attributed to high ascend rates and coupled degassing of magmatic volatiles.

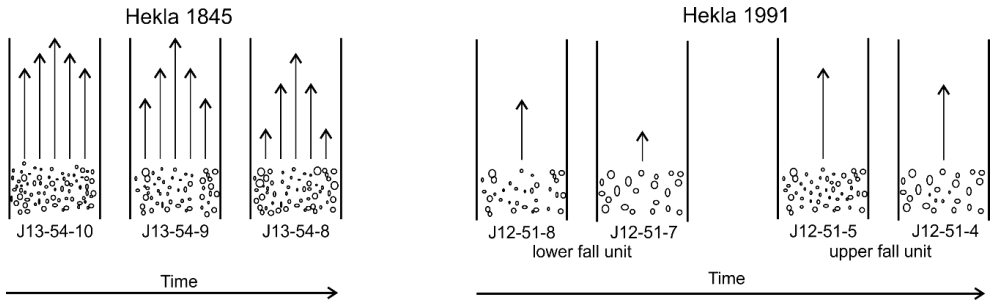

Figure 16: Schematic illustration of variance in ascend velocity with time during the opening phase of the 1991 and the 1845 eruptions. Arrows indicate relative speed of ascent, the multiple arrows for the 1845 conduit flow indicate cross conduit variance in speed. Variance in size of vesicles is used to indicate inferred larger vesicles along conduit walls. In the 1991 conduit model, the arrow length, number of vesicles and the vesicle size indicate inferred variance in ascent rate within each fall unit and between them. Original figure is presented in Paper 3.

5.4 General conclusions

Methods of mapping were successfully applied to the tephra fall deposits from the opening phases of the 1991 and 1845 Hekla eruptions. The 1845 tephra fall was constrained from 154 visited locations and mapped to mm accuracy. The tephra fall from the 1991 opening phase was remapped in the proximal region to supplement previously published isopach and isomass maps (Larsen et al., 1992). The tephra fall deposits were examined to evaluate the dispersal, sedimentation patterns, eruption source parameters, and fragmentation mechanisms.

The first sightings of the 1991 eruption plume on the 17 January indicate that gas was dominating the erupting material. Shortly after onset, the eruptive cloud became tephra laden (Þráinsson, 1991). In paper 1, it is concluded that the opening phase was pulsating, and the sedimentation patterns revealed two depositional units referred to as the upper and lower fall units. This pattern was not noticed during the eruption. The pulsating behaviour during the 1991 opening phase was further quantified in paper 3. Paper 3 demonstrates that the magma responsible for opening the conduit and deposited as the lower fall unit was affected by vesicle coalescence and outgassing. Slowed and/or stalled ascent during the opening of the conduit is the primary mechanism for decoupling the gas phase and resulting in patterns of outgassing as presented for the lower fall unit, as presented in paper 3. After the establishment of an open conduit, magma ascent became faster, resulting in higher vesicle number densities as recorded in the upper fall unit of the 1991 tephra (papers 1 and 3). The upper fall unit therefore represents material fragmented during the most intense pulse of the opening phase in Hekla 1991. The 50-minute-long opening phase had average mass eruption rate of 2.9×10^6 kg s^{-1} and produced tephra fall to the NNE (paper 1). Depositional patterns indicate size fractionation and decreasing turbulence over the first 65 km of transport, and as turbulence within the volcanic plume decreased sedimentation transitioned to a laminar regime. The grain-size distribution of the tephra fall deposit from the 1991 opening phase is bimodal, and the bimodality is attributed to the primary fragmentation.

The 1845 opening phase started abruptly with only few precursory earthquakes reported on the morning of 2 September (Erlendsson, 1847). In paper 3, the ascent dynamics are studied through vesicle size analysis. When the results are combined with the variation in grain-size

(paper 2), there are strong evidence for peak intensity of the 1845 opening phase early in the eruption. The intensity gradually decreased over the course of the 1 hour long explosive phase. At any given time, a velocity profile existed across the conduit, due to drag along conduit walls. With decreasing intensity, this variation increased. The magma flowing along the conduit walls had longer residence time and could evolve to a more mature bubble population. This variation finally lead to effective separation of the gas phase in the conduit, resulting in effusive rather than explosive activity as the 1845 transitioned into lava production. Tephra fall from the 1845 opening phase was to the ESE from a 19 km a.s.l. high eruption plume. The tephra fall deposit consists of two grain-size populations that reveal two different sedimentation mechanisms. The coarse subpopulation was sedimented by fractionation from the volcanic plume, making up the bulk of the fallout. The fine subpopulation aggregated in the volcanic plume, resulting in enhanced sedimentation of fine particles close to Hekla because of aggregation.

The grain-size distribution of the tephra fall deposit from both opening phases are bimodal. The cause for the bimodality is a result of the primary magma fragmentation. This is most likely due to pockets of contrasting permeability in the melt just prior to fragmentation. The coalescence in the pockets was more advanced, resulting in higher permeability and lower pressure difference and thus not preserving high enough pressure differentials at fragmentation and forming the dominant lapilli-sized populations. Where coalescence was not advanced, small bubbles remained unconnected and preserved high pressure differentials. This resulted in more intense fragmentation and formation of the ash-sized fraction of the deposit.

References

Andronico, D., Scollo, S., Lo Castro, M.D., Cristaldi, A., Lodato, L., Taddeucci, J., 2014. Eruption dynamics and tephra dispersal from the 24 November 2006 paroxysm at South-East Crater, Mt Etna, Italy. J. Volcanol. Geotherm. Res. 274, 78–91. doi:10.1016/j.jvolgeores.2014.01.009

Baker, D.R., Alletti, M., 2012. Fluid saturation and volatile partitioning between melts and hydrous fluids in crustal magmatic systems: The contribution of experimental measurements and solubility models. Earth-Science Rev. 114, 298–324. doi:doi.org/10.1016/j.earscirev.2012.06.005

Baker, D.R., Mancini, L., Polacci, M., Higgins, M.D., Gualda, G. a. R., Hill, R.J., Rivers, M.L., 2012. An introduction to the application of X-ray microtomography to the three-dimensional study of igneous rocks. Lithos 148, 262–276. doi:10.1016/j.lithos.2012.06.008

Behrens, H., Gaillard, F., 2007. Geochemical Aspects of Melts: Volatiles and Redox Behavior. Elements 2, 275 LP-280.

Biass, S., Bonadonna, C., 2014. TOTGS: Total grainsize distribution of tephra fallout.

Bjarnason, I.Þ., 2008. An Iceland hotspot saga. Jökull 3–16.

Björnsson, J., 1846. Fréttir frá Heklu. Úr Rangárvallasýslu. Ný Félagsrit VIII, 183–202.

Blake, S., 1984. Magma mixing and hybridization processes at the alkalic, silicic, Torfajökull central volcano triggered by tholeiitic Veidivötn fissuring, south Iceland. J. Volcanol. Geotherm. Res. 22, 1–31. doi:doi.org/10.1016/0377-0273(84)90033-7

Bonadonna, C., Cioni, R., Pistolesi, M., Elissondo, M., Baumann, V., 2015a. Sedimentation of long-lasting wind-affected volcanic plumes: the example of the 2011 rhyolitic Cordón Caulle eruption, Chile. Bull. Volcanol. 77, 13. doi:10.1007/s00445-015-0900-8

Bonadonna, C., Costa, A., 2012. Estimating the volume of tephra deposits: A new simple strategy. Geology 40, 415–418. doi:10.1130/G32769.1

Bonadonna, C., Costa, A., Folch, A., Koyaguchi, T., 2015b. Chapter 33 - Tephra Dispersal and Sedimentation, in: Sigurdsson, H. (Ed.), The Encyclopedia of Volcanoes (Second Edition). Academic Press, Amsterdam, pp. 587–597. doi:http://dx.doi.org/10.1016/B978-0-12-385938-9.00033-X

Bonadonna, C., Ernst, G.G.J., Sparks, R.S.J., 1998. Thickness variations and volume estimates of tephra fall deposits: the importance of particle Reynolds number. J. Volcanol. Geotherm. Res. 81, 173–187. doi:10.1016/S0377-0273(98)00007-9

Bonadonna, C., Genco, R., Gouhier, M., Pistolesi, M., Cioni, R., Alfano, F., Hoskuldsson, A., Ripepe, M., 2011. Tephra sedimentation during the 2010 Eyjafjallajkull eruption (Iceland) from deposit, radar, and satellite observations. J. Geophys. Res. Solid Earth 116. doi:10.1029/2011JB008462

Bonadonna, C., Houghton, B.F., 2005. Total grain-size distribution and volume of tephra-fall deposits. Bull. Volcanol. 67, 441–456. doi:10.1007/s00445-004-0386-2

Bonadonna, C., Phillips, J.C., 2003. Sedimentation from strong volcanic plumes. J. Geophys. Res. 108, 1–28. doi:10.1029/2002JB002034

Bonadonna, C., Phillips, J.C., Houghton, B.F., 2005. Modeling tephra sedimentation from a Ruapehu weak plume eruption 110, 1–22. doi:10.1029/2004JB003515

Brown, R.J., Bonadonna, C., Durant, A.J., 2012. A review of volcanic ash aggregation. Phys.

Chem. Earth, Parts A/B/C 45–46, 65–78. doi:doi.org/10.1016/j.pce.2011.11.001
Bursik, M.I., Sparks, R.S.J., Gilbert, J.S., Carey, S.N., 1992. Sedimentation of tephra by volcanic plumes: I. Theory and its comparison with a study of the Fogo A plinian deposit, Sao Miguel (Azores). Bull. Volcanol. 54, 329–344.
Carey, R.J., Houghton, B.F., Thordarson, T., 2009a. Tephra dispersal and eruption dynamics of wet and dry phases of the 1875 eruption of Askja Volcano, Iceland. Bull. Volcanol. 72, 259–278. doi:10.1007/s00445-009-0317-3
Carey, R.J., Houghton, B.F., Thordarson, T., 2009b. Abrupt shifts between wet and dry phases of the 1875 eruption of Askja Volcano: Microscopic evidence for macroscopic dynamics. J. Volcanol. Geotherm. Res. 184, 256–270. doi:10.1016/j.jvolgeores.2009.04.003
Carey, R.J., Houghton, B.F., Thordarson, T., 2008. Contrasting styles of welding observed in the proximal Askja 1875 eruption deposits I: Regional welding. J. Volcanol. Geotherm. Res. 171, 1–19. doi:10.1016/j.jvolgeores.2007.11.020
Carey, S., Sigurdsson, H., 1989. The intensity of plinian eruptions. Bull. Volcanol. 51, 28–40. doi:10.1007/BF01086759
Carey, S., Sparks, R.S.J., 1986. Quantitative models of the fallout and dispersal of tephra from volcanic eruption columns. Bull. Volcanol. 48, 109–125.
Carey, S.N., Sigurdsson, H., 1982. Influence of particle aggregation on deposition of distal tephra from the MAy 18, 1980, eruption of Mount St. Helens volcano. J. Geophys. Res. Solid Earth 87, 7061–7072. doi:10.1029/JB087iB08p07061
Cashman, K. V, 2004. Volatile Controls on Magma Ascent and Eruption. State Planet Front. Challenges Geophys. Geophys. 19, 109–124. doi:10.1029/150gm10
Cashman, K. V, 1992. Groundmass crystallization of Mount St. Helens dacite, 1980–1986: a tool for interpreting shallow magmatic processes. Contrib. to Mineral. Petrol. 109, 431–449. doi:10.1007/BF00306547
Criswell, C.W., 1987. Chronology and pyroclastic stratigraphy of the May 18, 1980, Eruption of Mount St. Helens, Washington. J. Geophys. Res. Solid Earth 92, 10237–10266. doi:10.1029/JB092iB10p10237
Dingwell, D.B., 1996. Volcanic dilemma: Flow or blow? Science (80-.). 273, 1054.
Dugmore, A.J., Larsen, G., Newton, A.J., 1995. Seven tephra isochrones in Scotland. The Holocene 5, 257–266. doi:10.1177/095968369500500301
Durant, A.J., Rose, W.I., 2009. Sedimentological constraints on hydrometeor-enhanced particle deposition: 1992 Eruptions of Crater Peak, Alaska. J. Volcanol. Geotherm. Res. 186, 40–59. doi:10.1016/j.jvolgeores.2009.02.004
Eichelberger, J.C., 1995. Silicic Volcanism: Ascent of Viscous Magmas from Crustal Reservoirs. Annu. Rev. Earth Planet. Sci. 23, 41–63. doi:10.1146/annurev.ea.23.050195.000353
Einarsson, P., 2008. Plate boundaries, rifts and transforms in Iceland. Jökull 58, 35–58.
Einarsson, P., 1991. Earthquakes and present-day tectonism in Iceland. Tectonophysics 189, 261–279. doi:10.1016/0040-1951(91)90501-I
Einarsson, P., Eiríksson, J., 1982. Earthquake fractures in the districts Land and Rangárvellir in the South Iceland Seismic Zone. Jökull 32, 113–120.
Engwell, S.L., Sparks, R.S.J., Carey, S., 2014. Physical characteristics of tephra layers in the deep sea realm : the Campanian Ignimbrite eruption, in: Austin, W.E.N., Abbott, P.M., Davies, S.M., Pearce, N.J.G., Wastegård, S. (Eds.), Marine Tephrochronology. Geological Society, London, Special Publications. London, pp. 47–64.
Erlendsson, O., 1847. Dagskrá um Heklugosið 1845-6 og afleiðingar þess, in: Ólafsson, E. (Ed.), Fjölrit Náttúrufræðistofnunar 3. H. Jóhannesson Prepared for Publication. Iceland Institute of Natural History, Reykjavík (Garðabær) 1986.
Eychenne, J., Cashman, K., Rust, A., Durant, A., 2015. Impact of the lateral blast on the

spatial pattern and grain size characteristics of the 18 May 1980 Mount St. Helens fallout deposit. J. Geophys. Res. Solid Earth 120, 6018–6038. doi:10.1002/2015JB012116

Eychenne, J., Pennec, J.-L., 2012. Sigmoidal particle density distribution in a subplinian scoria fall deposit. Bull. Volcanol. 74, 2243–2249. doi:10.1007/s00445-012-0671-4

Fierstein, J., Nathenson, M., 1992. Another look at the calculation of fallout tephra volumes. Bull. Volcanol. 54, 156–167. doi:10.1007/BF00278005

Folk, R.L., Ward, W.C., 1957. Brazos River Bar: A study in the significance of Grain Size Parameters. J. Sediment. Petrol. 27, 3–26.

Geirsson, H., Árnadóttir, T., Völksen, C., Jiang, W., Sturkell, E., Villemin, T., Einarsson, P., Sigmundsson, F., Stefánsson, R., 2006. Current plate movements across the Mid-Atlantic Ridge determined from 5 years of continuous GPS measurements in Iceland. J. Geophys. Res. Solid Earth 111, n/a-n/a. doi:10.1029/2005JB003717

Gjerløw, E., Höskuldsson, A., Pedersen, R.-B., 2015. The 1732 Surtseyan eruption of Eggøya, Jan Mayen, North Atlantic: deposits, distribution, chemistry and chronology. Bull. Volcanol. 77, 14. doi:10.1007/s00445-014-0895-6

Gonnermann, H.M., 2015. Magma fragmentation. Annu. Rev. Earth Planet. Sci. 43, 1–28.

Gonnermann, H.M., Manga, M., 2007. The Fluid Mechanics Inside a Volcano. Annu. Rev. Fluid Mech. 39, 321–356. doi:10.1146/annurev.fluid.39.050905.110207

Grönvold, K., Larsen, G., Einarsson, P., Thorarinsson, S., Saemundsson, K., 1983. The Hekla Eruption 1980-1981. Bull. Volcanol. 46, 349–363.

Gudmundsdottir, E., Larsen, G., Bj, S., Striberger, J., 2016. A new high-resolution Holocene tephra stratigraphy in eastern Iceland : Improving the Icelandic and North Atlantic tephrochronology. Quat. Sci. Rev. 150, 234–249. doi:10.1016/j.quascirev.2016.08.011

Gudmundsdóttir, E.H., Larsen, G., Eiríksson, J., 2011. Two new Icelandic tephra markers: The Hekla Ö tephra layer, 6060 cal. yr BP, and Hekla DH tephra layer, ~6650 cal. yr BP. Land-sea correlation of mid-Holocene tephra markers. The Holocene 21, 629–639. doi:10.1177/0959683610391313

Gudmundsson, A., 2012. Magma chambers: Formation, local stresses, excess pressures, and compartments. J. Volcanol. Geotherm. Res. 237–238, 19–41. doi:doi.org/10.1016/j.jvolgeores.2012.05.015

Gudmundsson, A., Oskarsson, N., Grönvold, K., Saemundsson, K., Sigurdsson, O., Stefansson, R., Gislason, S.R., Einarsson, P., Brandsdottir, B., Larsen, G., Johannesson, H., Thordarson, T., 1992. The 1991 eruption of Hekla, Iceland. Bull. Volcanol. 54, 238–246. doi:10.1007/BF00278391

Gudmundsson, A., Sæmundsson, K., 1992. Heklugosið 1991 : Gangur gossins og aflfræði Heklu 145–158.

Gudmundsson, M.T., Högnadóttir, T., 2007. Volcanic systems and calderas in the Vatnajökull region, central Iceland: Constraints on crustal structure from gravity data. J. Geodyn. 43, 153–169. doi:10.1016/j.jog.2006.09.015

Gudmundsson, M.T., Jónsdóttir, K., Hooper, A., Holohan, E.P., Halldórsson, S.A., Ófeigsson, B.G., Cesca, S., Vogfjörd, K.S., Sigmundsson, F., Högnadóttir, T., Einarsson, P., Sigmarsson, O., Jarosch, A.H., Jónasson, K., Magnússon, E., Hreinsdóttir, S., Bagnardi, M., Parks, M.M., Hjörleifsdóttir, V., Pálsson, F., Walter, T.R., Schöpfer, M.P.J., Heimann, S., Reynolds, H.I., Dumont, S., Bali, E., Gudfinnsson, G.H., Dahm, T., Roberts, M.J., Hensch, M., Belart, J.M.C., Spaans, K., Jakobsson, S., Gudmundsson, G.B., Fridriksdóttir, H.M., Drouin, V., Dürig, T., A\dhalgeirsdóttir, G., Riishuus, M.S., Pedersen, G.B.M., van Boeckel, T., Oddsson, B., Pfeffer, M.A., Barsotti, S., Bergsson, B., Donovan, A., Burton, M.R., Aiuppa, A., 2016. Gradual caldera collapse at Bárdarbunga volcano, Iceland, regulated by lateral magma outflow. Science (80-.). 353. doi:10.1126/science.aaf8988

Gudmundsson, M.T., Sigmundsson, F., Bjornsson, H., 1997. Ice-volcano interaction of the 1996 Gjalp subglacial eruption, Vatnajokull, Iceland. Nature 389, 954–957.

Gudmundsson, M.T., Sigmundsson, F., Björnsson, H., Högnadóttir, T., 2004. The 1996 eruption at Gjálp, Vatnajökull ice cap, Iceland: efficiency of heat transfer, ice deformation and subglacial water pressure. Bull. Volcanol. 66, 46–65. doi:10.1007/s00445-003-0295-9

Gudmundsson, M.T., Thordarson, T., Höskuldsson, Á., Larsen, G., Björnsson, H., Prata, F.J., Oddsson, B., Magnússon, E., Högnadóttir, T., Petersen, G.N., Hayward, C.L., Stevenson, J.A., Jónsdóttir, I., 2012. Ash generation and distribution from the April-May 2010 eruption of Eyjafjallajökull, Iceland. Sci. Rep. 2, 1–12. doi:10.1038/srep00572

Gudnason, J., Thordarson, T., Houghton, B.F., Larsen, G., 2017. The opening subplinian phase of the Hekla 1991 eruption: properties of the tephra fall deposit. Bull. Volcanol. 79. doi:10.1007/s00445-017-1118-8

Gurioli, L., Harris, A.J.L., Houghton, B.F., Polacci, M., Ripepe, M., 2008. Textural and geophysical characterization of explosive basaltic activity at Villarrica volcano 113, 1–16. doi:10.1029/2007JB005328

Horwell, C.J., Baxter, P.J., 2006. The respiratory health hazards of volcanic ash : a review for volcanic risk mitigation. Bull. Volcanol. 69, 1–24. doi:10.1007/s00445-006-0052-y

Höskuldsson, Á., Óskarsson, N., Pedersen, R., Grönvold, K., Vogfjörð, K., Ólafsdóttir, R., 2007. The millennium eruption of Hekla in February 2000. Bull. Volcanol. 70, 169–182. doi:10.1007/s00445-007-0128-3

Houghton, B., Carey, R.J., 2015. Chapter 34 - Pyroclastic Fall Deposits, in: Sigurdsson, H. (Ed.), The Encyclopedia of Volcanoes (Second Edition). Academic Press, Amsterdam, pp. 599–616. doi:doi.org/10.1016/B978-0-12-385938-9.00034-1

Houghton, B.F., Carey, R.J., Cashman, K. V., Wilson, C.J.N., Hobden, B.J., Hammer, J.E., 2010. Diverse patterns of ascent, degassing, and eruption of rhyolite magma during the 1.8ka Taupo eruption, New Zealand: Evidence from clast vesicularity. J. Volcanol. Geotherm. Res. 195, 31–47. doi:10.1016/j.jvolgeores.2010.06.002

Houghton, B.F., Gonnermann, H.M., 2008. Basaltic explosive volcanism: Constraints from deposits and models. Chemie der Erde - Geochemistry 68, 117–140. doi:10.1016/j.chemer.2008.04.002

Houghton, B.F., Wilson, C.J.N., 1989. A vesicularity index for pyroclastic deposits. Bull. Volcanol. 51, 451–462.

Houghton, B.F., Wilson, C.J.N., Fierstein, J., Hildreth, W., 2004. Complex proximal deposition during the Plinian eruptions of 1912 at Novarupta, Alaska. Bull. Volcanol. 66, 95–133. doi:10.1007/s00445-003-0297-7

Hreinsdóttir, S., Sigmundsson, F., Roberts, M.J., Björnsson, H., Grapenthin, R., Arason, P., Árnadóttir, T., Hólmjárn, J., Geirsson, H., Bennett, R.A., Gudmundsson, M.T., Oddsson, B., Ófeigsson, B.G., Villemin, T., Jónsson, T., Sturkell, E., Höskuldsson, Á., Larsen, G., Thordarson, T., Óladóttir, B.A., 2014. Volcanic plume height correlated with magma- pressure change at Grímsvötn Volcano , Iceland. Nat. Geosci. 7, 1–5. doi:10.1038/ngeo2044

Jakobsson, S., 1979. Petrology of recent basalts of the Eastern Volcanic Zone, Iceland. Acta Nat. Islandica 26.

Jakobsson, S.P., Jónasson, K., Sigurðsson, I. a., 2008. The three igneous rock series of Iceland. Jökull 58, 117–138.

Janebo, M.H., 2016. Historical explosive eruptions in Hekla and Askja Volcanoes; eruption dynamics and source paramters. University of Hawaii at Manoa.

Janebo, M.H., Houghton, B.F., Thordarson, T., Larsen, G., 2016a. Shallow conduit processes during the AD 1158 explosive eruption of Hekla volcano , Iceland. Bull. Volcanol. 78.

doi:10.1007/s00445-016-1070-z
Janebo, M.H., Thordarson, T., Houghton, B.F., Bonadonna, C., Larsen, G., Carey, R.J., 2016b. Dispersal of key subplinian – Plinian tephras from Hekla volcano , Iceland : implications for eruption source parameters. Bull. Volcanol. 78. doi:10.1007/s00445-016-1059-7
Jarosewich, E., Nelen, J.A., Norberg, J.A., 1980. Reference Samples for Electron Microprobe Analysis. Geostand. Newsl. 4, 43–47. doi:10.1111/j.1751-908X.1980.tb00273.x
Jóhannesson, H., Einarsson, S., 1990. Glefsur úr sögu hrauna og jarðvegs sunnan Heklu., in: Arnalds, A. (Ed.), Græðum Ísland. Landgræðslan, Reykjavik, pp. 123–136.
Jóhannesson, H., Sæmundsson, K., 1998. Geological map of Iceland, 1:500.000 Bedrock Geology. Reykjavik.
Jude-Eton, T.C., Thordarson, T., Gudmundsson, M.T., Oddsson, B., 2012. Dynamics, stratigraphy and proximal dispersal of supraglacial tephra during the ice-confined 2004 eruption at Grímsvötn Volcano, Iceland. Bull. Volcanol. 74, 1057–1082. doi:10.1007/s00445-012-0583-3
Kaminski, E., Jaupart, C., 1998. The size distribution of pyroclasts and the fragmentation sequence in explosive volcanic eruptions. J. Geophys. Res. 103, 29759–29779.
Kjartansson, E., Grönvold, K., 1983. Location of a magma reservoir beneath Hekla Volcano, Iceland. Nature 301, 139–141.
Klug, C., Cashman, K., Bacon, C., 2002. Structure and physical characteristics of pumice from the climactic eruption of Mount Mazama (Crater Lake), Oregon. Bull. Volcanol. 64, 486–501. doi:10.1007/s00445-002-0230-5
Klug, C., Cashman, K.V., 1996. Permeability development in vesiculating magmas : implications for fragmentation. Bull. Volcanol. 58, 87–100.
Klug, C., Cashman, K. V, 1994. Vesiculation of May 18, 1980, Mount St. Helens magma. Geology 22, 468–472.
Larsen, G., 2010. 3 Katla: Tephrochronology and Eruption History. Dev. Quat. Sci. 13, 23–49. doi:10.1016/S1571-0866(09)01303-7
Larsen, G., 2002. A brief overview of eruptions from ice-covered and ice-capped volcanic systems in Iceland during the past 11 centuries: frequency, periodicity and implications, in: Smellie, J.L., Chapman, M.G. (Eds.), Volcano-Ice Interaction on Earth and Mars. Geological Society, Special publication, London, pp. 81–90.
Larsen, G., 2000. Holocene eruptions within the Katla volcanic system, south Iceland: Characteristics and environmental impact. Jökull 49, 1–28.
Larsen, G., 1984. Recent volcanic history of the veidivötn fissure swarm, southern Iceland - An approach to volcanic risk assessment. J. Volcanol. Geotherm. Res. 22, 33–58.
Larsen, G., Dugmore, A., Newton, A., Larsen, G., 2013. The Holocene Geochemistry of historical-age silicic tephras in Iceland. doi:10.1191/095968399669624108
Larsen, G., Dugmore, a., Newton, a., 1999. Geochemistry of historical-age silicic tephras in Iceland. The Holocene 9, 463–471. doi:10.1191/095968399669624108
Larsen, G., Eiríksson, J., 2008. Late Quaternary terrestrial tephrochronology of Iceland-frequency of explosive eruptions, type and volume of tephra deposits. J. Quat. Sci. 23, 109–120.
Larsen, G., Gronvold, K., Thorarinsson, S., 1979. Volcanic eruption through a geothermal borehole at Namafjall, Iceland. Nature 278, 707–710.
Larsen, G., Sverrisdóttir, G., Jóhannesson, H., Hjartarson, Á., Einarsson, P., 2013. Hekla, in: Sólnes, J., Sigmundsson, F., Bessason, B. (Eds.), Náttúrvá Á Íslandi - Eldgos Og Jarðskjálftar. Viðlagatrygging/Háskólaútgáfan, Reykjavík, pp. 189–210.
Larsen, G., Thorarinsson, S., 1977. H4 and other acid Hekla tephra layers. Jökull 27, 28–46.
Larsen, G., Vilmundardóttir, E.G., 1992. Tvílit Gjóskulög austan Heklu: H-x, H-y og H-z.,

in: Veggspjaldaráðstefna, Jarðfræðafélags Íslands. pp. 27–29.
Larsen, G., Vilmundardóttir, E.G., Thorkelsson, B., 1992. Heklugosið 1991 : Gjóskufallið og gjóskulagið frá fyrsta degi gossins. Náttúrufræðingurinn 61, 159–176.
Mangan, M.T., Sisson, T.W., Hankins, W.B., 2004. Decompression experiments identify kinetic controls on explosive silicic eruptions. Geophys. Res. Lett. 31, 1–5. doi:10.1029/2004GL019509
Manzella, I., Bonadonna, C., Phillips, J.C., Monnard, H., 2015. The role of gravitational instabilities in deposition of volcanic ash. Geology 43, 211–214. doi:10.1130/G36252.1
Marsh, B.D., 2015. Chapter 8 - Magma Chambers, in: Sigurdsson, H. (Ed.), The Encyclopedia of Volcanoes (Second Edition). Academic Press, Amsterdam, pp. 185–201. doi:doi.org/10.1016/B978-0-12-385938-9.00008-0
Mastin, L.G.G., Guffanti, M., Servranckx, R., Webley, P., Barsotti, S., Dean, K., Durant, a., Ewert, J.W.W., Neri, a., Rose, W.I.I., Schneider, D., Siebert, L., Stunder, B., Swanson, G., Tupper, a., Volentik, a., Waythomas, C.F.F., 2009. A multidisciplinary effort to assign realistic source parameters to models of volcanic ash-cloud transport and dispersion during eruptions. J. Volcanol. Geotherm. Res. 186, 10–21. doi:10.1016/j.jvolgeores.2009.01.008
McBirney, A.R., Murase, T., 1970. Factors governing the formation of pyroclastic rocks. Bull. Volcanol. 34, 372–384. doi:10.1007/BF02596762
Melnik, O., 2000. Dynamics of two-phase conduit flow of high-viscosity gas-saturated magma: large variations of sustained explosive eruption intensity. Bull. Volcanol. 62, 153–170. doi:10.1007/s004450000072
Melnik, O., Barmin, A.A., Sparks, R.S.J., 2005. Dynamics of magma flow inside volcanic conduits with bubble overpressure buildup and gas loss through permeable magma. J. Volcanol. Geotherm. Res. 143, 53–68. doi:doi.org/10.1016/j.jvolgeores.2004.09.010
Melsted, P., 1846. Fréttir frá Heklu. Ný Félagsrit 6, 202–210.
Métrich, N., Wallace, P.J., 2008. Volatile Abundances in Basaltic Magmas and Their Degassing Paths Tracked by Melt Inclusions. Rev. Mineral. Geochemistry 69, 363 LP-402.
Moore, J.G., 1985. Structure and eruptive mechanisms at Surtsey Volcano, Iceland. Geol. Mag. 122, 649–661. doi:DOI: 10.1017/S0016756800032052
Mourtada-Bonnefoi, C.C., Laporte, D., 2004. Kinetics of bubble nucleation in a rhyolitic melt: An experimental study of the effect of ascent rate. Earth Planet. Sci. Lett. 218, 521–537. doi:10.1016/S0012-821X(03)00684-8
Mourtada-Bonnefoi, C.C., Laporte, D., 2002. Homogeneous bubble nucleation in rhyolitic magmas: An experimental study of the effect of H2O and CO2. J. Geophys. Res. Solid Earth 107. doi:10.1029/2001JB000290
Mourtada-Bonnefoi, C.C., Laporte, D., 1999. Experimental study of homogeneous bubble nucleation in rhyolitic magmas. Geophys. Res. Lett. 26, 3505–3508. doi:10.1029/1999GL008368
Murrow, P.J., Rose, W.I., Self, S., 1980. Determination of the total grain size distribution in a Vulcanian eruption column, and its implications to stratospheric aerosol perturbation. Geophys. Res. Lett. 7, 893–896. doi:10.1029/GL007i011p00893
Oddsson, B., Gudmundsson, M.T., Larsen, G., Karlsdóttir, S., 2012. Monitoring of the plume from the basaltic phreatomagmatic 2004 Grímsvötn eruption-application of weather radar and comparison with plume models. Bull. Volcanol. 74, 1395–1407. doi:10.1007/s00445-012-0598-9
Ofeigsson, B.G., Hooper, A., Sigmundsson, F., Sturkell, E., Grapenthin, R., 2011. Deep magma storage at Hekla volcano, Iceland, revealed by InSAR time series analysis. J. Geophys. Res. Solid Earth 116, 1–15. doi:10.1029/2010JB007576

Óladóttir, B.., Larsen, G., Sigmarsson, O., 2011. Holocene volcanic activity at Grímsvötn, Bárdarbunga and Kverkfjöll subglacial centres beneath Vatnajökull, Iceland. Bull. Volcanol. 73, 1187–1208. doi:10.1007/s00445-011-0461-4

Óladóttir, B.A., Sigmarsson, O., Larsen, G., Thordarson, T., Oladóttir, B.A., Sigmarsson, O., Larsen, G., Thordarson, T., 2008. Katla volcano, Iceland: Magma composition, dynamics and eruption frequency as recorded by Holocene tephra layers. Bull. Volcanol. 70, 475–493. doi:10.1007/s00445-007-0150-5

Óladóttir, B.A., Thordarson, T., Larsen, G., Sigmarsson, O., 2007. Survival of the Mýrdalsjökull ice cap through the Holocene thermal maximum: Evidence from sulphur contents in Katla tephra layers (Iceland) from the last 8400 years. Ann. Glaciol. 45, 183–188. doi:10.3189/172756407782282516

Papale, P., 1999. Strain-induced magma fragmentation in explosive eruptions. Nature 397, 425–428. doi:10.1038/17109

Papale, P., Neri, A., Macedonio, G., 1998. The role of magma composition and water content in explosive eruptions 1 . Conduit ascent dynamics. J. Volcanol. Geotherm. Res. 87, 75–93.

Parcheta, C.E., Houghton, B.F., Swanson, D. a., 2013. Contrasting patterns of vesiculation in low, intermediate, and high Hawaiian fountains: A case study of the 1969 Mauna Ulu eruption. J. Volcanol. Geotherm. Res. 255, 79–89. doi:10.1016/j.jvolgeores.2013.01.016

Parfitt, E. a, 2004. A discussion of the mechanisms of explosive basaltic eruptions. J. Volcanol. Geotherm. Res. 134, 77–107. doi:10.1016/j.jvolgeores.2004.01.002

Pedersen, G.B.M., Höskuldsson, A., Dürig, T., Thordarson, T., Jónsdóttir, I., Riishuus, M.S., Óskarsson, B.V., Dumont, S., Magnusson, E., Gudmundsson, M.T., Sigmundsson, F., Drouin, V.J.P.B., Gallagher, C., Askew, R., Guðnason, J., Moreland, W.M., Nikkola, P., Reynolds, H.I., Schmith, J., 2017. Lava field evolution and emplacement dynamics of the 2014–2015 basaltic fissure eruption at Holuhraun, Iceland. J. Volcanol. Geotherm. Res. doi:10.1016/j.jvolgeores.2017.02.027

Polacci, M., Baker, D.R., Bai, L., Mancini, L., 2008. Large vesicles record pathways of degassing at basaltic volcanoes. Bull. Volcanol. 70, 1023–1029. doi:10.1007/s00445-007-0184-8

Proussevitch, A.A., Sahagian, D.L., 1996. Dynamics of coupled diffusive and decompressive bubble growth in magmatic systems. J. Geophys. Res. Solid Earth 101, 17447–17455. doi:10.1029/96JB01342

Pyle, D.M., 1989. The thickness, volume and grainsize of tephra fall deposits. Bull. Volcanol. 51, 1–15.

Róbertsdóttir, B.G., 1992. Þrjú forsöguleg gjóskulög frá Heklu, HA, HB og HC, in: Veggspjaldaráðstefna, Jarðfræðafélags Íslands1. pp. 5–7.

Rose, W.I., Durant, A.J., 2011. Fate of volcanic ash: Aggregation and fallout. Geology 39, 895–896. doi:10.1130/focus092011.1

Rose, W.I., Durant, A.J., 2009a. El Chichón volcano, April 4, 1982: volcanic cloud history and fine ash fallout. Nat. Hazards 51, 363–374. doi:10.1007/s11069-008-9283-x

Rose, W.I., Durant, a. J., 2009b. Fine ash content of explosive eruptions. J. Volcanol. Geotherm. Res. 186, 32–39. doi:10.1016/j.jvolgeores.2009.01.010

Rust, a. C., Cashman, K. V., 2004. Permeability of vesicular silicic magma: Inertial and hysteresis effects. Earth Planet. Sci. Lett. 228, 93–107. doi:10.1016/j.epsl.2004.09.025

Sable, J.E., Houghton, B.F., Del Carlo, P., Coltelli, M., 2006. Changing conditions of magma ascent and fragmentation during the Etna 122 BC basaltic Plinian eruption: Evidence from clast microtextures. J. Volcanol. Geotherm. Res. 158, 333–354. doi:10.1016/j.jvolgeores.2006.07.006

Sæmundsson, K., 1991. Jarðfræði Kröflukerfisins, in: Garðarsson, A., Einarsson, Á. (Eds.),

Náttúra Mývatns. Hið íslenska náttúrufræðifélag, Reykjavík, pp. 25–95.
Sæmundsson, K., 1979. Outline of the geology of Iceland. Jökull 29, 7–32.
Sahagian, D.L., Proussevitch, A.A., 1998. 3D particle size distributions from 2D observations: stereology for natural applications. J. Volcanol. Geotherm. Res. 84, 173–196. doi:10.1016/S0377-0273(98)00043-2
Schneider, C.., Rasband, W.., Eliceiri, K.., 2012. NIH Image to ImageJ: 25 years of image analysis. Nat. Methods 9, 671–675.
Schythe, J.C., 1847. Hekla og dens sidste Udbrud, den 2den September 1845. København.
Sella, G.F., Dixon, T.H., Mao, A., 2002. REVEL: A model for Recent plate velocities from space geodesy. J. Geophys. Res. Solid Earth 107, ETG 11-1-ETG 11-30. doi:10.1029/2000JB000033
Sharma, K., Self, S., Blake, S., Thordarson, T., Larsen, G., 2008. The AD 1362 Öræfajökull eruption, S.E. Iceland: Physical volcanology and volatile release. J. Volcanol. Geotherm. Res. 178, 719–739. doi:10.1016/j.jvolgeores.2008.08.003
Shea, T., Houghton, B.F., Gurioli, L., Cashman, K. V., Hammer, J.E., Hobden, B.J., 2010. Textural studies of vesicles in volcanic rocks: An integrated methodology. J. Volcanol. Geotherm. Res. 190, 271–289. doi:10.1016/j.jvolgeores.2009.12.003
Sigmarsson, O., Condomines, M., Fourcade, S., 1992. A detailed Th, Sr and O isotope study of Hekla: differentiation processes in an Icelandic Volcano. Contrib. to Mineral. Petrol.
Sigmundsson, F., Einarsson, P., Bilham, R., 1992. Magma chamber deflation recorded by the global positioning system: The Hekla 1991 Eruption. Geophys. Res. Lett. 19, 1483–1486. doi:10.1029/92GL01636
Sigmundsson, F., Hooper, A., Hreinsdottir, S., Vogfjord, K.S., Ofeigsson, B.G., Heimisson, E.R., Dumont, S., Parks, M., Spaans, K., Gudmundsson, G.B., Drouin, V., Arnadottir, T., Jonsdottir, K., Gudmundsson, M.T., Hognadottir, T., Fridriksdottir, H.M., Hensch, M., Einarsson, P., Magnusson, E., Samsonov, S., Brandsdottir, B., White, R.S., Agustsdottir, T., Greenfield, T., Green, R.G., Hjartardottir, A.R., Pedersen, R., Bennett, R.A., Geirsson, H., La Femina, P.C., Bjornsson, H., Palsson, F., Sturkell, E., Bean, C.J., Mollhoff, M., Braiden, A.K., Eibl, E.P.S., 2015. Segmented lateral dyke growth in a rifting event at Bárðarbunga volcanic system, Iceland. Nature 517, 191–195.
Sigmundsson, F., Hreinsdottir, S., Hooper, A., Arnadottir, T., Pedersen, R., Roberts, M.J., Oskarsson, N., Auriac, A., Decriem, J., Einarsson, P., Geirsson, H., Hensch, M., Ofeigsson, B.G., Sturkell, E., Sveinbjornsson, H., Feigl, K.L., 2010. Intrusion triggering of the 2010 Eyjafjallajokull explosive eruption. Nature 468, 426–430.
Soosalu, H., Einarsson, P., 2004. Seismic constraints on magma chambers at Hekla and Torfajökull volcanoes, Iceland. Bull. Volcanol. 66, 276–286. doi:10.1007/s00445-003-0310-1
Soosalu, H., Einarsson, P., Jakobsdottir, S., 2003. Volcanic tremor related to the 1991 eruption of the Hekla volcano, Iceland. Bull. Volcanol. 65, 562–577. doi:10.1007/s00445-003-0285-y
Soosalu, H., Einarsson, P., Þorbjarnardóttir, B., 2005. Seismic activity related to the 2000 eruption of the Hekla volcano, Iceland. Bull. Volcanol. 68, 21–36. doi:10.1007/s00445-005-0417-7
Sparks, R., Wilson, L., Sigurdsson, H., 1981. The pyroclastic deposits of the 1875 eruption of Askja, Iceland. Phil Trans R Soc L. 229, 241–273.
Sparks, R.S.J., 1978. The dynamics of bubble formation and growth in magmas: A review and analysis. J. Volcanol. Geotherm. Res. 3, 1–37. doi:doi.org/10.1016/0377-0273(78)90002-1
Sparks, R.S.J., Bursik, M.I., Ablay, G.J., Thomas, R.M.E., Carey, S.N., 1992. Sedimentation of tephra by volcanic plumes. Part 2: controls on thickness and grain-size variations of

tephra deposits. Bull. Volcanol. 54, 685–695.
Sparks, R.S.J., Bursik, M.I., Carey, S.N., Gilbert, J.S., Glaze, L.S., Sigurdsson, H., Woods, A.W., 1997. Volcanic Plumes, 1st ed. John Wiley & Sons, Chichester.
Spieler, O., Kennedy, B., Kueppers, U., Dingwell, D.B., Scheu, B., Taddeucci, J., 2004. The fragmentation threshold of pyroclastic rocks. Earth Planet. Sci. Lett. 226, 139–148. doi:doi.org/10.1016/j.epsl.2004.07.016
Stevenson, J., Larsen, G., Thordarson, T., 2015. Physical volcanology of the prehistoric Hekla 3 and Hekla 4 eruptions, Iceland. EGU Gen. Assem. id.4207.
Sturkell, E., Agustsson, K., Linde, A.I., Sacks, S.I., Einarsson, P., Sigmundsson, F., Geirsson, H., Pedersen, R., La Femina, P., 2005. Geodetic constraints on the magma chamber of the Hekla volcano, Iceland. Eos Trans. AGU 86, V21D–0636.
Sverrisdottir, G., 2007. Hybrid magma generation preceding Plinian silicic eruptions at Hekla, Iceland: evidence from mineralogy and chemistry of two zoned deposits. Geol. Mag. 144, 643. doi:10.1017/S0016756807003470
Taddeucci, J., Pompilio, M., Scarlato, P., 2004. Conduit processes during the July – August 2001 explosive activity of Mt . Etna (Italy): inferences from glass chemistry and crystal size distribution of ash particles 137, 33–54. doi:10.1016/j.jvolgeores.2004.05.011
Thorarinsson, S., 1968. Heklueldar. Rangæingafélagið, Reykjavik.
Thorarinsson, S., 1967a. The eruption of Hekla 1947-1948. I. The eruptions of Hekla in historical times, a tephrochronological study. Soc. Sci. Islandica 1, 1–170.
Thorarinsson, S., 1967b. The eruption of Hekla 1947-1948. II, 3. The tephra fall from Hekla on March 29th 1947. Soc. Sci. Islandica 2, 1–68.
Thorarinsson, S., 1958. The Öræfajökull Eruption of 1362. Acta Nat. Islandica II, 1–99.
Thorarinsson, S., 1953. Some new aspects of the Grímsvötn problem. J. Glaciol. 2, 267–274.
Thorarinsson, S., Sigvaldason, G.E., 1972a. The Hekla Eruption of 1970. Bull. Volcanol. 36, 269–288. doi:10.1007/BF02596870
Thorarinsson, S., Sigvaldason, G.E., 1972b. Tröllagígar og Tröllahraun. Jökull 22, 1862–1864.
Thorarinsson, S., Sigvaldason, G.E., 1962. The eruption in Askja, 1961; a preliminary report. Am. J. Sci. 260, 641–651. doi:10.2475/ajs.260.9.641
Thordarson, T., Höskuldsson, A., 2008. Postglacial volcanism in Iceland. Jokull 58, 197–228.
Thordarson, T., Larsen, G., 2007. Volcanism in Iceland in historical time: Volcano types, eruption styles and eruptive history. J. Geodyn. 43, 118–152. doi:10.1016/j.jog.2006.09.005
Thordarson, T., Self, S., 2003. Atmospheric and environmental effects of the 1783-1784 Laki eruption: a review and reassessment 108. doi:10.1029/2001JD002042
Thordarson, T., Self, S., 1993. The Laki (Skaftár Fires) and Grímsvötn eruptions in 1783–1785. Bull. Volcanol. 55, 233–263. doi:10.1007/BF00624353
Thornber, B.C.R., Sherrod, D.R., Siems, D.F., Heliker, C.C., Gregory, P., Oscarson, R.L., Kauahikaua, J.P., 2002. Whole-rock and glass major-element geochemistry of Kilauea Volcano , Hawaii , near-vent eruptive products : September 1994 through September 2001. USGS, Open File Rep. 02-17 1–9.
Toramaru, A., 1989. Vesiculation process and bubble size distributions in ascending magmas with constant velocities. J. Geophys. Res. Solid Earth 94, 17523–17542. doi:10.1029/JB094iB12p17523
Tryggvason, E., 1994. Observed ground deformation at Hekla, Iceland prior to and during the eruptions of 1970, 1980–1981 and 1991. J. Volcanol. Geotherm. Res. 61, 281–291. doi:doi.org/10.1016/0377-0273(94)90009-4
Verhoogen, J., 1951. Mechanics of ash formation. Am. J. Sci. 249, 729–739.

doi:10.2475/ajs.249.10.729
Vogfjörð, K.S., Jakobsdóttir, S.S., Gudmundsson, G.B., Roberts, M.J., Ágústsson, K., Arason, T., Geirsson, H., Karlsdóttir, S., Hjaltadóttir, S., Ólafsdóttir, U., Thorbjarnardóttir, B., Skaftadóttir, T., Sturkell, E., Jónasdóttir, E.B., Hafsteinsson, G., Sveinbjörnsson, H., Stefánsson, R., Jónsson, T.V., 2005. Forecasting and Monitoring a Subglacial Eruption in Iceland. Eos, Trans. Am. Geophys. Union 86. doi:10.1029/eost2005EO26
Walker, G.P.L., 1981. Characteristics of two phreatoplinian ashes, and their water-flushed origin. J. Volcanol. Geotherm. Res. 9, 395–407.
Walker, G.P.L., 1973. Explosive volcanic eruptions - a new classification scheme. Geol. Rundschau 62, 431–556.
Wallace, P.J., Plank, T., Edmonds, M., Hauri, E.H., 2015. Chapter 7 - Volatiles in Magmas A2 - Sigurdsson, Haraldur BT - The Encyclopedia of Volcanoes (Second Edition). Academic Press, Amsterdam, pp. 163–183. doi:dx.doi.org/10.1016/B978-0-12-385938-9.00007-9
Wilson, L., 1972. Explosive Volcanic Eruptions-II The Atmospheric Trajectories of Pyroclasts. Geophys. J. Int. 30, 381–392.
Wohletz, K.H., 1986. Explosive magma-water interactions: Thermodynamics, explosion mechanisms, and field studies. Bull. Volcanol. 48, 245–264. doi:10.1007/BF01081754
Zimanowski, B., Büttner, R., Dellino, P., White, J.D.L., Wohletz, K.H., 2015. Chapter 26 - Magma–Water Interaction and Phreatomagmatic Fragmentation A2 - Sigurdsson, Haraldur BT - The Encyclopedia of Volcanoes (Second Edition). Academic Press, Amsterdam, pp. 473–484. doi:doi.org/10.1016/B978-0-12-385938-9.00026-2
Þráinsson, B.Þ., 1991. Iceland national radio, 19:00 news, January 17th 1991.

Paper 1

The opening subplinian phase of the Hekla 1991 eruption: properties of the tephra fall deposit

Jónas Guðnason, Þorvaldur Þórðarson, Bruce F. Houghton, Guðrún Larsen

Bulletin of Volcanology, 79, 34.

Bull Volcanol (2017) 79:34
DOI 10.1007/s00445-017-1118-8

RESEARCH ARTICLE

The opening subplinian phase of the Hekla 1991 eruption: properties of the tephra fall deposit

Jonas Gudnason[1,3] · **Thor Thordarson**[1] · **Bruce F. Houghton**[2] · **Gudrun Larsen**[3]

Received: 13 September 2016 / Accepted: 23 March 2017

Abstract The 1991 Hekla eruption started on 17th of January with an intense 50-min-long explosive phase that transitioned into fire fountain activity lasting for 2 days. The eruptive plume rose to maximum height in about 10 min and the total mass of tephra deposited from the opening phase was 8.6×10^9 kg (VEI 3 event). The principal axis of tephra fall is to the NNE of Hekla and grain-size analysis reveals a systematic decrease in grain-size away from source. Majority of sample sites show typically unimodal grain-size distributions, although a few have bimodal distributions where the secondary mode is a subtle finer peak. The calculated total grain-size distribution (TGSD) is bimodal, with a coarse primary peak (−3.5 to −2.5 φ) and a subordinate fine peak (2.5 to 3.5 φ). The coarse peak is lapilli-dominated and was deposited within the first 25 km of transport, whereas the fine peak is coarse-ash-dominated and fits well with the modal grain-size of samples deposited >65 km from Hekla. Ascent rate of the magma and conditions for vesiculation in the shallow conduit became increasingly uniform with time through the 1991 opening phase.

Editorial responsibility: C. Bonadonna

Electronic supplementary material The online version of this article (doi:10.1007/s00445-017-1118-8) contains supplementary material, which is available to authorized users.

✉ Jonas Gudnason
jog4@hi.is

[1] Faculty of Earth Sciences, University of Iceland, Reykjavík, Iceland

[2] Department of Geology and Geophysics, University of Hawaii, Honolulu, HI, USA

[3] Institute of Earth Sciences, University of Iceland, Reykjavík, Iceland

Keywords Hekla · Total grain size distribution · Vesicularity · Subplinian · Tephra

Introduction

Tephra fall deposits (i.e. pyroclasts deposited by fallout from an eruption plume) of volcanic eruptions contain invaluable information that can be used for assessing eruption parameters such as magnitude, intensity, and eruption plume heights (e.g. Walker 1973; Newhall and Self 1982; Carey and Sparks 1986; Pyle 1989; Bonadonna et al. 1998; Mastin et al. 2009). Selected dispersal parameters (e.g. thinning rate and half distances for clast size) are used to determine eruptive volume and intensity (Pyle 1989; Fierstein and Nathenson 1992; Bonadonna and Houghton 2005; Bonadonna and Costa 2012), while mechanisms of magma fragmentation and eruption dynamics are inferred from the study of the ejected pyroclasts (i.e. tephra clasts) (e.g. Kaminski and Jaupart 1998; Kueppers et al. 2006; Carey et al. 2009; Eychenne et al. 2011) and of total grain-size distribution (TGSD), which is also a critical parameter for numerical models of tephra transport and sedimentation (e.g. Carey and Sigurdsson 1982; Bonadonna and Houghton 2005; Durant et al. 2009; Eychenne et al. 2015). These parameters along with quantification of rates of magma ascent, degassing, and crystallization in the shallow conduit from studies of microtextures provide the best constraints on eruption dynamics (e.g. Houghton and Wilson 1989; Klug and Cashman 1996; Gurioli et al. 2005; Lautze and Houghton 2006; Polacci et al. 2006).

Hekla is one of the most active volcanic systems in Iceland, with at least 23 events in the last 900 years, 18 of which took place at the Hekla central volcano (Thordarson and Larsen 2007). Hekla eruptions start highly explosively (subplinian to Plinian intensity; Janebo et al. 2016; this study), and

Published online: 05 April 2017

typically with little warning, only tens of minutes (e.g. Thorarinsson 1968; Grönvold et al. 1983; Gudmundsson et al. 1992; Soosalu et al. 2003; Thordarson and Larsen 2007). The drivers for the high intensity of the opening phase are largely unexplored. The fact that the eruptions began with very little warning further emphasizes the importance of better understanding of the explosive opening phases of Hekla events.

The 1991 eruption is ideal for addressing the intricacies of Hekla's opening explosive phases, because its chronology and tephra fall are exceptionally well documented (Gudmundsson et al. 1992; Larsen et al. 1992). In this paper we investigate the 1991 opening phase in order to better quantify the dynamics of the explosive activity as well as the associated eruption source parameters. This is achieved by (1) reassessment of dispersal and volume of the 1991 tephra; (2) comparison of the measured plume height to conventional empirical estimates of plume height from field data; (3) grain-size analyses of strategically selected samples and determined TGSD; (4) density of pumice clasts; and (5) fining in grain-size with distance from source used to constrain rates of tephra sedimentation.

Hekla

Hekla central volcano (63.98°N, 19.70°W; 1490 m a.s.l.) sits within a SW-NE trending fissure swarm that is ~40 km long and ~19 km wide (Fig. 1; e.g. Jakobsson 1979; Jóhannesson and Sæmundsson 1998). Its NW to SE profile has the conical form that typifies stratovolcanoes, while its SW to NE profile is more elongate (Fig. 1c, d). The elongation reflects a ~5-km-long linear vent system that becomes partly or fully active during most eruptions (e.g. Thorarinsson 1968; Thorarinsson and Sigvaldason 1972; Grönvold et al. 1983; Gudmundsson et al. 1992; Larsen et al. 1992; Höskuldsson et al. 2007).

Hekla post glacial eruptive activity has been of three types: (I) effusive fissure eruptions, primarily basaltic; (II) Plinian eruptions of ~70 wt% SiO_2 magma; and (III) hybrid subplinan-Plinian explosive to effusive eruptions. Effusive fissure eruptions (type I) take place on the Hekla fissure swarm outside the Hekla central volcano. The most recent example is the 1913 Lambafit eruption to the NE of Hekla. Lava flows older than 4300 years and younger than 1500 years erupted SW and NE of Hekla, whereas between 4300 and 2000 years ago activity peaked SE and S of Hekla at Vatnafjöll (Jóhannesson and Einarsson 1990). Examples of Plinian eruptions (type II) are the silicic H1, H3, H4, and H5 tephra layers. These large eruptions produced tephra layers that cover up to 80% of Iceland and have volumes up to 13 km^3 (Larsen and Thorarinsson 1977; Stevenson et al. 2015; Janebo et al. 2016). The hybrid events (type III) represent the majority of the 18 documented historical eruptions, e.g. in 1300, 1693, 1766, 1845, 1947, 1970, 1991, 1980, and 2000. They start with a 30- to 60-min-long explosive phase, subplinian to Plinian in intensity. The opening phase is followed by a sharp drop in magma discharge and a transition into dominantly Strombolian/effusive activity with intense fountaining and relatively fast moving fountain-fed lava flows of icelandite to basaltic icelandite composition (Supplementary document 1). Another sharp drop in magma discharge occurs over the first 1–3 days (Fig. 2), and activity becomes localized to low-altitude vents on the main Hekla fissure or on short radial flank fissures. This activity is typified by Strombolian activity with relatively low discharge rates (<20 m^3 s^{-1}; Table 1).

The repose period of Hekla eruptions and the magnitude of the subsequent eruptions seem to correlate, as a longer repose most often results in a larger and more powerful eruption (e.g. Thorarinsson 1968). During historical times (i.e. since 874 CE), the repose period has ranged from 9 to 120 years with an average of 50 years. The eruptive activity in Hekla before 1947 (including the 1947 eruption) had, on average longer repose, more widespread tephra fall and more voluminous lavas (Thorarinsson 1968). After the 1947 eruption, activity has changed to shorter repose periods and smaller eruptions. Since 1970, Hekla volcano has produced four eruptions, in 1970, 1980 to 1981, 1991, and the last one in February 2000. All were typified by a 0.5–2-h-long opening subplinian phase with discharge ranging from 1100 to 2600 m^3 s^{-1}. In all four events, the sustained and relatively low-discharge (<20 m^3 s^{-1}) Strombolian/effusive phase lasted up to a few months (e.g. Thorarinsson and Sigvaldason 1972; Grönvold et al. 1983; Gudmundsson et al. 1992; Höskuldsson et al. 2007).

The Hekla 1991 eruption

The 1991 eruption was the 17th historical eruption of Hekla. It started on 17th of January 1991 and lasted 53 days, ending on 11th March 1991. Key events of the first 12 h are summarized in Table 1. The onset of the eruption was at 17:01 (Iceland Standard Time); elevated seismicity was first detected 30 min earlier (Soosalu et al. 2003). First observations were of three gas-rich jets, seen from a farm ~50 km WNW of Hekla, accompanied with a faint rumble (Þráinsson 1991). The three jets were seen for ~1 min until a tephra-laden eruption plume started rising from a fissure just north of the 1947 shoulder crater; 5 min later the eruption plume was visible from locations 80 km away from Hekla and it was first detected by radar at 17:10. The opening phase was a 50-min-long subplinian phase producing a 11.5 ± 1.2-km above sea level (a.s.l) high eruption plume in ~10 min, feeding a NE dispersing plume with significant tephra fall up to 370 km from the volcano (Fig. 3). The plume height was estimated by a weather radar of the Meteorological Office and from direct pilot observations (Gudmundsson et al. 1992). The error on measurements

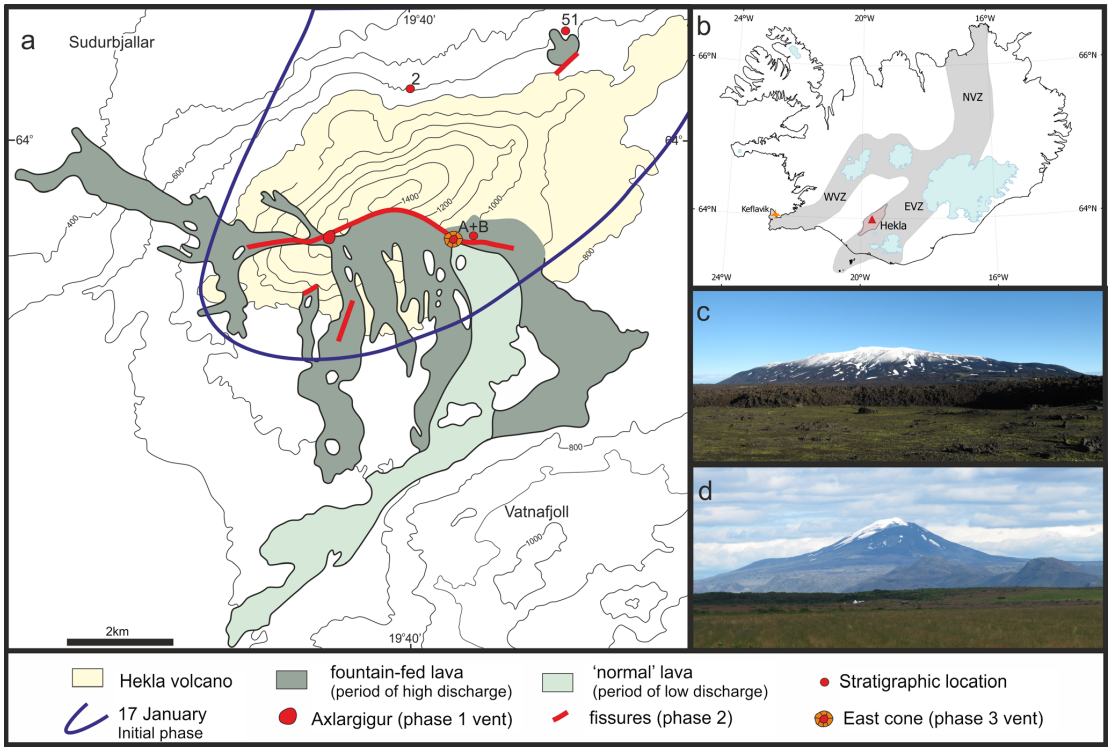

Fig. 1 **a** Distribution map of the 1991 products and active vents (see key for details). Stratigraphic locations indicated are opening phase loc. 51 and 2, transitional phase loc. A+B. **b** Location of Hekla on Iceland (*red triangle*), with the surrounding 720 km^2 fissure swarm (*outlined*). Also shown is the Western (*WVZ*), Eastern (*EVZ*), and Northern (*NVZ*) Volcanic Zones (*shaded grey*; modified after Sæmundsson 1979). **c** The elongate form of Hekla as seen from the east, perpendicular to the main fissure. **d** The conical form of Hekla as seen from the south along the main fissure

obtained with the weather radar increases with distance and at Hekla it is ±1.2 km (Oddsson et al. 2012). The rise velocity of the subplinian plume was in the range of 20–30 m s^{-1}, whereas the umbrella cloud propagated downwind at velocities of ~20 m s^{-1} (Larsen et al. 1992). A sharp onset of earthquakes at 17:52 marked the start of phase 2 (Table 1), which began with a stepwise opening of the Hekla fissure and the initiation of fountaining that propagated along the opening fissure. This phase of the eruption was typified by 300–500 m high eruptive fountains that fed lava flows that cascaded down the western and southern slopes of the volcano, reaching lengths of 4–5.5 km in <6 h (Fig. 1a). Shortly thereafter, additional fountains emerged from radial northern and southern fissures (Table 1). During the subplinian opening phase (i.e. first 50 min), the magma discharge was on the order of 1260 m^3 s^{-1} as calculated from tephra fall deposit volume and duration of the subplinian phase, whereas during the transitional phase 2, the discharge dropped to <50 m^3 s^{-1} over the course of 2 days (Fig. 2; Gudmundsson et al. 1992). This decline coincided with an eastward shift and progressive localization of the activity. By the third day of the eruption, the activity was typified by fountaining on a short fissure segment at the site which became known as the East cone (Fig. 1a). This activity supported only a weak convective plume (<2 km) and represents the switch to phase 3. From this time onwards, the activity was characterized by a single gas-rich fountain, carrying sporadic bombs to heights of several hundred meters with only minor ash. Coarse ejecta gradually accumulated around the vent to form an 80-m high and ~250-m wide scoria cone. At the same time, lava was discharged at rates of 1–12 m^3 s^{-1} (Fig. 2 inset), as several flows through separate vents at the base of the East cone (Fig. 1a). The eruption produced, in total, ~0.15 km^3 of icelandite lava and 0.02 km^3 of tephra fall deposits (Gudmundsson and Sæmundsson 1992; Gudmundsson et al. 1992; Larsen et al. 1992; Supplementary document 1), including a well-defined tephra blanket covering >20,000 km^2 (Fig. 3; Larsen et al. 1992). The movement of the tephra-laden plume to the NNE was monitored by weather radar, at the Keflavík airport, and tephra fall was constrained visually by residents in the NE part of the tephra sector. Details of the tephra fall from the 1991 eruption are published in Larsen et al. (1992).

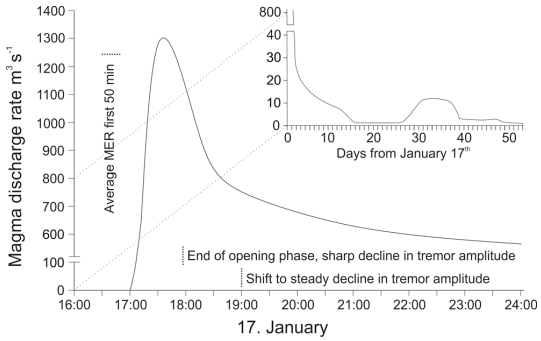

Fig. 2 Diagram showing magma discharge (DRE) versus time for the first hours of the 1991 Hekla eruption. The discharge curve is based on the following: the time averaged discharge during the opening phase, timing of decrease in discharge is based on changes in tremor amplitude (Soosalu et al. 2003), and calculated total output of magma during the first days (Gudmundsson et al. 1992). The *inset* (*top right*) shows the magma discharge during for the rest of the eruption (modified after Gudmundsson et al. 1992)

Methods

Sampling of 1991 tephra fall deposit

The Hekla 1991 tephra fall from the opening phase was sampled during and in the weeks after the eruption (Fig. 3). Within the central highlands, the tephra fall was quickly buried by snow and thus well preserved during the weeks following, although the longer term preservation of the deposit in the medial to distal regions is poor (Larsen et al. 1992). All samples (Supplementary Table 1) were collected from known surface areas (up to 1 m^2) along with entrained snow, which afterwards was melted and decanted off. Sample coverage was increased in 2012–2013, particularly in the proximal sector. The deposit thickness was measured along with mass per unit area and samples were collected for grain-size and vesicularity analysis. The combined 1991 and 2012–13 dataset has good coverage in the proximal and medial sectors, i.e. within the 0.75 kg m^{-3} isomass line, beyond that the coverage drops significantly (Fig. 3). Outer limits of tephra dispersal on 17th of January are well constrained through reports of tephra fall and eyewitness accounts (Larsen et al. 1992).

The key proximal section, location 51, is 5 km from the Hekla summit (Figs. 1a and 3b), and contains the entire proximal tephra fall from the opening phase, preserved beneath the lava flow from the northernmost vent of the 1991 eruption (Fig. 4). Samples were collected through the section, as illustrated in Fig. 5, for grain-size analyses and clast density measurements.

Density

Samples for density analysis were collected at two locations: location 51 (opening phase) and from a site just north of the East cone (phase 2) (Fig. 1a). Samples from four stratigraphic levels at location 51 represent the subplinian opening phase of the eruption, whereas the two samples (A and B, Fig. 1a) from the East cone are from the transitional phase (phase 2). From each density sample, a set of 100 clasts were measured after Houghton and Wilson (1989). A dense rock equivalent (DRE) value of 2620 kg m^{-3}, calculated using a water pycnometer, was used when converting from measured density to bulk vesicularity.

Grain-size and total grain-size distribution of Hekla 1991

Samples collected for grain-size analyses were manually sieved at half intervals down to 4 or 63 μm ($= -\log_2 d$, d is the particle diameter in mm). Max diameter (Max_φ), median diameter ($Md_\varphi = \varphi_{50}$), and sorting coefficient ($\sigma_\varphi = (\varphi_{84}-\varphi_{16})/2$) were calculated (Inman 1952). Two methods were used to analyse the fine tephra fraction. Firstly, a Beckmann Coulter LS230 at the University of Edinburgh was used to analyse the fraction finer than 1 mm. The output was binned in half intervals and combined with the sieving data based on mass finer than 1 mm in the sample, and the overlap of data from 1 mm to 63 μm was used to validate the data sets. Secondly, a SediGraph III at the University of Iceland was used to analyse the fraction smaller than 250 μm. The SediGraph uses horizontally collimated beam of X-rays to measure relative particle mass concentration in a liquid medium. The SediGraph then applies Stokes Law to determine relative percentage in each size class under known liquid conditions (density and viscosity) and known particle density (2620 kg m^{-3}). The output was binned in half intervals and combined with the sieving data based on mass finer than 250 μm in the sample. The data overlap from 250 to 63 μm was used to check if sieving and mechanical analyses gave consistent results. TGSD was calculated using a total of 26 samples, mostly from within the 0.75 kg m^{-2} isomass line (Fig. 3). All samples used for TGSD calculation are bulk samples, at location 51 (Fig. 1) where stratigraphic sampling was done, bulk sample of the deposit was collected for the TGSD calculation. The zero deposit line was determined from eyewitness accounts of tephra deposition on 17th of January (Fig. 3). The TGSD was determined by the Voronoi Tessellation method of Bonadonna and Houghton (2005), using an updated version of the code (Biass and Bonadonna 2014). This method assigns a polygonal Voronoi cell (see Supplementary Fig. 1) to each sample and the TGSD of the deposit is obtained as the area-weighted average of all the cells covering the deposit. Criteria for sample selection were to optimize deposit coverage. This method has successfully been applied to other eruptions where sampling was contemporaneous with eruption, e.g. the 1996 Ruapehu eruption, New Zealand

Table 1 Sequence of events of during the first hours of the Hekla 1991 eruption, summarizing phases 1 and 2 on 17th January to 18th January (Gudmundsson et al. 1992; Larsen et al. 1992; Linde et al. 1993; Soosalu et al. 2003)

Time	Seismicity	Eruptive vents	Interpretation
16:32	First volcano-tectonic earthquakes detected, growing in intensity (ML = 1–2) and frequency to 17:00. Strain contraction starts		Intrusion of magma rising through the Hekla conduit system. The magma travelled from holding chamber to the surface in ~30 min
17:01	Onset of volcanic tremor, which remained at high intensity levels to ~18:00	Three large gas jets rise emerge from a short fissure near the 1947 Shoulder Crater	Onset of visible eruption
17:02		Black tephra-laden column emerges from Shoulder Crater fissure	Appearance of subplinian column, start of phase 1
17:05–17:07		Rapidly rising eruption column at Hekla seen from several farms in S-Iceland. As its top decelerated it spread out before being deflected northwards by wind	Eruption column rising vertically above Hekla and forming a small umbrella cloud before downwind dispersal of the plume (to north)
17:10		Eruption plume first detected by the Iceland Meteorological Office weather radar, column and plume height ≥11.5 km	Fully developed eruption column constructed at rise velocities in the range of 20–30 m s^{-1}
17:52	Relatively strong earthquake (ML = 2.5)	Lava fountains appear from the Shoulder Crater fissure, signalling the onset of simultaneous explosive and lava fountain eruption	Termination of subplinian eruption (phase 1) and the initiation of phase 2. Duration of phase 1 = 50 min
18:00	Volcanic tremor decreases sharply between 18:00–19:00 h	Intense explosive activity on a new fissure down slope from Shoulder Crater fissure, propagating westward at the time and featuring a line 300–500 m high fountains supporting a 12 km high eruption column (as measured by Iceland air pilots in transit). Also, a new short fountaining fissure opened on the north flank of Hekla	Opening of the Hekla fissure with fire fountain activity on lengthening fissures marking a full transition to phase 2
18:06–18:40	Series of relatively strong earthquakes (ML = 2.0–2.3), lasting for 24 min (18:06 to 18:30), followed by sharp decrease in earthquake intensity and frequency over 40 min. Strain contraction stops at 18:40	Lava fountains first seen on radial fissures on south slope of Hekla, followed by a gradual lengthening of the Shoulder crater fissure and stepwise propagation of explosive and lava fountain activity, first to the NE along the crest of Hekla towards the Summit Crater and from there eastward, diagonally down the eastern slope of Hekla	Evolution of phase 2 activity marked by continued growth and lengthening of the Hekla fissure to the NE and associated explosive and lava fountain activity
19:00–20:00	Continued but gradual decrease of volcanic tremor. Slight increase in earthquake intensity and frequency from 19:05–19:40, followed by a 2-h-long period steady decline	Renewed growth of the phase 2 eruption plume close to Hekla volcano	Slight increase in phase 2 activity
20:00–21:00	Continued decline of seismic activity	Decreasing explosivity, with a lull in explosive activity around 21:00. Phase 2 eruption plume detached from the volcano at 20:50	Gradual temporary decrease in phase 2 activity
21:30–24:00	At 21:32: Relatively strong earthquake (ML = 2.3)	Eruption intensity decreases rapidly on SW-part of the Hekla fissure. Eastward lengthening of the Hekla fissure (at ~900 m a.sl.), coupled with renewed vigour of the activity on the segment of Hekla fissure that extends from the Summit Crater to the foot of the eastern flank	Renewed vigour of phase 2 activity in junction with a shift of the vents to NE part of the Hekla fissure
0:00–4:00	Earthquake intensity and frequency and volcanic tremor decrease at steady rate	Strong explosive and lava fountaining activity, of gradually decreasing intensity, continued into the night on NE part of the Hekla fissure	Intensity of phase 2 activity begins to drop off leading to gradual localization of the eruptive vents
>4:00	Volcanic tremor levels off to low but steady intensities and earthquakes taper off	Activity characterized by rapid decrease in eruption intensity coupled with progressive localization of the eruptive vents onto a short fissure segment at the foot of the east slope (i.e. at the site of the East Cone (= phase 3 vent))	Waning stages of phase 2 activity leading to the transition to phase 3 on 20 January. From then on, activity was confined to the East Cone vent and characterized by weak Strombolian explosions and quiet effusion of lava

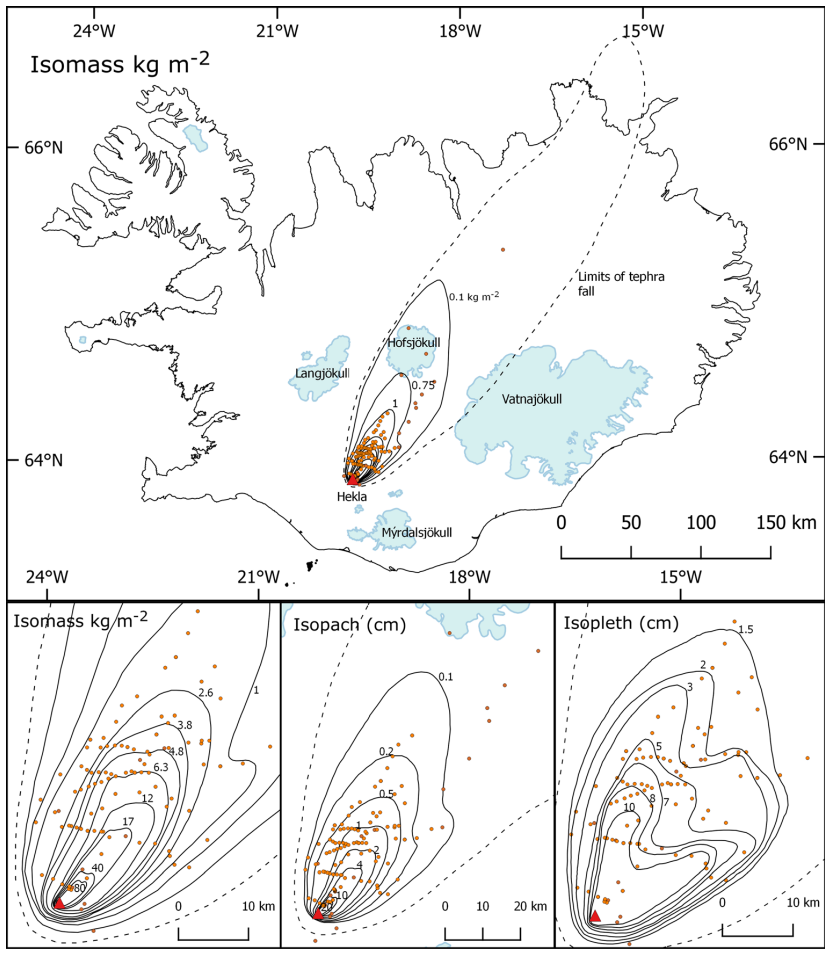

Fig. 3 Isomaps of the Hekla 1991 deposits. The *top panel* shows the extend of the 1991 tephra fall on land with isomass (kg m^{-2}) lines. Outermost limits of tephra fall are after sampled tephra and reports from the eruption. *Lower panel* shows the isomass (*far left*), isopach (*centre*), and isopleth (*far right*) maps for the proximal and medial sectors of the fall deposit. Based on Larsen et al. (1992), with additions from unpublished 1991 field data (Thordarson and Larsen) and new field observations in 2012 and 2013 by principal author

(Bonadonna and Houghton 2005), and the 2001 and 2002–03 eruptions at Mt. Etna, Italy (Scollo et al. 2007; Andronico et al. 2008).

Volume and mass of deposit

The volume of erupted tephra was calculated by integrating best fit lines on semi-log plots of deposit thickness and mass per unit area versus square root of area using multiple exponential segments (Fierstein and Nathenson 1992; Pyle 1989): power law (Bonadonna and Houghton 2005) and Weibull (Bonadonna and Costa 2012) functions. Transformation from mass per unit area to equivalent thickness for the data collected in 1991 was done using measured bulk densities from 400 to 940 kg m^{-3} (Larsen et al. 1992).

Plume height and mass eruption rate

Average mass eruption rate (MER) was calculated from the known duration of the opening phase and the calculated mass of the tephra deposits. In addition, to account for strong wind during the eruption, MER was calculated using the method of Degruyter and Bonadonna (2012). Magma temperature was varied according to magma composition from 1173 to 1373 K, the plume heights measured by the weather radar were used 8.8, 10, and 11.2 km above vent (10.3, 11.5, and 12.7 a.s.l., respectively) but wind speed was kept constant at 20 m s^{-1}, and the wind- and radial-entrainment coefficients were set to 0.5 and 0.1, respectively. The scaling parameter Π was also calculated to give insights into plume dynamics (Supplementary Table 2; Degruyter and Bonadonna 2012). Maximum plume height (H) was observed but was also calculated using the empirical relationships $H = 1.67\ Q^{0.259}$ (Sparks

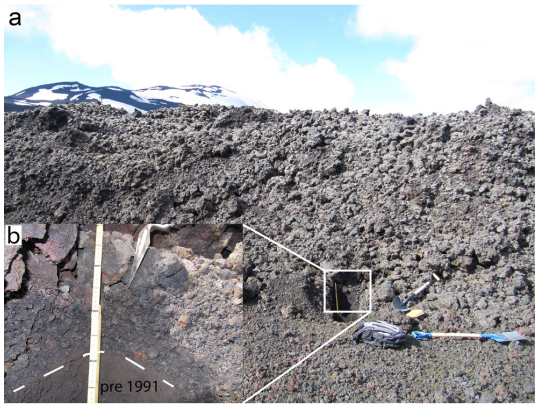

Fig. 4 **a** Location 51, the principal stratigraphic for the Hekla 1991 deposit (see Fig. 1 for geographic location). Photo taken on 27th of July 2012. At this site, the fall deposit is partly overlain by a small lava flow from the 1991 eruption. This site was chosen to ensure sampling of the Hekla 1991 fall deposit and not the subsequent Hekla 2000 event. **b** The deposit is 15 cm thick at location 51, the fine grained base in the image is pre 1991 and the larger grains at top are from the lava on top. *Black lines* on measuring stick are 5 cm apart

et al. 1997) and $H = 2.00\ Q^{0.241}$ (Mastin et al. 2009) (based on 34 historic eruptions, including the 1947, 1970, and 1980 Hekla events) where Q is the time-averaged MER.

Results

The 1991 tephra fall deposit—physical characteristics and dispersal

In the proximal region, up to 7 km from source, the 1991 deposit is made up of metallic bluish black scoria bombs and lapilli, and is poor in wall-rock lithics but with minor amounts of red cored bombs. Bombs are only common in the most proximal Hekla deposits. These bombs are fragile and have expanded after fragmentation with a concentration of very coarse vesicles in the cores. Beyond 7 km from source, the deposit is ash dominated.

The tephra dispersal from the subplinian phase forms a narrow (max 70 km wide) sector with the main dispersal axis trending NNE and a less distinct, secondary axis to the NE. The tephra thins rapidly along the dispersal axis; thinning half distance for the deposit is 5.5 km. At 13 km downwind of Hekla, the cross-wind half-distance is 3–4 km. The isomass and isopach contours are almost identical while the isopleth is crudely bilobate (Fig. 3), with two axes in the proximal area.

Two principal subunits were identified, described, and sampled at location 51 (Figs. 1, 5, and 6). Further away from Hekla, where deposits are <5 cm, subunits were not recognizable. At location 51, the basal subunit is a 7.5-cm-thick, very poorly sorted (σ_φ 2.1–2.9), inversely graded, lapilli-dominated fall. The basal subunit is overlain by a 0.5-cm-thick finer grained layer of medium to coarse ash, containing poorly sorted (σ_φ 1.3) fluidal and blocky juvenile clasts (Fig. 7). The overlying top subunit resembles the basal one; it is a 7-cm-thick, inversely graded, poorly sorted (σ_φ 1.4–1.7), clast-supported lapilli-dominated fall (Fig. 5). The tephra is homogeneous in terms of juvenile clast properties and the top subunit is distinctly lithic-poor. Lithic content in the basal sample (sample 8 in Fig. 5) is highest around 5% at −1.5 φ but averages around 1% of mass in the range −3 to 0 φ. Sample 7 is poorer in lithics. The lithic population is dominated by dark fragments of aphyric lava, with minor amounts of highly altered, light coloured, and red lava fragments.

Grain-size distribution

The grain-size distribution of individual samples is generally unimodal and show variation in maximum, minimum, and modal grain-size depending on distance from vent (Fig. 8a). However, bimodal grain-size samples are present, with the secondary peak in the <2 mm fraction. Sorting ranges from very well to poorly sorted (σ_φ 0.7 to 3; Fig. 8b) and median diameter ranges from −3.9 to 4 φ.

At location 51, the four grain-size samples from the lapilli fall units (Fig. 5) are bimodal whereas the grain-size sample from the ash layer (sample 6 in Fig. 5) is unimodal.

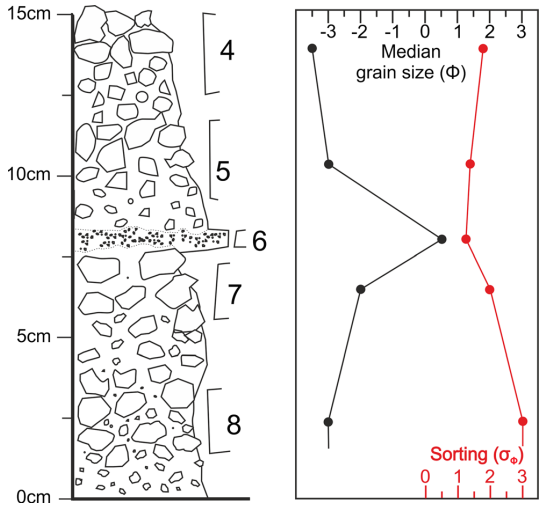

Fig. 5 Stratigraphic log of the Hekla 1991 tephra fall deposit at locality 51. Two principal fall units are identified separated by 0.5 cm thick parting of medium to coarse ash. Samples were collected for grain-size and density analyses. Grain-size samples were collected in subunits, samples (J12-51) 4–8 and density samples for 4, 5, 7, and 8. Sorting calculated after Inman (1952)

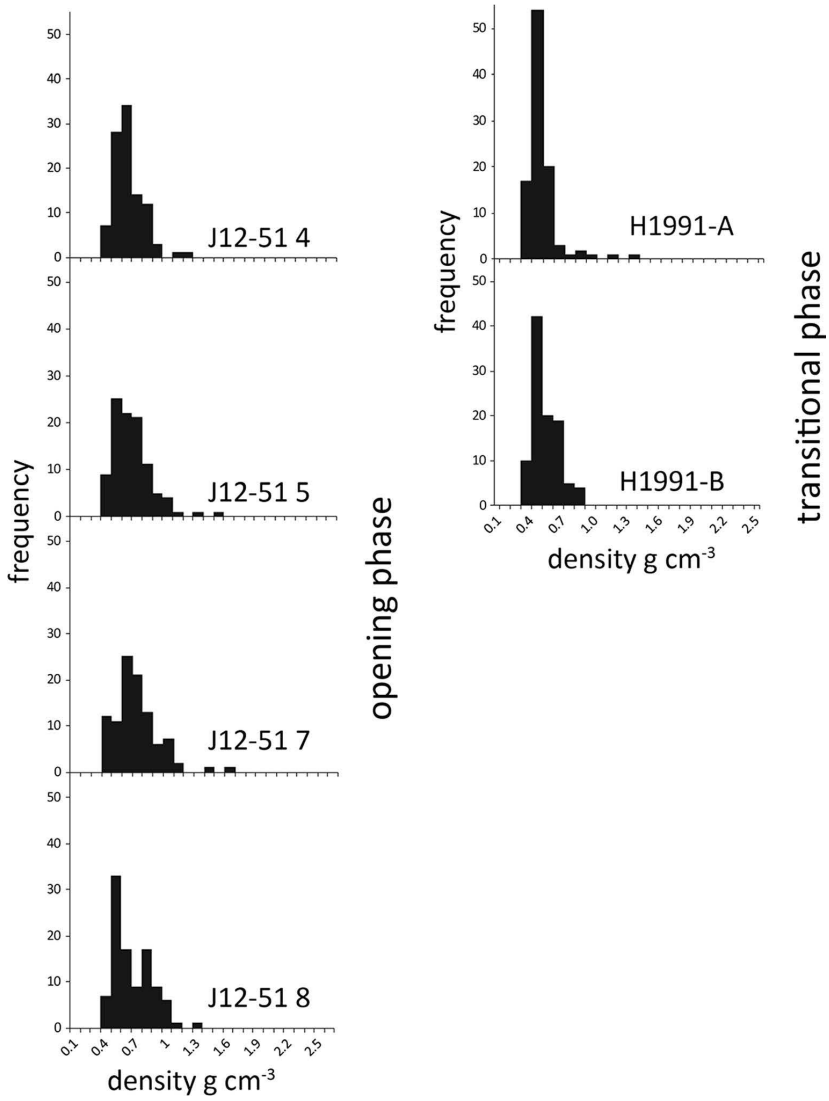

Fig. 6 Histograms showing the clast density measurements from both subunits (samples J12-51 4 to 8) at location 51. Also shown are clast density measurements from phase 2 tephra fall (samples H1991-A and B from the east cone location; Fig. 1a). The span in clast density is narrow, ranging from 520 to 880 kg m^{-3} and each sample exhibits a tight unimodal and log-normal distribution indicating a mean vesicularity of 77 to 79% for the analysed pumices, obtained via conversion of clast density using melt density of 2620 kg m^{-3}. Samples were analysed after the procedure of Houghton and Wilson (1989). Note, samples J12-51 4, H1991 A and B feature the tightest distributions

The bimodal samples have a primary coarser mode at −3.5 to −2.5 φ and a secondary finer mode at 3 to 4 φ (Fig. 5). There is a slight upward coarsening along with better sorting and lesser amounts of ash (<2 mm) in samples 4 and 5, compared to in samples 7 and 8 (Fig. 9). Samples 4 and 5 have Md_{φ} −3.5 to −3 φ and are better sorted (σ_{φ} 1.4 to 1.7) than samples 7 and 8 which have Md_{φ} −3.1 to −2.6 φ and σ_{φ} 2.1 to 3.

Along the main depositional axis, a size fractionation induced by transport and deposition becomes apparent. Samples along the main depositional axis show size fractionation with distance of the primary coarse mode (samples closer than 82 km, Fig. 8a). The two most proximal samples show slight bimodality, relatively broad coarse peaks at −3.5 and −1.5 φ, and smaller fine peaks around 3.5 φ. Bimodality is also seen in the medial samples (38, 52 km), sharper coarse peak at 0 to 2 φ and smaller finer peaks around 3.5 φ. Distal samples (82, 115, and 195 km from source) show only a broad fine peak at 3.5 to 4.5 φ (Fig. 8a). Another noteworthy feature is the small change of the grain-size mode of samples from 82 to 195 km from source (Fig. 8b), whereas over the same distance isomass values drop from 0.75 to 0.1 kg m^{-2} (Fig. 1a). Deposition of lapilli (64–2 mm;

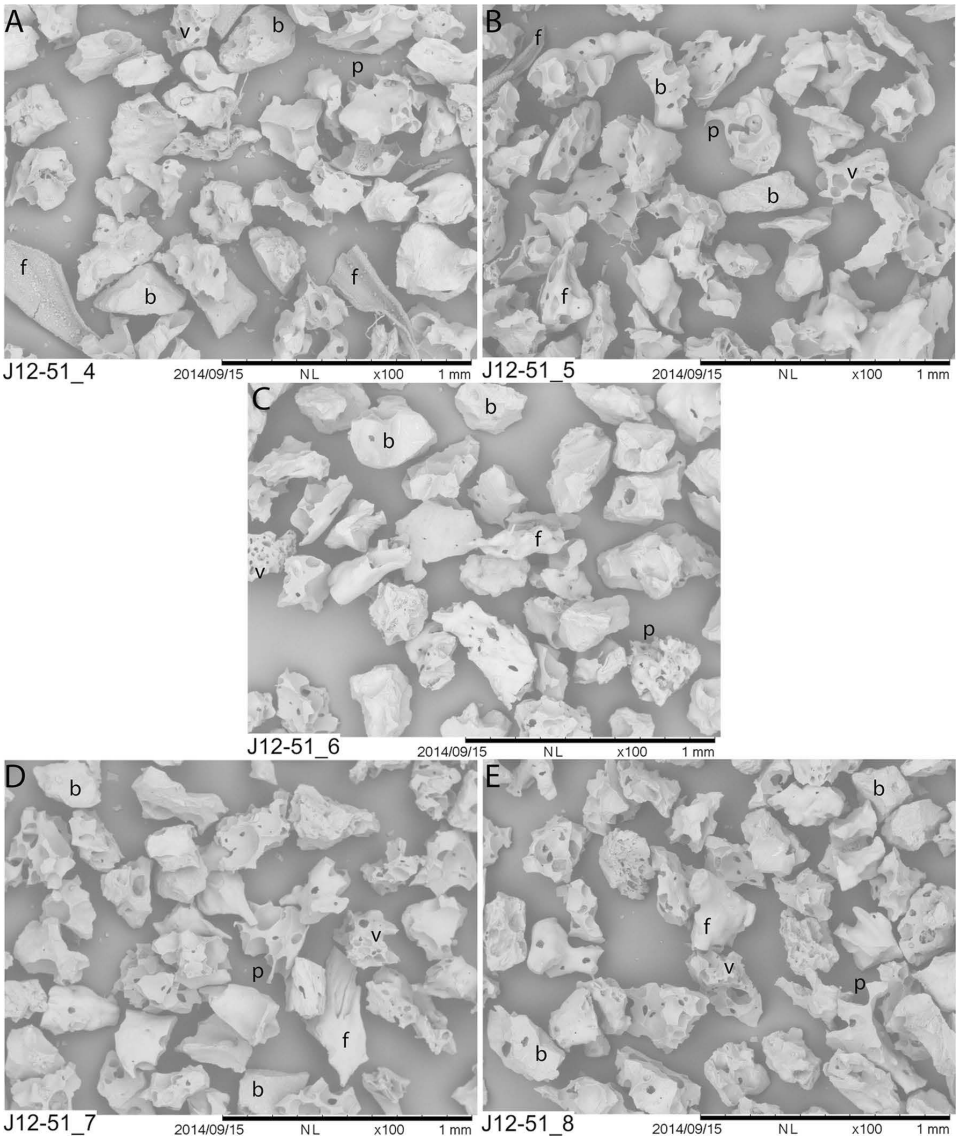

Fig. 7 Scanning electron microscope (SEM) images of grain-size samples from location 51. Grains were selected from the 2.5 φ bin in order to examine the finer grain-size peak observed in Fig. 9. Samples are shown in stratigraphical order from top left to bottom right. These moderately to highly vesicular ash grains have viscous fluidal or blocky shapes. The fluidal (*f*) grains typically have smooth shiny outer surfaces, which in some instances feature smaller sub-ten micron grains adhering to their surface (e.g. a. sample J12-51-4 grains at bottom left and right). The blocky (*b*) grains feature pristine curvi-planar surfaces typical of brittle fracturing. These grains also preserve small delicate protrusions (*p*) that have survived the transport through and deposition from the eruption plume

−6–1 φ) is concentrated during the first 25 km when it is the dominant grain-size (>60 wt%). From 25 km onwards, coarse ash becomes the dominant grain-size in the deposit, and fine ash becomes an important part of the deposit after 70 km. Changes in grain-size Md_φ, Max_φ, and σ_φ with distance from source (Fig. 8b) show that the most scatter for all parameters occur in the first 15 km. There is a steady decrease in Md_φ and Max_φ from ~0 to 65 km and then almost constant values from 65 to 195 km, where coarse ash is the dominant component (Fig. 8c). Over the same distance, σ_φ improves significantly out to 20 km and then shows no further significant variation.

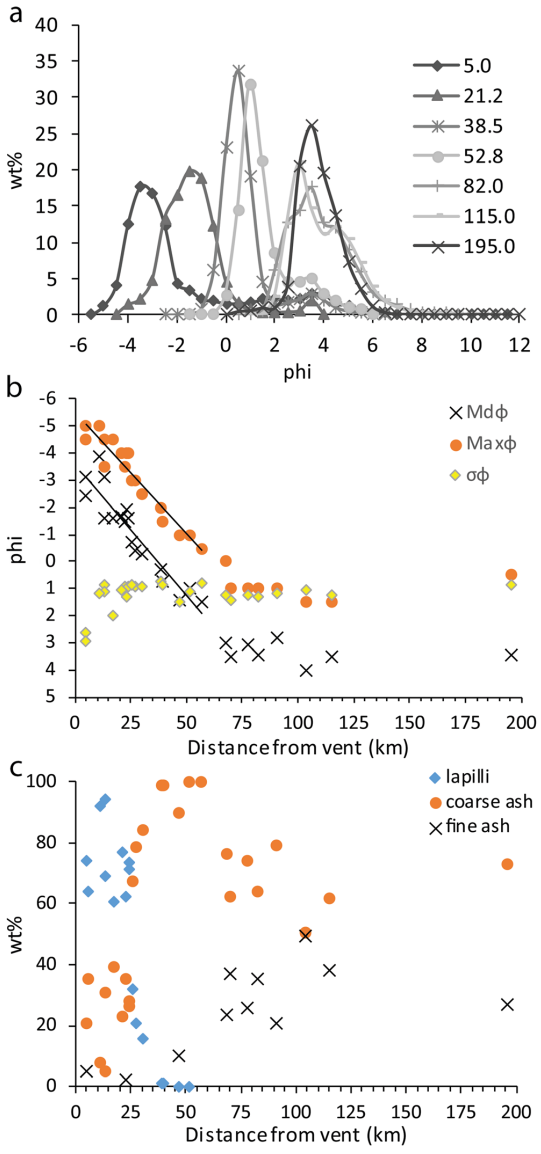

Fig. 8 **a** Grain-size distribution of selected samples along the principal dispersal axis of the Hekla 1991 tephra fall. *Each line* represents a sample at indicated distance from Hekla. **b** Variation of Md_φ, Max_φ, and sorting (σ_φ) of all Hekla 1991 grain-size samples as a function of distance from vent. Two lines show best fit through Md_φ and Max_φ data from 5 to 57 km from source. **c** Comparison of relative abundance of lapilli, coarse ash and fine ash with distance from source. Lapilli 64–2 mm, −6–1φ; coarse ash 2–0.063 mm, −1–4φ; fine ash <0.063 mm, >4φ

Total grain-size distribution

The TGSD (Fig. 10) is bimodal with a primary mode at −3.5 to −2.5 , and a secondary mode at 2.5 to 3.5 φ. Md_φ is −1.8 φ and σ_φ is 3.3. The ash fraction (<2 mm; ≥−1φ) amounts to 37% of the tephra mass, but fine ash (<63 μm; ≥4.5φ) accounts for only 6%.

Clast density

The density measurements of the 1991 pyroclasts show tight density/vesicularity distributions up through the type 51 section (Fig. 6). The range of mean clast density is 550 ± 140 to 600 ± 210 kg m^{-3}, corresponding to calculated mean vesicularities of 78 to 75%. The maximum measured juvenile clast density is 1520 kg m^{-3}, corresponding to a minimum vesicularity of 42%, while the minimum clast density is 310 kg m^{-3}, indicating a maximum vesicularity of 88% (Table 2). The density/vesicularity distributions are unimodal and weakly skewed towards higher densities, or lower vesicularity, with a standard deviation in the range of 140 to 210 kg m^{-3} for clast density and 5 to 8% for vesicularity (Fig. 6; Table 2). From the East cone location (Fig. 6, Table 2), samples H1991 A and B range in mean clast density from 520 ± 120 to 480 ± 150 kg m^{-3}, corresponding to calculated mean vesicularities of 80 to 81%. The maximum measured density is 1310 kg m^{-3}, which corresponds to a minimum vesicularity of 50%. The minimum clast density is 310 kg m^{-3}, corresponding to maximum vesicularity of 88%. The density/vesicularity distributions are unimodal, and less skewed towards higher densities than samples from location 51 with standard deviation of 120–150 kg m^{-3}, or 5–6% vesicularity (Fig. 6; Table 2).

Eruptive parameters

The estimates of volume of tephra fall from the opening phase using the three integration techniques ranges from 0.016 to 0.019 km^3 (Fig. 11a). The three-segmented exponential method gives 0.019 km^3, the power law 0.019 km^3, and the Weibull function 0.018 km^3, a difference of 0.001 km^3. The estimate of erupted mass derived by fitting three exponential segments (Fig. 11b) is 9.9×10^9 kg, the Weibull method gives 8.6×10^9 kg, whereas the power law results in 9.6×10^9 kg (corresponding to tephra volumes of 0.020, 0.017, and 0.019 km^3, respectively, using bulk density of 500 kg m^{-3}). The slightly lower values obtained here than the original estimate of 0.022 km^3 (Larsen et al. 1992) are due to the new mapping that better constrains thickness in the proximal area. The result from the integration using isomass data is considered the most reliable approaches to mass estimation of the opening phase, as no conversion to thickness is needed. All methods provide excellent fit to the data points (exponential $r^2 = 0.96$ to 0.98, Weibull $r^2 = 0.99$, and power law $r^2 = 0.97$). Here, the results from the Weibull are preferred as the most conservative estimate.

Using the estimates of 8.6×10^9 and 9.9×10^9 kg (0.003 and 0.004 km^3 DRE; Weibull and exponential, respectively),

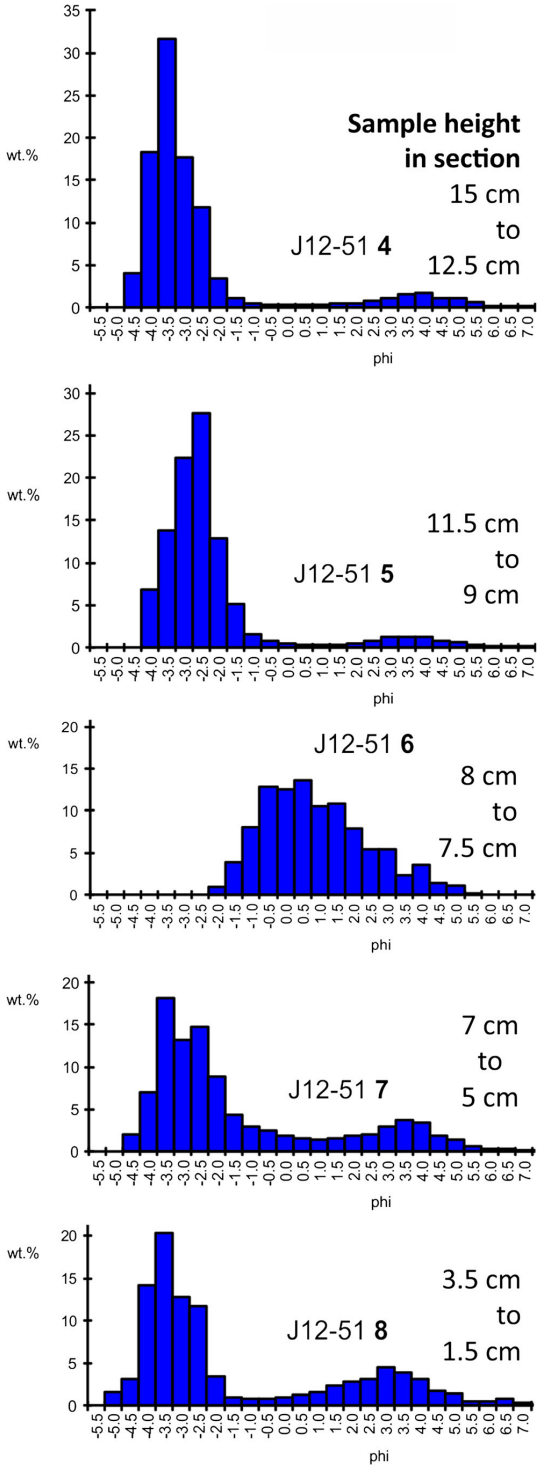

◀ **Fig. 9** Grain-size analyses for samples collected at location 51. Samples are bimodal except sample J12-51 6, the bimodal samples have principal coarse peak at −3.5 to −2.5 φ. The finer peak is at 3 to 4 φ. The lower fall unit (samples 7 and 8) has on average less defined coarse peak and higher mass contribution from the fine peak compared to the upper fall unit (samples 4 and 5)

the calculated time-averaged MER is between 2.9×10^6 and 3.3×10^6 kg s^{-1}. Conversion to volumetric MER, using DRE of 2620 kg m^{-3}, results in values of 1100 to 1260 m^3 s^{-1}. Plume heights empirically derived from the MER are 12 to 12.4 km a.s.l. (Mastin et al. 2009). This is in good agreement with the 11.5 km a.s.l. plume reported by Gudmundsson et al. (1992) and Larsen et al. (1992). Calculating the MER after Degruyter and Bonadonna (2012), and using the measured plume height by the radar (10 ± 1.2 km above vent), and wind speed of 20 m s^{-1} (Larsen et al. 1992), results in MER of 3.4×10^6 to 1.6×10^7 kg s^{-1} and scaling parameter Π of 0.20 to 0.26 (Supplementary Table 2).

Eruption type

The calculated maximum deposit thickness from the semi-log plot is 35 cm (Fig. 11a), and the thickest measured section is 28 cm. Following Walker (1973), the calculated dispersal index (D) is 460 km^2, and the fragmentation index (F) is 6.3%. These values are consistent with an explosive phase of subplinian intensity. Both the deposit volume and plume height would classify the eruption as a VEI 3 (Newhall and Self 1982) and the plume height equates to the M3 category of Mastin et al. (2009). However, using more recent classification methods that combine plume height with MER, the opening phase falls into the small to moderate category below the field of subplinian events (Bonadonna and Costa 2013).

Discussion

Explosive Hekla eruptions

Of the known post glacial explosive eruptive activity in Hekla, the 1970, 1980, 1991, and 2000 eruptions have produced the smallest volume of tephra fall and weakest intensity events (Fig. 12). Other historic Hekla (type III) eruptions are larger than the 1970 to 2000 activity, but smaller than the e.g. 1104 CE and H4 (type II) Hekla eruptions (Fig. 12; Larsen and Thorarinsson 1977; Thorarinsson and Sigvaldason 1972; Grönvold et al. 1983; Gudmundsson et al. 1992; Höskuldsson et al. 2007; Janebo et al. 2016). The 1991 eruption and other post 1947 Hekla eruptions are strikingly similar in sequence of events, composition of erupted materials, and eruption source parameters (Fig. 12; Supplementary document 1; Thorarinsson and Sigvaldason 1972; Grönvold

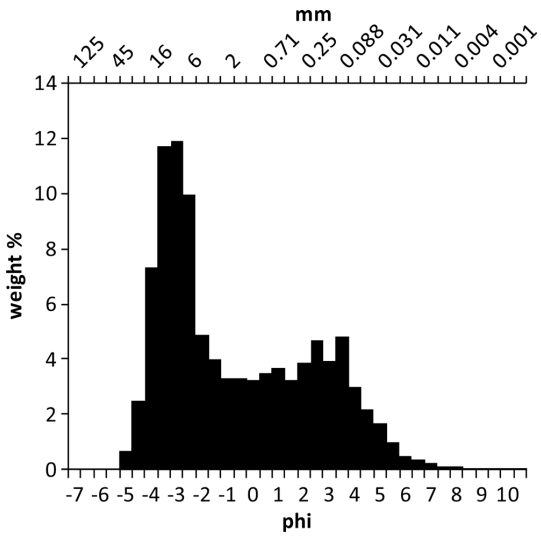

Fig. 10 Reconstructed TGSD of the opening phase tephra fall from the Hekla 1991 eruption. Note the bimodal distribution. The tighter coarse peak is around −3.5 to −2.5 φ, while the finer peak is broader, extending from around 2.5 to 3.5 φ. Spatial distribution of samples included in the calculation is shown in Supplementary Fig. 1

et al. 1983; Gudmundsson et al. 1992; Lacasse et al. 2004; Höskuldsson et al. 2007). But as illustrated here, there is potentiality for complex eruption dynamics in these short and smaller events.

Proximal tephra fall deposits

The threefold stratigraphy observed in the proximal tephra fall deposits, i.e. two coarse lapilli-dominated fall units separated by an ash parting as seen at location 51 (Fig. 5), cannot be explained by continuous deposition from a steadily rising and spreading plume. A plausible interpretation is that the opening phase of the eruption featured two distinct explosive phases, separated by a long enough break for the 0.5-cm-thick ash layer to accumulate. However, syn-eruptive observations as reported in Larsen et al. (1992) and tremor data (see Figs. 3 and 4 in Soosalu et al. 2003) do not indicate any pause in activity during the opening phase, rendering the above explanation unlikely.

At the most proximal site measured on 23 January 1991 (location 2, Fig. 1a), two lapilli fall units, which we interpreted to be the two beds at location 51, were separated by 4–5 cm of newly fallen snow. This suggests a short but distinct break in the lapilli accumulation.

We therefore suggest that the opening phase had a pulsating source with sustained atmospheric plume. Between the lapilli fall units, finer particles were aggregated by snow and deposited. Snow-induced aggregation may furthermore be the source for bimodality observed in the lapilli fall units (Fig. 9). Aggregation by snow commonly occurs in Iceland, e.g. in the 2000 Hekla eruption (Lacasse et al. 2004), the 2010 Eyjafjallajökull eruption (Thordarson, unpublished data), and in the 2011 Grímsvötn eruption (Gudnason, unpublished data).

Bilobate proximal isopleth lines (Fig. 3) indicate shift in wind direction during the opening phase, the bilobate shapes are not recognized in other isolines (Fig. 3). Indicating a relatively short temporal shift in wind direction, shift that is only recorded by large clasts, and thus not long enough to alter the general trend of the isopach map (Fig. 3). A more general shift in wind direction was recorded during the eruption, data from the weather radar indicates that the plume at 2 km a.s.l did shift from NNE at 17:50 to ENE at 23:50 (Larsen et al. 1992).

The reverse grading of each lapilli unit can be explained either by increasing eruption intensity and thus deposition from higher altitudes, or by shifts in the wind direction. Bilobation in the most proximal isopleth lines (Fig. 3) support wind shift. However, for two reversely graded fall units, wind shifts would need to be two. For the duration of the opening phase, that is not considered plausible. However, the reverse grading could be combination of the two, i.e. shift in wind direction and/or increasing eruption intensity.

Shallow conduit processes

The density data (Fig. 6) show minor variation over stratigraphic level (i.e. time). The lower lapilli unit at location 51 starts with a broad, slightly bimodal distribution that with time

Table 2 Vesicularity/density results from location 51 and the east cone. Four samples were analysed from location 51, stratigraphic height is illustrated in Fig. 9. Two samples from the east cone location were analysed (samples H1991 A and B)

	J12-51 4	J12-51 5	J12-51 7	J12-51 8	H1991-A	H1991-B
Mean vesicularity	78%	75%	75%	76%	80%	81%
Standard deviation	5%	8%	8%	7%	5%	6%
Maximum vesicularity	87%	88%	88%	88%	87%	88%
Minimum vesicularity	56%	42%	42%	52%	66%	50%
Mean density	0.55	0.57	0.6	0.59	0.52	0.48
Standard deviation	0.14	0.19	0.21	0.18	0.12	0.15
Maximum density	1.15	1.44	1.52	1.25	0.9	1.31
Minimum density	0.33	0.32	0.31	0.31	0.36	0.31

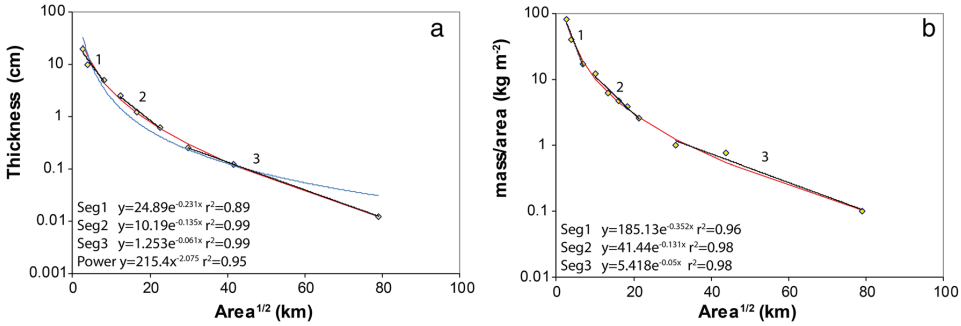

Fig. 11 Thickness vs √Area and mass per unit area vs √Area for the tephra fall deposit of the Hekla 1991 opening phase. Area of each isoline indicated by *yellow diamonds*. The data can be taken to define three exponential segments (*black solid lines*), best fit Power law solution (*blue dotted line*), and Weibull fit (*red solid line*). Equations for exponential fit, power law fit, and r^2 are shown in the lower left corner of each diagram

becomes unimodal. The upper lapilli unit shifts towards a narrower distribution over time. The broader initial density distribution is possibly due to partly degassed magma (i.e. gas flames in start of eruption), responsible for opening the conduit. The narrower density distributions towards the end of the opening phase indicate more stable conditions for vesiculation in the shallow conduit. Broad density distributions are thought to reflect heterogeneous textures in the magma, which could reflect heterogeneous vesiculation/degassing condition in the shallow conduit (e.g. Houghton et al. 2004). This could be linked to variation in rise speed during opening of the conduit in 1991, and resulting in less supersaturation and/or more loss of volatiles along the conduit walls. The somewhat narrower density distribution (samples 4 and 5; Fig. 6) is formed when the conduit is better established and less variation in ascend speed across conduit can be expected. Although interpretations of density data are only speculative without vesicle size distributions, it seems likely that throughout the opening phase of the 1991 eruption, vesiculation conditions became increasingly homogeneous. These conditions then continued in phase 2 of the eruption (as shown by the samples from the East cone location). This, together with the overall intensity decrease (Fig. 2) indicate that magmatic volatiles rose coupled to the magma in the beginning of the eruption but with time became decoupled as intensity decreased.

Eruptive parameters

The mass of tephra deposited during the opening phase of 8.6×10^9 kg reflects fine spatial resolution in the proximal and medial areas, and coarse resolution in the distal area. In fact, the most distal isomass contour is only constrained by

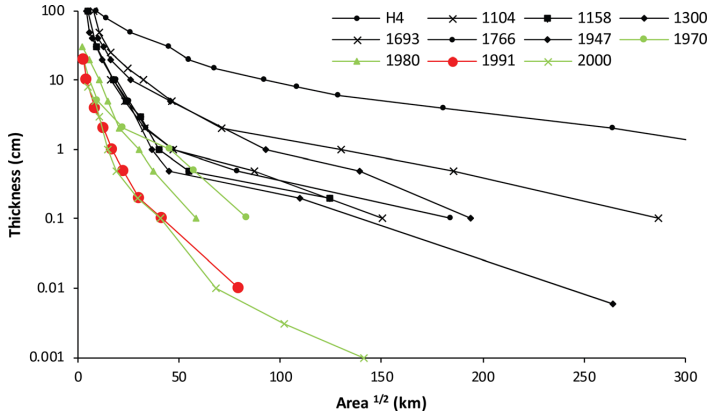

Fig. 12 Thickness vs √Area for selected post glacial explosive Hekla eruptions. Legend indicates year of eruption for all but H4 which is a ~4300-year-old event. *Black lines and symbols* are pre 1970 eruptions. *Green* are the 1970, 1980 and 2000 eruptions, and in *red* the 1991 eruption. Sources for thickness and area data: H4 from Larsen and Thorarinsson (1977), 1104 to 1766 from Janebo et al. (2016), 1947 from Thorarinsson (1968), 1970 from Thorarinsson and Sigvaldason (1972), 1980 from Grönvold et al. (1983), 2000 from Haraldsson (2001), and 1991 from this study

one point on the downwind side (Fig. 3a). Mass estimate of the tephra fall deposits without this 0.1 kg m^{-2} results in larger apparent mass for both exponential and Weibull fits (9.1 to 9.6 × 10^9 kg).

The MER (2.9 × 10^6 kg s^{-1}) obtained from the mass of the deposits and the duration of the opening phase is a time average value, although the empirically derived plume heights are in good agreement with observations in 1991 (Gudmundsson et al. 1992). The strong wind during the eruption affected tephra fall (Fig. 2) and likely decreased the plume height. The method of Degruyter and Bonadonna (2012), which takes the effect of wind into account, indicates that even a plume height of 10.3 a.s.l. would correspond to a MER of 3.4 to 4.3 × 10^6 kg s^{-1} whereas the reported plume height of 11.5 km a.s.l. would correspond to a MER of 6.9 to 8.6 × 10^6 kg s^{-1}, and plume height of 12.7 km a.s.l. results in MER of 1.3 to 1.6 × 10^7 kg s^{-1} (Supplementary Table 2). This indicates that at peak discharge in 1991 the MER was higher than the time averaged and the wind field did affect the ability of the eruption plume to rise fully. Nonetheless, the MER calculated from a 11.5-km a.s.l. high plume is probably at the higher end for Hekla 1991, as pilots and the weather radar report this altitude. Also Hekla eruption plumes are known to be vapour rich (i.e. 1947 eruption), and the weather radar will also detect the signal from ice and snow particles in the plume (Thorarinsson 1968; Lacasse et al. 2004). There is thus potentiality that the measured and observed plume top is higher than the buoyancy level of pyroclasts in the plume. Scaling parameter Π of 0.2 to 0.26 classifies the 1991 eruption plume as transitional similarly to the climactic Cordón Caulle plume (4–6 June, Bonadonna et al. 2015b) and parts of the May 2010 Eyjafjallajökull plume (Degruyter and Bonadonna 2012).

Conditions of tephra fall

Deposition from the opening phase was to the NNE of Hekla (Fig. 3). The short duration of the explosive activity coupled with a strong wind field probably did not result in a radially spreading umbrella cloud and minimal upwind deposition. A rapid initial drop in mass of tephra deposited along the dispersal axis coincides with deposition of predominantly lapilli during the first 25 km (Figs. 8b, c and 11b), and then more gradual decrease in mass deposition occurred as coarse ash dominates the deposit (>50 wt%). After 65 km, the proportion of fine ash becomes substantial in the deposit (40–20 wt%). This is consistent with size fractionation from a laterally spreading plume and gravitational settling in a turbulent to intermediate regime (Óskarsson 1980; Bursik et al. 1992; Sparks et al. 1992; Bonadonna et al. 1998). Along the dispersal axis, the distance where Md_φ and Max_φ values level out on Fig. 8b fits roughly with 1 kg m^{-2} isomass line and the 0.2-cm isopach line (60 and 50 km, respectively; Fig. 3) and the last break-in-slope on Fig. 11. Most likely deposition beyond 65 km was characterized by laminar-regime sedimentation (Bonadonna et al. 1998; Bonadonna and Phillips 2003). The deposited material has a mode at 2.5 to 3.5 φ, similar to the finer mode of the TGSD (Fig. 10). There is no significant decrease in grain-size with increasing distance from vent. This is consistent with models where decrease in thinning rate with distance is to be expected when fine ash becomes major part of the deposit (Bonadonna et al. 1998).

The changes in grain-size with transport are considered to reflect the settling velocity and continuous decrease in turbulence and carrying capacity of the plume until around 65 km from went. High sorting (0.9–3 σ_φ) values during the first 25 km reflect the limited carrying capacity of the plume as most of the mass is deposited within this distance (Figs. 8b and c). Premature sedimentation of ash could have been enhanced by various processes, e.g. induced by snow and as aggregates. Transition to a laminar sedimentation regime and dilution of the plume is marked with no drop in Md_φ and Max_φ.

Total grain-size distribution

Our results show a bimodal TGSD, with a coarse (−3.5 to −2.5 φ) and a fine peak (2.5 to 3.5 φ). The two subpopulations equate to the grain-size modes of samples <10 km from Hekla and 50–120 km from Hekla (Fig. 8a). Bimodal TGSD as reported here is not uncommon. It is a common feature of Hekla eruptions, e.g. from the eruptions in 1104, 1300, 1693, 1766, 1970, and 2000 (Óskarsson 1980; Biass et al. 2014; Janebo 2016). Polymodal TGSD have also been observed in eruptions from other volcanoes, e.g. Mt. St Helens 1980 (Carey and Sigurdsson 1982; Durant et al. 2009), Mt. Spurr 1992 (Durant and Rose 2009), and El Chichón 1982 (Varekamp et al. 1984; Rose and Durant 2009). However, for these non-Icelandic eruptions the polymodal distribution can largely be linked to coeval sedimentation from co-pyroclastic density current (PDC) plumes. For deposits with co-PDC contributions, the fine mode lies at ~5–6 φ (Eychenne et al. 2015), in comparison to at 2.5 to 3.5 φ for Hekla 1991. Deposition from a co-PDC plume cannot explain the bimodality for the Hekla 1991 TGSD, as no PDCs were observed during the eruption.

TGSD are very sensitive to the reconstruction method used, but other studies where the TGSD has been computed with same method as here show either unimodal or bimodal TGSDs. Unimodal TGSDs have been reported for, e.g. the Chaitén 2008 eruption (Alfano et al. 2016), the Ruapehu 1996 event (Bonadonna and Houghton 2005), and several subplinian eruptions of Etna (e.g. Scollo et al. 2007; Andronico et al. 2008; Andronico et al. 2009; Andronico et al. 2014) whereas a bimodal distribution is seen for the 2011 eruption of Cordón Caulle (Bonadonna et al. 2015a). In all these eruptions, the TGSD is a result of the primary fragmentation of the magma, and specifically for Cordón Caulle

2011, the shape of the TGSD and significant lack of particles in the 3 φ category was inferred to be a result of complex textural features of the highly vesicular magma (Bonadonna et al. 2015a). The reason for bimodal TGSD is not obvious, but for Hekla 1991 we consider the possibility that the bimodal distribution is a result of the primary fragmentation mechanism of the magma in the shallow conduit. However, the eruptive products of the Hekla 1991 eruption do not show variable texture matching that of the 2011 Cordón Caulle products. Based on the available data, other processes leading to bimodal TGSD cannot be ruled out. Possibilities are e.g. phreatomagmatic activity (which however is unlikely at Hekla), poor sample cover or secondary granulation of lapilli-sized clasts in the conduit, thrust region or the rising plume similarly to what has been proposed to be the source for bimodality of the TGSD from Mt. Spurr 1992 (Durant and Rose 2009).

Although the Voronoi method is designed for non-uniform deposits, the lack of data points between 125 and 195 km from Hekla must be addressed as possible source for TGSD bimodality. Gaps in the dataset might produce TGSDs that are not representative of the associated tephra deposits (Alfano et al. 2016). Lack of the most distal data points however, does not significantly alter the TGSD (Bonadonna et al. 2015a; Alfano et al. 2016). This is due to lower mass contribution and less variability in grain-size distribution of distal samples. The sample gap from 115 to 195 km downwind in the 1991 Hekla dataset (Fig. 8; Supplementary Fig. 1) is in area of low mass accumulation (Fig. 3a) and stable deposited grain-size distribution (Fig. 8b). Therefore, the source of bimodality is not considered to be the spacing of samples. However, this probably results in underestimation of mass contribution of fines in the TGSD (Fig. 10). Thus, the TGSD is considered good approximation and a conservative estimate of mass contributions by ash.

In eruptions where secondary granulation of particles has been proposed as source for bimodal TGSD (i.e. Mt. Spurr 1992) and by co-ignimbrite plumes (i.e. Mt. St Helens 1980), fine ash (<63 μm; >4 φ) is a substantial component of the TGSD (Durant and Rose 2009). In Hekla 1991, fine ash is not a substantial component (Fig. 10).

Therefore, we consider the bimodal TGSD of the Hekla 1991 tephra fall to be a product of the primary fragmentation mechanism(s) taking place in the shallow conduit, and possibly influenced by the pulsating behaviour of the eruption.

Summary and conclusions

The 50-min-long opening subplinian phase of the Hekla 1991 eruption produced a deposit of 8.6×10^9 kg and 0.17 km^3 (0.003 km^3 DRE), with an average mass eruption rate of 2.9×10^6 kg s^{-1} (1100 m^3 s^{-1}). The transitional volcanic plume rose to 11.5 ± 1.2 km in ~10 min. The eruption cloud drifted to the NNE producing a well-defined tephra layer made up of lapilli fall deposits and early-sedimented fines over the first 25 km. There was a gradual decrease in plume turbulence over the first 65 km of transport from vent, as is illustrated by good sorting (from 25 km) and effective size fractionation of tephra. At the 65-km mark, particle sedimentation transitioned to a laminar regime marked with no drop in Md_φ and Max_φ. This coupled with the TGSD indicates that the lapilli-dominated TGSD mode was deposited mostly during the first 25 km of transport. From 25 to 65 km, coarse ash dominates the deposit, whereas the finer TGSD mode coincides with grain-sizes of samples from 65 km onwards. The proximal deposits indicate deposition of tephra from a sustained atmospheric plume with a pulsating source, and snow-enhanced deposition of fines. The calculated TGSD of the deposit is bimodal, and inferred to reflect the primary fragmentation of the magma.

Acknowledgements This work was supported by Icelandic Centre for Research grant 110077-0061, the Landsvirkjun Energy Research Fund grant 02-2012, the south Iceland research fund 2014, and NSF EAR-12-20596. Special thanks to William Moreland, Christopher Lofthouse, Lee Masson, Simon N. Lauritssen, Elísa Ólafsdóttir, Maria Janebo, and Sigurður Gústafsson for fieldwork assistance. The manuscript was improved significantly by comments from M. Janebo, two anonymous reviewers, executive editor J.D.L White, and editor C. Bonadonna.

References

Alfano F, Bonadonna C, Watt S, Connor C, Volentic A, Pyle DM (2016) Reconstruction of total grain size distribution of the climactic phase of a long-lasting eruption: the example of the 2008–2013 Caitén eruption. Bull Volcanol 78:46. doi:10.1007/s00445-016-1040-5

Andronico D, Scollo S, Caruso S, Cristaldi A (2008) The 2002-03 Etna explosive activity: tephra dispersal and features of the deposits. Journal of Geophysical Research: Solid Earth 113(4):1–16

Andronico D, Scollo S, Cristaldi A, Ferrari F (2009) Monitoring ash emission episodes at Mt. Etna: the 16 November 2006 case study. J Volcanol Geotherm Res 180:123–134

Andronico D, Scollo S, Lo Castro MD, Cristaldi A, Lodato L, Taddeucci J (2014) Eruption dynamics and tephra dispersal from the 24 November 2006 paroxysm at South-East Crater, Mt Etna, Italy. J Volcanol Geotherm Res 274:78–91

Biass, S., & Bonadonna, C. (2014). TOTGS: Total grainsize distribution of tephra fallout. Retrieved from https://vhub.org/resources/3297

Biass S, Scaini C, Bonadonna C, Folch A, Smith K, Höskuldsson A (2014) A multi-scale risk assessment for tephra fallout and airborne concentration from multiple Icelandic volcanoes—part 1: hazard assessment. Nat Hazards Earth Syst Sci 14:2265–2287

Bonadonna C, Costa A (2012) Estimating the volume of tephra deposits: a new simple strategy. Geology 40(5):415–418

Bonadonna C, Costa A (2013) Plume height, volume, and classification of explosive volcanic eruptions based on the Weibull function. Bull Volcanol 75:1–19

Bonadonna C, Houghton BF (2005) Total grain-size distribution and volume of tephra-fall deposits. Bull Volcanol 67(5):441–456

Bonadonna C, Phillips JC (2003) Sedimentation from strong volcanic plumes. J Geophys Res 108:1–28

Bonadonna C, Ernst GGJ, Sparks RSJ (1998) Thickness variations and volume estimates of tephra fall deposits: the importance of particle Reynolds number. J Volcanol Geotherm Res 81(3–4):173–187

Bonadonna C, Cioni R, Pistolesi M, Elissondo M, Baumann V (2015a) Sedimentation of long-lasting wind-affected volcanic plumes: the example of the 2011 rhyolitic Cordón Caulle eruption, Chile. Bull Volcanol 77:13

Bonadonna C, Pistolesi M, Cioni R, Degruyter W, Elissondo M, Baumann V (2015b) Dynamics of wind-affected volcanic plumes: the example of the 2011 Cordón Caulle eruption, Chile. Journal of Geophysics Research: Solid Earth 120:2242–2261

Bursik MI, Sparks RSJ, Gilbert JS, Carey SN (1992) Sedimentation of tephra by volcanic plumes: I. Theory and its comparison with a study of the Fogo A Plinian deposit, Sao Miguel (Azores). Bull Volcanol 54:329–344

Carey SN, Sigurdsson H (1982) Influence of particle aggregation on deposition of distal tephra from the May 18, 1980, eruption of Mount St. Helens volcano. Journal of Geophysical Research: Solid Earth 87(B8):7061–7072. doi:10.1029/JB087iB08p07061

Carey S, Sparks RSJ (1986) Quantitative models of the fallout and dispersal of tephra from volcanic eruption columns. Bull Volcanol 48: 109–125

Carey RJ, Houghton BF, Thordarson T (2009) Tephra dispersal and eruption dynamics of wet and dry phases of the 1875 eruption of Askja Volcano, Iceland. Bull Volcanol 72(3):259–278

Degruyter W, Bonadonna B (2012) Improving on mass flow rate estimates of volcanic eruptions. Geophys Res Lett 39:1–6

Durant AJ, Rose WI (2009) Sedimentological constraints on hydrometeor-enhanced particle deposition: 1992 eruptions of Crater Peak, Alaska. J Volcanol Geotherm Res 186(1–2):40–59

Durant AJ, Rose WI, Carey S, Volentik ACM (2009) Hydrometeor-enhanced tephra sedimentation: constraints from the 18 May 1980 eruption of Mount St. Helens. Journal of Geophysical Research 114: 1–21

Eychenne J, Pennec J-L, Troncoso L, Gouhier M, Nedelec J-M (2011) Causes and consequences of bimodal grain-size distribution of tephra fall deposited during the August 2006 Tungurahua eruption (Ecuador). Bull Volcanol 74(1):187–205

Eychenne J, Cashman K, Rust A, Durant A (2015) Impact of the lateral blast on spatial pattern and grain size characteristics of the 18 May 1980 Mount St. Helens fallout deposits. J Geophys Res Solid Earth 120:6018–6038

Fierstein J, Nathenson M (1992) Another look at the calculation of fallout tephra volumes. Bull Volcanol 54(2):156–167

Grönvold K, Larsen G, Einarsson P, Thorarinsson S, Saemundsson K (1983) The Hekla eruption 1980-1981. Bull Volcanol 46:350–363

Gudmundsson A, Sæmundsson K (1992) Heklugosið 1991: Gangur gossins og aflfræði Heklu. Náttúrufræðingurinn 61:145–158

Gudmundsson A, Oskarsson N, Grönvold K, Saemundsson K, Sigurdsson O, Stefansson R, Thordarson T (1992) The 1991 eruption of Hekla, Iceland. Bull Volcanol 54(3):238–246

Gurioli L, Houghton BF, Cashman KV, Cioni R (2005) Complex changes in eruption dynamics during the 79 AD eruption of Vesuvius. Bull Volcanol 67(2):144–159. doi:10.1007/s00445-004-0368-4

Haraldsson KÖ (2001) The Hekla 2000 eruption, distribution of ash from the first days of the eruption (in Icelandic). BSc thesis. University of Iceland, Reykjavík

Höskuldsson Á, Óskarsson N, Pedersen R, Grönvold K, Vogfjörð K, Ólafsdóttir R (2007) The millennium eruption of Hekla in February 2000. Bull Volcanol 70(2):169–182

Houghton BF, Wilson CJN (1989) A vesicularity index for pyroclastic deposits. Bull Volcanol 51:451–462

Houghton BF, Wilson CJN, Del Carlo P, Coltelli M, Sable JE, Carey R (2004) The influence of conduit processes on changes in style of basaltic Plinian eruptions: Tarawera 1886 and Etna 122 BC. J Volcanol Geotherm Res 137:1–14

Inman D (1952) Measures for describing the size distribution of sediments. J Sediment Petrol 22(3):125–145

Jakobsson S (1979) Petrology of recent basalts of the Eastern Volcanic Zone, Iceland. Acta Naturalia Islandica 26:1–103

Janebo MH (2016) Historical explosive eruptions in Hekla and Askja volcanoes; eruption dynamics and source parameters. PhD dissertation. University of Hawaii at Manoa, Honolulu

Janebo MH, Thordarson T, Houghton BF, Larsen G, Carey RJ (2016) Dispersal of key subplinian-Plinian tephra from Hekla volcano, Iceland: implications for eruption source parameters. Bull Volcanol 78. doi:10.1007/s00445-016-1059-7

Jóhannesson H, Einarsson S (1990) Glefsur úr sögu hrauna og jarðvegs sunnan Heklu. In: Arnalds A (ed) Græðum Ísland. Landgræðslan, Reykjavik, pp 123–136

Jóhannesson H, Sæmundsson K (1998) Geological map of Iceland, 1: 500.000 bedrock geology, Reykjavik. Náttúrufræðistofnun Íslands, Reykjavík

Kaminski E, Jaupart C (1998) The size distribution of pyroclasts and the fragmentation sequence in explosive volcanic eruptions. J Geophys Res 103(98):29759–29779

Klug C, Cashman KV (1996) Permeability development in vesiculating magmas: implications for fragmentation. Bull Volcanol 58:87–100

Kueppers, U., Scheu, B., Spieler, O., & Dingwell, D. B. (2006). Fragmentation efficiency of explosive volcanic eruptions: a study of experimentally generated pyroclasts, 153, 125–135

Lacasse C, Karlsdóttir S, Larsen G, Soosalu H, Rose WI, Ernst GGJ (2004) Weather radar observations of the Hekla 2000 eruption cloud, Iceland. Bull Volcanol 66:457–473

Larsen G, Thorarinsson S (1977) H4 and other acid Hekla tephra layers. Jökull 27:28–46

Larsen G, Vilmundardóttir EG, Thorkelsson B (1992) Heklugosið 1991 : Gjóskufallið og gjóskulagið frá fyrsta degi gossins. Náttúrufræðingurinn 61:159–176

Lautze NC, Houghton BF (2006) Linking variable explosion style and magma textures during 2002 at Stromboli Volcano, Italy. Bull Volcanol 69(4):445–460

Linde AT, Agustsson K, Sacks IS, Stefansson R (1993) Mechanism of the 1991 eruption of Hekla from continuous borehole strain monitoring. Nature 365(21):737–740

Mastin LG, Guffanti M, Servranckx R, Webley P, Barsotti S, Dean K, Waythomas CF (2009) A multidisciplinary effort to assign realistic source parameters to models of volcanic ash-cloud transport and dispersion during eruptions. J Volcanol Geotherm Res 186(1–2): 10–21

Newhall CG, Self S (1982) The volcanic explosivity index (VEI) an estimate of explosive magnitude for historical volcanism. J Geophys Res 87(C2):1231

Oddsson B, Gudmundsson MT, Larsen G, Karlsdóttir S (2012) Monitoring of the plume from the basaltic phreatomagmatic 2004 Grímsvötn eruption—application of weather radar and comparison with plume models. Bull Volcanol 74:1395–1407

Óskarsson N (1980) The interaction between volcanic gases and tephra: fluorine adhering to tephra of the 1970 Hekla eruption. J Volcanol Geotherm Res 8:251–266

Polacci M, Baker DR, Mancini L, Polacci M, Baker DR, Mancini L, Tromba G (2006) Three dimensional investigation of volcanic textures by X-ray microtomography and implications for conduit processes. Geophys Res Lett 33:1–5

Pyle DM (1989) The thickness, volume and grainsize of tephra fall deposits. Bull Volcanol 51:1–15

Rose WI, Durant AJ (2009) El Chichón volcano, April 4, 1982: volcanic cloud history and fine ash fallout. Nat Hazards 51(2):363–374

Sæmundsson K (1979) Outline of the geology of Iceland. Jökull 29:7–28

Scollo S, Del Carlo P, Coltelli M (2007) Tephra fallout of 2001 Etna flank eruption: analysis of the deposit and plume dispersion. J Volcanol Geotherm Res 160(1–2):147–164

Soosalu H, Einarsson P, Jakobsdottir S (2003) Volcanic tremor related to the 1991 eruption of the Hekla Volcano, Iceland. Bull Volcanol 65(8):562–577

Sparks RSJ, Bursik MI, Ablay GJ, Thomas RME, Carey SN (1992) Sedimentation of tephra by volcanic plumes. Part 2: controls on thickness and grain-size variations of tephra deposits. Bull Volcanol 54:685–695

Sparks RSJ, Bursik MI, Carey SN, Gilbert JS, Glaze LS, Sigurdsson H, Woods AW (1997) Volcanic plumes, 1st edn. Wiley, Chichester

Stevenson, J., Larsen, G., & Thordarson, T. (2015). Physical volcanology of the prehistoric Hekla 3 and Hekla 4 eruptions, Iceland. *EGU General Assembly*, *abstract id.4207*

Thorarinsson S (1968) Heklueldar. Rangæingafélagið, Reykjavik

Thorarinsson S, Sigvaldason GE (1972) The Hekla eruption of 1970. Bull Volcanol 36(2):269–288

Thordarson T, Larsen G (2007) Volcanism in Iceland in historical time: volcano types, eruption styles and eruptive history. J Geodyn 43(1): 118–152

Þráinsson, B. Þ. (1991). *Iceland national radio, 19:00 news*, January 17th 1991

Varekamp JC, Luhr JF, Prestegaard KL (1984) The 1982 eruptions of El Chichón Volcano (Chiapas, Mexico): character of the eruptions, ash-fall deposits, and gas phase. J Volcanol Geotherm Res 23(1–2):39–68

Walker GPL (1973) Explosive volcanic eruptions—a new classification scheme. Geol Rundsch 62(2):431–556

Supplementary document 1

The opening subplinian phase of the Hekla 1991 eruption: properties of the tephra fall deposit

Jonas Gudnason[1,3], Thor Thordarson[1], Bruce F. Houghton[2] and Gudrun Larsen[3]

[1]Faculty of Earth Sciences, University of Iceland

[2]Department of Geology and Geophysics, University of Hawaii

[3]Institute of Earth Sciences, University of Iceland

Corresponding author: Jonas Gudnason jog4@hi.is

Chemical composition

Glass chemistry of the 1991 tephra was analysed on a WDS Cameca SX100 electron microprobe at the Laboratoire Magmas et Volcans, Clermont –Ferrand (LMV). Standard used was natural glass from Kilauea (A99), the analytical conditions used were 15 kV voltage and 4 nA current and 10 µm beam diameter. Counting time was 10 s for Na, CA, Ti, P and Si; 20 s for Mg and Al; 30 s for Mn and 40 s for Fe and K. Before the session 10 points were measured on the standard (A99), when compared to other reported results they are indistinguishable apart from systematically higher titanium at LMV (Table 1; Jarosewich et al., 1980; Oladottir et al., 2011; Thornber et al., 2002).

The 1991 products are intermediate transitional alkalic and are basaltic icelandites (Table 1; Jakobsson et al 2008). Holocene magmatic activity at Hekla features an igneous rock series extending from mildly alkaline basalt to a sub-alkaline rhyolite, including transitional basaltic icelandites and subalkaline icelandites. Isotopic studies indicate that they are genetically unrelated and that the formation of the basaltic icelandites results from fractional crystallization of the basaltic parental magma (Sigmarsson, 1992).

When comparing the major elemental composition of tephra from the opening phase and later formed lava in the basaltic icelandite eruptions at Hekla during the latter half of the 20th century the observed differences are minimal (Table 2). For example, the difference in concentration of highly incompatible elements, such as K_2O, between the tephra and lava is <0.25 wt %, and the difference in SiO_2 concentration is only 0.65 wt % (i.e. ≤1%; Table 2). The magma produced by other post 1947 Hekla eruptions are very similar to that produced by the 1991 event (Table 2; Gronvold et al., 1983; Gudmundsson et al., 1992; Höskuldsson et al., 2007; Thorarinsson & Sigvaldason, 1970; Thorarinsson, 1968). Of the 20th century events, only the 1947 eruption exhibits significant temporal variation in terms of major element composition, where the tephra from the

initial phase is high silica icelandite (SiO_2, 62.11 wt %) while the later formed lava is basaltic icelandite (SiO_2, 54.25 wt%; Table 2).

Table 1: Chemical composition of the standard VG-A99 as acquired on the electron microprobe at Laboratorie Magmas et Volcans LMV (this study) compared to published values: USGS (Thornber et al 2000), USNM (Jarosewich et al 1979), LMV (A) (Oladottir et al 2011). Numbers in brackets are one sigma standard deviation

	VG-A99			
	USGS	USNM	LMV (A)	LMV (this study)
SiO_2	51.06 (0.46)	50.94	51.00 (0.54)	50.85 (0.35)
TiO_2	3.95 (0.09)	4.06	4.17 (0.06)	4.16 (0.06)
Al_2O_3	12.44 (0.13)	12.49	12.65 (0.15)	12.65 (0.10)
FeO	13.15 (0.16)	13.3	13.20 (0.29)	13.31 (0.18)
MnO	0.19 (0.02)	0.15	0.20 (0.07)	0.20 (0.007)
MgO	5.04 (0.1)	5.08	5.01 (0.09)	5.02 (0.07)
CaO	9.04 (0.11)	9.3	9.14 (0.09)	9.16 (0.04)
Na_2O	2.72 (0.16)	2.66	2.69 (0.11)	2.77 (0.11)
K_2O	0.82 (0.03)	0.82	0.86 (0.02)	0.85 (0.02)
P_2O_5	0.43 (0.03)	0.38	0.46 (0.02)	0.44 (0.05)
Total	98.84	99.18	99.35	99.42

Table 2: Comparison of the 20th century Hekla eruptions; Hekla 1947 tephra and lava [1](Thorarinsson and Sigvaldason 1970); Hekla 1970 tephra and lava [1](Thorarinsson and Sigvaldason 1970); Hekla 1980 tephra and lava [2](Gronvold et al. 1980); Hekla 1991 tephra average of 10 glass shards (this study) 1991 lava (Gudmundsson et al 1992) and H2000 average of 20 tephra and lava samples, according to authors undistinguishable between the two products [4](Hoskuldsson et al. 2007).

Hekla	1947		1970		1980		1991		2000
	tephra - opening phase	lava - effusive phase	tephra - opening phase	lava - effusive phase	tephra - opening phase	lava - effusive phase	**tephra - opening phase**	lava - effusive phase	Average of lava and tephra
SiO_2	62.11	54.25	55.21	54.52	54.50	54.60	**55.45**	54.90	55.52
TiO_2	1.02	1.54	1.83	1.91	1.91	1.91	**2.32**	2.09	2.07
Al_2O_3	16.17	16.34	15.16	14.80	14.60	14.70	**13.71**	14.30	14.54
FeO	7.75	11.28	11.52	11.78	11.70	11.40	**12.30**	11.59	11.79
MnO	0.18	0.26	0.26	0.26	0.22	0.24	**0.33**	0.27	0.28
MgO	1.63	3.39	2.86	3.03	2.90	2.87	**2.82**	2.91	2.89
CaO	5.24	5.24	6.81	6.76	7.09	7.12	**6.26**	7.06	6.82
Na_2O	4.12	4.12	4.16	4.08	4.03	3.98	**3.59**	4.18	4.01
K_2O	0.98	0.98	1.26	1.24	1.16	1.19	**1.45**	1.22	1.21
P_2O_5	0.34	0.34	0.68	0.71	0.85	0.86	**1.25**	1.34	0.87
Total	99.54	97.74	99.75	99.09	98.96	98.87	**99.47**	99.86	100.00
Source	1	1	1	1	2	2	**This study**	3	4

References

Grönvold, K., Larsen, G., Einarsson, P., Thorarinsson, S., & Saemundsson, K. (1983). The Hekla

Eruption 1980-1981. *Bulletin of Volcanology*.

Gudmundsson, A., Oskarsson, N., Grönvold, K., Saemundsson, K., Sigurdsson, O., Stefansson, R., … Thordarson, T. (1992). The 1991 eruption of Hekla, Iceland. *Bulletin of Volcanology*, *54*(3), 238–246. doi:10.1007/BF00278391

Höskuldsson, Á., Óskarsson, N., Pedersen, R., Grönvold, K., Vogfjörð, K., & Ólafsdóttir, R. (2007). The millennium eruption of Hekla in February 2000. *Bulletin of Volcanology*, *70*(2), 169–182. doi:10.1007/s00445-007-0128-3

Jakobsson, S. P., Jónasson, K., & Sigurðsson, I. a. (2008). The three igneous rock series of Iceland. *Jökull*, *58*(58), 117–138.

Jarosewich, E., Nelen, J. A., & Norberg, J. A. (1980). Reference Samples for Electron Microprobe Analysis. *Geostandards Newsletter*, *4*(1), 43–47. doi:10.1111/j.1751-908X.1980.tb00273.x

Oladottir, B. a., Sigmarsson, O., Larsen, G., & Devidal, J.-L. (2011). Provenance of basaltic tephra from Vatnajokull subglacial volcanoes, Iceland, as determined by major- and trace-element analyses. *The Holocene*, *21*(7), 1037–1048. doi:10.1177/0959683611400456

Thorarinsson, S., & Sigvaldason, G. E. (1972). The Hekla Eruption of 1970. *Bulletin Volcanologique*, *36*(2), 269–288. doi:10.1007/BF02596870

Thornber, B. C. R., Sherrod, D. R., Siems, D. F., Heliker, C. C., Gregory, P., Oscarson, R. L., & Kauahikaua, J. P. (2002). Whole-rock and glass major-element geochemistry of Kilauea Volcano , Hawaii , near-vent eruptive products : September 1994 through September 2001. *USGS, Open File Report 02-17*, 1–9.

Supplementary table 1 Locations of grain-size samples

Sample	distance from Hekla (km)	Latitude	Longitude
J12-51	5	64.021830	-19.599870
150-140	5	64.032750	-19.613000
10	23	64.173930	-19.446980
33	21	64.157540	-19.461880
41	24	64.190390	-19.484150
47	24	64.199410	-19.593650
120	27	64.206820	-19.399080
37	30	64.166400	-19.210930
105	39	64.305940	-19.343340
108	52	64.414900	-19.171880
51	47	64.286600	-18.999920
55	40	64.195730	-19.005370
8	26	64.189170	-19.375620
90	13	64.075970	-19.487370
93	17	64.057100	-19.359880
19	13	64.107470	-19.684330
21	11	64.085580	-19.620730
Kö	57	64.359810	-18.858320
Blau	82	64.658795	-18.965257
EY	91	64.615119	-18.473532
Svart	78	64.533758	-18.660314
Dratt	70	64.479534	-18.757478
Stó	68	64.449473	-18.747272
Hofsjökull 4	115	64.961300	-18.856416
Þjórsárjökull	104	64.795395	-18.592445
Lundabrekka	196	65.458267	-17.394550

Supplementary table 2 Results from the MER calculation after Degruyter and Bonadonna (2012)

Wind speed ($m\ s^{-2}$)	Magma temp. (K)	Plume height above vent (km)	Plume height a.s.l. (km)	Scaling parameter (II)	MER ($kg\ s^{-1}$)
20	1373	8.8	10.3	0.2068	3.4×10^6
20	1173	8.8	10.3	0.2068	4.3×10^6
20	1373	10	11.5	0.2336	6.9×10^6
20	1173	10	11.5	0.2336	8.6×10^6
20	1373	11.2	12.7	0.2628	1.3×10^7
20	1173	11.2	12.7	0.2628	1.6×10^7

Supplementary figure 1: The Hekla 1991 tephra fall, sample locations, and Voronoi polygons.

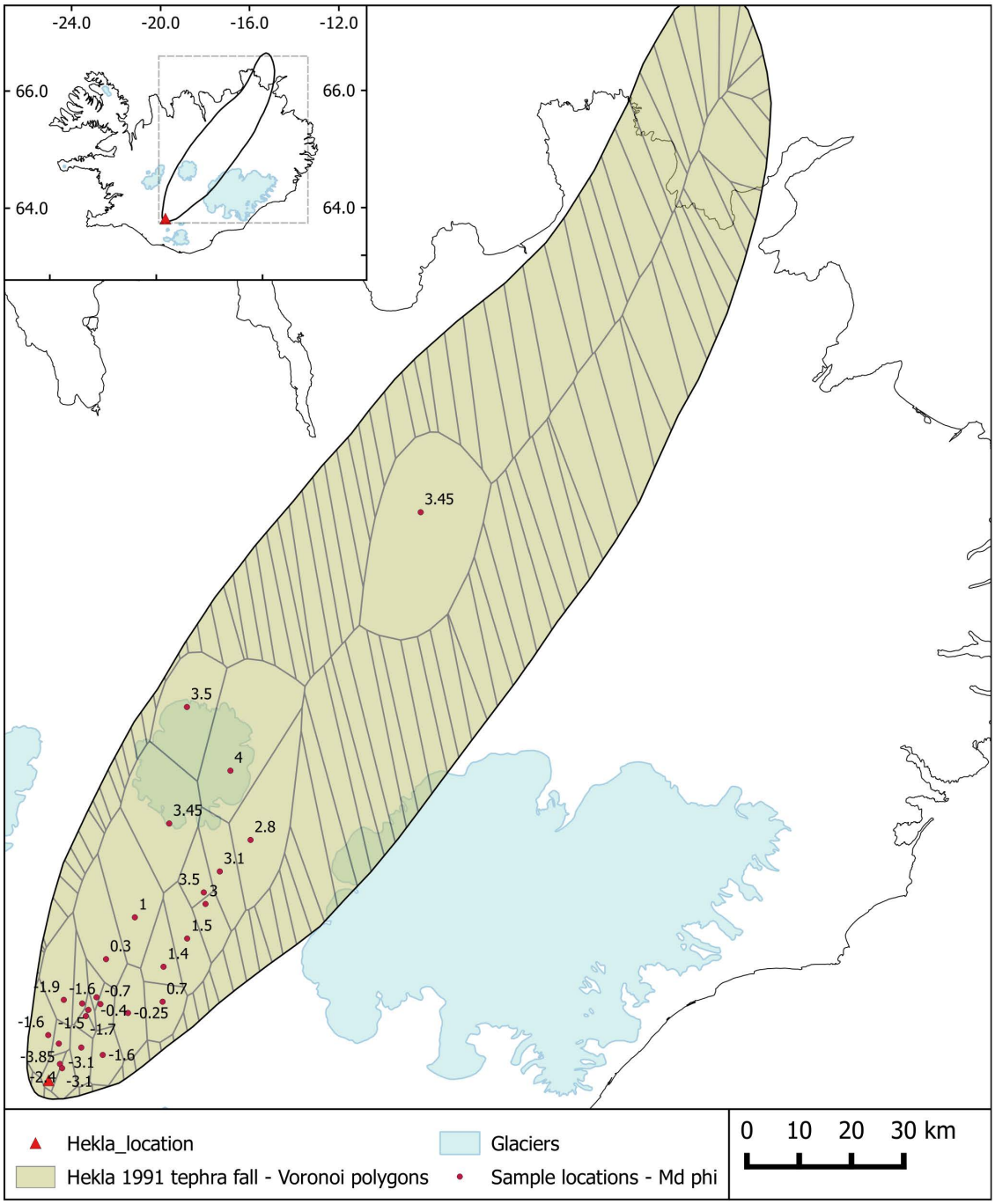

Paper 2

The 1845 Hekla eruption: grain-size characteristics of a tephra layer

Jónas Guðnason, Þorvaldur Þórðarson, Bruce F. Houghton, Guðrún Larsen

Submitted to Journal of Volcanology and Geothermal Research

The 1845 Hekla eruption: grain-size characteristics of a tephra layer.

Jonas Gudnason[1,3], Thor Thordarson[1], Bruce F. Houghton[2] and Gudrun Larsen[3]

[1]Faculty of Earth Sciences, University of Iceland

[2]Department of Geology and Geophysics, University of Hawaii

[3]Institute of Earth Sciences, University of Iceland

Corresponding author: Jonas Gudnason jog4@hi.is

Keywords Hekla; total grain-size distribution; aggregation; tephra

Acknowledgements This work was supported by Icelandic Centre for Research grant 110077-0061, the Landsvirkjun Energy Research Fund grant 02-2012, the south Iceland research fund 2014, and NSF EAR-12-20596. Special thanks to William Moreland, Christopher Lofthouse, Simon N. Lauritsen, Elísa Ólafsdóttir, Maria Janebo, and Sigurður Gústafsson for fieldwork assistance.

Manuscript submitted to the Journal of Volcanology and Geothermal Research

Abstract

The 1845 eruption is commonly viewed as a typical Hekla eruption. It is a key event in the eruptive history of the volcano, as it is one of the best documented Hekla eruptions, in terms of contemporary accounts and observations. The eruption started on 2 September 1845 with an intense, hour long explosive phase that transitioned into effusive activity, ending on the 16th of March 1846. The amount of tephra produced in the opening phase was 0.13 km^3 / 7.5 x 10^{10} kg. The total grain-size distribution of the deposit is bimodal with a dominating coarse mode at -2.5 ϕ (5.6 mm) and a broader finer mode at 3 to 4.5 ϕ (0.125 to 0.045 mm). Premature deposition of ash throughout the opening phase and across the whole deposit is reflected in the bimodal grain-size distribution. Deconvolved grain-size distributions exhibit distinctly different sedimentation patterns of the coarse and fine subpopulations. The coarser lapilli dominated subpopulation fines rapidly with transport, while the finer ash dominated subpopulation shows less changes with distance, indicating premature sedimentation of fines by aggregation from the 1845 volcanic plume. Tephra deposition was to the ESE of the volcano from a 19 km (a.s.l.) high eruption plume. Tephra was transported at speeds of 16–19 m s^{-1}. Deposition was reported on and near the Faroe and Shetland Islands, 700 to 1100 km away from Hekla, illustrating the potential of even moderate-sized Hekla eruptions to affect very large parts of European air-space.

1. Introduction

Explosive volcanic eruptions in Iceland pose threats to the local population, livestock, and infrastructure through deposition of tephra (e.g., Óskarsson, 1980; Horwell and Baxter, 2006; Gíslason et al., 2011; Biass et al., 2014). Ash-laden eruption plumes can also cause widespread disruption to air traffic via dispersal of fine ash into atmospheric levels travelled by jet aircraft (e.g., Durant and Rose, 2009; Gudmundsson et al., 2012; Kueppers et al., 2014; Stevenson et al., 2015). Hekla (63.98°N, 19.70°W; 1490 m a.s.l.) and its surrounding volcanic system sits within the Eastern Volcanic Zone (EVZ) in southern Iceland (Fig. 1). It is the central volcano for the Hekla volcanic system, which is 60 km long and 19 km wide and covers 720 km^2. Hekla volcano is elongated SW–NE with a linear vent system that stretches ~5 km and becomes fully, or nearly fully, active during most eruptions (e.g., Erlendsson, 1847; Thorarinsson and Sigvaldason, 1972; Grönvold et al., 1983).

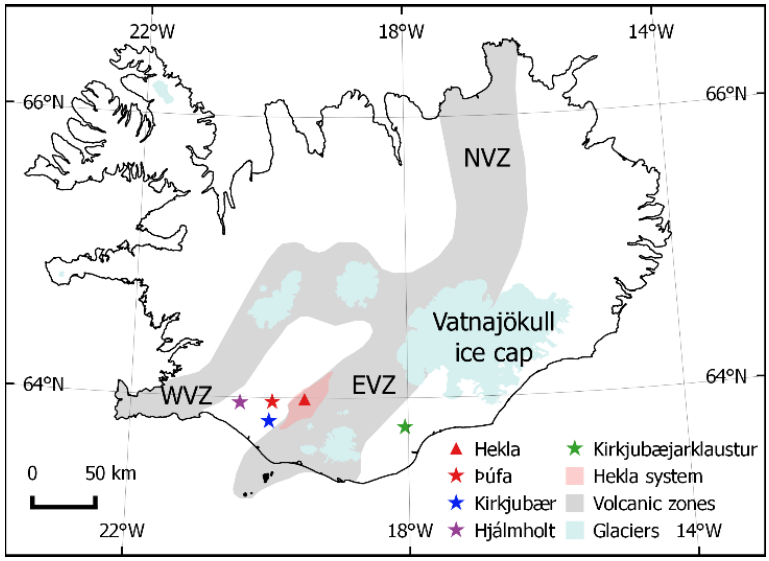

Fig. 1. Hekla volcano and its location in Iceland (red triangle). The Hekla volcanic system is shaded in pink and sits within the Eastern Volcanic Zone (EVZ). The grey areas depict the active volcanic zones of Iceland, Western Volcanic Zone (WVS) and the Northern Volcanic Zone (NVZ). Major ice caps in Iceland are shown in pale blue. The colored stars indicate where contemporary observations were made (see key and text for further details).

Hekla is one of the most frequently active Icelandic volcanoes, with 18 explosive eruptions (Thordarson and Larsen, 2007) in historical times, i.e., since the settlement of Iceland (874 CE). The average repose period was 53 years from 1104 to 1970. Since 1970, the activity has changed to more frequent eruptions (occurring on ~10 year intervals), which are smaller, less intense, and with lower SiO_2 contents (e.g., Thorarinsson and Sigvaldason, 1972; Grönvold et al., 1983; Gudmundsson et al., 1992; Höskuldsson et al., 2007; Gudnason et al., 2017). In historical times, Hekla eruptions span the range in intensity and composition from basaltic lava-producing fissure eruptions to silicic tephra-producing Plinian eruptions (e.g., Thorarinsson, 1967a; Janebo et al., 2016; Gudnason et al., 2017). The post-1500 eruptions at Hekla have been typified by hybrid eruptions that start with (1) an explosive opening phase with associated tephra fall, then (2) a transitional phase with fountaining along the main Hekla fissure and formation of fountain-fed lava, is followed by (3) Strombolian activity and lava effusion from discrete vents (e.g., Thorarinsson, 1967a; 1968; Gudnason et al., 2017). The 1845 eruption is one of the best documented Hekla eruptions, and typifies the 1500–1970 activity. The observations include accounts of precursors, vent activity, flooding of rivers, and tephra fall on and off shore (Björnsson, 1846; Erlendsson, 1847; Schythe, 1847). Additional information regarding source parameters (i.e., erupted volume, mass eruption rate (MER), plume height, and duration), however, is required to quantify the opening phase of the 1845 eruption. The dynamics of explosive activity in volcanic eruptions can be inferred from rates of thinning and fining of fall deposits (Kaminski and Jaupart, 1998; Houghton and Gonnermann, 2008; Carey et al., 2009; Perugini et al., 2011; Bonadonna et al., 2015; Houghton and Carey, 2015). For the historical Hekla eruptions, the major tephra-producing phase is always the opening phase (e.g., Thorarinsson, 1967a; 1967b; Janebo et al., 2016). Therefore, we focus on the opening phase to quantify the tephra fall and the total grain-size distribution (TGSD). The TGSD allows for assessment of hazards associated from the eruption to aviation, both by being a source input into forecast models and by quantification of the mass of fine ash.

2. The 1845 eruption

2.1 contemporary accounts

Detailed descriptions of the Hekla eruption in 1845 and its effects via observations by Oddur Erlendsson at the farm Þúfa in Land (Erlendsson, 1847), Jóhann Björnsson at the farm Kirkjubær á Rangárvöllum (Björnsson, 1846), Páll Melsted at Hjálmholt (Melsted, 1846) (Fig. 1) and contemporary accounts of the tephra fall from the opening phase as observed in the area around Kirkjubæjarklaustur about 85 km to the ESE of Hekla (Schythe, 1847). The first observations on 2 September include noise from Hekla along with ground movements (Table 1; Erlendsson, 1847), followed by a dark cloud rising from the summit of Hekla, and casting a shadow over the farming district to the west of the volcano (Erlendsson, 1847). Sightings of a dark cloud in the mountains between W and NW from the coastal region ESE from Hekla are reported around 10 in the morning and the plume reached Kirkjubæjarklaustur one hour later or around 11 in the morning (Schyte, 1847). From around 11 to 12 o'clock, the tephra fall was so dense that people working in the fields could not find their way home. The deposited material was described as greyish yellow, the average size similar to a fox shot, and the thickness was about half Danish inch (≃1.3 cm; Schythe, 1847). At around 12 o'clock, the dense fallout started to dissipate and the light was like an early morning. Following the hour-long fallout, the material was described as finer and darker "volcanic sand", and daylight was not restored until 3 in the afternoon (Schythe, 1847). Later in the same day, larger discrete earthquakes could be felt at Þúfa, superimposed on underlying tremor, and by the evening Erlendsson (1847) described lava fountains from the southern part of the Hekla fissure (i.e., along the crest of Hekla), and outpouring of lava on to the western slopes. In the area around Kirkjubæjarklaustur fallout of tephra continued throughout the rest of the day, and stopped just before midday on 3 September 1845 (Schythe, 1847). Schythe (1847) furthermore describes the deposit to be composed of gravel, sand, and ash. In "several places" in the area around Kirkjubæjarklaustur and in Skaftártungur (Fig. 2A), the layer was 1–1.5 inch (≃2.6–3.9 cm) thick. Schythe (1847) also notes that the gravel can float on water while the ash cannot. The thickness of the tephra layer was reported to be much thinner east of Geirlandsá (Fig. 2A; Schythe, 1847).

By 3 September lava was flowing from Hekla and Erlendsson (1947) describes the plume height to be three times the height of Hekla (~1300 m above surrounding topography; i.e., ≥ 3.9 km a.s.l). On 4 September wind carried the tephra to the NE but, by that time, only minimal amounts of tephra were produced, and lava was instead the main product. These wind and eruption conditions remained until 12 September (Björnsson, 1846; Melsted, 1846; Erlendsson, 1847). Jóhann Björnsson and five other individuals went to Hekla on the 9th to examine the activity. They noted three weakly explosive vents, situated just NW of the summit, and the activity from the middle vent was the most vigorous. At that time, the erupted lava had produced a 30-m thick flow field with a circumference of 15 km (Björnsson, 1846). On 13 September, the wind shifted, dispersing the plume to the west from Hekla with subsequent ash fall in the farming district of the Southern Lowlands, which lasted through the 15 September. This ash fall caused the grass in the fields to wither such that the grazing livestock did not take to it and their milk-yield dropped dramatically, or up to 65–75%. Later, fluorosis was noted in the livestock from these areas. From 15 September, the eruption continued with very low intensity explosive activity and lava production, forming a near-circular, thin tephra deposit around Hekla (Thorarinsson, 1967a; 1968). The last day of major lava production was 16 March 1846, however, sporadic explosions occurred until 25 September 1846 (Erlendsson, 1847).

Table 1. Key events and chronology of activity during the opening phase of the Hekla 1845 eruption. The timing of events is partly authors interpretation. Dates and observations are after [1]Erlendsson (1847) and [2]Schythe (1847).

Date	From start of eruption	Observations	Interpretation
2 Sept.	~0	Shortly after mid-morning rumbles and violent murmurings were suddenly heard from the east by farmers around Hekla[1]	Low frequency seismic activity in relation to the unrest immediately prior to onset of eruption
2 Sept.	~0	3–4 earthquakes[1]	Seismic activity associated with opening of the conduit and the top crater
2 Sept.	~0	Rising greyish black cloud[1]	Rising eruption plume
2 Sept.	~15 min	Shadow cast to the east of Hekla[1]	Shadow from the rising plume
2 Sept.	~60 min	Darkness dissipated, sound changes from constant to episodic and became louder[1]	Change in activity, less dense eruptive cloud lets sun rays through and the activity changes from sustained (constant sound) to non-sustained (episodic noise)
2 Sept.	~60 min	Tephra fall to the ESE of Hekla and at 85 km distance, total darkness during the time of heaviest tephra fall[2]	Most dense tephra fall is described as total darkness, with coarse ash sized particles, followed by fine ash and slowly dissipating tephra fall
2 Sept.	~2 hrs	Tephra fall dissipates (85 km downwind), finer material is deposited. Darkness lifts gradually over 3 hrs.[2]	The change from coarse to fine ash fallout represents most likely transition from the opening phase to the transitional phase of the eruption.
2 Sept.	~2 hrs	Floods in river Ytri Rangá and Markarfljót[1]	Flood water from melted snow/ice on the W flanks of Hekla to Ytri Rangá, less voluminous flood in Markarfljót with rafted pumice
2 Sept.	~6 hrs	Two big earthquakes[1]	Earthquakes related to the opening/elongation of the Hekla fissure
2 Sept.	~12 hrs	Big earthquake[1]	Earthquakes related to the opening/elongation of the Hekla fissure
2 Sept.	~12 hrs	Clear sky, fire visible in SW part of Hekla fissure, main tephra production up slope towards top of Hekla, big blocks of rock thrown up[1]	Some tephra production and fire fountain activity at the top and shoulder crater
2 Sept.	~12 hrs	Clear sky, fire visible in SW part of Hekla fissure, main tephra production up slope towards top of Hekla[1]	The main lava producing part of the fissure is active on the SW part of Hekla fissure
3 Sept.	~24 hrs	Wind from WSW, plume height three times height of Hekla[1]	Tephra fall to the ENE, plume > 3 km high
3 Sept.	~24 hrs	Fire, smoking lava, tumbling boulders from lava front[1]	Further transition into effusive activity and growth of the lava field
3 Sept.	~36 hrs	Fire fountains, smoking lava, tumbling boulders from lava front[1]	Further transition into effusive activity and growth of the lava field
4 Sept.	~50 hrs	Bad visibility, rumble from Hekla, rain and wind from SE[1]	Effusive activity, tephra fall to the NW
5 Sept.	~70 hrs	Bad visibility, bad weather[1]	Continued activity

Deposition of tephra produced by the opening phase was reported outside of Iceland by three separate vessels; one close to Faeroe Islands, one in the Orkney Islands, and one by the Shetland Islands. Tephra fall was also reported from the Faroe and Shetland islands. Details on the positions of the ships and the timing of tephra arrival are shown in Fig. 2B and listed in Table 2 (Schythe, 1847).

Table 2. Ships and locations from where tephra fall was reported in 1845. Date, location, and time is reported by the ships (Schyte, 1847). The information is not as detailed from the Faroe and Shetland Islands and hence time, location, and distance are approximated.

Vessel	N	W	Date	Time	Distance from Hekla (km)
St. Helena	61.0250	-7.9667	2 September	21:00	685
Anna Charlotte	60.4167	-3.8667	2 September	20:45	910
Johanne	59.0833	-1.5833	3 September	05:00	1090
Faroe Islands	62.2449	-7.1564	2 September	Evening	~685
Shetland Islands	60.7977	-0.8243	3rd September		~1020

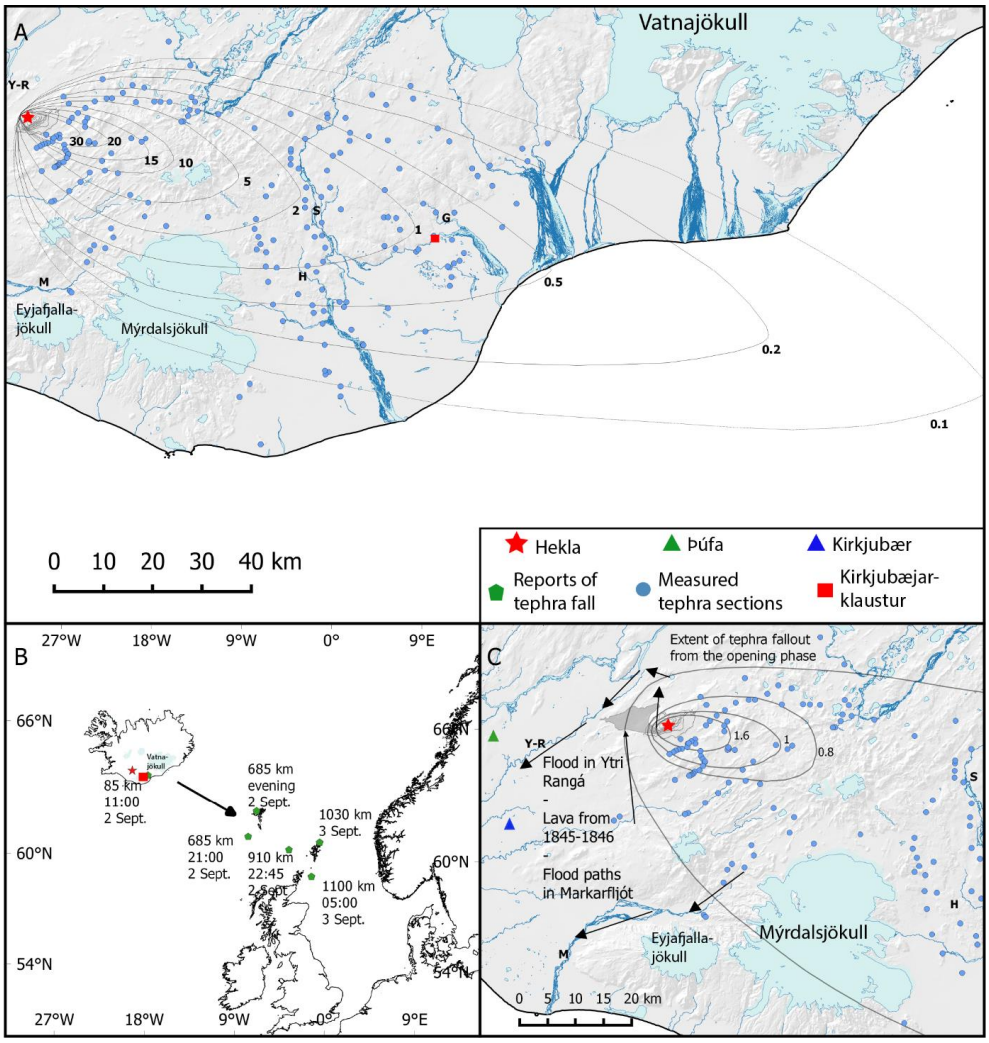

Fig. 2. Hekla and the tephra fall from the opening phase of the 1845 eruption. A: Isopach (cm) map of the tephra fall, blue-filled circles indicate sites of field observation, measurements, and sampling. B: Sites outside of Iceland where tephra fall was detected and reported, with timing of tephra deposition indicated. Locations and time for offshore tephra deposition after Schythe (1847). C: Isopleth (cm) map for the opening phase tephra fall deposit. The black line indicates the outermost extent of the fall (= 0.1 cm isopach). Also shown (black arrows) are the paths of the floods in the rivers Ytri Rangá and Markarfljót. Abbreviations are: Y-R Ytri Rangá river, M Markarfljót river, S Skaftá river and the Skaftártungur district, H Hólmsá river, G Geirlandsá river.

The eruption had shorter and longer lasting hazards. Flash floods passed through the rivers Ytri-Rangá and Markarfljót. The Ytri-Rangá river was flooded with meltwater produced by melting snow on the western and northern slopes of Hekla and the high temperature of the flood water killed the fish. An unrelated flood in Markarfljót river, to the east of Hekla, was a result from melting of snow by the tephra fall from the opening phase. Fluorosis was reported in grazing animals, both associated with the opening phase tephra and tephra from latter phases of the eruption, and had a widespread impact on the population in southern Iceland (Björnsson, 1846; Erlendsson, 1847).

2.2 The 1845 eruption, previous studies

The products of the 1845 Hekla eruption were studied by several scientists who visited Iceland following the eruption (see overview in Thorarinsson, 1967a; 1968). The journal from Erlendsson (1847), the report from Björnsson (1846), and the compilation of data by Schythe (1847) provide the framework for constraining the opening phase of the 1845 Hekla eruption. Glass chemistry of the tephra and lava composition has been published, with a SiO_2 content of ~60 wt% (Thorarinsson, 1968), 60.93 wt%(Thordarson et al., 1998) is and 59.70 wt% (Sverrisdottir, 2007).

An extended overview of the 1845 tephra is presented in the pioneering work of Sigurður Þórarinsson (Thorarinsson, 1967a; 1968) who mapped and compiled data on the 1845 tephra distribution and produced the first volume and dispersal estimates for the opening phase tephra. According to the dispersal map by Thorarinsson (1967a; 1968), the tephra fall from the opening phase covers 1740 km^2 within the 1 cm isopach and he states that the volume of freshly fallen tephra is 0.23 km^3. This value is clearly a mistake, because when the volume of the tephra deposit is calculated using the thickness and area values listed in his monographs (Thorarinsson 1967a; 1968), the volume amounts to 0.09 km^3 when obtained from the isopachs, which is equal to 0.145 km^3 of freshly fallen tephra using his conversion factor of 1.6 (Thorarinsson, 1958, 1968). It is noteworthy that the 0.23 km^3 of freshly fallen tephra is a factor of 1.6 larger than the value of 0.145 km^3 obtained in the recalculation (Thorarinsson, 1968, 1967a).

3. Methods

3.1 Field methods

We examined 195 soil profiles and the 1845 tephra fall deposits were identified at 154 sites. At each site, thickness, general appearance, and stratigraphic position in relation to adjacent tephra layers were documented, grain-size samples were collected, and, where possible, weighed samples were taken from area of known size, which proved most successful in the more proximal, thicker sectors of the deposit. The 1845 tephra is a key marker layer in the top part of the historical soil section in the Fire districts (i.e., Skaftártunga to Fljótshverfi; ESE of Hekla; Fig. 2), because it is distinct from the more numerous Katla tephra layers that dominate the sequence. The tephra is easily identifiable both from its appearance, as brown coarse ash in the area and typically coarser-grained than the black Katla tephra layers (e.g., Thordarson et al., 1998; Larsen, 2000; Fig. 3).

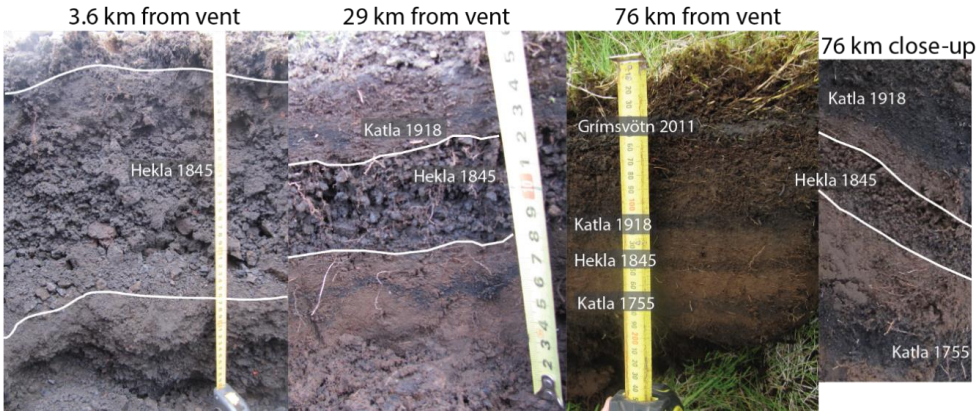

Fig. 3. The 1845 tephra layer at 3.6, 29, and 76 km distance from Hekla. The image on the right is a close up of the 76 km site. Note the difference in appearance to the adjacent Katla layers.

3.2 Eruption Source Parameters

The contemporary accounts (see section 4.1) have been re-examined in order to narrow down the starting time of the eruption. We examined the plume travel velocity as determined by records of onset of tephra fall at Kirkjubæjarklaustur and at locations outside of Iceland (Table 2). The plume travel velocity was calculated for each of the locations assuming five different starting times; 9:00, 9:15; 9:30, 9:45, and 10:00 am (Supplement A).

Eruptive tephra volume was calculated on the basis of the area enclosed by each isopach (Fig. 2). The volume was obtained by fitting two exponential segments, power law, and Weibull curves to the data on a semi-log thickness vs. square root of area plot (Pyle, 1989; Fierstein and Nathenson, 1992; Bonadonna and Houghton, 2005; Bonadonna and Costa, 2012). For calculating plume height (H) for the opening phase, three different methods were used. Firstly, the plume height (H) is estimated from the time averaged MER using the Mastin et al. (2009) empirical formula, $H=2.00\ Q^{0.241}$ (where Q is the volumetric MER rate in $m^3\ s^{-1}$). Secondly, it was estimated using the obtained tephra volume (V) and the relationship $H = 25.9 + 6.64\log_{10}V$ (Mastin et al., 2009). Lastly, the isopleth map (Fig. 1c), constructed from the average of the five largest lithic clasts (maximum lithics, ML) at each site, was used to estimate plume height and the wind speed following the method of Carey and Sparks (1986) (assuming a clast density of 2500 kg m^{-3}). MER (Q) was calculated using the deposit volume and the duration of the opening phase, as deduced from contemporary accounts (Björnsson 1846; Erlendsson 1847; Schythe 1847). Effects of wind on the estimated MER are also computed after Degruyter and Bonadonna (2012) for which magma temperature was kept at 1273 K, plume height was varied from 17 to 31.5 km, and wind speed was set at 16 m s^{-1}, 19 m s^{-1}, and 24 m s^{-1} (corresponding to onset at 09:30, 09:45, and 10:00, respectively). Wind speed was derived from the arrival time over 85 km, or the distance to Kirkjubæjarklaustur (Fig. 2B).

3.3 Grain-size analysis

48 samples were selected for grain-size analysis. These samples were selected to best represent the whole deposit spatially (Fig. 4). The samples were dried and hand-sieved at half ϕ intervals down to 4 ϕ (0.63 mm) ($\phi=-\log_2 D$, where D is the particle diameter in mm). Material finer than 3 ϕ (0.125 mm) was further analyzed using a SediGraph 5120 X-ray particle analyzer down to 10 ϕ (0.001 mm). The sieve and X-ray data was combined, using the overlap from 0.125 mm to 0.063 mm. The mass percent finer than 0.125 mm of the sample was used to merge the data from sieving and fine grain analysis. Median and sorting values were calculated after Folk and Ward (1957). A melt density of 2470 kg m^{-3} was measured using water pycnometer. Bulk tephra density of 600 kg m^{-3} was determined by measure sample volume in the field, weigh dried sample, and take average of 25 samples.

3.4 Deconvolution

Because the majority of grain-size samples are bimodal, further processing of the grain-size data was required. Deconvolution of the two subpopulations—CS (coarse) and FS (fine)—was done using the fully automated program Decolog 5.2.1 (decolog.org). Decolog has previously been used on similar sample sets (e.g., Eychenne et al., 2015; Janebo, 2016). The program fits nonlinear Weibull or power law functions to the grain-size data and calculates the statistical parameters for each fitted function. The output thus allows for examination of the two subpopulation independent of each other (see section 3.3). The program calculates median and sorting values for each subpopulation according to Folk and Ward (1957; supplement B).

3.5 Total grain-size distribution

A total grain-size distribution (TGSD) was reconstructed using the Voronoi Tesselation method as outlined in Bonadonna and Houghton (2005) and Biass and Bonadonna (2014). The outer limit selected for the TGSD calculation was set as the 0.1 cm isopach (Fig. 2A).

3.6 Componentry

Componentry analysis was done on selected samples from three locations (Fig. 4): one proximal (J13-53), one medial (J13-42), and one distal (J12-42). Two samples (lower and upper) were analyzed for the proximal location, whereas single bulk samples were analyzed for the other two sites. In each sample, the relative proportions of each components in the lapilli fraction of the deposits (i.e., ≥2 mm) was determined by weight in each half phi intervals. For the ash sized portion, the relative abundance of the componentry groups was determined by counting a minimum of 200 grains. The components identified in the 1845 tephra fall deposits are; lithic fragments, microvesicular juvenile clasts, and scoriaceous juvenile clasts. The microvesicular clasts are most often lighter (brown) colored while the scoriaceous are darker (black).

3.7 Scanning Electron Microscopy

Qualitative examination on aggregation with a Hitatchi TM3000 scanning Electron Microscope (SEM) was carried out on two sample sets with, with 15 kV acceleration voltage in analysis mode. The first set was from the modal peak of FS selected across the deposit (red stars in Fig. 4). The second set consisted of a thin section through each tephra layer, sampled in situ (see supplement C for details of sample preparation) at locations indicated on Fig. 4.

3.8 Chemistry

Glass chemistry of the opening phase tephra was analyzed with WDS Cameca SX100 electron microprobe for completeness and to compare to previously published values. See supplement D for detailed description of methods and results.

4 Results

Preservation of the 1845 tephra in the distal sector where its thickness ranges from 0.5–3 cm is good (present > 90% of sites examined). This is true for the coarser fallout, which was described during the first hour of the tephra fall (Schythe, 1847). However, the fallout of fine material as described in the contemporary accounts is never found capping the coarse fallout despite of abundant vegetation and high soil accumulation rates in area east of the rivers Hólmsá and Skaftá and west of Geirlandsá, which is presumed to provide optimal conditions for preservation (Fig. 2A). Within the proximal sector, where the thickness of the tephra is >20 cm (typically <10 km from Hekla), the preservation is fairly good and the 1845 deposit was present in >60% of sites examined.

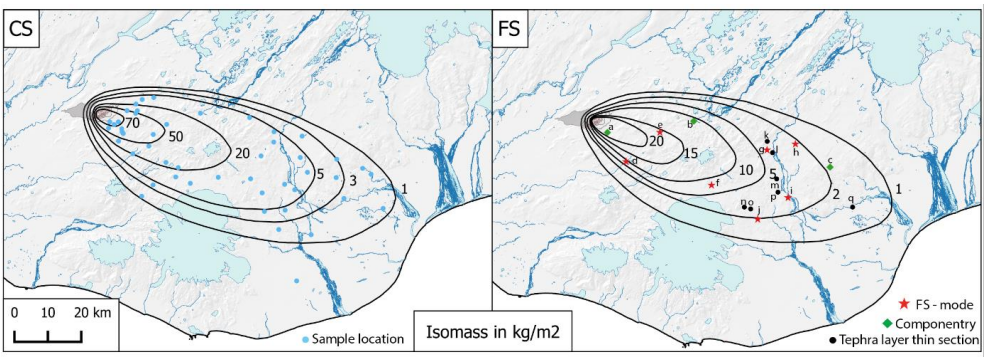

Fig. 4. Isomass maps of the two subpopulations CS and FS. Both the CS and FS are constructed from the same number of grain-size samples indicated on the CS map as blue dots. Locations of selected grain-size sub groups used for SEM examination are shown on the FS map. Red stars are locations of samples for which the mode of the FS was examined with SEM (Fig. 5), green diamonds are locations of samples componentry analyzed (Table 5) and black dots are locations of samples of which thin sections were made (Fig. 6). Sample labels: a J13-53; b J13-42; c J12-42; d J13-95; e J13-106; f J14-06; g J12-49; h J12-35; I J13-17; j J12-44; k J13-67; l J13-75; m J13-19; n J13-05; o J13-09; p J12-74 and q J13-37.

In this sector, the tephra is preserved within the regolith and soil is more or less absent. The 1845 tephra is discriminated from other tephra layers, including the more recent 1947 and other 20th century Hekla events, by its distinct appearance (i.e., color, grain-size, and thinning characteristics) as well as by its stratigraphical position in the regolith in relation to known tephra layers from other volcanic systems (in particular from the Katla and Bárðarbunga-Veiðivötn systems). The poorest preservation of the 1845 tephra is in the medial sector (i.e., the area north of Mýrdalsjökull), between the 20 cm and the 5 cm isopachs (Fig. 2A). This area is mountainous with inter-dispersed glacial outwash plains (Fig. 2), and the regolith is poorly developed and soil is sparse. Descriptions by sheep herders, who gathered sheep immediately after the opening phase from the highland pastures affected by the proximal and medial sectors of the tephra fall, indicate that the tephra fall deposit was subjected to immediate wind erosion for number of days in September 1845 (Björnsson, 1846).

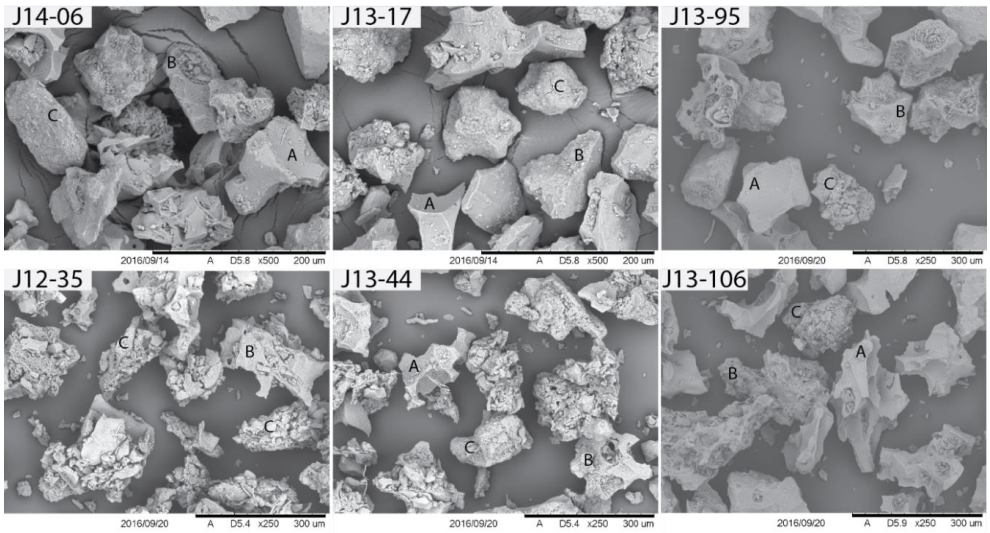

Fig. 5. SEM images of clasts from the FS of six different samples, selected across the deposit. Size fractions imaged are from modal peaks of FS, either 3 or 4 phi. Three principal types of grains are recognized: A – glass shards, B – coated particles, and C – ash clusters.

4.1 Plume and tephra dispersal

The start of the 1845 eruption at 09:00 as given by Thorarinsson (1968), based on Erlendsson´s (1847) accounts, is here considered too early for onset of eruption (see section 5.1). The contemporary descriptions (Björnsson, 1846; Erlendsson, 1847; Schythe, 1847) and evaluation of plume velocities (supplement A) shows the most compatibility with the inferred onset in the period 9:30 to 9:45 am, resulting in wind speed of 16–19 m s^{-1}.

The historical accounts describe deposition on the dispersal axis near Kirkjubæjarklaustur (Schythe, 1847), as a 1-hour-long heavy fallout of coarse pyroclasts, followed by 3 hours of deposition of finer material (Schythe, 1847). Based on these descriptions, Thorarinsson (1967a; 1968) interpreted this to indicate that the opening phase lasted 4 hours. In light of our current understanding of activity in the early stages of Hekla eruptions, where the eruptions begin with 0.5 to 1 hour long opening phase, followed by a 2–3 day long transitional phase and weeks to months long effusive phase (e.g., Thordarson and Larsen, 2007; Larsen et al., 1992; Janebo et al., 2016; Gudnason et al., 2017), we interpret the accounts as that the opening phase lasted for 1 hour. The opening phase was then succeeded by 3-hour-long ash fall, which we infer to be from the transitional phase of the eruption. The tephra fall on the 2 and the tephra fall on the 3rd correspond to the waning part of the transitional phase and complete transition into Strombolian/effusive activity as described by Erlendsson (1847).

4.2 Eruption source parameters

The reconstructed isopachs for the deposits are elongated in the downwind direction (i.e., to the ESE) and are slightly asymmetrical around the dispersal axis and skewed to the south (Fig. 2A). The thinning half distance is 10 km and at that point, the cross-wind width of the deposits is 34 km (20 km to the south and 14 to the north). The thinning half distance in the cross-wind direction are ~5 km. The isopleth map, in contrast to the isopach map, is asymmetrical to the north of the dispersal axis (Fig. 2C). The total area cover of the 0.1 cm isopach is 9000 km^2 and the area enclosed by the thickest isopach of 30 cm is 35.5 km^2. The maximum thickness of the Hekla 1845 tephra deposit, as obtained by extrapolating segment (a) on Fig. 7, is 50 cm and the break-in-slope is at 38 km.

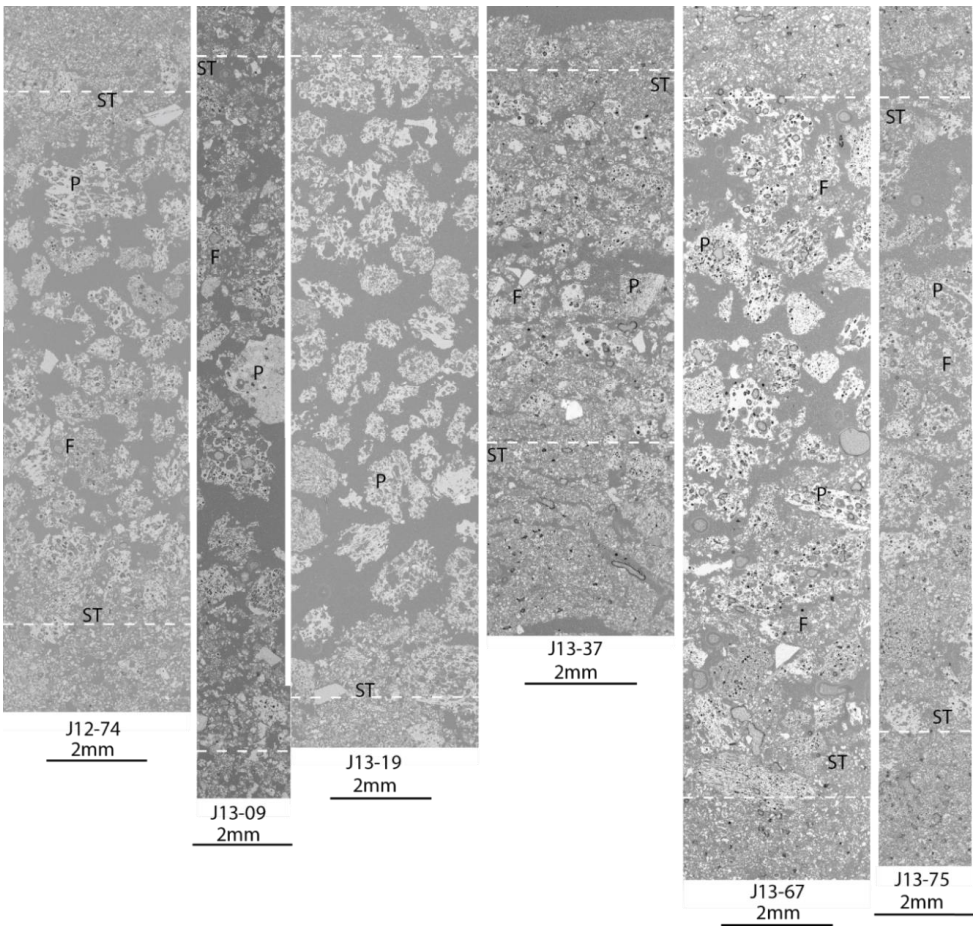

Fig. 6. Backscatter electron image of the full thickness of the 1845 tephra layer in situ, from six distal localities (Fig. 4). Fine material at the top and base of each sample is soil. Icelandic soil is rich in tephra, thus little variance is seen in backscatter properties of soil vs. tephra. Dashed white line indicates soil and tephra boundaries. Labels are P = pumice, F = fine material (shards) and ST = soil and tephra mixture at tephra layer boundaries. In many instances, the fines (F) cluster, possibly indicating aggregation. See supplement C for description of sampling technique and preparation of the tephra sections.

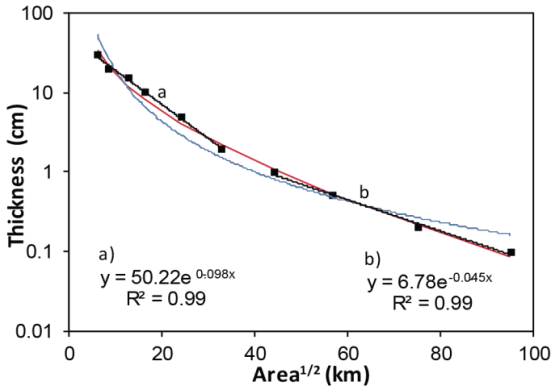

Fig. 7. Thickness vs square root of area plot of the isopach data. Three functions were fitted to the data. Black straight segments are exponential (Pyle, 1989; Fierstein and Nathenson, 1992); red line is the Weibull function (Bonadonna and Costa, 2012); and blue is the Power law (Bonadonna and Houghton, 2005).

The tephra volume from the opening phase is in the range from 0.13–0.22 km^3, depending on which approach (Fig. 7) is used. Using a melt density of 2470 kg m^{-3} and tephra bulk density of 600 kg m^{-3} gives a dense rock equivalent (DRE) volume of 0.03–0.05 km^3 for the opening phase (Table 3). The power law produces the largest volume estimate of 0.22 km^3, and has the second best fit to the data (r^2 = 0.96). The Weibull function has the worst fit to the data (r^2 = 0.93) and results in the same volume as obtained by fitting two exponential segments, 0.13 km^3, which corresponds to a DRE volume of 0.03 km^3.

	Tephra (km^3)	Tephra (kg)	r^2	DRE (km^3)
Exponential 2 segments	0.13	7.5 x 10^{10}	0.99	0.03
Power Law	0.22	1.3 x 10^{11}	0.96	0.05
Weibull	0.13	8.1 x 10^{10}	0.93	0.03

Table 3. Volume and mass of the tephra deposits obtained from integrating the functions in Fig. 7.

The time averaged MER for the opening phase of Hekla 1845 was determined to be 2.1 x 10^7 kg s^{-1} (8300 m^3 s^{-1} DRE), using the DRE volume from the exponential fit which had the best fit to the data (Table 3), and a duration of 1 hour corresponding to the deposition time of the coarse fallout. The MER via the method of Degruyter and Bonadonna (2012), ranges from 4.7 x 10^7 to 7.5 x 10^8 kg s^{-1} for the plume heights obtained with all methods (Table 4). These numbers are consistently higher than the time averaged MER of 2.1 x 10^7 kg s^{-1} given above.

The plume height derived from the time averaged MER, following Mastin et al., (2009) is 19 km a.s.l. whereas the plume height derived from the volume (Mastin et al., 2009) is 17 km a.s.l. In contrast, the plume height derived from the isopleth map (Fig. 2C) using the method of Carey and Sparks (1986), is significantly higher, in the range of 24.5 to 31.5 km a.s.l. The wind speed derived from the isopleth data is 23 to 25 m s^{-1}, which is at the higher end of wind speeds inferred from the contemporary accounts for the downwind plume velocity. For onset of eruption at 09:30, 09:45 and 10:00, wind speeds are 16, 19, and 24 m s^{-1} respectively (supplement A).

The average plume height and MER values would classify the 1845 eruption as subplinian (Bonadonna and Costa, 2013), and the volume as a VEI 4 Plinian event (Houghton et al., 2013).

Table 4. MER of Hekla in 1845 after correction for wind advection. The wind speed and wind entrainment are dominant factors on the rise of the plume, illustrated by scaling parameter values <1 (Degruyter and Bonadonna, 2012). Temperature assumed for the magma in 1845 is 1273 K, plume height above vent is used for the calculation, plume height a.s.l. for table. The range of plume heights 17–31.5 km a.s.l. are the same as obtained by empirical methods and from the isopleth map (Fig. 2C).

Plume height a.s.l. (km)	Wind speed (m s^{-1})	MER (kg s^{-1})	Scaling parameter (Π)
17	24	6.3 x 10^7	0.3019
19	-	1.0 x 10^8	0.3444
24.5	-	2.9 x 10^8	0.4726
31.5	-	7.5 x 10^8	0.6648
17	19	5.3 x 10^7	0.3814
19	-	8.7 x 10^7	0.4350
24.5	-	2.5 x 10^8	0.5970
31.5	-	6.5 x 10^8	0.8397
17	16	4.7 x 10^7	0.4529
19	-	7.7 x 10^7	0.5165
24.5	-	2.2 x 10^8	0.7089
31.5	-	6.0 x 10^8	0.9972

4.3 Grain-size

Grain-size analysis revealed multiple populations within each grain-size distribution. There are both unimodal and bimodal distributions found. After deconvolution of the grain-size distributions, the subpopulations are referred to as CS for the coarser lapilli fraction and FS for the finer ash fraction. There is no spatial relationship observed between unimodal and bimodal grain-size samples across the deposit. Examples of the deconvolved grain-size distributions are on Fig. 8. Only one of the measured sample is comprised solely of FS (J15-3; Fig. 8).

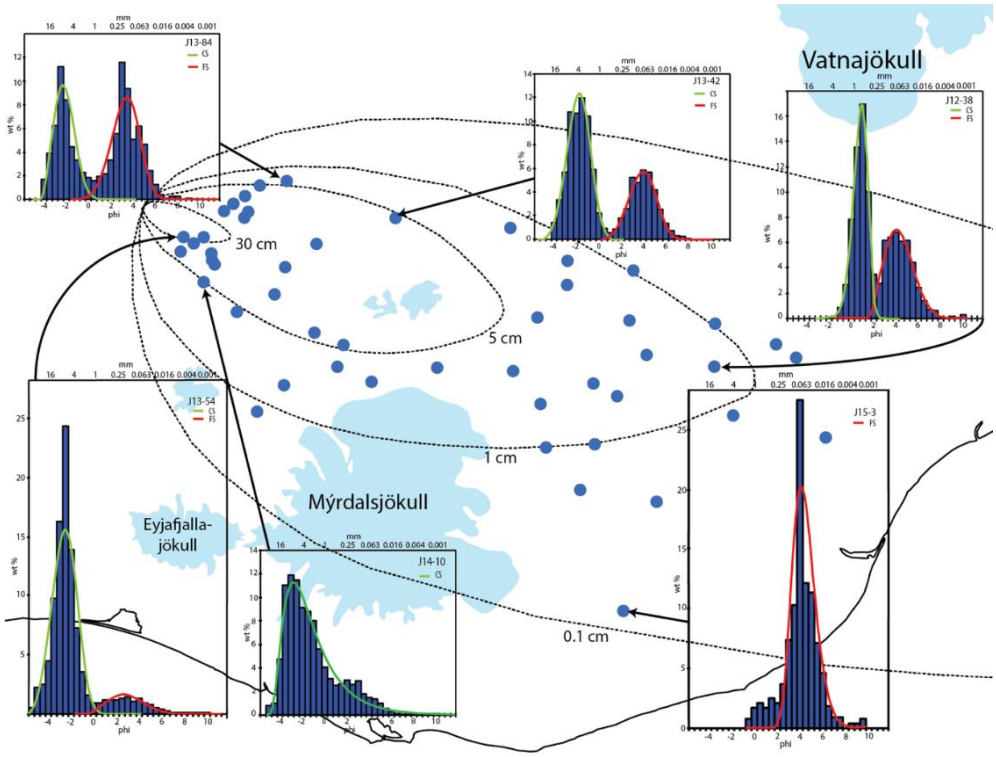

Fig. 8. Map of distribution of samples selected for: grain-size analysis, deconvolution, and TGSD calculation. Isopach lines of 30, 5, 1, and 0.1 cm are shown for reference, see Fig. 2 for complete isopach map. Example grain-size distribution and deconvolved populations are shown in insets. Blue bars represent whole sample grain-size distribution, green curve represents coarse subpopulation (CS) and red curve represents fine subpopulation (FS). Individual subgroups are also represented: unimodal (sample J14-10; J15-3), bimodal with dominant coarse population (J13-54, J13-42 and J12-38), bimodal with equally weighted populations (J13-84), and unimodal fine subpopulation dominant sample (J15-3).

The relative mass contribution of lapilli (2–64 mm; ≤-1 ϕ), coarse ash (0.063–2 mm; -0.5–4 ϕ) and fine ash (<0.063 mm; >4 ϕ) becomes more systematic beyond 30 km from Hekla (Fig. 9). During the first 30 km of sedimentation, lapilli is the major size group (≥ 50% wt%), coarse ash (-0.5–4 ϕ) most commonly contributes 10–40 wt%, with three samples containing 45–50 wt% and one as much as 80 wt%, and fine ash (<4 ϕ) is in the range of 3–18 wt% (Fig. 9). Beyond 30 km from source, deposition of ash dominates, rising sharply over the 30 to 50 km from source interval from ~50 wt% to ~85 wt% and then levels out and remains in the 80–90 wt% range up to 90 km from source. Throughout (i.e., from 30 to 90 km from source), the deposition of fine ash is persistent at about 5–20 wt% and defines a near-horizontal trend with distance from source (Figs. 9, 10).

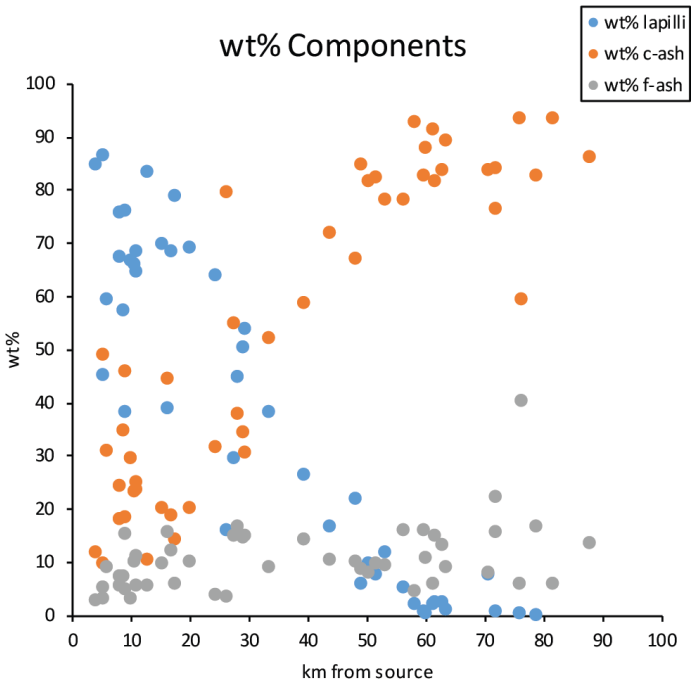

Fig. 9. Weighted abundances of the lapilli (2 to 64 mm; ≤-1φ), coarse ash (0.063 mm to 2 mm; 0 to 4 φ) and fine ash (<0.063 mm; >4φ) grain-size groups in Hekla 1845 tephra samples.

The grain-size distribution for the whole, non-deconvolved samples (small inset on Fig. 10) exhibits a tight negative sloping trend of Md_ϕ over distance from source. Scatter is largest in the most proximal samples, which exhibit the largest variance in sorting (σ_ϕ). Md_ϕ shows a consistent decline from around 10 km to 90 km, -2.5 ϕ to 1.5 ϕ. Over the same distance, the sorting generally improves, especially from 30 km to 90 km, over which σ_ϕ decreases from 2.5 to 1.5.

When the subpopulations are examined individually, the trend of the sample collection is fining of the Md_ϕ for both FS and CS with transport (Fig. 10). The CS subpopulation fines significantly along the dispersal axis. The rate of fining is steepest from 0 to 15 km, and decreases outward along the axis. Sorting for the CS subpopulations improves with distance down axis which is consistent with progressive loss of the largest clasts during transport. The median diameter for the FS population is very consistent at 2.5 to 4 ϕ, a feature that would be consistent with the deposition as ash aggregates.

CS distributions are, in general poorly to moderately sorted (σ_ϕ 1.8 to 0.4), and FS are more poorly sorted (σ_ϕ 2.1 to 0.5), which furthermore supports the notion that the latter were, at least in part, sedimented as aggregates. Sorting for both populations improves over distance travelled (Fig. 10).

The relative proportion of both subpopulations vary throughout the deposit, especially in the proximal part, while a degree of convergence is seen in the distal part (Fig. 11A), as identified on the isopach map (Fig. 2A). The largest difference in depositional trends is the relatively large mass deposition during the first 20 km of transport as revealed on Figs. 9, 11B as well as the isomass maps of CS and FS on Fig. 4.

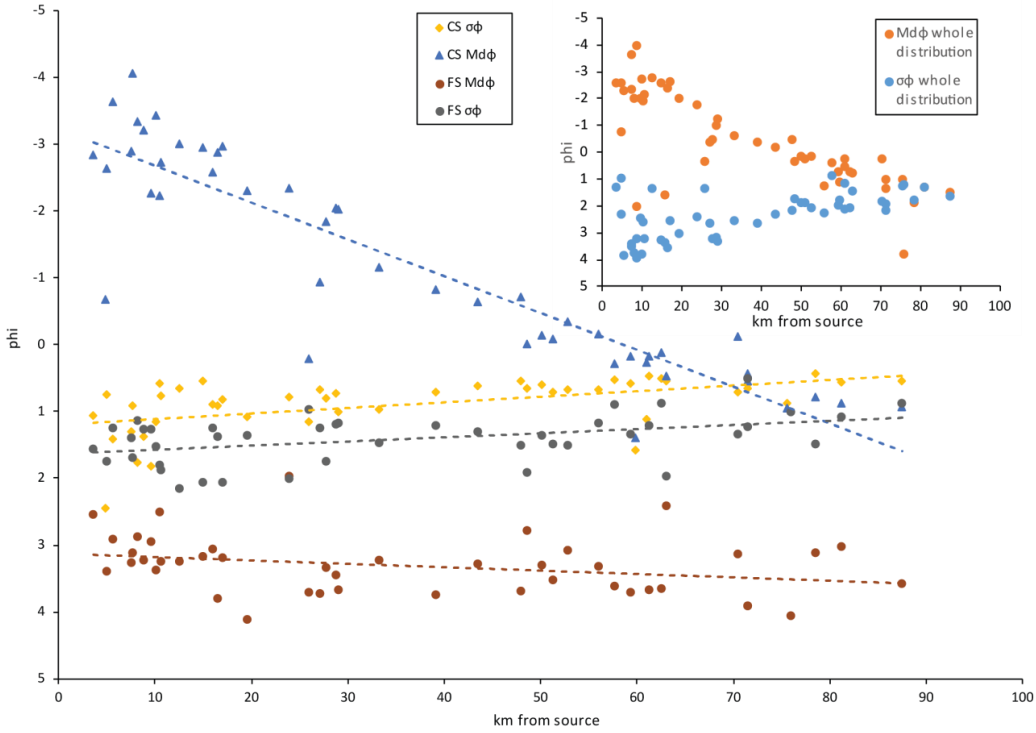

Fig. 10. Change in Md_φ and σ_φ with distance from source for CS and FS. Small inset shows the same parameters for the sample set as a whole. CS Md_φ (blue triangles) drops with distance transported more than FS Md_φ (Red dots) which shows only a slight change in Md_φ with distance from vent over 87.5 km. Sorting of the two populations improves (i.e., approaches zero) over the sampled distance and at similar rate.

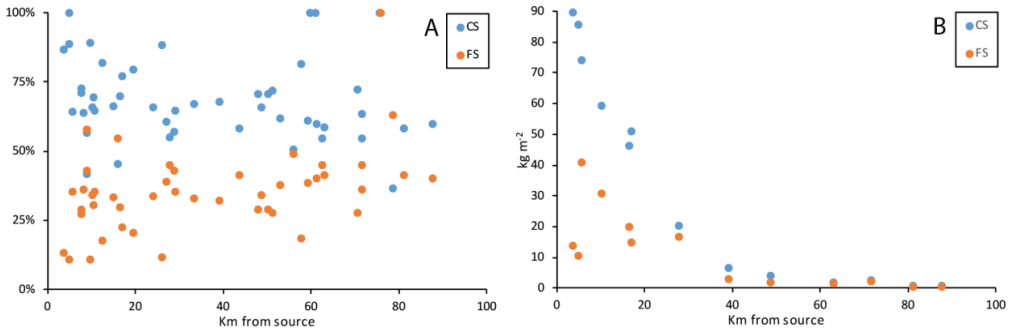

Fig. 11. A: The relative fraction of CS and FS at each location against distance from vent, illustrating a highly variable CS to FS proportions at distance <20 km and more uniform proportions beyond 25 km. B: mass in kg m^{-2} for the CS and FS at locations along the dispersal axis, similarly illustrating a more uniform mass distribution between the subpopulations during deposition beyond 25 km.

4.3.1 Proximal grain-size characteristics

The proximal deposit (J13-53) is inversely-to-normally graded, with a 15 cm thick base that that grades sharply into a 10 cm thick top (Fig. 12). Grain-size samples from the two major fall units show near-unimodal distributions dominated by lapilli and a long tail of fines, with a weak secondary peak at about 4 ϕ. For sample J13-53-3, Md_ϕ is -4 ϕ while for J13-53-2 it is -2.5 ϕ. The wall rock lithic content of the deposit is 1 to 5 wt% in the grain-size samples from section J13-53 (Table 5; Fig. 12). Lithics are most abundant (2 wt%) in the -2 ϕ (4 mm) size fraction.

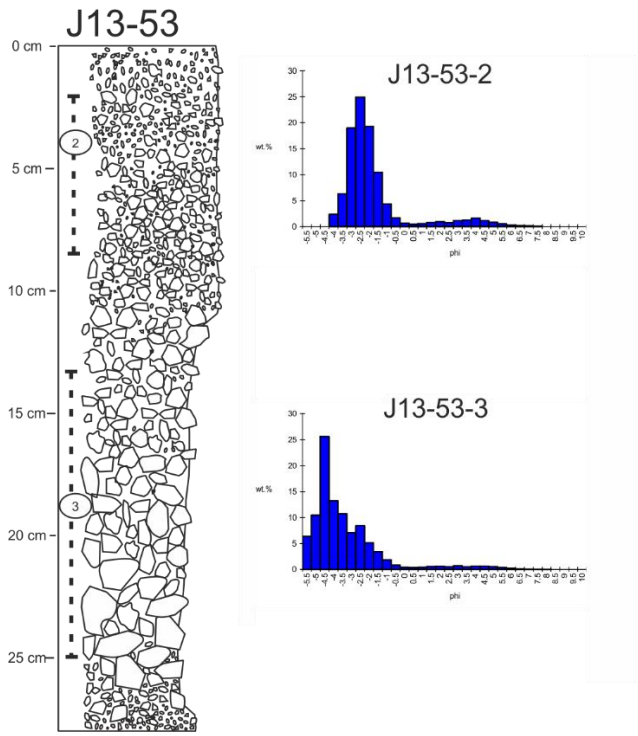

Fig. 12. From section J13-53, two samples (J13-53-2 and 3) were collected for grain-size measurements. Vertical extend of sampling is indicated by the numbered broken lines on the left side of the log. The results of the grain-size analysis are shown in histograms to the right of the log.

4.4 Textural components of the deposits

Size fractionation during transport is evident in deposits (e.g., Figs. 8, 9, 10). To examine the role of density fractionation, samples were selected from three locations (Fig. 4B).

The CS fraction of these four samples contains three components: scoriaceous (S) and microvesicular (M) juvenile clasts as well as accidental lithics. Results in Table 5 show that the relative proportions of individual components in the CS subpopulation of the analyzed samples do not change significantly from the proximal to the distal sector of the fall deposit.

Table 5. Results for componentry of four grain-size samples from three locations. J13-53 has separate samples from the upper and lower parts of the section, J13-42 and J12-42 are bulk samples. The componentry analysis covers CS of each sample. Numbers in brackets are scaled to 100%, for comparison between samples.

Sample	Lithics (wt%)	Microvesicular (wt%)	Scoriaceous (wt%)	wt% of sample analyzed
J13-53-2 (top)	5 (6)	49 (55)	35 (39)	89
J13-53-3 (base)	1 (1)	55 (59)	38 (40)	94
J13-42	1 (2)	40 (63)	22 (35)	63
J12-42	1 (1)	43 (57)	31 (41)	75

4.5 Ash aggregation

The bimodality of individual tephra samples from the 1845 deposits (Fig. 8) and the uniform abundance of fine ash to the deposit across the tephra sector (Fig. 9) suggests premature deposition of ash during the 1845 fallout. In order to qualitatively examine weather this premature deposition may have been the consequence of ash aggregation in the plume, we examined SEM images of

selected size bins (i.e., 3 to 4 ϕ size fraction; Fig. 5) from the FS peak (e.g., Fig. 8) in samples that span the aerial extent of the 1845 deposit (red stars on Fig. 4). Similarly, thin sections representing a cross section of the tephra layer (Fig. 6), at specific sites in the distal sector of the tephra fall (black dots on Fig. 4), were examined under the SEM (Fig. 6).

Fig. 5 shows that the FS fraction of the 1845 deposit contains coarse ash size aggregates of fine ash. It also contains particles that are coated with fine ash particles. Three principal clast types are identified in the samples examined: Type A are clean ash grains with straight and concave surfaces, the latter representing broken bubble walls; Type B are grains that are similar to those of type A but coated with significant amounts of fine ash (<63 µm); and type C are a few hundred microns-wide aggregates of fine ash (<63 µm) (i.e., ash clusters).

The thin sectioned tephra layer (Fig. 6) indicate no apparent size grading; coarser and finer particles are equally dispersed vertically throughout the layer. The coarse ash fraction is predominantly made up of pumice, consistent with the contemporary descriptions. The pumices contain abundant sub-100 micron vesicles plus a few that approach to 500 micron diameter (Fig. 6). Finer particles are shards similar to those in Fig. 5. In the six samples prepared as sections (Fig. 6), fine particles are a major component in all samples but one (J13-19). Porosity of the tephra layer is also relatively high, especially where fines are sparse (Fig. 6). In many of the thin sections ash clusters were inferred where fines were observed (Fig. 6).

4.6 Total grain-size

The total grain-size distribution (TGSD) of the opening phase of Hekla 1845 is shown in Fig. 13. The distribution is bimodal with a coarse peak at -2.5 ϕ with a hint of a shoulder centered on 1 ϕ, and a subordinate fine peak from 3 ϕ to 4.5 ϕ. The proportions of lapilli, coarse ash and fine ash produced in the opening phase are: 46% lapilli (2 to 64 mm; -1 to -6 ϕ), 43% coarse ash (0.063 to 2 mm; 4 to 0 ϕ), and 11% fine ash (< 0.063 mm; >4 ϕ). This amounts to 3.5 x 10^{10} kg of lapilli, 3.2 x 10^{10} kg of coarse ash and 8.3 x 10^{9} kg of fine ash.

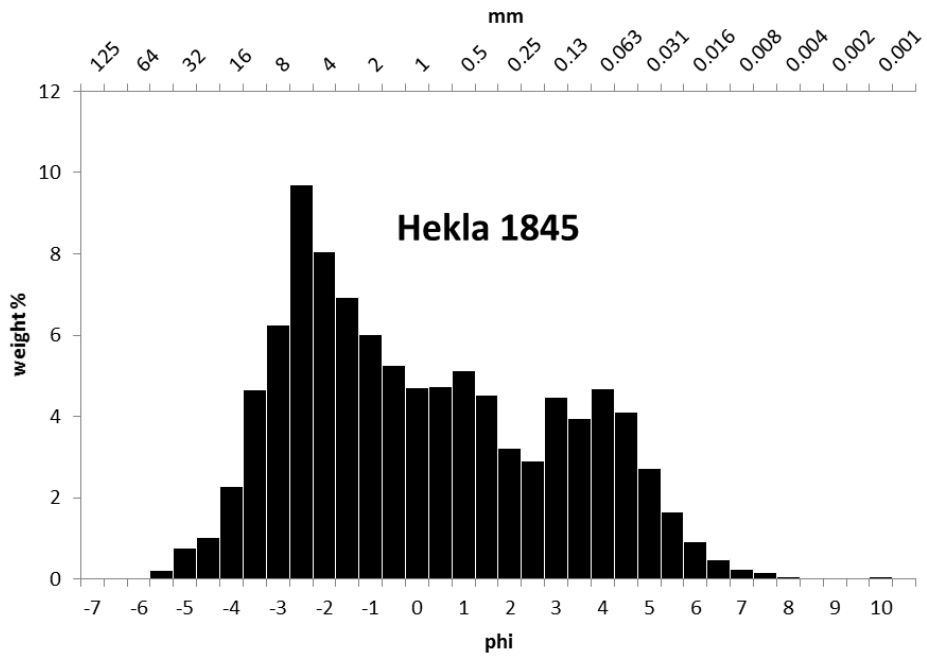

Fig. 13. Total grain-size distribution of the opening phase of Hekla 1845. The distribution is bimodal with primary, coarser peak at -2.5 φ and a shoulder centered at 1 φ, and a secondary, finer peak at 4φ.

5 Discussion

5.1 Contemporary accounts

There is some ambiguity regarding the exact onset of the eruption. Erlendsson (1847) states that the eruption started in the early part of the mid-morning division of the solar day ("ofanverðum dagmálum" in Icelandic). Thorarinsson (1967a; 1968) took this to mean 9 am. However, the term "dagmál" is one of the eight three-hour-long division of the solar day, namely the one extending from 9 to 12 am. The fact that Erlendsson states it began during the early part of "dagmál", implies that it began sometime after 9 am. This understanding is further supported by the statement by Björnsson (1846) that the tephra fall began at Kirkjubæjarklaustur in the latter part of "dagmál" ("hallandi dagmálum" in Icelandic), which we know from other sources began around 11 am (Schyte, 1847) or towards the end of the division "dagmál". We also know that the plume was first seen from the coastal region ESE of Hekla around 10 am, which places the onset of the eruption in the hour of 9 to 10 am. This implies the onset of activity is closer to 10 am rather than 9 am, because typical rise-time to maximum heights for 20th century Hekla plumes can be as low as 10 minutes (Thorarinsson, 1967a; 1968; Larsen et al., 1992; Gudnason et al., 2017;). Therefore, we interpret the onset of the 1845 eruption to be sometime between 9:30 and 9:45. This is compatible with wind speed of 16–19 m s^{-1} to Kirkjubæjarklaustur and ships listed in Table 2.

All 20th century opening phases of Hekla eruptions illustrate that each eruption starts abruptly and explosively with maximum productivity attained in few minutes. The contemporary accounts (Schythe, 1846; Erlendsson, 1847) do not imply anything other than a powerful opening phase peaking within 30 minutes and featuring intense tephra fall for about one hour, as inferred here. This compares well with duration of the opening phase in the 1947, 1970, 1980, 1991, and 2000 eruptions, which are on the order of 0.5 to 3 hours with MER from 10^6 to 10^7 kg s^{-1} (Thorarinsson and Sigvaldason, 1972; Grönvold et al., 1983; Gudmundsson et al., 1992; Höskuldsson et al 2007; Gudnason et al., 2017).

5.2 Volume of deposits

The three different approaches (exponential, power law, and Weibull) used yield similar volumes of tephra from the opening phase (Table 3). The volume estimate obtained via exponential segments and the Weibull function are compatible, whereas the power law overestimates the deposit thickness in the distal sector, thus resulting in a larger volume. The tephra layer is well preserved in the distal region and shows no signs of being modified by erosion. Furthermore, the tephra deposition was at the end of summer when vegetation coverage is at its maximum. Therefore, we conclude that the overestimation of distal thicknesses by the power law fit is real, and the exponential and Weibull fits are a better representation of the data. However, the thinning trend is only represented with two exponential segments which implies minimum volume estimates for the opening phase. Ideally, tephra deposits should be described by three segments (Bonadonna et al., 1998). Bonadonna and Houghton (2005) demonstrated that exponential fit can underestimate the volume by 40–70% if thickness constraints are missing from the distal and the proximal sectors. Bonadonna and Costa (2012) pointed out that estimates based on a Weibull fit are sensitive to how well constrained the thickness changes are in the proximal and distal sectors. For the 1845 tephra fall deposit, the proximal and distal parts of the deposit were the best constrained. However, as mentioned above, the deposit is only represented by two exponential segments, indicating caveats in the most proximal area. That area is partly covered by younger lava flows and is poorly accessible. Although we consider the results from the exponential segments as being more representative than the power law and Weibull, due to a better fit to the whole dataset (Fig. 7), it should be stressed that the results (0.13 km^3 / 0.03 km^3 DRE and 7.5 x 10^{10} kg) are a minimum estimate for the volume and mass of 1845 tephra fall deposit.

Comparing the 1845 tephra fall deposit to tephra fall deposits from other historical Hekla eruptions shows that the 1845 eruption is in the lower end of the historical spectrum (i.e., since the 1104

eruption), but within the same magnitude as the eruptions in 1104, 1158, 1300, 1693, 1766, and 1947 (Thorarinsson, 1968; Janebo et al., 2016). It is also an order of magnitude larger than the 1980, 1991, and 2000 eruptions (Thorarinsson, 1968; Thorarinsson and Sigvaldason, 1972; Grönvold et al., 1983; Gudmundsson et al., 1992; Larsen et al., 1992; Höskuldsson et al., 2007; Gudnason et al., 2017; Fig. 14).

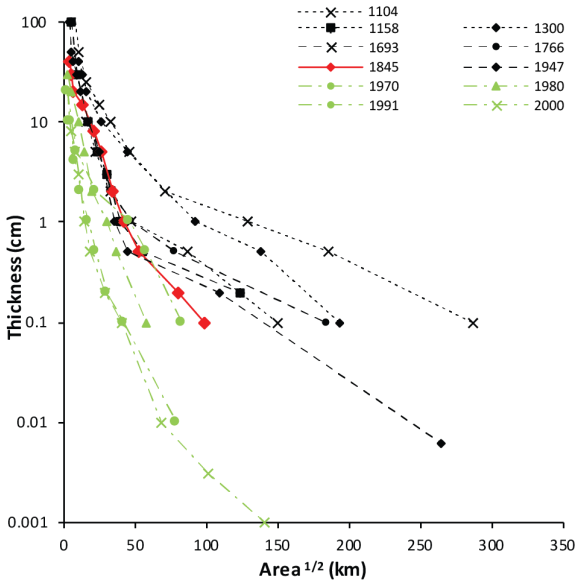

Fig. 14. Thickness vs. square root of area covered for historical Hekla tephra fall deposits. The 1845 tephra fall deposit falls roughly in the middle of the historical spectrum.

5.3 Dispersal and volume of the 1845 tephra fall deposits, comparison with previous studies

The new isopach map (Fig. 2) is based on 154 visited locations, whereas the old isopach map by Thorarinsson (1967a; 1968) was based on only about 30 points. The two maps, however, compare reasonably well. They illustrate the axis of deposition but the geometry of the fall deposit is in general better defined in the revised map. To compare the results from the measured 154 sites to Thorarinsson´s (1967a; 1968) results, volume was calculated from the original data from Thorarinsson (1968) using the same approaches as in Fig. 7. This results in volumes of 0.08 km^3, 0.1 km^3 and 0.35 km^3 of tephra by one-exponential segment, Weibull, and the Power law (0.02 km^3, 0.02 km^3 and 0.09 km^3 DRE, respectively). Although the volume difference between the two isopach maps is not big, the range in volume is larger and less information can be drawn from the isopach map constructed from the much more limited amount of data points. 30 points are adequate to get a rough estimate of the tephra fall volume for the 1845 deposits. In spite of the much large number of measured sites for the revised map, the proximal area possibly remain underrepresented.

5.4 Plume height and duration of the explosive phase

The calculated plume height and MER are based on duration of tephra deposition in distal parts of the deposits (Schythe, 1947). The length of the opening phase is not precisely known but the 1 hour long deposition of coarse ejecta is interpreted here as duration of the opening phase.

We consider the 19 km a.s.l. to be a time-average height. Most likely a higher eruption plume characterized the first half hour of the opening phase, possibly similarly to the 1947 Hekla eruption plume, which rose to 30 km in 30 minutes (Thorarinsson 1967a; 1968). This is also supported by the

decrease in intensity inferred from changes in grain-size with time in the proximal 1845 deposit (Fig. 12) and indications of a higher plume of 24.5–31.5 km a.s.l. from the isopleth data.

5.5 Bimodality of individual grain-size samples

The downwind decrease in grain-size of the tephra layer and especially the coarse subpopulation (Figs. 8, 9) reflects fractionation during transport in a turbulent volcanic umbrella cloud that had a wide initial range of entrained grain-sizes (e.g., Sparks et al., 1992; Bonadonna et al., 1998). The results from the grain-size analysis and the deconvolution show that the sedimentation processes of the two populations (Fig. 10) was more complex than anticipated from the uniform appearance of the deposit (Fig. 9B). The question is whether the two grain-size populations sedimented independently of each other or simultaneously.

The contemporary accounts describe fallout of coarse material succeeded by sedimentation of fines (Schythe, 1947). This could indicate that there is simply a temporal evolution in production and sedimentation from CS to FS. However, only minor temporal changes in grain size are seen in proximal sections (Fig. 12), none in medial sections (Fig. 9B), and in distal sections no stratification is observed and there is an overall non-graded appearance of the tephra layer (Fig. 6). The mass proportions of the two subpopulations are on average 60/40 (CS/FS) and so sedimentation of CS prior to FS would be expected to result in stratified deposits. The overall appearance of the tephra layer therefore favors simultaneous sedimentation of the two populations. This could be explained by premature settling of fines by aggregation. Aggregates are found throughout the deposit (Figs. 4, 5, 6), and we therefore interpret the sedimentation pattern on Fig. 10 as premature sedimentation of fines by aggregation and, consequently, favor simultaneous sedimentation of the CS and FS from the Hekla 1845 volcanic cloud. The temporal variation of the fallout, described by Schythe (1847), probably involved only a very small proportion of the erupted mass, i.e., most of the ash also deposited during the sedimentation of the lapilli fraction, and the 'fine tail' during waning intensity was volumetrically insignificant.

5.6 Total grain-size distribution

The Hekla 1845 TGSD is bimodal (Fig. 13). This is not an unusual feature of Hekla deposits. e.g. The deposits from the 1970, 1991, and 2000 Hekla eruptions are also bimodal (Óskarsson, 1980; Biass et al., 2014; Gudnason et al., 2017). Other historical Hekla eruptions like 1104, 1300, 1693, and 1766 have also produced bimodal tephra layers (Janebo, 2016), as well as the prehistorical H3 and H4 Hekla tephra layers (Stevenson et al., 2015).

Bimodal TGSDs are known from other eruptions such as Mt St Helens 1980 (Carey and Sigurdsson 1982; Rose and Durant, 2009), Mt Spurr 1992 (Durant et al., 2009), El Chichón 1982 (Varekamp et al., 1984; Rose and Durant, 2009), and the Campania Ignimbrite (Engwell et al., 2014). The bimodality in these eruptions has been linked to sedimentation from plumes associated with pyroclastic density currents (co-PDC plumes). The source of the secondary peak in the 1845 Hekla TGSD (Fig. 13) is not thought to be a result of a co-PDC plume as PDC deposits are lacking and there is no mention of such events in the contemporary accounts. An alternative explanation for bimodal TGSD could be secondary fragmentation by external water. Although some water/ice was present in the summit region of Hekla in 1845, as source for flood water (Fig. 2C; Erlendsson, 1847), Hekla lacks a significant amount of ice on the summit to induce secondary fragmentation by external water. The cause for the bimodal TGSD is therefore considered related to the primary fragmentation, similar to what was proposed for bimodality in the 1991 Hekla eruption (Gudnason et al., 2017).

6 Conclusions

The opening phase of the 1845 eruption was 1 hour long sustained explosive phase, starting around 9:30–9:45 on the 2 September. During the opening phase, 7.5 x 10^{10} kg and 0.13 km^3 (0.03 km^3 DRE) tephra was deposited from a 19 km a.s.l. high eruption plume to the ESE of Hekla.

Intensity (i.e., plume height and MER) was highest early in the opening phase and decreased with time. Tephra was transported with speed of 16–19 m s^{-1} to locations in Iceland, and ships and Islands up to 1100 km away, within 24 hrs from onset of the eruption.

The TGSD of Hekla 1845 is bimodal, with peaks at -2.5 ϕ and 3 to 4.5 ϕ. Of the erupted tephra, lapilli, coarse and fine ash amounts to 3.4 x 10^{10}, 3.2 x 10^{10} kg and 8.2 x 10^{9} kg (46%, 44% and 11% of the total mass, respectively). The bimodality of the total grain-size distribution is attributed to the primary fragmentation of the magma whereas the bimodality of individual grain-size samples can be explained by premature deposition of fine particles by aggregation.

A future explosive event of similar size and character as Hekla 1845 has the potential to disrupt air traffic through injection of ash into the atmosphere, reaching mainland Europe in ~24 hrs. It can also have severe effect on local population health by depositing large amounts of fine particles close to the volcano.

References:

Biass, S., Scaini, C., Bonadonna, C., Folch, A., Smith, K., & Höskuldsson, A. (2014). A multi-scale risk assessment for tephra fallout and airborne concentration from multiple Icelandic volcanoes – Part 1: Hazard assessment. Natural Hazards and Earth System Sciences, (14), 2265–2287. doi.org/10.5194/nhess-14-2265-2014

Biass, S., Bonadonna, C. (2014). TOTGS: Total grainsize distribution of tephra fallout. https://vhub.org/resources/3297

Björnsson, J. (1846). Fréttir frá Heklu. Úr Rangárvallasýslu. Ný Félagsrit, VIII, 183–202.

Bonadonna, C., Cioni, R., Pistolesi, M., Elissondo, M., & Baumann, V. (2015). Sedimentation of long-lasting wind-affected volcanic plumes: the example of the 2011 rhyolitic Cordón Caulle eruption, Chile. Bulletin of Volcanology, 77(2), 13. doi.org/10.1007/s00445-015-0900-8

Bonadonna, C., & Costa, A. (2013). Plume height, volume, and classification of explosive volcanic eruptions based on the Weibull function. Bulletin of Volcanology, 75, 1–19. doi.org/10.1007/s00445-013-0742-1

Bonadonna, C., & Costa, A. (2012). Estimating the volume of tephra deposits: A new simple strategy. Geology, 40(5), 415–418. doi.org/10.1130/G32769.1

Bonadonna, C., Ernst, G. G. J., & Sparks, R. S. J. (1998). Thickness variations and volume estimates of tephra fall deposits: the importance of particle Reynolds number. Journal of Volcanology and Geothermal Research, 81(3–4), 173–187. doi.org/10.1016/S0377-0273(98)00007-9

Bonadonna, C., & Houghton, B. F. (2005). Total grain-size distribution and volume of tephra-fall deposits. Bulletin of Volcanology, 67(5), 441–456. doi.org/10.1007/s00445-004-0386-2

Carey, R. J., Houghton, B. F., & Thordarson, T. (2009). Tephra dispersal and eruption dynamics of wet and dry phases of the 1875 eruption of Askja Volcano, Iceland. Bulletin of Volcanology, 72(3), 259–278. doi.org/10.1007/s00445-009-0317-3

Carey, S. N., & Sigurdsson, H. (1982). Influence of particle aggregation on deposition of distal tephra from the MAy 18, 1980, eruption of Mount St. Helens volcano. Journal of Geophysical Research: Solid Earth, 87(B8), 7061–7072. doi.org/10.1029/JB087iB08p07061

Carey, S., & Sparks, R. S. J. (1986). Quantitative models of the fallout and dispersal of tephra from volcanic eruption columns. Bulletin of Volcanology, 48, 109–125.

Degruyter, W., & Bonadonna, C. (2012). Improving on mass flow rate estimates of volcanic eruptions. Geophysical Research Letters, 39(16). doi.org/10.1029/2012GL052566

Durant, A. J., & Rose, W. I. (2009). Sedimentological constraints on hydrometeor-enhanced particle deposition: 1992 Eruptions of Crater Peak, Alaska. Journal of Volcanology and Geothermal Research, 186(1–2), 40–59. doi.org/10.1016/j.jvolgeores.2009.02.004

Engwell, S. L., Sparks, R. S. J., & Carey, S. (2014). Physical characteristics of tephra layers in the deep sea realm : the Campanian Ignimbrite eruption. Geological Society, London, Special Publications, 398, 47–64.

Erlendsson, O. (1847). Dagskrá um Heklugosið 1845-6 og afleiðingar þess. In: Ólafsson, E. (ed.) Fjölrit Náttúrufræðistofnunar 3. Prepared for publication by Jóhannesson, H. Náttúrufræðistofnun Íslands, Reykjavík (Garðabær), 1986.

Eychenne, J., Cashman, K., Rust, A., Durant, A., 2015. Impact of the lateral blast on the spatial pattern and grain size characteristics of the 18 May 1980 Mount St. Helens fallout deposit. .Journal of Geophysical Research: Solid Earth 120, 6018–6038. doi:10.1002/2015JB012116

Fierstein, J., & Nathenson, M. (1992). Another look at the calculation of fallout tephra volumes. Bulletin of Volcanology, 54(2), 156–167. doi.org/10.1007/BF00278005

Folk, R. L., & Ward, W. C. (1957). Brazos River Bar: A study in the significance of grain size parameters. Journal of Sedimentary Petrology, 27(1), 3–26.

Gíslason, S.R., Hassenkam, T., Nedel, S., Bovet, N., Eiriksdottir, E.S., Alfredsson, H.A., Hem, C.P., Balogh, Z.I. (2011). Characterization of Eyjafjallajökull volcanic ash particles and a protocol for rapid risk assessment. PNAS. 108. doi:10.1073/pnas.1015053108

Grönvold, K., Larsen, G., Einarsson, P., Thorarinsson, S., & Saemundsson, K. (1983). The Hekla Eruption 1980-1981. Bulletin Volcanologique, 46 (4), 349-363.

Gudmundsson, A., Oskarsson, N., Grönvold, K., Saemundsson, K., Sigurdsson, O., Stefansson, R., Thordarson, T. (1992). The 1991 eruption of Hekla, Iceland. Bulletin of Volcanology, 54(3), 238–246. doi.org/10.1007/BF00278391

Gudmundsson, M.T., Thordarson, T., Höskuldsson, Á., Larsen, G., Björnsson, H., Prata, F.J., Oddsson, B., Magnússon, E., Högnadóttir, T., Petersen, G.N., Hayward, C.L., Stevenson, J. a., Jónsdóttir, I. (2012). Ash generation and distribution from the April-May 2010 eruption of Eyjafjallajökull, Iceland. Scientific Reports, 2, 1–12. doi:10.1038/srep00572

Gudnason, J., Thordarson, T., Houghton, B.F., Larsen, G. (2017). The opening subplinian phase of the Hekla 1991 eruption: properties of the tephra fall deposit. Bulletin of Volcanology 79, 34. doi:10.1007/s00445-017-1118-8

Horwell, C. J., & Baxter, P. J. (2006). The respiratory health hazards of volcanic ash : a review for volcanic risk mitigation, 1–24. doi.org/10.1007/s00445-006-0052-y

Höskuldsson, Á., Óskarsson, N., Pedersen, R., Grönvold, K., Vogfjörð, K., & Ólafsdóttir, R. (2007). The millennium eruption of Hekla in February 2000. Bulletin of Volcanology, 70(2), 169–182. doi.org/10.1007/s00445-007-0128-3

Houghton, B. F., & Gonnermann, H. M. (2008). Basaltic explosive volcanism: Constraints from deposits and models. Chemie Der Erde - Geochemistry, 68(2), 117–140. doi.org/10.1016/j.chemer.2008.04.002

Houghton, B. F., Swanson, D. A., Rausch, J., Carey, R. J., Fagents, S. A., & Orr, T. R. (2013). Pushing the Volcanic Explosivity Index to its limit and beyond : Constraints from exceptionally weak explosive eruptions at Kılauea in 2008. Geology, 41(6). doi.org/10.1130/G34146.1

Houghton, B., Carey, R.J. (2015). Chapter 34 - Pyroclastic Fall Deposits Eds. Sigurdsson, H. In - The Encyclopedia of Volcanoes (Second Edition). Academic Press, Amsterdam, pp. 599–616. doi.org/10.1016/B978-0-12-385938-9.00034-1

Janebo, M. H. (2016). Historical explosive eruptions in Hekla and Askja Volcanoes; eruption dynamics and source parameters. University of Hawaii at Manoa.

Janebo, M. H., Thordarson, T., Houghton, B. F., Bonadonna, C., Larsen, G., & Carey, R. J. (2016). Dispersal of key subplinian–Plinian tephras from Hekla volcano, Iceland: implications for eruption source parameters. Bulletin of Volcanology 78, 66. doi.org/10.1007/s00445-016-1059-7

Kaminski, E., & Jaupart, C. (1998). The size distribution of pyroclasts and the fragmentation sequence in explosive volcanic eruptions. Journal of Geophysical Research, 103(98), 29759–29779.

Kueppers, U., Cimarelli, C., Hess, K., Taddeucci, J., & Wadsworth, F. B. (2014). The thermal stability of Eyjafjallajökull ash versus turbine ingestion test sands, Journal of Applied Volcanology 3 (4), doi.org/10.1186/2191-5040-3-4

Larsen, G. (2000). Holocene eruptions within the Katla volcanic system, south Iceland: Characteristics and environmental impact. Jökull, 49, 1–28.

Larsen, G., Vilmundardóttir, E. G., & Thorkelsson, B. (1992). Heklugosið 1991 : Gjóskufallið og gjóskulagið frá fyrsta degi gossins. Náttúrufræðingurinn, 61, 159–176.

Mastin, L. G., Guffanti, M., Servranckx, R., Webley, P., Barsotti, S., Dean, K., Waythomas, C. F. (2009). A multidisciplinary effort to assign realistic source parameters to models of volcanic ash-cloud transport and dispersion during eruptions. Journal of Volcanology and Geothermal Research, 186(1–2), 10–21. doi.org/10.1016/j.jvolgeores.2009.01.008

Melsted, P. (1846). Fréttir frá Heklu. Ný Félagsrit 6.árgangur. p. 202–210.

Óskarsson, N. (1980). The interaction between volcanic gases and tephra: fluorine adhering to tephra of the 1970 Hekla eruption. Journal of Volcanology and Geothermal Research, 8, 251–266.

Perugini, D., Speziali, A., Caricchi, L., & Kueppers, U. (2011). Application of fractal fragmentation theory to natural pyroclastic deposits: Insights into volcanic explosivity of the Valentano scoria cone (Italy). Journal of Volcanology and Geothermal Research, 202(3–4), 200–210. doi.org/10.1016/j.jvolgeores.2011.02.008

Pyle, D. M. (1989). The thickness, volume and grainsize of tephra fall deposits. Bulletin of Volcanology, 51, 1–15.

Rose, W. I., & Durant, A. J. (2009). El Chichón volcano, April 4, 1982: volcanic cloud history and fine ash fallout. Natural Hazards, 51(2), 363–374. doi.org/10.1007/s11069-008-9283-x

Schythe, J. C. (1847). Hekla og dens sidste Udbrud, den 2den September 1845. København.

Sparks, R.S.J., Bursik, M.I., Ablay, G.J., Thomas, R.M.E., Carey, S.N. (1992). Sedimentation of tephra by volcanic plumes. Part 2: controls on thickness and grain-size variations of tephra deposits. Bulletin Volcanology 54, 685–695.

Stevenson, J., Larsen, G., & Thordarson, T. (2015). Physical volcanology of the prehistoric Hekla 3 and Hekla 4 eruptions, Iceland. EGU General Assembly, id.4207.

Sverrisdottir, G. (2007). Hybrid magma generation preceding Plinian silicic eruptions at Hekla, Iceland: evidence from mineralogy and chemistry of two zoned deposits. Geological Magasine 144, 643. doi:10.1017/S0016756807003470

Thorarinsson, S. (1958). The Öræfajökull Eruption of 1362. Acta Nat. Islandica II, 1–99.

Thorarinsson, S. (1967a). The eruption of Hekla 1947-1948. I. The eruptions of Hekla in historical times, a tephrochronological study. Societas Scientiarum Islandica, I, 1–170.

Thorarinsson, S. (1967b). The eruption of Hekla 1947-1948. II, 3. The tephra fall from Hekla on March 29th 1947. Societas Scientiarum Islandica, I, 1–68.

Thorarinsson, S. (1968). Heklueldar. Reykjavik: Rangæingafélagið.

Thorarinsson, S., & Sigvaldason, G. E. (1972). The Hekla Eruption of 1970. Bulletin Volcanologique, 36(2), 269–288. doi.org/10.1007/BF02596870

Thordarson, T., & Larsen, G. (2007). Volcanism in Iceland in historical time: Volcano types, eruption styles and eruptive history. Journal of Geodynamics, 43(1), 118–152. doi.org/10.1016/j.jog.2006.09.005

Thordarson, T., Miller, D. J., & Larsen, G. (1998). New data on the age and origin of the Leiðólfsfell Cone Group in south Iceland. Jökull, (46).

Varekamp, J. C., Luhr, J. F., & Prestegaard, K. L. (1984). The 1982 eruptions of El Chichón Volcano (Chiapas, Mexico): Character of the eruptions, ash-fall deposits, and gasphase. Journal of Volcanology and Geothermal Research, 23(1–2), 39–68. doi.org/10.1016/0377-0273(84)90056-8

The 1845 Hekla eruption: grain-size characteristics of a tephra layer.

Jonas Gudnason[1,3], Thor Thordarson[1], Bruce F. Houghton[2] and Gudrun Larsen[3]

[1]Faculty of Earth Sciences, University of Iceland

[2]Department of Geology and Geophysics, University of Hawaii

[3]Institute of Earth Sciences, University of Iceland

Corresponding author: Jonas Gudnason jog4@hi.is

Supplement A

Wind speed estimation and travel time for tephra on the 2nd September 1845.

	Time of arrival of ash fall	Eruption start on 2nd of Sept.	Distance (m)	Time (sec)	V (m s^{-1})	Source
Kirkjubæjarklaustur	11:00	10:00	85000	3600	24	Schythe, 1847
		09:45	**85000**	**4500**	**19**	
		09:30	**85000**	**5400**	**16**	
		09:15	85000	6300	13	
		09:00	85000	7200	12	
Ships						
Sloop Helena	21:00	10:00	685000	39600	17	
61°1.5'N		**09:45**	**685000**	**40500**	**17**	
7°58'W		**09:30**	**685000**	**41400**	**17**	
		09:15	685000	42300	16	
		09:00	685000	43200	16	
Schooner Anna Charlotta	22:45	10:00	910000	45900	20	
60°25'N		**09:45**	**910000**	**46800**	**19**	
3°52'W		**09:30**	**910000**	**47700**	**19**	
		09:15	910000	48600	19	
		09:00	910000	49500	18	
Johanne	05:00	10:00	1100000	68400	16	
59°5'N		**09:45**	**1100000**	**69300**	**16**	
1°35'W		**09:30**	**1100000**	**70200**	**16**	
		09:15	1100000	71100	15	
		09:00	1100000	72000	15	

References:

Schythe, J.C., 1847. Hekla og dens sidste Udbrud, den 2den September 1845. København.

The 1845 Hekla eruption: grain-size characteristics of a tephra layer

Jonas Gudnason[1,3], Thor Thordarson[1], Bruce F. Houghton[2] and Gudrun Larsen[3] [1]Faculty of Earth Sciences, University of Iceland
[2]Department of Geology and Geophysics, University of Hawaii
[3]Institute of Earth Sciences, University of Iceland
Corresponding author: Jonas Gudnason jog4@hi.is Supplement B

sample	distance from vent (km)	thickness (cm)	lat	long	wt% lapilli	wt% c-ash	wt% f-ash	Mean	Max ϕ	Mdϕ	σϕ	CS	Mean	Mode	Mdϕ	σϕ	Variance	Skewness	Kurtosis	FS	Mean	Mode	Mdϕ	σϕ	Variance	Skewness	Kurtosis
J13-54_7	3.6	37	63.9684	19.6165	85	12	3	1.0	-5.5	-2.5	3.0	87%	-2.9	-2.8	-2.8	1.1	1.2	0.0	2.7	13%	2.7	2.3	2.5	1.6	2.5	0.4	2.9
J13-87_1	7.6	13	63.9979	19.5132	76	18	6	1.0	-5	-1.1	3.0	73%	-3.9	-4.5	-4.1	0.9	0.9	1.0	4.2	27%	3.1	3.3	3.1	1.7	2.9	-0.1	2.8
J13-53_2	5	28	63.9614	19.5903	87	10	3	1.0	-4	-2.3	4.0	89%	-2.6	-2.8	-2.6	0.8	0.6	0.7	3.8	11%	3.6	3.1	3.4	1.7	3.0	0.6	3.7
J13-50_1	12.5	8	64.0269	19.4222	84	11	6	1.0	-4	-2.3	3.0	82%	-3.0	-3.0	-3.0	0.7	0.4	0.1	2.7	18%	3.3	3.2	3.3	2.1	4.6	0.1	2.7
J13-51_1	10.6	4	63.9974	19.4514	65	24	11	1.0	-4	0.0	3.0	65%	-2.7	-2.7	-2.7	0.8	0.6	0.2	2.7	35%	3.2	3.4	3.3	1.9	3.5	0.0	2.7
J12-46_1	47.9	1	63.8190	18.7736	22	67	10	2.0	-2.5	1.0	4.0	71%	-0.7	-0.8	-0.7	0.5	0.3	0.3	2.8	29%	3.6	3.8	3.7	1.5	2.3	-0.1	2.8
J13-89_1	5.6	15	63.9685	19.5649	60	31	9	1.0	-5.5	-0.7	3.0	64%	-3.4	-4.1	-3.6	1.4	2.0	0.7	3.4	36%	3.1	2.6	2.9	1.2	1.5	0.6	3.2
J13-42_1	29	5	63.9911	19.0737	54	31	15	1.0	-4	0.6	4.0	65%	-2.1	-2.0	-2.0	1.0	1.0	-0.1	2.8	35%	3.6	3.7	3.7	1.2	1.4	-0.1	2.7
J12-48	48.6	1.8	63.8791	18.7111	6	85	9	2.0	-2	1.2	4.5	66%	-0.1	0.1	0.0	0.7	0.4	-0.5	3.3	34%	3.1	2.1	2.8	1.9	3.7	0.8	3.6
J12-36	59.8	1.5	63.8750	18.4764	1	88	11	2.0	-1.5	1.8	3.5	100%	1.6	0.9	1.4	1.6	2.5	0.7	3.4								
J12-37	63	1	63.8362	18.4333	1	89	9	2.0	-1.5	1.5	3.0	59%	0.4	0.6	0.5	0.6	0.3	-0.5	3.3	41%	2.6	2.1	2.4	2.0	3.9	0.4	2.9
J12-38	71.5	0.8	63.8222	18.2612	1	77	22	2.0	-1	2.4	4.0	55%	0.5	0.7	0.5	0.7	0.4	-0.5	3.2	45%	4.0	3.7	3.9	1.2	1.5	0.4	2.9
J12-43	61	1.2	63.7363	18.5671	2	92	6	2.0	-1.5	0.8	5.0	100%	0.5	-0.2	0.3	1.1	1.2	2.1	12.2								
J12-49	51.2	1.2	63.9155	18.6349	8	82	10	2.0	-1.5	1.3	3.5	72%	-0.1	-0.1	-0.1	0.7	0.5	0.0	2.7	28%	3.7	3.1	3.5	1.5	2.2	0.6	3.2
J12-42	70.4	0.7	63.8705	18.2578	8	84	8	2.0	-1.5	1.2	3.5	72%	-0.1	-0.1	-0.1	0.7	0.5	0.0	2.7	28%	3.1	3.3	3.1	1.3	1.8	-0.2	2.8
J12-50	43.5	2	63.9798	18.7794	17	72	11	2.0	-2	1.3	3.5	58%	-0.7	-0.5	-0.6	0.6	0.4	-0.6	3.6	42%	3.2	3.5	3.3	1.3	1.7	-0.4	3.0
J12-35	59.3	0.7	63.9312	18.4653	1	83	16	2.0	-1.5	1.7	4.5	61%	0.2	0.1	0.2	0.6	0.4	0.5	3.0	39%	3.7	3.8	3.7	1.3	1.8	-0.1	2.7
J12-44	56	1.1	63.7330	18.6909	5	79	16	2.0	-2	1.8	3.0	51%	-0.2	-0.1	-0.2	0.7	0.4	-0.1	2.8	49%	3.4	3.2	3.3	1.2	1.4	0.4	2.9
J12-45	52.8	1.3	63.7819	18.7043	12	78	10	2.0	-2.5	1.3	4.0	62%	-0.4	-0.2	-0.3	0.7	0.5	-0.6	3.4	38%	3.2	2.9	3.1	1.5	2.3	0.4	2.9

sample	distance from vent (km)	thickness (cm)		lat	long	wt% lapilli		wt% c-ash		wt% f-ash		Mean		Max ϕ		Mdϕ		σϕ		Variance		Skewness		Kurtosis		FS		Mean		Mode		Mdϕ		σϕ		Variance		Skewness		Kurtosis	
J13-85_1	10.5	10	64.0150	19.4597	69	25	6	1.0	-3.5	-0.1	3.0	69%	-2.2	-2.3	-2.2	0.6	0.3	0.5	3.0	31%	2.5	2.6	2.5	1.8	3.3	0.0	2.7													
J13-84_1	16	5	64.0322	19.3530	39	45	16	1.0	-4	0.7	3.0	45%	-2.5	-2.7	-2.6	0.9	0.8	0.3	2.8	55%	3.0	3.2	3.1	1.2	1.5	-0.2	2.8													
J13-106_1	19.5	15	63.9617	19.2760	69	20	10	1.0	-4.5	-0.2	4.0	80%	-2.2	-2.5	-2.3	1.1	1.2	0.5	3.0	20%	4.1	4.2	4.1	1.4	1.8	-0.2	2.8													
J13-95_1	15	4	63.8848	19.4785	70	20	10	1.0	-4	-0.1	4.0	66%	-3.0	-2.9	-3.0	0.5	0.3	-0.2	2.8	34%	3.2	3.2	3.2	2.1	4.3	0.1	2.7													
J13-103_1	16.5	10	63.9354	19.3559	69	19	12	1.0	-4.5	0.0	4.0	70%	-2.8	-3.1	-2.9	0.9	0.8	0.5	3.1	30%	3.8	3.9	3.8	1.4	1.9	-0.1	2.8													
J12-68_1	27.7	6	63.8483	19.2062	45	38	17	1.0	-3	0.9	4.0	55%	-1.8	-2.0	-1.8	0.8	0.7	0.6	3.2	45%	3.4	3.1	3.3	1.7	3.0	0.4	2.8													
J12-69_1	26	2.5	63.8029	19.3571	16	80	4	2.0	-2.5	0.4	0.0	88%	0.1	0.2	0.2	1.2	1.4	-0.4	3.1	12%	3.9	3.3	3.7	1.0	1.0	0.9	3.8													
J12-74	57.7	1.5	63.8045	18.5696	2	93	5	2.0	-1.5	0.7	4.0	81%	0.2	0.4	0.3	0.5	0.3	-0.4	3.1	19%	3.5	3.8	3.6	0.9	0.8	-0.5	3.3													
J12-67	23.9	7	63.8620	19.2802	64	32	4	1.0	-3.5	-0.5	0.0	66%	-2.3	-2.4	-2.3	0.8	0.6	0.2	2.8	34%	2.2	1.5	2.0	2.0	4.0	0.6	3.2													
J12-70	27.1	1	63.7729	19.4251	30	57	13	2.0	-2.5	1.3	0.0	61%	-0.9	-1.1	-0.9	0.7	0.5	0.5	3.0	39%	3.7	3.8	3.7	1.3	1.6	-0.1	2.7													
J13-109_1	8.2	8	63.9426	19.5427	58	35	7	1.0	-5.5	-0.8	3.0	64%	-3.0	-4.2	-3.3	1.8	3.2	1.0	4.2	36%	3.0	2.6	2.9	1.1	1.3	0.5	3.1													
J13-110_1	8.8	5	63.9379	19.5361	38	46	16	1.0	-5	0.1	3.0	42%	-3.1	-3.4	-3.2	1.4	1.9	0.3	2.9	58%	3.3	3.0	3.2	1.3	1.6	0.4	3.0													
J12-65_2	17	8	63.9049	19.3825	79	15	6	1.0	-5	-1.2	3.0	77%	-3.0	-2.9	-3.0	0.8	0.7	0.1	2.7	23%	3.2	3.2	3.2	2.1	4.2	0.1	2.7													
J13-108_1	7.55	15	63.9503	19.5448	68	25	8	1.0	-5.5	-0.6	4.5	71%	-2.8	-3.0	-2.9	1.3	1.7	0.3	2.8	29%	3.4	3.1	3.3	1.4	2.0	0.4	2.9													
J13-98	10.1	13	63.9907	19.4613	66	24	10	1.0	-5.5	-0.5	3.0	66%	-3.4	-3.5	-3.4	1.2	1.3	0.2	2.7	34%	3.4	3.4	3.4	1.5	2.3	0.1	2.7													
J13-77	50.1	1	63.9425	18.6335	10	82	8	2.0	-3	1.1	0.0	71%	-0.2	0.0	-0.1	0.6	0.4	-0.7	3.8	29%	3.2	3.5	3.3	1.4	1.9	-0.3	3.0													
J13-17	61.2	2	63.7901	18.5093	3	82	15	2.0	-2	1.9	0.0	60%	0.1	0.3	0.2	0.5	0.2	-0.8	4.0	40%	3.6	3.9	3.7	1.2	1.5	-0.4	3.1													
J15-3	75.9	0.1	63.5488	18.4978	0	60	40	3.0	-0.5	3.8	0.0									100%	4.2	3.9	4.1	1.0	1.0	0.5	3.3													
J15-8	75.6	1	63.7671	18.2146	0	94	6	2.0	-1	1.5	0.0	100%	1.0	0.8	0.9	0.9	0.8	0.6	3.5																					
J15-10	71.5	0.5	63.6712	18.4113	0	84	16	2.0	-0.5	2.1	4.0	64%	0.4	0.6	0.4	0.6	0.4	-0.8	3.9	36%	3.9	4.0	3.9	0.5	0.3	-0.8	4.0													
J15-17	62.5	0.6	63.6851	18.6048	3	84	13	2.0	-1	1.9	4.5	55%	0.1	0.2	0.1	0.5	0.3	-0.1	2.7	45%	3.6	3.8	3.7	0.9	0.8	-0.5	3.2													
J15-23	87.5	0.7	63.7409	17.9802	0	86	14	2.0	-0.5	2.3	4.0	60%	0.9	1.0	0.9	0.6	0.3	-0.4	3.0	40%	3.5	3.8	3.6	0.9	0.8	-0.5	3.2													
J13-26	81.2	0.7	63.8310	18.0524	0	94	6	2.0	-0.5	1.8	0.0	59%	0.8	1.0	0.9	0.6	0.3	-0.3	2.9	42%	3.0	3.0	3.0	1.1	1.2	0.1	2.7													
J13-27	78.5	0.6	63.8464	18.1030	0	83	17	2.0	-1	2.4	0.0	37%	0.8	0.7	0.8	0.4	0.2	0.4	2.9	63%	3.2	3.0	3.1	1.5	2.2	0.3	2.8													
J14-04	28.7	2.5	63.8238	19.2215	51	35	15	1.0	-3	0.8	3.0	57%	-1.9	-2.2	-2.0	0.7	0.5	0.7	3.3	43%	3.4	3.5	3.5	1.2	1.4	0.0	2.7													
J14-05	33.2	2.6	63.8070	19.1343	39	52	9	2.0	-3.5	0.6	3.0	67%	-1.2	-1.0	-1.1	1.0	1.0	-0.4	3.1	33%	3.2	3.3	3.2	1.5	2.2	-0.1	2.8													
J14-06	39.1	2.9	63.8230	18.9672	27	59	14	2.0	-2.5	1.2	3.5	68%	-0.9	-0.7	-0.8	0.7	0.5	-0.6	3.5	32%	3.7	3.9	3.7	1.2	1.5	-0.2	2.8													
J14-10	9.6	7	63.9180	19.5640	67	30	3	1.0	-5	-1.1	3.0	89%	-1.9	-3.3	-2.3	1.8	3.3	1.3	5.1	11%	3.1	2.5	2.9	1.3	1.6	0.8	3.6													
J14-14	4.9	8	63.9521	19.6235	45	49	6	2.0	-3.5	-0.1	0.0	100%	-0.1	-2.1	-0.7	2.5	6.0	1.3	5.4																					

The 1845 Hekla eruption: grain-size characteristics of a tephra layer.

Jonas Gudnason[1,3], Thor Thordarson[1], Bruce F. Houghton[2] and Gudrun Larsen[3]

[1]Faculty of Earth Sciences, University of Iceland

[2]Department of Geology and Geophysics, University of Hawaii

[3]Institute of Earth Sciences, University of Iceland

Corresponding author: Jonas Gudnason jog4@hi.is

Keywords Hekla; total grain-size distribution; deconvolution; aggregation; tephra

Corresponding author: Jonas Gudnason jog4@hi.is

Supplement C

The method of sampling the tephra layer in situ, and make thin section will by described and illustrated here.

Firstly, the tephra layer is identified in a soil section, and soil from above the tephra layer is partly removed. A tube of known diameter is punched through soil and tephra. By this the tephra layer is preserved between the soil above and below (Fig. C1).

Fig. C1: Sampling method of tephra by tube, the soil above and below the tephra layer preserves it in situ.

In the lab, the tubes (soil and tephra) were cut in two (Fig. C2) and dried for 48 hours at 60°C.

Fig. C2: Sample tubes cut in two and ready to be dried. Scale on right is in cm.

Fig. C3: Preparation for thin-section. Epoxy was poured over soil and tephra. When epoxy had set loose material (i.e., soil and tephra) was removed and thin-section prepared. Orientation of the tephra layer was always documented.

Epoxy was then poured over the tephra layer (Fig. C3), and as the tephra is more porous than the soil, the epoxy penetrated it well. The soil was also preserved in the epoxy (Fig. C4). A total of seven thin sections from the tephra layer of the 1845 Hekla eruption were prepared this way.

Fig. C4: Thin section of tephra in situ, soil above and below is the brown finer grained material while in the center the tephra layer is preserved. Up direction on the thin section corresponds to the up direction for the tephra layer as seen in soils.

This method of sampling and preparing the tephra layer allows for multiple examinations, e.g., study by imagery in SEM or microscope, and componentry or chemistry can also be done.

The technique can be further improved, especially since the tephra layer is a week point in the soil/tephra structure, and therefore tends to break along the tephra. This was not noticed until thin sections were finished, and to prevent this some sort of confinement above and below (the tube supports the sides) is needed from the cutting stage until epoxy has cured. Example of this can be seen in Fig. C5.

Fig. C5: Another thin sectioned tephra layer, this illustrates how the tephra layer is a weak point in the structure and confinement is needed during preparation.

Qualitative observations were done on the thin sections with scanning electron microscopy Fig. C6. See main text for details and discussion.

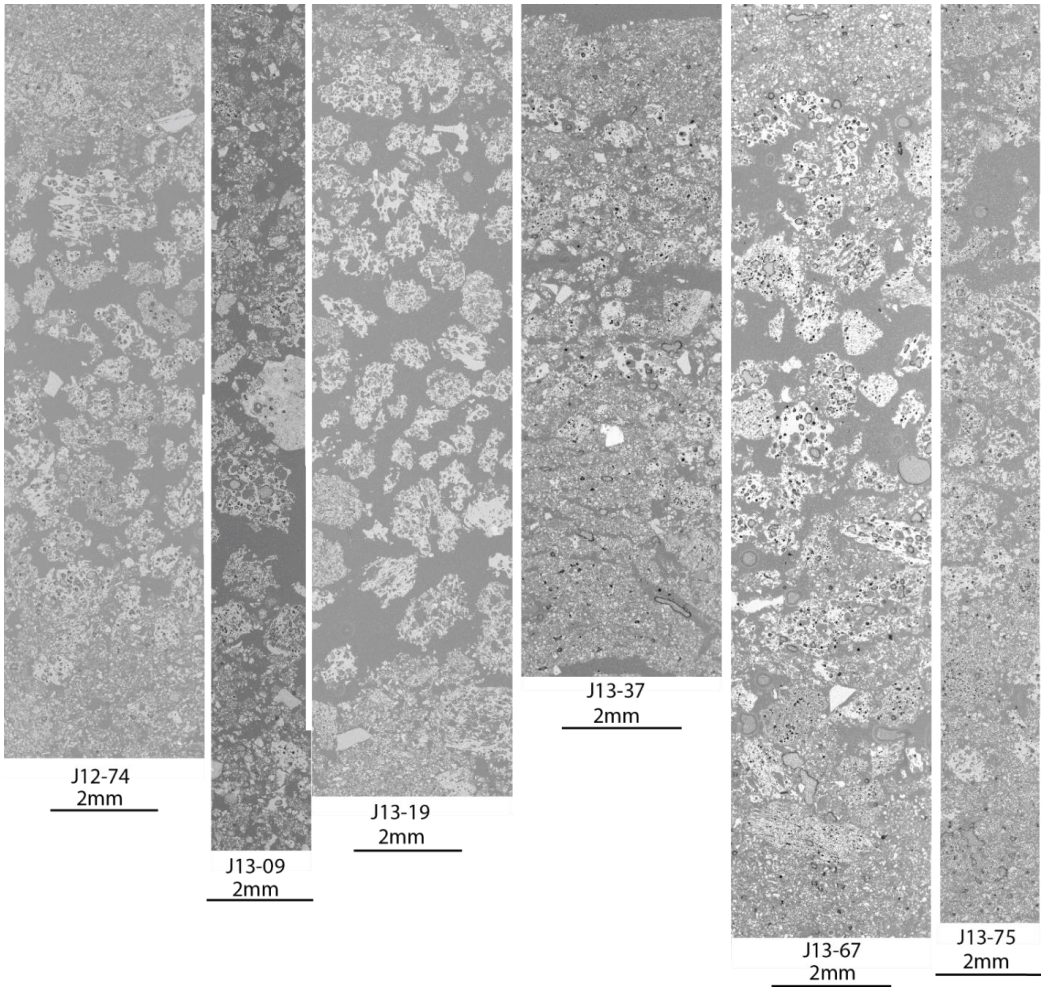

Fig. C6: Final product, imaged with Scanning Electron Microscope using back scatter detector. Grey back ground is epoxy lighter colors are tephra.

The 1845 Hekla eruption: grain-size characteristics of a tephra layer

Jonas Gudnason[1,3], Thor Thordarson[1], Bruce F. Houghton[2] and Gudrun Larsen[3]

[1]Faculty of Earth Sciences, University of Iceland

[2]Department of Geology and Geophysics, University of Hawaii

[3]Institute of Earth Sciences, University of Iceland

Corresponding author: Jonas Gudnason jog4@hi.is

Supplement D

Chemical composition

Glass chemistry of the 1845 tephra was analysed on a WDS Cameca SX100 electron microprobe at the Laboratoire Magmas et Volcans, Clermont –Ferrand (LMV). Standard used was natural glass from Kilauea (A99). The analytical conditions used were 15 kV voltage, 4 nA current, and 10 µm beam diameter. Counting time was 10 s for Na, CA, Ti, P and Si; 20 s for Mg and Al; 30 s for Mn and 40 s for Fe and K. Before the session, 10 points were measured on the standard (A99), and when compared to other reported results they are indistinguishable apart from systematically higher titanium at LMV (Table D1; Jarosewich et al., 1980; Óladóttir et al., 2011; Thornber et al., 2002).

The 1845 products are intermediate transitional alkalic and are icelandites (Table D2; Jakobsson et al., 2008). Holocene magmatic activity at Hekla features an igneous rock series extending from mildly alkaline basalt to a sub-alkaline rhyolite, including transitional basaltic icelandites and subalkaline icelandites. Isotopic studies indicate that they are genetically unrelated and that the formation of the basaltic icelandites results from fractional crystallization of the basaltic parental magma (Sigmarsson et al., 1992).

Table D1: Chemical composition of the standard VG-A99 as acquired on the electron microprobe at Laboratorie Magmas et Volcans LMV (this study) compared to published values: USGS (Thornber et al 2000), USNM (Jarosewich et al 1979), LMV (A) (Oladottir et al 2011). Numbers in brackets are one sigma standard deviation

	VG-A99			
	USGS	USNM	LMV (A)	LMV (this study)
SiO_2	51.06 (0.46)	50.94	51.00 (0.54)	50.85 (0.35)
TiO_2	3.95 (0.09)	4.06	4.17 (0.06)	4.16 (0.06)
Al_2O_3	12.44 (0.13)	12.49	12.65 (0.15)	12.65 (0.10)
FeO	13.15 (0.16)	13.3	13.20 (0.29)	13.31 (0.18)
MnO	0.19 (0.02)	0.15	0.20 (0.07)	0.20 (0.007)
MgO	5.04 (0.1)	5.08	5.01 (0.09)	5.02 (0.07)
CaO	9.04 (0.11)	9.3	9.14 (0.09)	9.16 (0.04)
Na_2O	2.72 (0.16)	2.66	2.69 (0.11)	2.77 (0.11)
K_2O	0.82 (0.03)	0.82	0.86 (0.02)	0.85 (0.02)
P_2O_5	0.43 (0.03)	0.38	0.46 (0.02)	0.44 (0.05)
Total	98.84	99.18	99.35	99.42

When comparing the major elemental composition of tephra from the opening phase and later formed lava in the basaltic icelandite eruptions at Hekla during the latter half of the 20th century the observed differences are minimal (Table D3). For example, the difference in concentration of highly incompatible elements, such as K_2O, between the tephra and lava is <0.25 wt%, and the difference in SiO_2 concentration is only 0.65 wt% (i.e. ≤1%; Table D3). The magma produced by the post 1947 are very similar, and show no temporal changes from the opening phase to the effusive phase (Table D3; Grönvold et al., 1983; Gudmundsson et al., 1992; Gudnason et al., 2017; Höskuldsson et al., 2007; Sverrisdottir, 2007; Thorarinsson, 1968; Thorarinsson and Sigvaldason, 1972). Of the 20th century events, only the 1947 eruption exhibits significant temporal variation in terms of major element composition, where the tephra from the initial phase is high silica icelandite (SiO_2, 62.11 wt%) while the later formed lava is basaltic icelandite (SiO_2, 54.25 wt%; Table 3D). The range in silica content for the tephra from the opening phase of the 1845 eruption is 57–61 wt% (Table D2) and the lava from the effusive phase 54.80 wt%, similar to the range in the 1947 eruptive products (tephra from the opening phase 61.26 wt% and lava from the effusive phase 54.25 wt% SiO_2)(Table D3).

Table D2: Glass chemistry of the 1845 tephra

SiO_2	57.59	58.30	58.34	58.54	58.66	58.78	59.07	59.90	59.93	59.97	60.80	61.26
TiO_2	1.77	1.64	1.55	1.56	1.73	1.77	1.74	1.55	1.61	1.62	1.23	1.20
Al_2O_3	14.49	13.87	14.83	15.43	13.02	14.83	14.80	15.12	14.53	14.60	15.43	15.69
FeO	10.49	10.25	10.70	9.94	9.43	10.46	9.44	10.65	10.27	10.60	9.16	8.65
MnO	0.22	0.28	0.13	0.37	0.08	0.36	0.34	0.33	0.20	0.35	0.30	0.34
MgO	2.42	1.97	2.26	1.87	1.60	2.38	1.88	2.15	2.22	2.28	1.81	1.66
CaO	5.68	4.81	5.26	5.31	5.00	5.65	5.07	5.30	5.32	5.25	5.15	5.03
Na_2O	3.27	3.24	3.94	3.85	4.51	3.55	3.99	3.95	3.93	3.77	3.73	4.14
K_2O	1.67	1.89	1.76	1.65	2.08	1.50	1.96	1.50	1.64	1.67	1.87	1.66
P_2O_5	0.85	0.94	0.92	0.81	0.96	0.88	0.89	0.60	0.72	0.70	0.52	0.37
Total	98.44	97.20	99.70	99.33	97.06	100.16	99.20	101.05	100.38	100.83	100.01	100.02

Table D3: Comparison of the 20th century Hekla eruptions; Hekla 1947 tephra and lava [1](Thorarinsson and Sigvaldason 1970); Hekla 1970 tephra and lava [1](Thorarinsson and Sigvaldason 1970); Hekla 1980 tephra and lava [2](Gronvold et al. 1980); Hekla 1991 tephra average of 10 glass shards [3](Gudnason et al., 2017) 1991 lava[4] (Gudmundsson et al 1992) and H2000 average of 20 tephra and lava samples, according to authors undistinguishable between the two products [5](Hoskuldsson et al. 2007), effusive phase tephra sampled on the Hekla fissure [6](Thorarinsson, 1968) and 1845 lava and opening phase tephra [7](Sverrisdottir, 2007).

Hekla	1845	1845	1845	1947		1970		1980		1991		2000
	Tephra – opening phase	Tephra – effusive phase	Lava – effusive phase	tephra - opening phase	lava - effusive phase	tephra - opening phase	lava - effusive phase	tephra - opening phase	lava - effusive phase	tephra - opening phase	lava - effusive phase	Average of lava and tephra
SiO_2	59.70	56.89	54.80	62.11	54.25	55.21	54.52	54.50	54.60	55.45	54.90	55.52
TiO_2	1.17		1.88	1.02	1.54	1.83	1.91	1.91	1.91	2.32	2.09	2.07
Al_2O_3	15.2	14.18	14.66	16.17	16.34	15.16	14.80	14.60	14.70	13.71	14.30	14.54
FeO	7.39	13.35	10.54	7.75	11.28	11.52	11.78	11.70	11.40	12.30	11.59	11.79
MnO	0.22	0.54	0.25	0.18	0.26	0.26	0.26	0.22	0.24	0.33	0.27	0.28
MgO	1.77	4.05	2.97	1.63	3.39	2.86	3.03	2.90	2.87	2.82	2.91	2.89
CaO	5.06	6.23	6.53	5.24	5.24	6.81	6.76	7.09	7.12	6.26	7.06	6.82
Na_2O	4.52	2.35	4.20	4.12	4.12	4.16	4.08	4.03	3.98	3.59	4.18	4.01
K_2O	1.60	2.65	1.31	0.98	0.98	1.26	1.24	1.16	1.19	1.45	1.22	1.21
P_2O_5	0.41	-	0.94	0.34	0.34	0.68	0.71	0.85	0.86	1.25	1.34	0.87
Total	97.04	100.23	98.08	99.54	97.74	99.75	99.09	98.96	98.87	99.47	99.86	100.00
Source	7	6	7	1	1	1	1	2	2	3	4	5

References

Grönvold, K., Larsen, G., Einarsson, P., Thorarinsson, S., Saemundsson, K., 1983. The Hekla Eruption 1980-1981. Bull. Volcanol.

Gudmundsson, A., Oskarsson, N., Grönvold, K., Saemundsson, K., Sigurdsson, O., Stefansson, R., Gislason, S.R., Einarsson, P., Brandsdottir, B., Larsen, G., Johannesson, H., Thordarson, T., 1992. The 1991 eruption of Hekla, Iceland. Bull. Volcanol. 54, 238–246. doi:10.1007/BF00278391

Gudnason, J., Thordarson, T., Houghton, B.F., Larsen, G., 2017. The opening subplinian phase of the Hekla 1991 eruption: properties of the tephra fall deposit. Bull. Volcanol. 79, 34. doi:10.1007/s00445-017-1118-8

Höskuldsson, Á., Óskarsson, N., Pedersen, R., Grönvold, K., Vogfjörð, K., Ólafsdóttir, R., 2007. The millennium eruption of Hekla in February 2000. Bull. Volcanol. 70, 169–182. doi:10.1007/s00445-007-0128-3

Jarosewich, E., Nelen, J.A., Norberg, J.A., 1980. Reference Samples for Electron Microprobe Analysis. Geostand. Newsl. 4, 43–47. doi:10.1111/j.1751-908X.1980.tb00273.x

Óladóttir, B.A., Sigmarsson, O., Larsen, G., Devidal, J.-L., 2011. Provenance of basaltic tephra from Vatnajokull subglacial volcanoes, Iceland, as determined by major- and trace-element analyses. The Holocene 21, 1037–1048. doi:10.1177/0959683611400456

Sigmarsson, O., Condomines, M., Fourcade, S., 1992. A detailed Th, Sr and O isotope study of Hekla: differentiation processes in an Icelandic Volcano. Contrib. to Mineral. Petrol.

Sverrisdottir, G., 2007. Hybrid magma generation preceding Plinian silicic eruptions at Hekla, Iceland: evidence from mineralogy and chemistry of two zoned deposits. Geol. Mag. 144, 643. doi:10.1017/S0016756807003470

Thorarinsson, S., 1968. Heklueldar. Rangæingafélagið, Reykjavik.

Thorarinsson, S., Sigvaldason, G.E., 1972. The Hekla Eruption of 1970. Bull. Volcanol. 36, 269–288. doi:10.1007/BF02596870

Thornber, B.C.R., Sherrod, D.R., Siems, D.F., Heliker, C.C., Gregory, P., Oscarson, R.L., Kauahikaua, J.P., 2002. Whole-rock and glass major-element geochemistry of Kilauea Volcano , Hawaii , near-vent eruptive products : September 1994 through September 2001. USGS, Open File Rep. 02-17 1–9.

Paper 3

The 1991 and 1845 eruptions at Hekla: Nature of the explosive opening phases inferred from vesicle volume distributions

Jónas Guðnason, Þorvaldur Þórðarson, Bruce F. Houghton

In preparation for Bulletin of Volcanology.

The 1991 and 1845 eruptions at Hekla: Nature of the explosive opening phases inferred from vesicle volume distributions.

Jonas Gudnason[1,3], Bruce F. Houghton[2] and Thor Thordarson[1]

[1]Faculty of Earth Sciences, University of Iceland

[2]Department of Geology and Geophysics, University of Hawaii

[3]Institute of Earth Sciences, University of Iceland

Corresponding author: Jonas Gudnason jog4@hi.is

Keywords: Hekla, Vesicle size distribution, explosive eruptions, fragmentation, ascent dynamics

Acknowledgements This work was supported by Icelandic Centre for Research grant 110077-0061, the Landsvirkjun Energy Research Fund grant 02-2012, the south Iceland Research Fund 2014, and NSF EAR-12-20596. Special thanks to Sigurður Gústafsson, Maria Janebo, and Rebecca Carey for fieldwork assistance.

Abstract

Hekla is one of Iceland´s most frequently erupting volcanoes. Hekla has erupted 18 times in historical times (i.e., since 874 CE), typically with little warning. The eruptions in 2000, 1991, 1980, 1970, 1947, 1845, 1766, 1693, 1389, and 1300 are known to be hybrid in nature (i.e., starting explosively and then transitioning into effusive activity). The explosive activity peaks, in terms of discharge rate, within minutes and the eruption plume rises to more than 10 km a.s.l. in 10 minutes from the onset of eruption. Here we examine the opening phases of the 1991 and 1845 Hekla eruptions, with a focus on constraining the vesiculation process over time. The opening phase of the 1991 eruption was a pulsating explosive event resulting from variable ascent rates seen in temporal trends of decreasing vesicle number densities in the pyroclasts. The opening phase of the 1845 eruption, on the other hand, was steady with a gradual decrease in intensity over time revealed by decreasing vesicle number densities, and increasing variation in ascent rate across the shallow conduit, throughout the opening phase.

1. Introduction

Hekla central volcano, in the Eastern Volcanic Zone, is one of Iceland's most active volcanoes with 18 explosive eruptions since the settlement of the island in 874 CE (Thordarson and Larsen 2007). The historical activity at Hekla is typified by three styles of eruptions: Type I, mafic fissure eruptions on the Hekla fissure swarm, primarily lava producing. Type II, powerful silicic explosive eruptions with little or no effusive activity (e.g., 1104 and 1158). Type III, hybrid eruptions that start explosively and gradually pass into fissure-fed and then single vent effusive activity (e.g., 1991, 1970, 1845, 1766). Since the first historical Hekla eruption in 1104 CE, the repose interval of type II and III Hekla eruptions span the range of 9 to 120 years, with an average of 53 years. However, in the late 20th century eruption frequency increased, resulting in repose period of 9 to 11 years (i.e., eruptions in: 1970, 1980–81, 1991, and 2000). At present, 17 years have passed since the most recent eruption, and in 2013 Hekla had inflated to a state similar to that prior to the 2000 eruption (Sturkell et al. 2013).

Types II and III are confined to the central volcano. Type II events are the largest and most intense eruptions, forming the most widespread deposits while type III events are the most frequent style of eruptions in historic times. We focus here on the products of two such type III eruptions, in 1845 and 1991. The opening explosive phase of the type III eruptions are typically of Plinian to subplinian intensity and produce widespread tephras (e.g., Thorarinsson 1968; Larsen and Eiríksson 2008; Janebo et al. 2016a, b; Gudnason et al. 2017a).

Mass eruption rates for the opening phase of well-characterized historic eruptions ranges from 10^6 to 10^8 kg s^{-1} and the tephra fall volumes range from of 0.17 to 1 km^3 (Thorarinsson 1967, 1968; Óskarsson 1980; Janebo et al. 2016b; Gudnason et al. 2017a, b). However, much less is known about the role of subsurface processes, such as magma ascent, vesiculation, and fragmentation within the shallow conduit, in controlling the nature and intensity of the opening explosive phases. So far, only one microtextural study has been carried out on the products of a Hekla opening phase; the 1158 eruption, which was a type II event (Janebo et al. 2016a). To characterize the more frequent hybrid or type III eruptions, we have undertaken a microtextural study on the pyroclasts from the opening phases of the 1845 icelandite and 1991 basaltic icelandite eruptions. The 1845 eruption typifies the activity at Hekla in the period from 1947 back to at least 1510 CE (Thorarinsson 1967). The opening phase of the 1845 event was one hour long and of Plinian intensity, dispersing tephra to the ESE of Hekla (Fig. 1b and c), with tephra reaching beyond the Faroe islands and as far as the Shetland isles (e.g., Gudnason et al. 2017b). The 1991 eruption is typical for eruptions post-1970 (i.e., up until 2000). Like the 1845 event it began with a 50-minute-long explosive phase, of subplinian intensity, dispersing a tephra-laden plume to the north-northeast from the volcano at velocities of 20 m s^{-1} (Fig. 1b and c), producing a tephra fall that reached the northern coast of Iceland in 5 hours. The explosive activity from both of these eruptions and the associated tephra fall are a threat to aviation, population, and livestock. Hence, improved knowledge of the mechanisms driving explosive activity in type II Hekla eruptions (i.e., ascent, vesiculation, and fragmentation) informs understanding of short-lived explosive eruptions of intermediate magma compositions and is essential for comprehensive hazard assessment and mitigation for future Hekla eruptions.

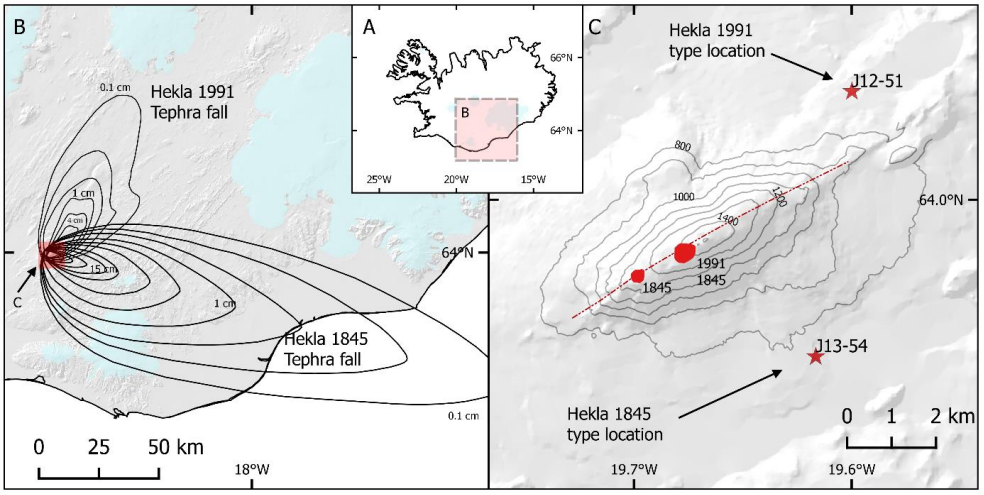

Fig. 1: A) Iceland and its location with the coverage of B). On B) is close up of the isopach maps of the 1991 and 1845 tephra fall after Gudnason et al. (2017a, b), illustrating the difference in areal extend of individual isopcahs. C) is close up of Hekla and with red stars indicating type locations sampled for this study. The section from the 1991 deposits is NE of Hekla (J12-51) and ESE of Hekla is the type location for the 1845 tephra fall deposits (J13-54). The Hekla fissure is indicated with red dashed line and the opening phase craters are shown in red

2. Approach to study

2.1 Type locations and sample selection

The study is centred on one type sections for each eruption, located about 4–5 km downwind from the summit of Hekla (Fig. 1). At these type sections, the deposit is 37 cm thick in case of the 1845 event and 15 cm thick in case of 1991 (Fig. 2).

2.1.1 Hekla 1991

At section J12-51 (Figs. 1, 2), the tephra fall deposit from the 1991 eruption has two principal subunits: a lower, lapilli-dominated fall unit (samples J12-51-8 and -7 on Fig. 2) and an upper, lapilli-dominated fall unit (samples J12-51-5 and -4 on Fig.2). The upper and lower fall units are separated by a parting of ash (Gudnason et al. 2017a). Both lapilli fall units were analysed for this study, with samples from both the base and the top of each unit (Fig. 2). The pyroclast textures are homogeneous and clasts selected for more detailed analysis have modal densities/vesicularities that represent the majority of the erupted magma in the opening phase of the 1991 eruption (Fig. 3).

2.1.2 Hekla 1845

At section J13-54, the 1845 tephra fall deposit is normally graded and lapilli dominated (Gudnason et al. 2017b). Samples for analysis were collected at three intervals at different stratigraphic heights through the deposit (Fig.2). The lowermost sample was selected to represent the coarsest/lowermost part of the deposits, the middle sample to represent the change in grain-size, and the top to represent the upper and finer part of the deposit (Fig. 2). The 1845 tephra was subdivided into three textural classes: microvesicular (M), scoriaceous (S), and transitional (T). The M clasts have on average smaller vesicles and are generally lighter (brown) colored, while the S clasts are darker (black) with larger vesicles, and the T clasts is a mixture of the other two. The clasts selected for detailed analysis were from the modes of the M and S classes (Fig. 3; Gudnason et al. 2017b).

2.2 Density/Bulk Vesicularity analysis

The seven samples were collected from vertically narrow stratigraphic intervals, and each sample contained a minimum of 100 clasts in the size range 8 to 32 mm. The density/bulk vesicularity of each clasts was determined using the method of Houghton and Wilson (1989). Melt density, to convert from clast specific density to bulk vesicularity was measured using a water pycnometer, and it was determined to be 2470 kg m^{-3} for Hekla 1845 and 2620 kg m^{-1} for Hekla 1991 (Gudnason et al. 2017a, b).

From each sample, a subset of clasts representing the modal peak, was selected for thin-sectioning and detailed vesicle-size distribution measurements (section 2.3).

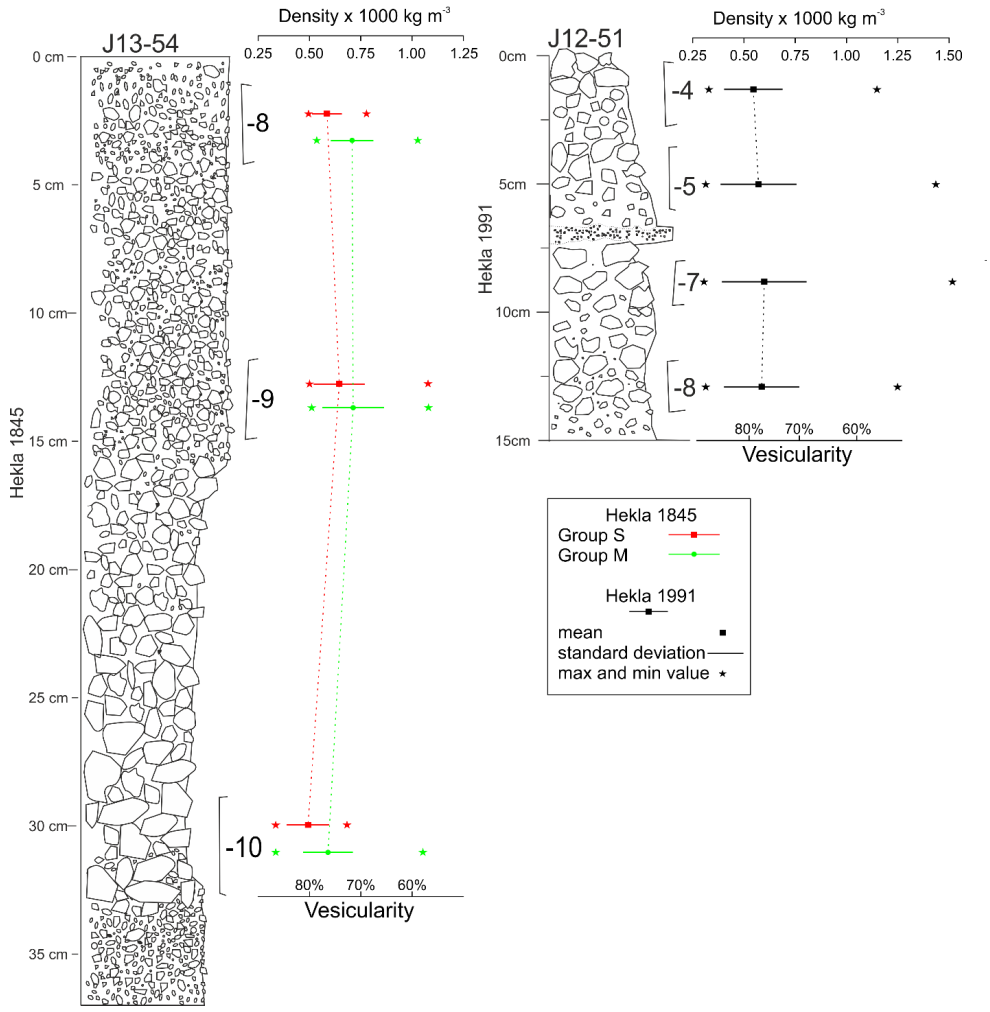

Fig. 2: Stratigraphic logs of the type sections for Hekla 1845 (left) and 1991 (right) sampled for this study. Depth of section is indicated by scale bar on the left columns and the raster in each log indicates qualitatively the vertical changes in grain size. The vertical bars on the left of the column indicate the sample position and the vertical thickness sampled. The figures next to the bar are the sample numbers, e.g., J13-54-10 in case of the lowest sample in the 1845 log. Density and vesicularity values indicated on the graph with mean, maximum, and minimum values and the standard deviation from the mean. The colors in the 1845 sections refer to componentry groups as indicated in the box: red is the scoriaceous componentry group S and green is microvesicular group M. The upper and lower lapilli-dominated fall units can be seen on the J12-51 log represented by samples J1251-8 and -7 (lower) and J12-51-5 and -4 (upper). The J12-51 log of the 1991 tephra fall is after Gudnason et al. (2017a) and accordingly has only one component type analyzed

2.3 Vesicle size measurements

Pyroclasts commonly contain vesicles with diameters spanning 4–5 orders of magnitude (e.g., Fig. 4; Klug et al. 2002). Therefore, to ensure a statistically valid sampling of vesicle sizes for measurements, images were collected at several magnifications. First images were collected using a flatbed scanner imaging whole clasts and secondly on a scanning electron microscope (SEM) (Shea et al., 2010). The scanned images were obtained with transmitted light at 1200 to 3200 dpi (47.2 to 126.0 dpmm). SEM images, in backscatter electron mode, were collected at four magnifications, in nested trees following Shea et al. (2010). SEM images were acquired using two different SEM´s: a JEOL-5900lv operating with 15 kV acceleration voltage at the University of Hawaii (UH) and a TM3000 Hitachi

table top microscope with 15 kV acceleration voltage at the University of Iceland (UI). For the 1845 samples, clasts were imaged at UI, and from the Hekla 1991 sample set, clasts were imaged both at UH and at UI.

The lowest possible magnification for the TM3000 instrument is 50x opposed to 25x on the JEOL. To minimize the magnification jump from the scan to the SEM images, and to be comparable to other studies (e.g., Carey et al. 2009; Gurioli et al. 2008; Houghton et al. 2010; Parcheta et al. 2013; Janebo et al. 2016a;), a set of 5 images at 50x magnification was collected with overlap of at least 30% on the TM3000 instrument, and combined into one image. These are the 50x images J12-51-4-97 and J12-51-5-65 in Fig. 4. For all other magnifications, no adjustments are needed. The images were merged using the photomerge command in Adobe Photoshop, choosing the reposition layout, to avoid any distortion. The 50x images cover the same, or a larger, area as the 25x magnification images used in the other studies (Gurioli et al. 2008; Janebo et al. 2016a), and is thus large enough to record the largest bubbles that would be recorded in an equivalent 25x image. As a result of acquiring images on two SEM´s with different resolutions, the lower limit of measured vesicles was set at 22 pixels on images from the JEOL and 15 pixels on images from the TM3000, which at 250x magnification results in a minimum size equivalent diameter of 9 µm. This relatively high cut off is in concordance to e.g. Janebo et al. (2016a) and results in minimal misinterpretation of pixels (see supplement 1).

The images were processed in Adobe Photoshop and made binary, with melt (and microlites) in white and vesicles in black. The open source software ImageJ was then used to measure the area of each vesicle in 2D and to determine the vesicle number density per unit area relative to glass content (Na) (Schneider et al. 2012). Conversion to 3D was made using the stereological conversion by Sahagian and Proussevitch (1998) and vesicles per unit volume of melt (Nv), vesicle volume distributions (VVD) and vesicle size distributions (VSD) were also calculated. The stereological conversion technique takes into account both that smaller vesicles are less likely than larger vesicles to be intersected, and the probability of not cutting a vesicle at the largest diameter (Sahagian and Proussevitch 1998). The drawback is that the method assumes spherical vesicle shapes. In the case for the Hekla pyroclasts studied here, spherical shapes are more common amongst the smaller vesicles (Figs. 4, 5), but no alternative method is available for converting irregular shaped bubbles. Correction for the vesicle volume (N_{Vm}) was also applied to avoid underestimating vesicle number densities (VND), which can be an issue in highly vesicular samples (Klug et al. 2002).

2.4 Microprope analysis

Glass compositions of the matrix in the 1991 and 1845 pumices from the clast density samples were measured by a JEOL JXA-8230 Superprobe at the Institute of Earth Sciences, University of Iceland (UI). The analytical conditions were 15 kV voltage, 19.3 µm current, and 5 µ beam diameter. The standard used was natural glass from Kilauea (A99). When compared to other reported results they are indistinguishable (supplement 2; Jarosewich et al. 1980; Thornber et al. 2002; Óladóttir et al. 2011 Gudnason et al. 2017). Between 10 and 20 point measurements were obtained from each sample. An overview of the glass chemistry of the Hekla 1991 and 1845 tephra is provided in electronic supplement 2 along with comparison with post 1845 Hekla eruptions.

3. Results

3.1 Hekla 1991

3.1.1 Macroscopic textures

At the type locality, the Hekla 1991 deposit is homogeneous in terms of pyroclast textures. It primarily consists of blue-black pumices that are blocky and rather coarsely vesicular, with semi circular bubbles reaching up to 2 mm in diameter. Phenocrysts are plagioclase and olivine and make up less than ~2 vol.%. Evidence of post fragmentation expansion of the tephra clasts, such as bread-crusted surfaces or obvious size increase of bubbles toward the clast centre (e.g., Klug and Cashman 1994), were not detected in the clasts analysed in this study.

3.1.2 Density and bulk vesicularity

The 1991 Hekla pumice clasts are dominantly highly vesicular (60–80% vesicles; 57% of clasts) and secondly extremely vesciular (>80% vesicles; 41% of clasts) (Houghton and Wilson 1989). Only a few clasts are moderately vesicular (2%) (Gudnason et al. 2017a). Clast density measurements show tight, slightly positively skewed distributions with density values between 310 and 1520 kg m^{-3}. The stratigraphically lowermost sample (J12-51-8), representing the onset of the eruption, exhibits a bimodal density distribution with peaks at 500 and 800 kg m^{-3}, whereas remaining samples, representing the later stages of the opening phase, are all unimodal with peaks at 500 or 600 kg m^{-3}. Samples from the upper fall unit (J12-51-4 and 5) exhibit a slightly tighter distribution (standard deviation of 140–190 kg m^{-3}) compared to the lower fall unit (standard deviation of 180–210 kg m^{-3}). The calculated mean vesicularity for all four samples fall within the very narrow range of 77–79 vol.% and is unchanged with respect to time (i.e., stratigraphic height) during the opening phases (Fig. 3; Table 1).

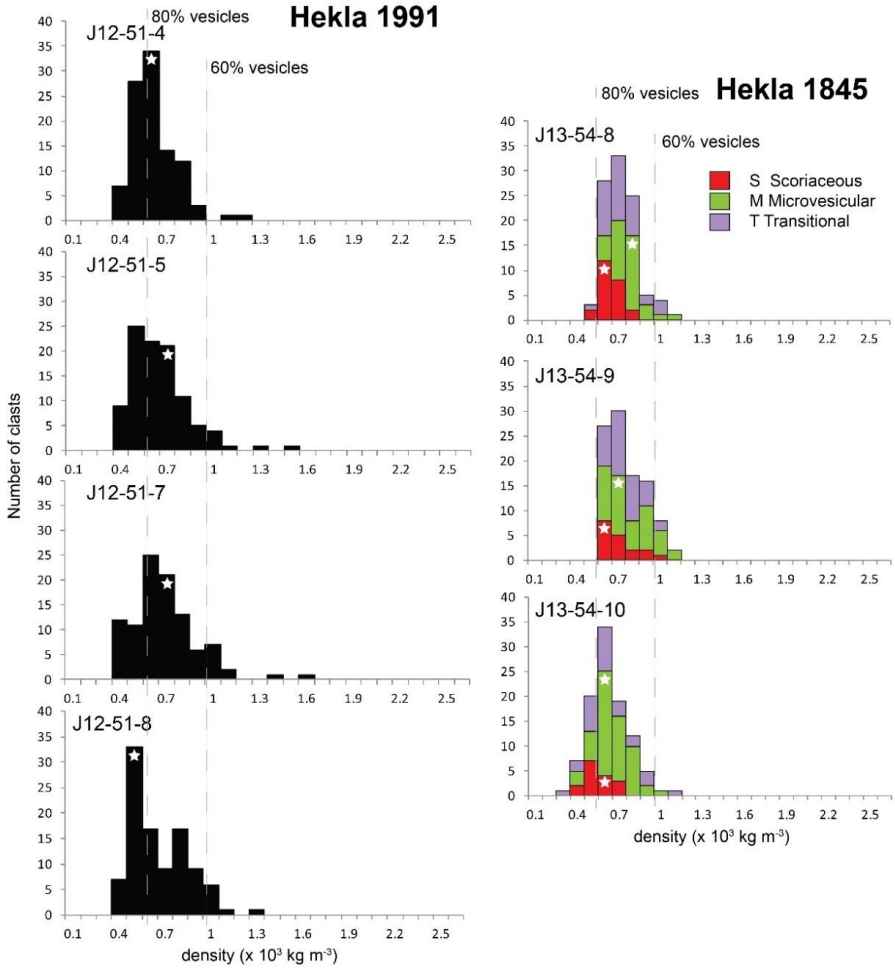

Fig. 3: Clast density distribution of Hekla 1991 samples from location J12-51 (left panel) and Hekla 1845 samples at location J13- 54 (right panel). The clast measurements from the Hekla 1991 deposit define tight and slightly positively skewed density distributions, with clast density ranging from 310–1520 kg m^{-3} and mean density from 550–600 kg m^{-3}, corresponding to mean vesicularity between 76 and 78 vol.% (see text for further details). The bars in the Hekla 1991 distributions are shown black because it is typified by one clast type, pumice. The clast measurements from the Hekla 1845 deposit define a tight and very weakly skewed unimodal distributions with clast densities ranging from 300–1080 kg m^{-3} and mean densities of 490–710 kg m^{-3}, corresponding to mean vesicularity between 70 and 80 vol.%. White stars indicate the bins that clasts for microtextural analysis were selected from. For the Hekla 1845 clasts were selected from two componentry (S and M) groups to cover the range in patterns of vesiculation (see text for further details)

3.1.3 Microscopic textures – Qualitative data

The microtextural properties of the tephra from the 1991 opening phase are fairly uniform. Vesicles of intermediate to large sizes (100 to 400 µm and >400 µm) are commonly polylobate, while the smallest vesicles (<100 µm) are typically sub-spherical to spherical.

Clast 88 from sample J12-51-8 and clast 99 from sample J12-51-7 represent the modal vesicularity of the magma at the start and towards the end of the lower fall unit (Fig. 4). The vesicles in these two clasts are comparable in size range. The only notable difference is in abundance of small vesicles (<100 µm), which are more numerous in J12-51-8-88 compared to J12-51-7-99 (Fig. 4). The more numerous small vesicles result in apparently thinner vesicle walls in J12-51-8-88 between the

smallest vesicles (1-15 μm). Vesicles of large (>400 μm) and intermediate (100–400 μm) sizes are similar in abundance in the clasts. In both clasts, the largest vesicles (>400um) are polylobate with round or concave walls (Fig. 4), indicating growth by coalescence with a few trains of partly coalesced vesicles observed. Coalescence of large vesicles with both intermediate sized and small vesicles is observed. Intermediate sized vesicles are dominantly sub-spherical but a minority are polylobate with signs of coalescence. The smallest vesicles show the highest degree of sphericity and are coalesced to the least extent (Fig. 4). Thickness of vesicle walls is on average 2–15 μm in both samples from the lower fall unit.

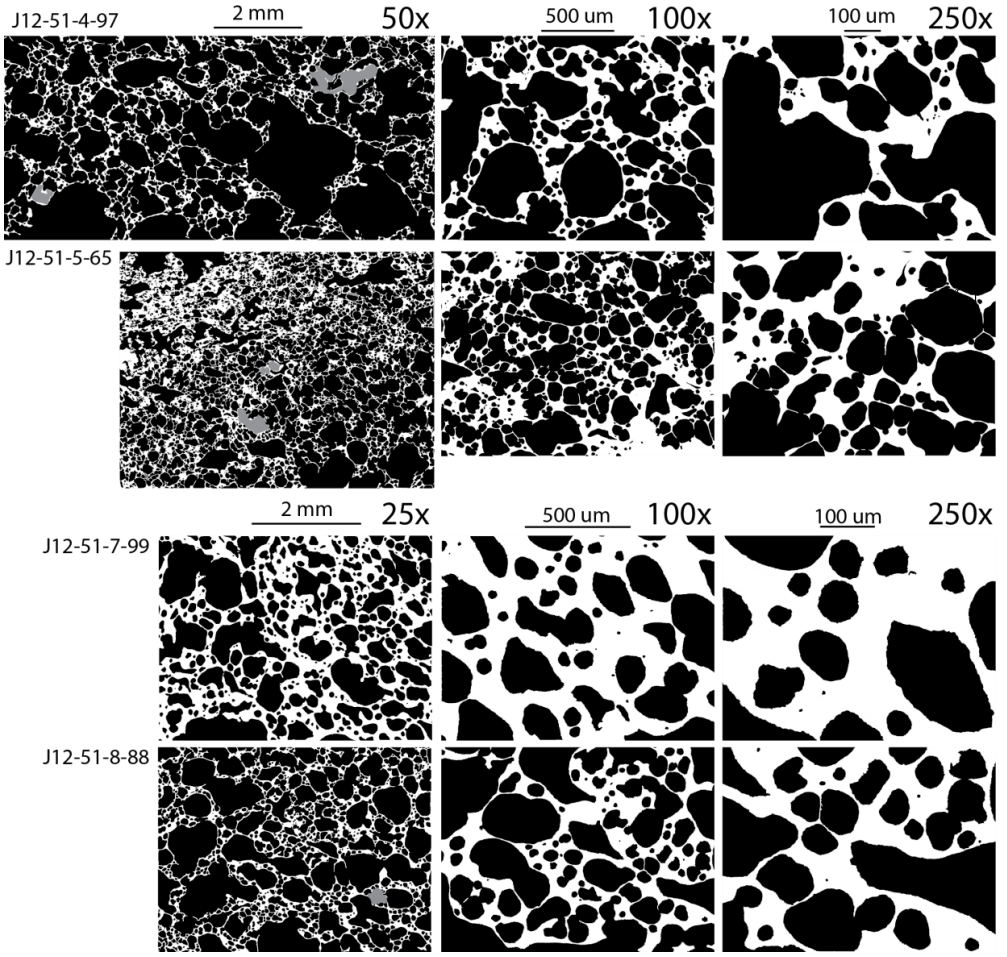

Fig.4: Binary images for the Hekla 1991 clasts arranged in stratigraphical order and used here to illustrate qualitatively the nature of the vesicle population at four stages during the explosive opening phase. Clasts J12-51-8-88 and J12-51-7-99 are from the bottom and top of the lower fall unit, while J12-51-5-65 and J12-51-4-97 represent the same pairing for the upper fall unit. Magnifications are from 25–250x; vesicles are black, crystals are grey and glass is white

Clast 65 from sample J12-51-5 and clast 97 from sample J12-51-4 represent the modal vesicularity of the magma at the start of and towards the end of the upper fall unit of the 1991 tephra fall deposits (Fig. 3). Clast J12-51-4-97 features a rather uniform vesicle population. Clast J12-51-5-65 exhibits some degree of heterogeneity. There are areas of apparently contrasting vesiculatrities, i.e. dominantly thin vesicle walls and all size ranges of vesicles vs. areas of dominantly smaller vesicles with thicker vesicle walls (Fig. 4). This heterogeneity does not appear to be related to post fragmentation expansion as domains with very large vesicles are present at the edge of the clast.

During image acquisition, the glassy and less vesiculated regions were avoided if possible (see Fig. 4, clast J12-51-5-65, 50x magnification upper left corner vs. lower right for example). The largest vesicles in clast J12-51-4-97 are qualitatively larger and more coalesced than in clast J12-51-5-65 (Fig. 4). The vesicle shapes of the largest vesicles (>400 µm) are polylobate after coalescence with smaller vesicles, similar to the pumices from the lower fall unit. Intermediate (100–400 µm) sized vesicles are sub-spherical, and only few are polylobate (Fig. 4). Small vesicles (<100 µm) are sub-spherical to spherical, and evenly distributed with minor coalescence. Bubble wall thickness for both samples is 2–15 µm. There are no signs of shearing or stretching of vesicles.

3.2 Hekla 1845

3.2.1 Macroscopic textures

The 1845 tephra fall deposits are normally graded and principally consists of two parts (Fig. 2): a lower, coarser part and upper, slightly finer part (Gudnason et al. 2017b). There are three types of juvenile clasts (M, S, and T as defined in 2.1.2). The variation in colour and clast characteristics is subtle and is rather a continuum between the M and S endmembers.

Type M comprises 24–56% of the sample set. The abundance decreases upwards from 56% at the base (sample J13-54-10) to 45% in the middle (sample J13-54-9) to 24% at the top (sample J13-54-8; Fig. 3). The transitional (T) clasts is the second most abundant component type. The T type pumices increase in abundance from 28% (base) to 37% (middle) and 38% (top). The third component (S) is rich in coarse vesicles especially compared to M. The S component increases like T from 16% to 18% and in sample J12-54-8 it is 24% of the deposit (Fig. 3).

3.2.2 Density and bulk vesicularity

The three analysed density samples show slightly positively skewed distributions (Fig. 3), and all of the three components are contributing to the main peak. However, the S group is consistently in the low-density end and the M and T groups are consistently in the high-density end of the distribution (Fig. 3).

The range of densities for the 1845 fall deposits is 300 to 1080 kg m^{-3} and vesicularity 56 to 88 vol.%. Mean clast densities for the three samples (Fig. 3) are 560, 690 and 660 kg m^{-3} (samples J13-54-10, -9 and -8), and the corresponding vesicularities are 76 vol.%, 71 vol.% and 73 vol.%. The mean densities range from 590 to 710 kg m^{-3} for group M, from 550 to 690 kg m^{-3} for group T, and from 490 to 640 kg m^{-3} for group S. The corresponding vesicularities are 70–75 vol.% (group M), 72–76 vol.% (group T), and 73– 80 vol.% (group S). Based on the vesicularity of the whole sample set, the 1845 fall deposit is classified as moderately (i.e., 40–60% vesicles) to extremely vesicular (i.e., 60–80% vesicles). There is an overall trend of decreasing vesicularity with time (Fig. 3), both in terms of decreasing abundance of highly vesicular clasts and increasing mean density. Sample J13-54-10 at the base of the deposit contains 28% highly vesicular clasts, whereas sample J13-54-8 at the top of the deposit only contains 1% of highly vesicular clasts.

3.2.3 Microscopic textures – Qualitative data

The clasts selected (Table 1) for examination of microscopic textures from the 1845 deposit represent the modal peaks of the density histograms for the M and S componentry groups (Fig. 3). The tight density (i.e., vesicularity) distributions imply that the selected clasts are a reasonable representation of the vesicle populations in the erupted magma (Fig. 3). Although the M and S clasts exhibit distinct macroscopic differences, the vesicularity of each type is consistent throughout the opening phase (Table 1). All the clasts contain microlites, increasing in abundance upward from ~5 vol.% at the base of the tephra fall unit to ~10 vol.% at the top. Vesicles are distributed uniformly in the glass regardless of size, and the majority of the vesicles are equant with sub-spherical to spherical forms.

There is a general increase in size of large vesicles from base to top of the section and from group M to group S in each sample (Fig. 5). Coalescence is seen in vesicles larger than 50 µm. With increasing size, vesicles become polylobate with convex and concave walls (Fig. 5). Coalescence of both intermediate (100–400 µm) and small vesicles is also observed. The smallest vesicles show the highest degree of sphericity and are coalesced to the least extent.

The contrast between group M and S (Fig. 5) are consistent with the macroscopic differences. The vesicle population in group S is much more mature, reflected by larger vesicles, complex vesicle shapes reflecting higher degrees of coalescence, and fewer vesicles on average (Table 1).

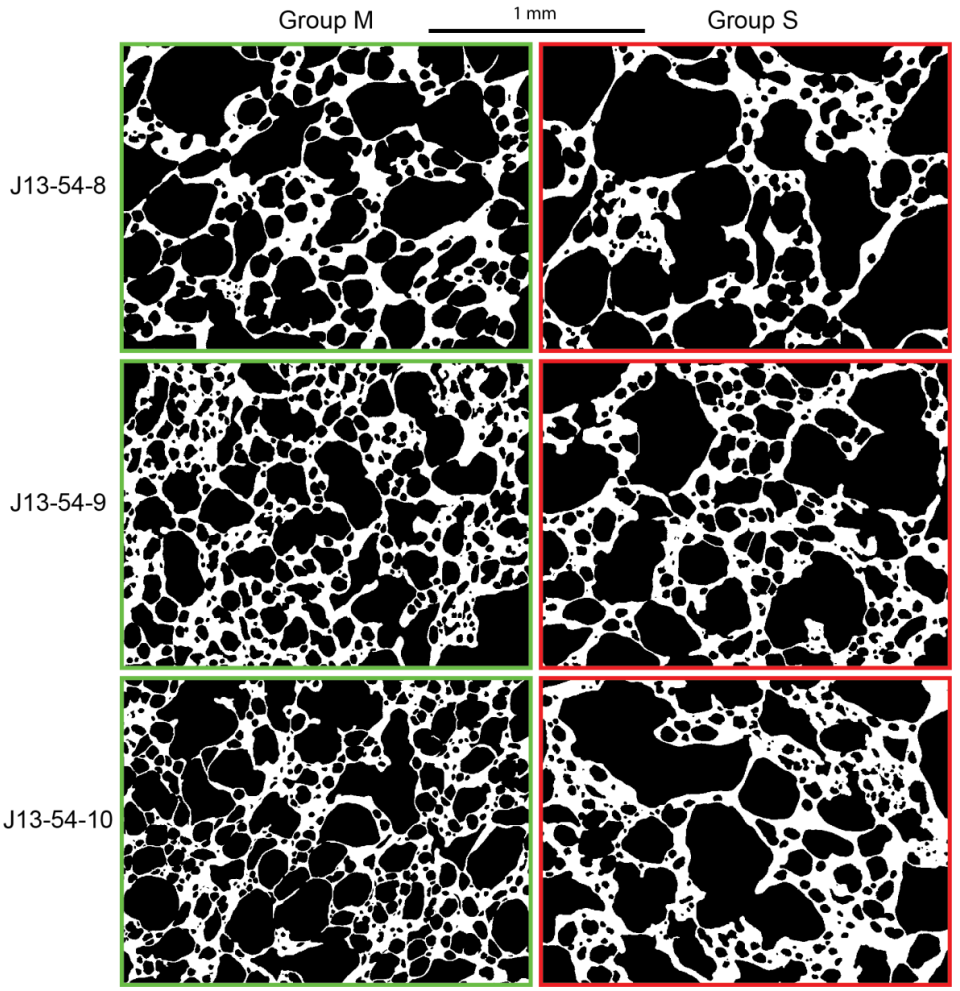

Fig. 5: Binary images of analyzed clasts from the Hekla 1845 deposits. Magnification is 100x in all images, vesicles appear black and glass white. The left panel with green border is the M componentry group and the right panel with red border is the S componentry group. Images are arranged in stratigraphic order according to Fig. 2

4. Quantitative textural analysis

4.1 Hekla 1991

Clasts from the lower fall unit have vesicle number densities (N_{Vm}) of 2.3 x 10^4 mm^{-3} (base, J12-51-8-88) and 1.5 x 10^4 mm^{-3} (top, J12-51-7-99). Equivalent values for the upper fall unit are 4.7 x 10^4 (base, J12-51-5-65) and 2.4 x 10^4 mm^{-3} (top, J12-51-4-97). The fall units show parallel trends of lower VND

at the top, and although within one order of magnitude the upper fall unit has more vesicles (Fig. 6; Table 1). On Fig. 6 it is illustrated how these values are up to an order of magnitude higher than recorded from basaltic Strombolian and Hawaiian ejecta (e.g., Lautze and Houghton 2006; Stovall et al. 2011; Parcheta et al. 2013), but one to two orders of magnitude lower than large silicic Plinian eruptions (e.g., Gurioli et al. 2005; Adams et al. 2006; Carey et al. 2009). The values are similar to those measured for basaltic Plinian eruptions (e.g., Sable et al. 2006, 2009; Costantini et al. 2010).

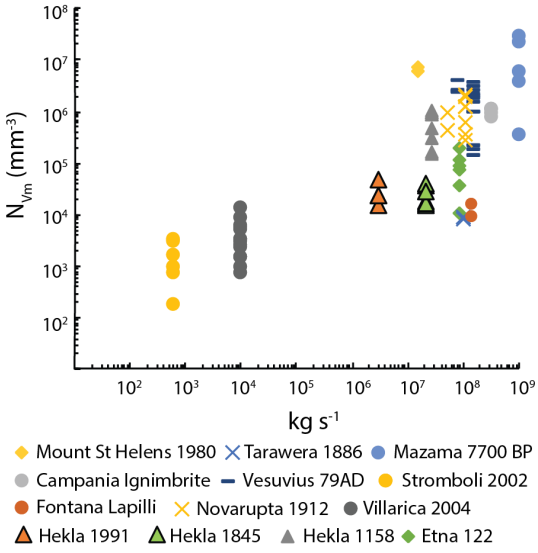

Fig. 6: Vesicle number density (N_{Vm}) as a function of mass eruption rate (kg s^{-1}). Selected eruptions are: Hekla 1991 (this study), Hekla 1845 (this study), Etna 122 BC (Sable et al. 2006), Stromboli 2002 (Lautze and Houghton 2005, 2008), Vesuvius AD 79 (Civetta et al. 1991; Gurioli et al. 2005), Campania Ignimbrite (Polacci et al. 2003), Mt St Helens 1980 (Carey and Sigurdsson 1990; Criswell 1987; Klug and Cashman 1994), Mazama 7700 BP (Klug et al. 2002), Kilauea Iki (Stovall et al. 2011), Villarrica 2004 (Gurioli et al. 2008), Hekla 1158 (Janebo et al. 2016a), Novarupta 1912 (Fierstein and Hildreth 1992; Adams et al. 2006) and Tarawera 1886 (Cole 1970; Sable et al. 2009)

Table 1: Summary of quantitative textural analyses of Hekla 1991 opening phase. Numbers reported are N_a number of vesicles per area, N_v number of vesicles per volume of melt corrected for phenocrysts, N_{Vm} number density of vesicles corrected for phenocrysts and vesicles

Eruption	Sample no.	Group	Clast no.	Density (kg m^{-3})	Ves. %	Na (mm^{-2})	Nv (mm^{-3})	N_{Vm} (mm^{-3})	No. Vesicl. Included	Median vesicle diameter (µm)
1991	J12-51-4	Na.	97	540	79.2	1.85 x 10^2	4.94 x 10^3	2.37 x 10^4	1796	300
1991	J12-51-5	Na.	65	610	76.7	2.97 x 10^2	1.05 x 10^4	4.72 x 10^4	3305	140
1991	J12-51-7	Na.	99	670	74.4	7.68 x 10^1	3.79 x 10^3	1.48 x 10^4	1049	720
1991	J12-51-8	Na.	88	460	82.5	1.59 x 10^2	4.02 x 10^3	2.30 x 10^4	1442	380
1845	J13-54-8	M	89	720	70.9	2.00 x 10^2	5.52 x 10^3	1.92 x 10^4	1477	210
1845	J13-54-8	S	82	520	78.8	1.16 x 10^2	3.20 x 10^3	1.51 x 10^4	1628	290
1845	J13-54-9	M	91	630	74.6	3.18 x 10^2	9.70 x 10^3	3.82 x 10^4	4454	170
1845	J13-54-9	S	92	560	77.5	1.37 x 10^2	3.80 x 10^3	1.69 x 10^4	1348	200
1845	J13-54-10	M	99	600	75.8	2.92 x 10^2	1.00 x 10^4	4.15 x 10^4	1945	260
1845	J13-54-10	S	92	540	78.1	1.77 x 10^2	6.07 x 10^3	2.77 x 10^4	1477	160

One of the vesicle volume distributions (VVD) for Hekla 1991 is unimodal and three are bimodal (Fig. 7). From the lower fall unit, clast J12-51-8-88 (base) is bimodal with a principal mode at 138 µm and a secondary mode at 870 µm, whereas clast J12-511-7-99 (top) is weakly bimodal with the dominant mode at 870 µm and subordinate peak at 350 µm. From the upper fall unit, clast J12-51-5-65 (base) is unimodal with peak at 140 µm, whereas clast J12-51-4-97 (top) has two peaks at 140 and 350 µm (Fig. 7). Small vesicles are more common in the upper fall unit, where the equivalent median diameters are 140 µm (J12-51-5-65) and 300 µm (12-51-4-97; Table 1). In the lower fall unit, median bubble diameter are 380 µm (J12-51-8-88) and 720 µm (J12-51-7-99; Table 1).

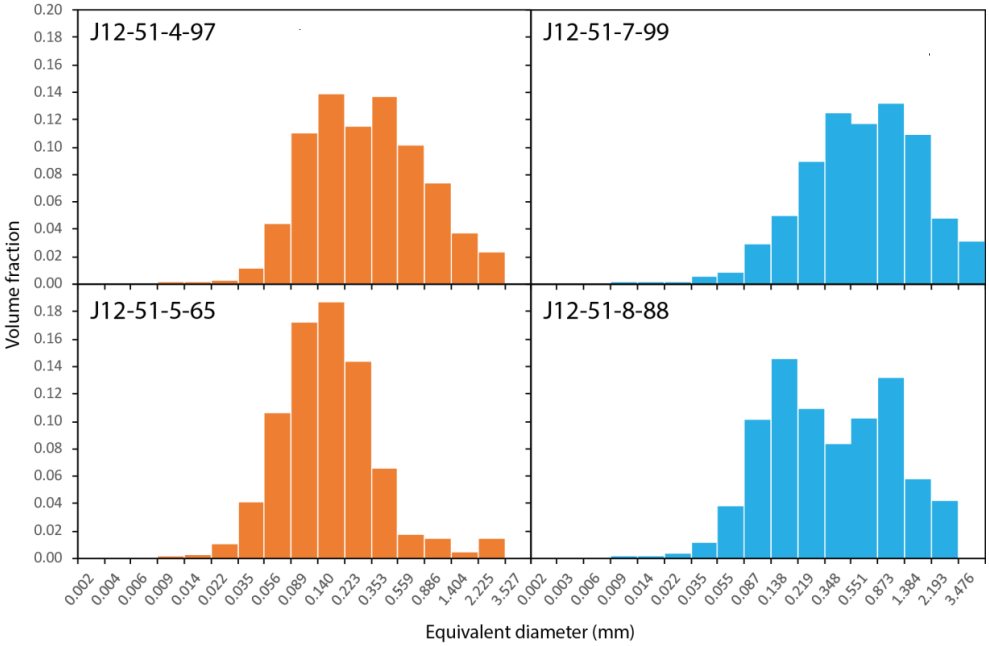

Fig. 7: Vesicle volume distribution of the analyzed samples from the Hekla 1991 deposit. Orange (left panel) is the upper fall unit and blue (right panel) is the lower fall unit from the opening phase of the eruption. The bin size on the horizontal scale is calculated from the smallest measured vesicle using a geometric bin factor $10^{0.1}$

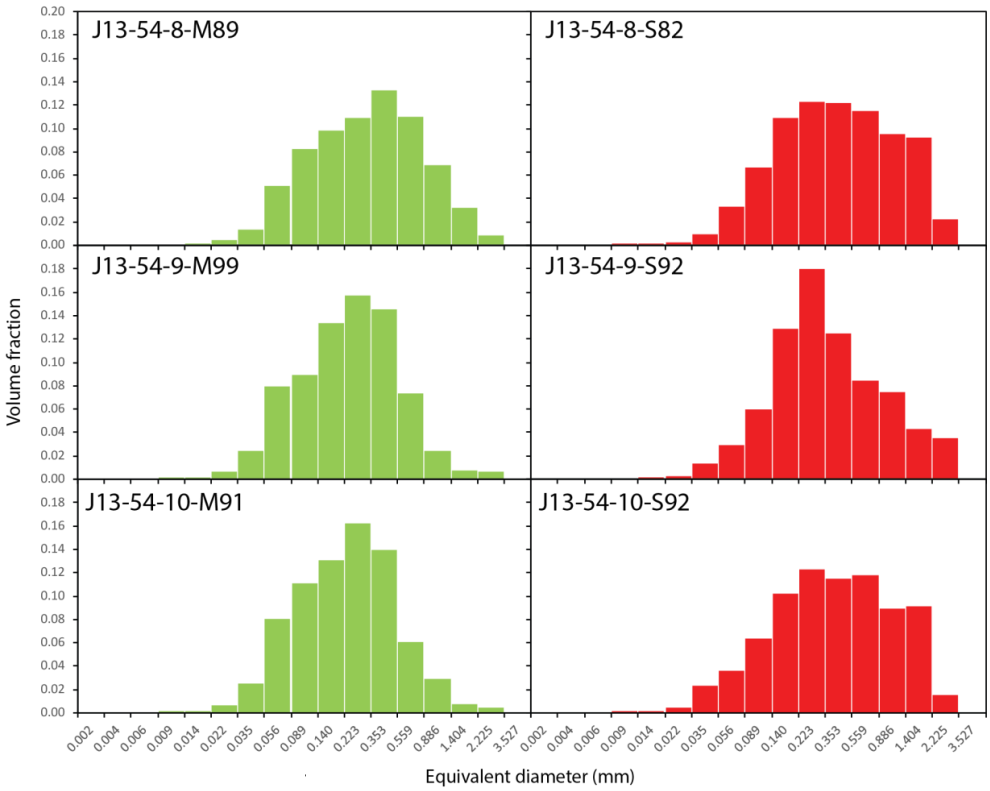

Fig. 8: Vesicle volume distribution from the Hekla 1845 deposit. Green distributions (left panel) are clasts from the microvesicular componentry group (M), red (right panel) are clasts from the scoriaceus componentry group (S). Samples are arranged in stratigraphic order. The horizontal scale is calculated from the smallest measurable vesicle using a geometric bin factor $10^{0.1}$

4.2 Hekla 1845

The VVD from the analysed clasts of Hekla 1845 are all unimodal, two clasts (J13-54-10-S92; J13-54-8-S82) have shoulder on the distribution at 1.4 mm (Fig. 8). The VVD distributions (Fig. 8) of the M group are negatively skewed with a shoulder on the left side of the distribution (i.e., skewed towards smaller vesicles), while the S group is positively skewed with a shoulder on the right side of the distribution (i.e., skewed towards coarser vesicles). Only one clast of the S group has a distinct peak in the VVD distribution (220 µm; J13-54-9-S92), whereas the other two have broad plateau-like distributions from 100 µm to 1400 µm (Fig. 8). In contrast to the S group, the M group has distinct modal peaks of the vesicle distribution, at 350 µm in clast J13-54-8-M89, and at 220 µm in the other clasts (Fig. 8). With time (i.e., from bottom up), there is a trend of VND (N_{Vm}) (Table 1). The basal clasts (J13-54-10-M91 and -S92) contain the highest N_{Vm} for each componentry group of 2.8×10^4 mm^{-3} (S) and 4.2×10^4 mm^{-3} (M), in the middle of the 1845 deposits (J13-54-9-M99 and -S92) VND (N_{Vm}) drops to 1.7×10^4 mm^{-3} (S) and 3.8×10^4 mm^{-3} (M). At the top of the fall unit (J13-54-8-M89 and -S82), VND (N_{Vm}) is 1.5×10^4 mm^{-3} (S) and 1.9×10^4 mm^{-3} (M). The cumulative vesicle volume distributions curves (CVVD) for the 1845 tephra fall (Fig. 9), shows sigmoidal distributions for 4 out of the 6 clasts. The broad plateau like distributions of clasts J13-54-8-S82 and J13-54-10-S92 have nearly straight segments due to the large volume of large vesicles. The CVVD curves also illustrates how the M and S groups of the 1845 fall deposits differ, especially the concentration of small vesicles in J13-54-10-M99 and J13-54-9-M91 compared to larger vesicles in J13-54-10-S92 and J13-54-S82. The 1991 CVVD curves (Fig. 9) are also nearly all sigmoidal, the only exception being the strongly bimodal clast J12-51-8-88. The 1991 CVVD curves (Fig. 9) also illustrates the fundamental difference between the

upper and lower fall units. The clasts from the lower fall unit have on average fewer small vesicles than the clasts from the upper fall unit. The top of the upper fall unit (J12-51-4-97) and the base from the lower fall unit (J12-51-7-99) are very similar in terms of volume distribution (Fig. 9).

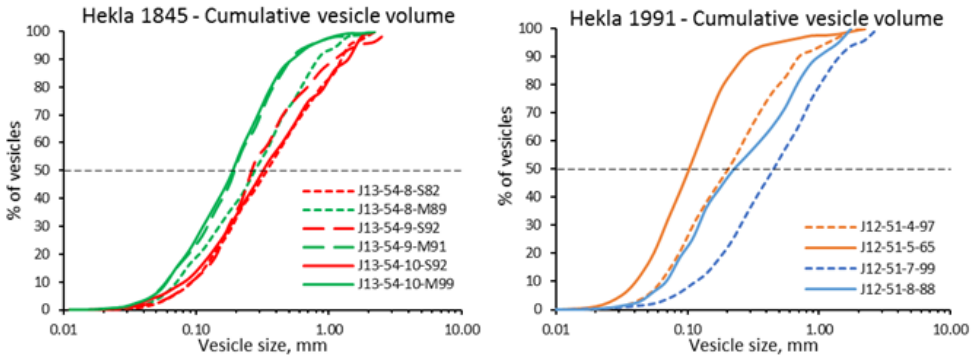

Fig. 9: Cumulative volume percent vesicles vs. the equivalent diameter of vesicles in the analyzed clasts from the 1991 and 1845 Hekla eruptions

5. Interpretation and discussion

During magma ascent, the nucleation of vesicles will start after a critical level of supersaturation of the melt has been achieved (Mangan et al. 2004). Numerical and experimental studies have shown that degree of volatile supersaturation, and hence decompression rate, modulate the vesicle nucleation rate and therefore VND in erupting magmas (e.g., Mourtada-Bonnefoi and Laporte 2004; Toramaru 2006). The VND scales with original volatile concentration and thus with silica content in the magma (e.g., Rust and Cashman 2011) and the rate of decompression (e.g., Mourtada-Bonnefoi and Laporte 2002, 2004; Mangan et al. 2004; Toramaru 2006; Hamada et al. 2010). We will illustrate here that decreasing intensity during the opening phase of the Hekla 1991 and 1845 eruptions is recorded by a drop in the VND, and illustrated by changes in both the VVD and VSD. We will propose a simple model for the rising magma in the shallow conduit and compare the textural analysis to published total grain-size distribution.

5.1 Hekla 1845 eruption dynamics

Previously published data on the 1845 eruption demonstrates an upward (i.e., temporal) fining of the proximal tephra. This tephra was deposited during steady wind conditions and thus the change in grain-size reflects a gradual decline in eruption intensity during the one-hour-long opening phase (Gudnason et al. 2017b). Contemporary descriptions of the eruption (Erlendsson 1847; Schythe 1847) indicate speedy waxing of explosive activity at the onset of the eruption, reaching peak intensities (mass eruption rate of 2.1×10^7) soon after onset of eruption (Gudnason et al. 2017b). This waxing period is followed by slower waning of eruption intensity, declining over a period of several days. Thus, the 1845 event conforms well with typical type III Hekla eruptions (Thorarinsson 1968; Thordarson and Larsen 2007; Larsen and Eiríksson 2008).

The data presented here conforms well with the previously published data on the 1845 eruption and demonstrates how decreasing VND are connected to increasing cross conduit variation and decreasing ascent rate during the opening phase of the 1845 eruption.

The presence of M and S clasts in all samples (Fig. 3) suggests that there was a consistent cross-conduit variation in the vesicularity of the magma parcels fragmenting at any one time (e.g., Figs. 3, 5, 8). The VVD for the M and S groups span the same size range in all samples (Fig. 8). However, the fundamental difference is lower VND in S than M at any given time and domination of larger vesicles in S compared to M. On a plot of volume ratio of vesicles to melt (V_G/V_L; Gardner et al. 1996) versus

VND (N_{Vm}) both groups show decreasing VND with time (Fig. 11), interpreted here as combination of coalescence, decreasing nucleation rate, and outgassing (possibly from M to S) for the M component (Fig. 10). Although all clasts are within one order of magnitude, there is an approximately decrease by a factor of 2 in VND (N_{Vm}) from sample J13-54-10 to J13-54-8 for both group S and M over the course of the opening phase (Table 1); Fig. 10), reflecting a decrease in the eruption intensity and thus slowed ascent. We therefore suggest that the melt that resulted in the S group has a more mature vesicle population, potentially evolved from M melt by coalescence. Coalescence was coeval with nucleation of bubbles during ascent (Figs. 5, 8), possibly a result of lower ascent rate of S compared to M. With time, relative volume of slower ascending melt (S) increases as compared to the relatively faster ascending melt (M; Figs. 3, 11). The textures and data are most consistent with a vesicularity gradient developed across the conduit in which melt at the margins ascends more slowly with greater opportunity for bubble-bubble interaction and maturation (Adams et al. 2006, Sable et al. 2006). This probably was accentuated during rapid (non-linear) acceleration of the magma up the shallowest conduit.

5.1.1 Hekla 1845 eruption scenario

Based on the results presented herein, we suggest a following scenario for the 1845 eruption (Fig. 11). The eruption began and escalated rapidly, driven by rapid ascent and continuous nucleation of bubbles in the newly arrived batch of melt. The ascent rate then slowly waned through the opening phase, accompanying a gradual decline in the rate of nucleation of bubbles. At any given time, a velocity profile existed across the conduit due to drag along the conduit walls (Fig. 11). The melt ascending adjacent to the conduit walls (S), had longer residence time in the conduit to evolve to a mature bubble population than melt rising through the middle of the conduit (M; Fig. 11). As the eruption progressed the declining ascent and discharge rates led to a shift from coupled to decoupled degassing, i.e., a shift from explosive to fountaining eruption, and then discharge of largely outgassed lava from fissure vents.

5.2 Hekla 1991 eruption dynamics

The Hekla 1991 samples analysed in this study span the duration of the opening phase and as such should reveal any changes in the ascending magma during that time (e.g., Gudnason et al. 2017a). The 1991 opening phase was interpreted to be pulsating based on grain-size variation in the proximal deposits (Gudnason et al. 2017a). The results presented here illustrates temporal variation in nucleation rates and thus supports the previously assumed pulsation of the 1991 opening phase.

5.2.1 Lower fall unit

The temporal evolution of the lower fall unit—increasing volume contribution of large vesicles with time (Figs. 7, 9), and decreasing VND (Table 1)—indicates a drop in the rate of nucleation with time. We interpret the shift from a bimodal VVD (clast J12-51-8-88, Fig, 7) with peaks at 140 and 870 μm, to a unimodal VVD with a peak at 870 μm (clast J12-51-7-99) as resulting from a decrease in nucleation rate combined with primarily growth by coalescence and partial outgassing of the magma during ascent (Fig. 10).

5.2.2 Upper fall unit

The overall temporal evolution of the upper fall unit from the 1991 opening phase is, decrease in VND with increasing VSD (Figs. 7, 9; Table 1). The increased size of the vesicle population is a result of coalescence and growth during ascent (Fig. 10). We interpret this as representing a drop in ascent rate with time permitting more maturing of the vesicle population by growth and coalescence during a decrease in the bubble nucleation rate (Fig. 10).

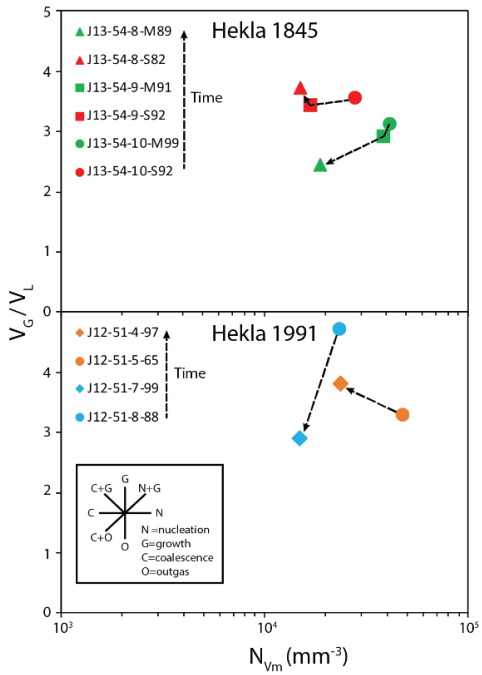

Fig. 10: Volume ratio of vesicles to melt (V_G/V_L) versus melt-referenced vesicle number density (N_{Vm}). For the 1845 deposits the componentry groups are shown in red (S) and green (M) while individual horizons in the deposits are grouped by shape. For the 1991 deposits the individual fall units have same color: orange is the upper fall unit and blue is the lower fall unit. For 1991 circles represent clasts from the base and diamonds are clasts from top of each unit. Key on lower figure is to interpret processes driving trends in the data.

5.2.3 Hekla 1991 eruption scenario

We suggest the following scenario for the 1991 opening phase. The lower fall unit is the product of the establishment of an open conduit and slow ascent during the conduit opening. Represented by a single initial burst of bubbles that during ascent grew by coalescence and was partly outgassed. After establishment of the open conduit, faster ascent was possible. This is represented by the upper fall unit, where the clasts contain a population dominated by numerous small bubbles, commensurate with more rapid ascent, and fragmentation which interrupted ongoing bubble nucleation and growth. Both fall units show increasing median vesicle size and decreasing VND with time, illustrating the evolution of each magma batch with decreasing rates of nucleation and growth of bubbles during ascent. The difference in VND between the upper and lower fall units represent higher ascend rates for the upper fall unit (Fig. 11).

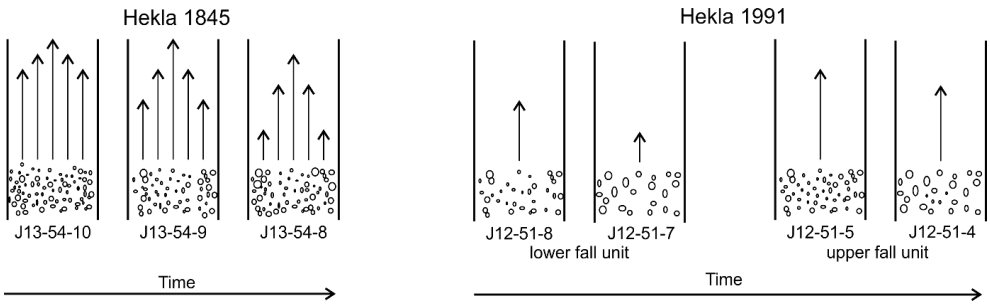

Fig. 11: Schematic model for the magma ascent in the conduit during the 1845 eruption. The magma batch which sample J13-54-10 represents was the first one to erupt, with high velocity and almost symmetrical profile across conduit. The last magma batch sampled (J13-54-8) has the largest variance in ascent rate across the conduit resulting in relatively fast ascending magma in the center relative to along the margins. Hekla 1991 is represented by two separate fall units, both show indications of reduced speed with time independently.

5.3 Magma fragmentation

The previously published total grain-size distributions (TGSD) for the opening phases of 1991 and 1845 are bimodal (Fig. 12; Gudnason et al. 2017a, b). The bimodality was interpreted as a consequence of the primary fragmentation based on deposit characteristics and surface conditions (Gudnason et al. 2017a, b). When the TGSD and VVD are compared (Fig. 12), the TGSD overlaps with the VVD. Since these two measured objects are intrinsically different, direct comparison is not possible. However, if the two overlap, that indicates a direct relationship between the kinetics of bubble vesiculation and fragmentation of the magma (Rust and Cashman 2011; Cashman and Sparks, 2013). Based on this we suggest an explanation for the process creating the bimodal TGSD. The possible mechanism is development of pockets of contrasting permeability in the melt immediately prior to fragmentation. In these pockets, the coalescence was more advanced and connectivity and high permeability permitted formerly trapped gas to escape and high pressure differentials were not preserved at fragmentation (Klug and Cashman 1996). These parts of the magma formed the dominant lapilli-sized subpopulations, where multiple outgassed bubbles are enclosed in each pyroclasts. Where coalescence was not advanced, the subpopulation of small bubbles remained unconnected and at high Δ pressure. Fragmentation of this material was therefore more intense generating the ash fraction with sizes that equate approximately to the dimensions of individual bubbles or rather, the glass walls that surrounded bubbles.

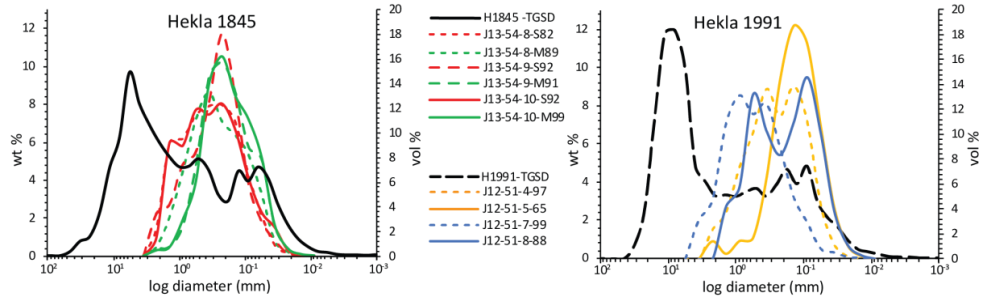

Fig. 12: Comparison of TGSD and VVD for the opening phases of 1991 and 1845. The finer mode of the bimodal TGSD and VVD overlap in both eruptions. The x-axis is the same, but the scale of the y-axis Is wt% for the TGSD and vol.% for the VVD.

6. Concluding remark

Both the 1845 and 1991 events are very typical of recent activity at Hekla, occurred with short warning times, and became most powerful during the first hour of the eruption (opening phase). The hazards posed to local population and air traffic with this type of activity is therefore acute. The pulsating behaviour of the 1991 opening phase and the resulting complexities in the vesiculation history were not noticed during the eruption (Gudmundsson et al. 1992; Larsen et al. 1992), but was inferred from proximal tephra stratigraphy (Gudnason et al. 2017) and now confirmed with temporal changes in vesicle number densities. The 1845 opening phase was on a gradual decline after initial high intensity, with increasing cross conduit heterogeneity and gradual increase in coalescence and development of larger vesicles in the conduit. The overlap between the total grain-size distribution and the vesicle volume distribution supports the notion by Gudnason et al. (2017a, b) that the bimodal total grain-size distribution is a result of the primary magma fragmentation.

This study indicates that during type III Hekla eruptions, the high intensity and explosivity of the opening phase is a direct result of coupled degassing of rapidly ascending magma. The decreasing intensity and changes in eruptive regime from explosive to effusive that follows during type III Hekla eruptions is a result of decreasing ascent rate and change from coupled to decoupled degassing.

References

Adams, N.K., Houghton, B.F., Hildreth, W., 2006. Abrupt transitions during sustained explosive eruptions: examples from the 1912 eruption of Novarupta , Alaska 189–206. doi:10.1007/s00445-006-0067-4

Carey, R.J., Houghton, B.F., Thordarson, T., 2009. Abrupt shifts between wet and dry phases of the 1875 eruption of Askja Volcano: Microscopic evidence for macroscopic dynamics. J. Volcanol. Geotherm. Res. 184, 256–270. doi:10.1016/j.jvolgeores.2009.04.003

Carey, S., Sigurdsson, H., Gardner, J.E., Criswell, W., 1990. Variations in column height and magma discharge during the May 18, 1980 eruption of Mount St. Helens. J. Volcanol. Geotherm. Res. 43, 99–112. doi.org/10.1016/0377-0273(90)90047-J

Cashman, K. V, Sparks, R.S.J., 2013. How volcanoes work: A 25 year perspective. Geol. Soc. Am. Bull. 125, 664–690. doi:10.1130/B30720.1

Civetta, L., Galati, R., Santacroce, R., 1991. Magma mixing and convective compositional layering within the Vesuvius magma chamber. Bull. Volcanol. 53, 287–300. doi:10.1007/BF00414525

Cole, J.W., 1970. Petrology of the basic rocks of the Tarawera Volcanic Complex. New Zeal. J. Geol. Geophys. 13, 925–936. doi:10.1080/00288306.1970.10418210

Costantini, L., Houghton, B.F., Bonadonna, C., 2010. Constraints on eruption dynamics of basaltic explosive activity derived from chemical and microtextural study: The example of the Fontana Lapilli Plinian eruption, Nicaragua. J. Volcanol. Geotherm. Res. 189, 207–224. doi:10.1016/j.jvolgeores.2009.11.008

Criswell, C.W., 1987. Chronology and pyroclastic stratigraphy of the May 18, 1980, Eruption of Mount St. Helens, Washington. J. Geophys. Res. Solid Earth 92, 10237–10266. doi:10.1029/JB092iB10p10237

Erlendsson, O., 1847. Dagskrá um Heklugosið 1845-6 og afleiðingar þess. Garðabær.

Fierstein, J., Hildreth, W., 1992. The plinian eruptions of 1912 at Novarupta, Katmai National Park, Alaska. Bull. Volcanol. 54, 646–684. doi:10.1007/BF00430778

Gardner, J.E., Thomas, R.M.E., Jaupart, C., Tait, S., 1996. Fragmentation of magma during Plinian volcanic eruptions. Bull. Volcanol. 58, 144–162. doi:10.1007/s004450050132

Gudmundsson, A., Oskarsson, N., Grönvold, K., Saemundsson, K., Sigurdsson, O., Stefansson, R., Gislason, S.R., Einarsson, P., Brandsdottir, B., Larsen, G., Johannesson, H., Thordarson, T., 1992. The 1991 eruption of Hekla, Iceland. Bull. Volcanol. 54, 238–246. doi:10.1007/BF00278391

Gudmundsson, A., Sæmundsson, K., 1992. Heklugosið 1991 : Gangur gossins og aflfræði Heklu 145–158.

Gudnason, J., Thordarson, T., Houghton, B.F., Larsen, G., 2017a. The opening subplinian phase of the Hekla 1991 eruption: properties of the tephra fall deposit. Bull. Volcanol. 79, 34. doi:10.1007/s00445-017-1118-8

Gudnason, J., Thordarson, T., Houghton, B.F., Larsen, G., 2017b. The 1845 Hekla eruption: grain-size characteristics of a tephra layer. Submitted to Journal of Volcanology and Geothermal Research. May 2017.

Gurioli, L., Harris, A.J.L., Houghton, B.F., Polacci, M., Ripepe, M., 2008. Textural and geophysical characterization of explosive basaltic activity at Villarrica volcano 113, 1–16. doi:10.1029/2007JB005328

Gurioli, L., Houghton, B.F., Cashman, K. V., Cioni, R., 2005. Complex changes in eruption dynamics during the 79 AD eruption of Vesuvius. Bull. Volcanol. 67, 144–159. doi:10.1007/s00445-004-0368-4

Hamada, M., Laporte, D., Cluzel, N., Koga, K.T., Kawamoto, T., 2010. Simulating bubble number density of rhyolitic pumices from Plinian eruptions: constraints from fast decompression experiments. Bull. Volcanol. 72, 735–746. doi:10.1007/s00445-010-0353-z

Houghton, B.F., Carey, R.J., Cashman, K. V., Wilson, C.J.N., Hobden, B.J., Hammer, J.E., 2010. Diverse patterns of ascent, degassing, and eruption of rhyolite magma during the 1.8ka Taupo eruption, New Zealand: Evidence from clast vesicularity. J. Volcanol. Geotherm. Res. 195, 31–47. doi:10.1016/j.jvolgeores.2010.06.002

Houghton, B.F., Wilson, C.J.N., 1989. A vesicularity index for pyroclastic deposits. Bull. Volcanol. 51, 451–462.

Houghton, B.F., Wilson, C.J.N., Smith, I.E.M., 1999. Shallow-seated controls on styles of explosive basaltic volcanism: A case study from New Zealand. J. Volcanol. Geotherm. Res. 91, 97–120. doi:10.1016/S0377-0273(99)00058-X

Janebo, M.H., Houghton, B.F., Thordarson, T., Larsen, G., 2016a. Shallow conduit processes during the AD 1158 explosive eruption of Hekla volcano , Iceland. Bull. Volcanol. doi:10.1007/s00445-016-1070-z

Janebo, M.H., Thordarson, T., Houghton, B.F., Larsen, G., Carey, R.J., 2016b. Dispersal of key subplinian-Plinian tephra from Hekla volcano, Iceland: implications for eruption source parameters. Bull. Volcanol. 78, 66.

Jarosewich, E., Nelen, J.A., Norberg, J.A., 1980. Reference Samples for Electron Microprobe Analysis. Geostand. Newsl. 4, 43–47. doi:10.1111/j.1751-908X.1980.tb00273.x

Klug, C., Cashman, K., Bacon, C., 2002. Structure and physical characteristics of pumice from the climactic eruption of Mount Mazama (Crater Lake), Oregon. Bull. Volcanol. 64, 486–501. doi:10.1007/s00445-002-0230-5

Klug, C., Cashman, K.V., 1996. Permeability development in vesiculating magmas : implications for fragmentation. Bull. Volcanol. 58, 87–100.

Klug, C., Cashman, K. V, 1994. Vesiculation of May 18, 1980, Mount St. Helens magma. Geol. 22, 468–472.

Larsen, G., Eiríksson, J., 2008. Late Quaternary terrestrial tephrochronology of Iceland-frequency of explosive eruptions, type and volume of tephra deposits. J. Quat. Sci. 23, 109–120.

Larsen, G., Vilmundardóttir, E.G., Thorkelsson, B., 1992. Heklugosið 1991 : Gjóskufallið og gjóskulagið frá fyrsta degi gossins. Náttúrufræðingurinn 61, 159–176.

Lautze, N.C., Houghton, B.F., 2008. Single explosions at Stromboli in 2002: Use of clast microtextures to map physical diversity across a fragmentation zone. J. Volcanol. Geotherm. Res. 170, 262–268. doi:10.1016/j.jvolgeores.2007.10.011

Lautze, N.C., Houghton, B.F., 2006. Linking variable explosion style and magma textures during 2002 at Stromboli volcano, Italy. Bull. Volcanol. 69, 445–460. doi:10.1007/s00445-006-0086-1

Lautze, N.C., Houghton, B.F., 2005. Physical mingling of magma and complex eruption dynamics in the shallow conduit at Stromboli volcano, Italy. Geology 33, 425–428. doi:10.1130/G21325.1

Linde, A.T., Agustsson, K., I.S., S., Stefansson, R., 1993. Mechanism of the 1991 eruption of Hekla from continuous borehole strain monitoring. Nature 365.

M.H, J., B.F., H., Thordarson, T., Bonadonna, C., 2016. Total grain size distributino of four subplinian-Plinian tephra from Hekla volcano, Iceland: Implications for fragmentation dynamics and eruption source parameters. prep.

Mangan, M.T., Sisson, T.W., Hankins, W.B., 2004. Decompression experiments identify kinetic controls on explosive silicic eruptions. Geophys. Res. Lett. 31, 1–5. doi:10.1029/2004GL019509

Mastin, L.G., Christiansen, R.L., Thornber, C., Lowenstern, J., Beeson, M., 2004. What makes hydromagmatic eruptions violent? Some insights from the Keanakāko'i Ash, Kīlauea Volcano, Hawai'i. J. Volcanol. Geotherm. Res. 137, 15–31. doi.org/10.1016/j.jvolgeores.2004.05.015

Mourtada-Bonnefoi, C.C., Laporte, D., 2004. Kinetics of bubble nucleation in a rhyolitic melt: An experimental study of the effect of ascent rate. Earth Planet. Sci. Lett. 218, 521–537. doi:10.1016/S0012-821X(03)00684-8

Mourtada-Bonnefoi, C.C., Laporte, D., 2002. Homogeneous bubble nucleation in rhyolitic magmas: An experimental study of the effect of H2O and CO2. J. Geophys. Res. Solid Earth 107, ECV 2-1–ECV 2-19. doi:10.1029/2001JB000290

Óladóttir, B.A., Sigmarsson, O., Larsen, G., Devidal, J.-L., 2011. Provenance of basaltic tephra from Vatnajokull subglacial volcanoes, Iceland, as determined by major- and trace-element analyses. The Holocene 21, 1037–1048. doi:10.1177/0959683611400456

Óskarsson, N., 1980. The interaction between volcanic gases and tephra: fluorine adhering to tephra of the 1970 hekla eruption. J. Volcanol. Geotherm. Res. 8, 251–266.

Parcheta, C.E., Houghton, B.F., Swanson, D. a., 2013. Contrasting patterns of vesiculation in low, intermediate, and high Hawaiian fountains: A case study of the 1969 Mauna Ulu eruption. J. Volcanol. Geotherm. Res. 255, 79–89. doi:10.1016/j.jvolgeores.2013.01.016

Polacci, M., Pioli, L., Rosi, M., 2003. The Plinian phase of the Campanian Ignimbrite eruption (phlegrean fields, Italy): Evidence from density measurements and textural characterization of pumice. Bull. Volcanol. 65, 418–432. doi:10.1007/s00445-002-0268-4

Rust, A. C., Cashman, K. V., 2011. Permeability controls on expansion and size distributions of pyroclasts. J. Geophys. Res. 116, B11202. doi:10.1029/2011JB008494

Sable, J.E., Houghton, B.F., Del Carlo, P., Coltelli, M., 2006. Changing conditions of magma ascent and fragmentation during the Etna 122 BC basaltic Plinian eruption: Evidence from clast microtextures. J. Volcanol. Geotherm. Res. 158, 333–354. doi:10.1016/j.jvolgeores.2006.07.006

Sable, J.E., Houghton, B.F., Wilson, C.J.N., Carey, R.J., 2009. Eruption mechanisms during the climax of the Tarawera 1886 basaltic Plinian eruption inferred from microtextural characteristics of the deposits, in: Thordarson, T., Self, S., Larsen, G., Rowland, S.K., Hoskuldsson, A. (Eds.), Studies in Volcanology: The Legacy of George Walker. The Geological Society, London, pp. 129–154.

Sahagian, D.L., Proussevitch, A.A., 1998. 3D particle size distributions from 2D observations: stereology for natural applications. J. Volcanol. Geotherm. Res. 84, 173–196. doi:10.1016/S0377-0273(98)00043-2

Schneider, C., Rasband, W.., Eliceiri, K.., 2012. NIH Image to ImageJ: 25 years of image analysis. Nat. Methods 9, 671–675.

Schythe, J.C., 1847. Hekla og dens sidste Udbrud, den 2den September 1845. København.

Shea, T., Houghton, B.F., Gurioli, L., Cashman, K. V., Hammer, J.E., Hobden, B.J., 2010. Textural studies of vesicles in volcanic rocks: An integrated methodology. J. Volcanol. Geotherm. Res. 190, 271–289. doi:10.1016/j.jvolgeores.2009.12.003

Stovall, W.K., Houghton, B.F., Hammer, J.E., Fagents, S. a., Swanson, D. a., 2011. Vesiculation of high fountaining Hawaiian eruptions: episodes 15 and 16 of 1959 Kīlauea Iki. Bull. Volcanol. 74, 441–455. doi:10.1007/s00445-011-0531-7

Sturkell, E., Ágústsson, K., Linde, A.T., Sacks, S.I., Einarsson, P., Sigmundsson, F., Geirsson, H., Pedersen, R., LaFemina, P.C., Ólafsson, H., 2013. New insights into volcanic activity from strain and other deformation data for the Hekla 2000 eruption. J. Volcanol. Geotherm. Res. 256, 78–86. doi:10.1016/j.jvolgeores.2013.02.001

Thorarinsson, S., 1968. Heklueldar. Rangæingafélagið, Reykjavik.

Thorarinsson, S., 1967. The eruption of Hekla 1947-1948. II, 3. The tephra fall from Hekla on March 29th 1947. Soc. Sci. Islandica I, 1–68.

Thordarson, T., Larsen, G., 2007. Volcanism in Iceland in historical time: Volcano types, eruption styles and eruptive history. J. Geodyn. 43, 118–152. doi:10.1016/j.jog.2006.09.005

Thornber, B.C.R., Sherrod, D.R., Siems, D.F., Heliker, C.C., Gregory, P., Oscarson, R.L., Kauahikaua, J.P., 2002. Whole-rock and glass major-element geochemistry of Kilauea Volcano , Hawaii , near-vent eruptive products : September 1994 through September 2001. USGS, Open File Rep. 02-17 1–9.

Toramaru, A., 2006. BND (bubble number density) decompression rate meter for explosive volcanic eruptions. J. Volcanol. Geotherm. Res. 154, 303–316. doi:10.1016/j.jvolgeores.2006.03.027

Jonas Gudnason[1,3], Bruce F. Houghton[2] and Thor Thordarson[1]
[1]Faculty of Earth Sciences, University of Iceland

[2]Department of Geology and Geophysics, University of Hawaii

[3]Institute of Earth Sciences, University of Iceland

Corresponding author: Jonas Gudnason jog4@hi.is

Supplementary material 1

For this study, images were acquired from two different SEM´s (section 2.3). The selected cut off therefore has to be compared in micrometres, rather than in number of pixels, in order for the geometric binning of vesicle sizes to be comparable. This was important for the vesicle study of the 1991 deposits.

SEM	Lower cut off pixels	Lower cut off mm	Resolution at 250 times magnification (pix mm^{-1})
JEOL SEM	22	0.0087	2520
TM 3000	15	0.0088	1693

For the 1845 deposit, all images were acquired at the University of Iceland, using a TM 3000 Hitachi SEM. 15 pixels were selected for the lower cut off to be consistent with the Hekla 1991 study. The 15 pixel lower cut of also minimizes misinterpretation of vesicles. According to Shea et al. (2010), the % error for one misinterpreted pixel in a 15 pixel diameter object is less than 2%, and this error would increase to 5% if 5 pixels are used for the lower cut off.

Hekla 1845

The chosen magnifications for the Hekla 1845 study were flat bead scanner, combined with 50x, 100x and 250x SEM images. With a 15 pixel lower cut off, at the highest magnification and resolution of 1693 pixels mm^{-1}, the smallest vesicle analysed has an equivalent diameter of 0.009 mm.

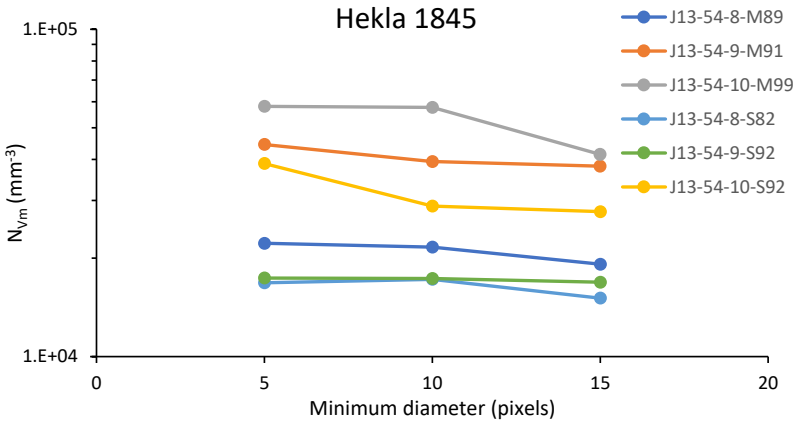

Lower cut off effects on vesicle number densities (VND), expressed as melt corrected values, can be seen on Fig. S1.1. All VND values are with in an order of magnitude when lower cut off is decreased from 15 to 5 pixels. The largest increase in VND with decreasing lower cut of is in clasts from the

basal sample, indicating that this sample has clasts containing the highest number of small vesicles. All clasts do not show significant increase in with lowering the cut of limit from 15 to 5 pixels.

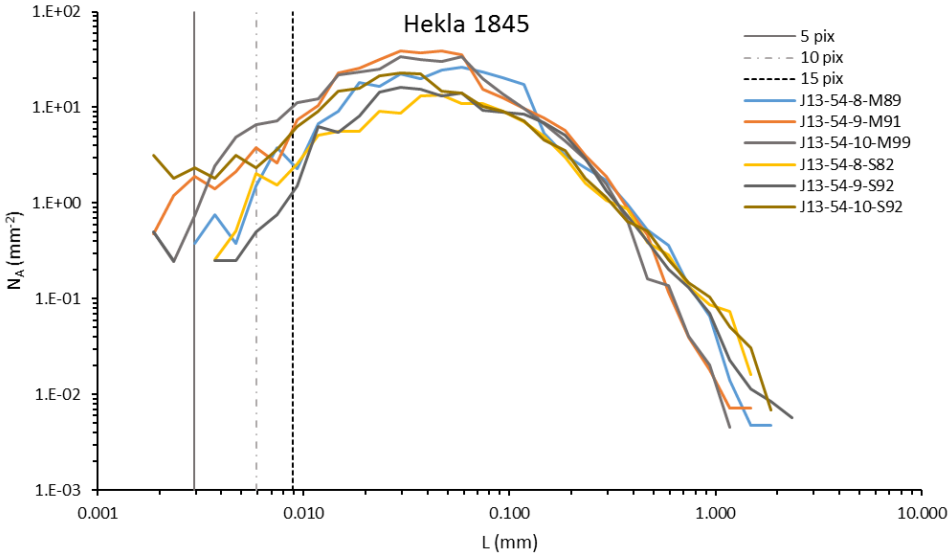

On Fig. S1.2 the number of vesicles (N_A) versus the apparent diameter (L) in mm is plotted. After 15 pixels, the lines representing each clast become more jagged. This is especially pronounced for clasts J13-54-10-S92 and J13-54-10-M99, both of which show the highest increase in N_{Vm} from 15 to 5 pixels. According to Shea et al. (2010), the irregularity of the segments increase when a certain size threshold has been passed and an error increase can therefore be expected.

As is illustrated in Figs. S1.1 and S1.2, there is no significant advantage of decreasing the lower cut off from 15 to 5 pixels for the study of the 1845 deposit. The added N_{Vm} is not significant enough to justify the potential error to the analysis that would result from decreasing the lower cut off limit.

Hekla 1991

For the Hekla 1991 study, the chosen lower cut off is 22 and 15 pixels (Table S1.1). Similarly, to the 1845, we do not see any advantage of lowering the cut off and increasing the error on the analysis, as no significant change in N_{Vm} results from lowering the cut off (Fig. S1.3).

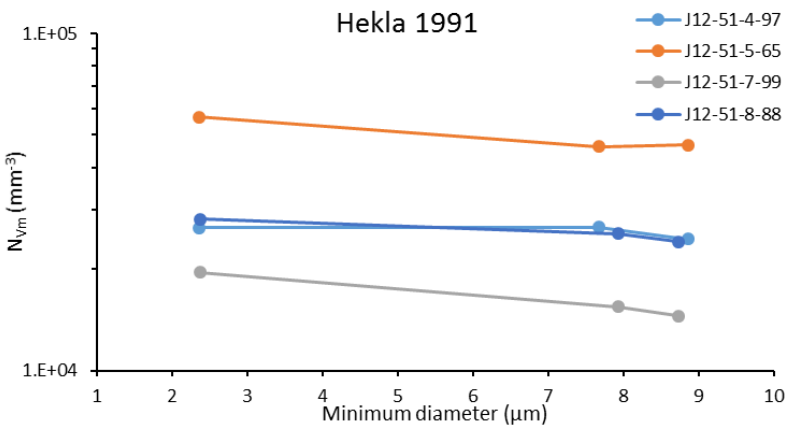

Similarly to the 1845 dataset, the selected magnifications cover the whole range of vesicles present in the set of clasts analyzed (Fig. S1.4). We are therefore confident that the lower cut off limit of 15 and 22 pixels for the aquired images from the two SEM´s used in the 1991 study produced representative results (Table S1.1).

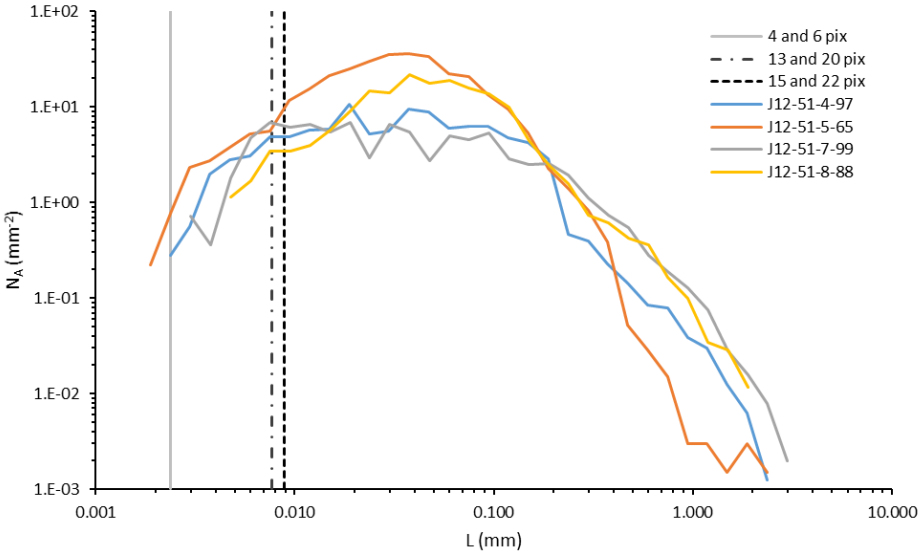

References:

Shea, T., Houghton, B.F., Gurioli, L., Cashman, K. V., Hammer, J.E., Hobden, B.J., 2010. Textural studies of vesicles in volcanic rocks: An integrated methodology. J. Volcanol. Geotherm. Res. 190, 271–289. doi:10.1016/j.jvolgeores.2009.12.003

The 1991 and 1845 eruptions at Hekla:
Nature of the explosive opening phases inferred from vesicle volume distributions.

Jonas Gudnason[1,3], Bruce F. Houghton[2] and Thor Thordarson[1]

[1]Faculty of Earth Sciences, University of Iceland

[2]Department of Geology and Geophysics, University of Hawaii

[3]Institute of Earth Sciences, University of Iceland

Corresponding author: Jonas Gudnason jog4@hi.is

Supplementary material 2

Chemical composition Hekla 1991

Methods

Glass chemistry of the 1991 and 1845 tephra was analysed on on a JEOL jxa-8230 superprobe at the Institute of Earth Sciences, University of Iceland (UI). At UI the analytical conditions were 15 kV voltage, 10 nA current and 5 µ, beam diameter. The standard used was natural glass from Kilauea (A99). When compared to other reported results they are indistinguishable (Table S2.1; Jarosewich et al 1980; Thornber et al 2002; Óladóttir et al 2011).

Results

The 1991 products are mildly alkalic basaltic icelandites (Table S2.2; Jakobsson et al 2008). When major elemental compositions of tephra from the opening phase and lava of latter phases are compared variation is minimal (Table S2.2). The composition of Hekla 1991 magma is very similar to the other post-1947 Hekla eruptions, and all of these eruptions show no temporal changes in SiO_2 with time, as has been reported for larger events including the 1947 Hekla eruption (Table S2.3; Thorarinsson1968; Thorarinsson and Sigvaldason 1970; Grönvold et al 1983; Gudmundsson et al 1992; Höskuldsson et al 2007).

The 1845 products are mildly alkalic icelandites (Table S2.2; Jakobsson et al 2008). When major elemental compositions of tephra from the opening phase and lava of latter phases are compared there is a noticable decrease in SiO_2 with time (Fig. S2.1)

The average silica content of the 1991 glass analysis ranges from 55.14–57.01 wt%. The standard deviation ranges 0.29–0.62 wt% (Table S2.2). For each clast analysed from the 1991 tephra the SiO_2 is: Sample J12-51-8-100 ranges in SiO_2content from 55.55–56.82 wt%, sample J12-51-8-98 from 54.98–56.34 SiO_2 wt%, J12-51-7-87 from 55.83–57.01 wt% SiO_2, J13-51-7-6 from 55.68–56.68 wt% SiO_2, J12-51-5-98 from 54.38–56.48 wt% SiO_2, J12-51-76 from 54.65–55.87 wt% SiO_2, J12-51-4-75 from 56.43–57.49 wt% SiO_2, J12-51-4-63 from 56.23–57.8 wt% SiO_2 and J12-51-4-59 from 55.05–56.09 wt% SiO_2. For the 1991 deposit there is no statistical difference in the glass chemistry, and it overlaps with the composition of the lava from the effusive phase (Table S2.3).

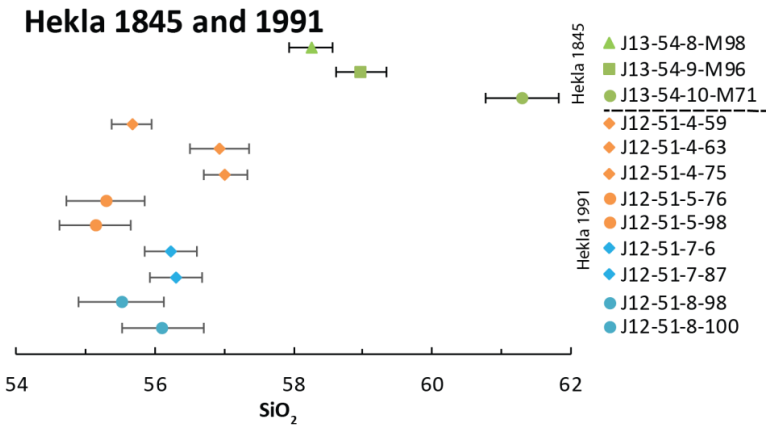

Fig. S2.1: Silica content as SiO_2 wt % in the glass from the 1991 and 1845 opening phase tephras. One standard deviation is depicted with lines. Samples are illustrated according to stratigraphic height for each eruption. Green symbols are Hekla 1845 and blue and orange Hekla 1991

The 1845 tephra is higher in SiO_2 content ranging from 58.3 wt% to 61.2 wt%, the variance in each sample from the 1845 tephra fall deposits is: J13-54-10-M71 from 60.65-62.03 wt% SiO_2, J13-54-9-M96 from 58.42–59.53 wt% SiO_2 and J13-54-8-M98 from 57.62–59.61 wt% SiO_2. The average values and associated standard deviation indicates that there is systematic change in the SiO_2 content over time in the 1845 tephra (Fig. S.21; Table S2.2). The highest SiO2 concentration is in the basal layer and from there decreases with time (Fig. S2.1), by about 3 wt % (Table S2.2).

There is not observed systematic change in SiO_2 content of the 1991 (Fig. S2.1; Table S2.2) magma while the 1845 magma had higher wt% SiO_2 at the start of the eruption and gradually decreased until the effusive phase (Fig. S2.1; Table S2.2, S.2.3).

Table S2.1: Chemical composition of the standard VG-A99 as acquired on the electron microprobe at Laboratorie Magmas et Volcans (LMV) and University of Iceland (UI) and compared to published values (USGS, USNM, LMV (A), LMV (B); Jarosewich et al. 1979; Thornber et al. 2002; Óladóttir et al. 2011; Gudnason et al. 2017). Numbers in brackets are one standard deviation

	VG-A99				
	USGS	USNM	LMV (A)	LMV (B)	UI
SiO_2	51.06 (0.46)	50.94	51.38 (0.12)	50.90 (0.35)	50.91 (0.31)
TiO_2	3.95 (0.09)	4.06	4.04 (0.05)	4.18 (0.06)	3.93 (0.12)
Al_2O_3	12.44 (0.13)	12.49	12.75 (0.25)	12.67 (0.07)	12.60 (0.10)
FeO	13.15 (0.16)	13.3	13.14 (0.21)	13.21 (0.16)	13.23 (0.13)
MnO	0.19 (0.02)	0.15	0.21 (0.01)	0.15 (0.07)	0.20 (0.02)
MgO	5.04 (0.1)	5.08	4.92 (0.06)	5.04 (0.03)	5.03 (0.11)
CaO	9.04 (0.11)	9.3	9.27 (0.32)	9.13 (0.03)	9.18 (0.18)
Na_2O	2.72 (0.16)	2.66	2.61 (0.12)	2.77 (0.09)	2.65 (0.10)
K_2O	0.82 (0.03)	0.82	0.85 (0.01)	0.84 (0.02)	0.83 (0.02)
P_2O_5	0.43 (0.03)	0.38	0.44 (0.04)	0.43 (0.06)	0.45 (0.03)
Total	98.84	99.18	99.61	99.34	98.99

Table S.2.2: Average chemical composition of the glass analysis of the 1991 and 1845 tephra, samples are arranged in stratigraphic order same as in Fig. S2.1. Number of points and the standard deviation is indicated for each sample.

1845												
number of point	analysis	SiO_2	TiO_2	Al_2O_3	FeO	MnO	MgO	CaO	Na_2O	K_2O	P_2O_5	Total
15	J13-54-8-M98	58.26	1.67	14.65	10.56	0.27	2.35	5.45	3.48	1.67	0.79	99.14
	std. dev.	0.53	0.05	0.22	0.63	0.03	0.15	0.35	0.67	0.20	0.04	0.30
19	J13-54-9-M96	58.98	1.45	14.82	10.66	0.29	2.18	5.19	3.06	1.82	0.66	99.09
	std. dev.	0.36	0.05	0.29	0.37	0.02	0.10	0.18	0.33	0.15	0.03	0.34
18	J13-54-10-M71	61.31	1.13	15.70	8.93	0.24	1.63	5.03	2.85	1.64	0.46	98.92
	std. dev.	0.31	0.03	0.10	0.21	0.01	0.04	0.09	0.10	0.05	0.04	0.27
1991												
20	J12-51-8-98	55.51	2.39	12.97	12.72	0.32	2.59	6.08	2.81	1.60	1.22	98.48
	std. dev.	0.62	0.16	0.35	0.60	0.02	0.16	0.38	0.40	0.07	0.09	0.63
10	J12-51-8-100	56.11	2.28	13.22	12.52	0.30	2.65	5.86	2.83	1.55	1.13	98.45
	std. dev.	0.59	0.16	0.33	0.65	0.02	0.19	0.36	0.44	0.09	0.08	0.60
14	J12-51-5-76	55.29	2.00	14.43	11.51	0.29	2.86	6.54	2.91	1.35	0.99	98.16
	std. dev.	0.56	0.15	0.31	0.71	0.02	0.20	0.40	0.60	0.14	0.08	0.61
17	J12-51-4-59	55.66	2.05	14.53	11.60	0.29	2.95	6.55	2.99	1.34	1.01	98.97
	std. dev.	0.32	0.03	0.27	0.29	0.02	0.10	0.15	0.25	0.05	0.02	0.32
15	J12-51-7-87	56.30	2.43	12.99	12.38	0.33	2.52	6.08	3.42	1.60	1.25	99.30
	std. dev.	0.38	0.12	0.38	0.44	0.04	0.13	0.54	0.46	0.10	0.04	0.66
15	J12-51-7-6	56.23	2.47	12.62	12.55	0.33	2.48	6.14	2.91	1.74	1.27	98.74
	std. dev.	0.39	0.09	0.18	0.77	0.03	0.17	0.47	0.38	0.10	0.05	0.49
15	J12-51-4-63	56.93	2.34	12.72	12.13	0.31	2.25	5.84	2.59	1.69	1.09	97.92
	std. dev.	0.42	0.07	0.14	0.39	0.03	0.07	0.14	0.12	0.06	0.03	0.23
10	J12-51-5-98	55.14	2.16	13.82	12.29	0.30	2.91	6.20	3.16	1.44	1.10	98.54
	std. dev.	0.52	0.10	0.27	0.54	0.03	0.14	0.30	0.49	0.13	0.07	0.45
20	J12-51-4-75	57.01	2.35	12.69	12.22	0.31	2.26	5.88	2.64	1.66	1.13	98.15
	std. dev.	0.29	0.06	0.11	0.32	0.01	0.06	0.19	0.11	0.04	0.04	0.40

Table S2.3: Comparison of the 20th century Hekla eruptions; Hekla 1947 tephra and lava [1](Thorarinsson and Sigvaldason 1970); Hekla 1970 tephra and lava [1](Thorarinsson and Sigvaldason 1970); Hekla 1980 tephra and lava [2](Gronvold et al. 1980); Hekla 1991 tephra average of 10 glass shards [3](Gudnason et al. 2017) 1991 lava[4] (Gudmundsson et al 1992) and H2000 average of 20 tephra and lava samples, according to authors undistinguishable between the two products [5](Hoskuldsson et al. 2007), effusive phase tephra sampled on the Hekla fissure [6](Thorarinsson, 1968) and 1845 lava and opening phase tephra [7](Sverrisdottir, 2007).

Hekla	1845	1845	1845	1947		1970		1980		1991		2000
	Tephra – opening phase	Tephra – effusive phase	Lava – effusive phase	tephra - opening phase	lava - effusive phase	tephra - opening phase	lava - effusive phase	tephra - opening phase	lava - effusive phase	tephra - opening phase	lava - effusive phase	Average of lava and tephra
SiO_2	59.70	56.89	54.80	62.11	54.25	55.21	54.52	54.50	54.60	55.45	54.90	55.52
TiO_2	1.17		1.88	1.02	1.54	1.83	1.91	1.91	1.91	2.32	2.09	2.07
Al_2O_3	15.2	14.18	14.66	16.17	16.34	15.16	14.80	14.60	14.70	13.71	14.30	14.54
FeO	7.39	13.35	10.54	7.75	11.28	11.52	11.78	11.70	11.40	12.30	11.59	11.79
MnO	0.22	0.54	0.25	0.18	0.26	0.26	0.26	0.22	0.24	0.33	0.27	0.28
MgO	1.77	4.05	2.97	1.63	3.39	2.86	3.03	2.90	2.87	2.82	2.91	2.89
CaO	5.06	6.23	6.53	5.24	5.24	6.81	6.76	7.09	7.12	6.26	7.06	6.82
Na_2O	4.52	2.35	4.20	4.12	4.12	4.16	4.08	4.03	3.98	3.59	4.18	4.01
K_2O	1.60	2.65	1.31	0.98	0.98	1.26	1.24	1.16	1.19	1.45	1.22	1.21
P_2O_5	0.41	-	0.94	0.34	0.34	0.68	0.71	0.85	0.86	1.25	1.34	0.87
Total	97.04	100.23	98.08	99.54	97.74	99.75	99.09	98.96	98.87	99.47	99.86	100.00
Source	7	6	7	1	1	1	1	2	2	3	4	5

References:

Grönvold, K., Larsen, G., Einarsson, P., Thorarinsson, S., Saemundsson, K., 1983. The Hekla Eruption 1980-1981. Bull. Volcanol. 46 (4), 349-363.

Gudmundsson, A., Oskarsson, N., Grönvold, K., Saemundsson, K., Sigurdsson, O., Stefansson, R., Gislason, S.R., Einarsson, P., Brandsdottir, B., Larsen, G., Johannesson, H., Thordarson, T., 1992. The 1991 eruption of Hekla, Iceland. Bull. Volcanol. 54, 238–246. doi:10.1007/BF00278391

Gudnason, J., Thordarson, T., Houghton, B.F., Larsen, G., 2017. The opening subplinian phase of the Hekla 1991 eruption: properties of the tephra fall deposit. Bull. Volcanol. 79. doi:10.1007/s00445-017-1118-8

Höskuldsson, Á., Óskarsson, N., Pedersen, R., Grönvold, K., Vogfjörð, K., Ólafsdóttir, R., 2007. The millennium eruption of Hekla in February 2000. Bull. Volcanol. 70, 169–182. doi:10.1007/s00445-007-0128-3

Jakobsson, S.P., Jónasson, K., Sigurðsson, I. a., 2008. The three igneous rock series of Iceland. Jökull 58, 117–138.

Jarosewich, E., Nelen, J.A., Norberg, J.A., 1980. Reference Samples for Electron Microprobe Analysis. Geostand. Newsl. 4, 43–47. doi:10.1111/j.1751-908X.1980.tb00273.x

Óladóttir, B.A., Sigmarsson, O., Larsen, G., Devidal, J.-L., 2011. Provenance of basaltic tephra from Vatnajokull subglacial volcanoes, Iceland, as determined by major- and trace-element analyses. The Holocene 21, 1037–1048. doi:10.1177/0959683611400456

Sverrisdottir, G., 2007. Hybrid magma generation preceding Plinian silicic eruptions at Hekla, Iceland: evidence from mineralogy and chemistry of two zoned deposits. Geol. Mag. 144, 643. doi:10.1017/S0016756807003470

Thorarinsson, S., 1968. Heklueldar. Rangæingafélagið, Reykjavik.

Thorarinsson, S., Sigvaldason, G.E., 1972. The Hekla Eruption of 1970. Bull. Volcanol. 36, 269–288. doi:10.1007/BF02596870

Thornber, B.C.R., Sherrod, D.R., Siems, D.F., Heliker, C.C., Gregory, P., Oscarson, R.L., Kauahikaua, J.P., 2002. Whole-rock and glass major-element geochemistry of Kilauea Volcano , Hawaii , near-vent eruptive products : September 1994 through September 2001. USGS, Open File Rep. 02-17 1–9.